# Hydro-Chemical Evaluation of Bentonite-Fly ash Mix as Liners in Near Surface Waste Disposal Facility

*A Thesis*

*Submitted in partial fulfillment of the requirements*

*for the degree of*

## Doctor of Philosophy

by

**Chandra Bhanu Gupt**
**(Roll No. 146104024)**

**Department of Civil Engineering**
**Indian Institute of Technology Guwahati**
**Guwahati- 781039**
**November-2022**

INDIAN INSTITUTE OF TECHNOLOGY GUWAHATI
DEPARTMENT OF CIVIL ENGINEERING

# CERTIFICATE

It is certified that the present work contained in the thesis entitled **Hydro-Chemical Evaluation of Bentonite-Fly ash Mix as Liners in Near Surface Waste Disposal Facility** submitted by **Mr. Chandra Bhanu Gupt** (Roll No. 146104024) to the Indian Institute of Technology Guwahati for the award of the Doctor of Philosophy has been carried out under my supervision in the Department of Civil Engineering, Indian Institute of Technology Guwahati, Assam, India. I certify that he has been fulfilled all the requirements according to the rules of this institute regarding the investigations embodied in his thesis. This work has not been submitted elsewhere for the award of any other degree.

**Date:** 17-4-2023
**Place:** IIT Guwahati

**Dr. Sreedeep S.**
Professor

Department of Civil Engineering
Indian Institute of Technology Guwahati
Guwahati 781039, Assam, India

INDIAN INSTITUTE OF TECHNOLOGY GUWAHATI
DEPARTMENT OF CIVIL ENGINEERING

# STATEMENT

I hereby declare that the work embodied in this thesis entitled **Hydro-Chemical Evaluation of Bentonite-Fly ash Mix as Liners in Near Surface Waste Disposal Facility** carried out by me in the Department of Civil Engineering, Indian Institute of Technology Guwahati, Assam, India, under the supervision of **Dr. Sreedeep S**. Wherever I have consulted the research findings of others in the creation of this work, I have given due credit by citing them in the text of the thesis and giving their details in the references.

Chandra Bhanu Gupt.

**Date:** 17-4-2023

**Place** IIT Guwahati

**Chandra Bhanu Gupt:**
**Roll No. 146104024**
Department of Civil Engineering
Indian Institute of Technology Guwahati
Guwahati 781039, Assam, India

# Acknowledgements

I would like to express my sincere gratitude and respect to my supervisor, **Dr. Sreedeep S.**, for his unconditional guidance, support and advice throughout this research. Working with **Dr. Sreedeep S.** has been an invaluable learning experience for me. This research would not have been possible without his support and guidance. I am also thankful to my doctoral committee members, **Dr. Anil Kumar Mishra, Dr. Abhishek Kumar and Dr. Suresh A. Kartha** for their advice and encouragement during my research.

I am very thankful to my thesis reviewer for their positive comments and valuable suggestions.

I highly appreciate **Ministry of Human Resource Development (MHRD), India** for providing me the fellowship. I am also thankful to **Department of Science of Technology (DST), Govt. of India**, for their financial support. I thank Director of the Institute, Head of the Civil Engineering Department, Dean Academics, and Dean of Research and Development section of IIT Guwahati for strengthing the research environment of the institute to conduct my research.

I am thankful to **Central Instrumental Facility** and **Centre for the Environmnet**, IIT Guwahati for the allowance of sample analysis to accomplish my PhD thesis objectives. I am also thankful to the **Environmnetal Engineering**, Department of Civil Engineering for allow me always to use the laboratory facility for the completion of my PhD work.

I express my heartfelt gratitude and thanks to the technical officer of Geotechnical Engineering Laboratory **Mr. Samarjyoti Kalita**, for extending all possible support for my experiments. I also acknowledge the unconditional and invaluable help of **Mr. Hari Ram Upadhyaya** and **Miss. Syeda Reshima Begum** for my experimental works. Furthermore, I would like to thank the staff of Civil Engineering Department office, for their support in official works.

It is a great pleasure for me to acknowledge **Mr. Utla Chandra Sekhar** for his support in my thesis formating, which make me able to accomplish my PhD thesis.

Special thanks to **Mr. Chitta Ranjan Medhi, Mr. Payodhar Pathak, and Mr. Upen Gohain** for their support in conducting the experiment and fabrication.

I also want to thank my fellow research scholars and postgraduate friends for their love, timely help, moral support, and friendship. In particular, **Dr. Sudheer Kumar Yamsani,**

**Dr. Abhijit Deka, Dr. Sanandam Bordoloi, Dr. Vinay Kumar Gadi, Dr. Janarul Shaikh, Dr. Shiv Shankar, Dr. Tanmoy Deb, Mr. Pawan Kishore, Mr. Bikash Kumar Sah, Mr. Naveen Kumar, Dr. Chandi Patra, Dr. Lalit Goswami, Dr. Rajneesh Kumar, Dr. Deepa Sachan, Dr. Dr. Suchit Patel, Mr. Deepak Patwa, Mr. Ajit Kumar, Mr. Himanshu Kumar Yadav, Mr. Ankti Srivastava, Mr. Bharat Ratan, Dr. Abhishek Saha, Dr. Arya Anuj, Dr. Krishanu Mukherjee, and Dr. Argdeep Biswas**, who have offered their generous help with my research and made my life enjoyable here.

I appreciate the help and support rendered by my juniors **Mr. Niranjan Kumar Bhatlu, Mr. Prashant Kumar Jha, Mr. Rakesh Kumar Sahoo, Mr. Abhishek Kumar Jha, Mr. Vikash Kumar, Miss Ranita Ray, Mr. Prabal** and **Mr. Charakho N. Nath**.

Last, but most importantly I am very grateful to my parents whose unconditional love, faith and patience encouraged me throughout the journey to achieve this. I am thankful to my elder brother **(Vinay)** who are always beside me for everything. I am thankful to my little gems, **Bhanu Priya, Pragyan Lakshya, and Pushpendra** for making me feel happy by their innocent and cute activities and bringing smile on my face in every situation.

I thank the Almighty God for showering his blessing upon me that I could reach upto here.

**Chandra Bhanu Gupt:**

Roll No. 146104024

# Abstract

Hazardous industrial wastes are contained in engineered shallow near-surface disposal facilities or landfills. To minimize the migration of waste from landfills and protection of geoenvironment and groundwater, low permeable compacted liners are provided, which act as hydraulic and contaminant barriers. In normal practice, bentonite-sand (B-S) mixtures are recommended as liner material. Due to shortage, there is a need to explore the possibility of using alternate waste materials like fly ash (FA) as a substitute for sand (S). To ensure its application in compacted liner, the B-FA mixes should qualify hydro-chemical requirements laid out by different regulatory bodies like Environmental Protection Agency (EPA). The detailed hydro-chemical evaluation includes hydraulic conductivity determination, contaminant retention properties, adequate strength and volumetric shrinkage characteristics. Additionally, when two reactive materials (B and FA) are mixed together, it is important to ensure its compatibility over a period of time. A detailed study is needed to make sure that there are no undesirable interactions between B and FA leading to poor performance of liner. This necessitate long-term interaction studies of B-FA mixes for vital properties such as hydraulic conductivity and contaminant retention.

This study investigated in detail the hydraulic conductivity of B-FA mixes under constant volume (swelling completely restricted) and free swelling conditions at time (t) varying from 0 days (immediately after compaction) to four years of interaction. Every measurement was carried out for extended duration of 90 days to ensure steady state condition. Since the hydraulic conductivity determination of low permeable liner materials is highly time intensive, this study demonstrated the use of geotechnical centrifuge for determining flow properties in short duration of time. A detailed study was performed to evaluate contaminant retention characteristics of B-FA mixes for t varying from 0 days to four years. Additionally, the strength and volumetric shrinkage characteristics of B-FA mixes was determined. The results of B-FA mixes were compared with conventional B-S mixes, wherever applicable. Based on the results, this study demonstrated the utility of B-FA mixes and also identified an optimal mix that ensures maximum utility of FA.

**Keywords**: hazardous waste, landfill liner, bentonite, fly ash, sand, interaction, hydraulic conductivity, contaminant retention, swelling, strength, volumetric shrinkage.

# Contents

# List of Figures

# List of Tables

# List of Abbrevations

| Syntax | Abbrevation |
|---|---|
| **AAS** | Atomic Absorption Spectrophotometer |
| **AEV** | Air entry value |
| **B1** | Bentonite 1 |
| **B2** | Bentonite 1 |
| **B3** | Bentonite 1 |
| **B4** | Bentonite 1 |
| **B/BX** | Barmer bentonite |
| **BFA** | Badarpur fly ash |
| **BAS** | Batch adsorption study |
| **EDX** | Energy dispersive spectroscopy |
| **EGME** | Ethylene glycol monoethyl ether |
| **FESEM** | Scanning electron microscope |
| **FFA** | Farakka fly ash |
| **FSI** | Free swell index |
| **FTIR** | Fourier transform infrared spectroscopy |
| **kPa** | Kilopascal |
| **LL** | Liquid limit |
| **LOI** | Loss on ignition |
| **L/S** | Liquid to solid ratio |
| **MDD** | Maximum dry density |
| **NTPC** | National thermal power plant |
| **NFA** | Neyveli fly ash |
| **OMC** | Optimum moisture content |
| **PA** | Pond ash |
| **PI** | Plastic index |
| **PL** | Plastic limit |
| **$R^2$** | Regression coefficient |
| **RH** | Relative humidity |
| **SL** | Shrinkage limit |
| **SSA** | Specific surface area |
| **SWCC** | Soil water characteristics curve |
| **XRD** | X-ray diffraction |

# List of Symbols

| Symbol | Description |
|---|---|
| $\mathbf{A}$ | Crossectional area of the soil sample |
| $\mathbf{a}$ | Crossectional area of the stand pipe |
| $\mathbf{C}_e$ | Equilibrium concentration of metal ion |
| $\mathbf{C}_o/\mathbf{C}_i$ | Initial concentration of metal ion (mg.L$^{-1}$or mg/L |
| $\boldsymbol{e}$ | Void ratio |
| $\boldsymbol{e}_L$ | Void ratio |
| $\boldsymbol{e}_{AE}$ | Void ratio at air entry |
| $\mathbf{G}_s$ | Specific gravity |
| $\mathbf{h}_1$, $\mathbf{h}_2$, | Pressure head |
| $\boldsymbol{i}$ | hydraulic gradient |
| $\boldsymbol{i}_m$ | hydraulic gradient in model |
| $\boldsymbol{k}$ | hydraulic conductivity |
| $\boldsymbol{k}_m$ | hydraulic conductivity in model |
| $\boldsymbol{k}_m$ | hydraulic conductivity in prototype |
| $\mathbf{g}$ | acceleration due to gravity |
| $\mathbf{L}$ | liter |
| $\mathbf{mg}$ | miligram |
| $\mathbf{N}$ | Centrifuge acceleration level |
| $\mathbf{N}$ | Centrifuge acceleration level |
| $\mathbf{Q}_m$ | Maximum adsorption capacity |
| $\mathbf{q}_e$ | Adsorption capacity |
| $\mathbf{S}_r$ | Degree of saturation |
| $\mathbf{t}$ | time in second |
| $\boldsymbol{w}_L$ | Liquid limit |
| $\boldsymbol{w}_P$ | Plastic limit |
| $\boldsymbol{w}_S$ | Shrinkage limit |
| $\boldsymbol{w}$ | Water content |
| $\boldsymbol{w}_{AE}$ | Water content at air entry |

# 1

# Introduction

## 1.1 General

Low level radioactive waste and hazardous industrial wastes are disposed into shallow near surface disposal facility or landfills. To minimize the migration of waste from landfills to geoenvironment and groundwater, low permeable compacted liners are provided, which act as hydraulic and contaminant barrier. In normal practice, bentonite-sand mixtures are recommended liner material in hazardous waste management. In recent times, there is intense shortage of sand even in the construction industry. Therefore, there is a need to explore the possibility of using alternate waste materials like fly ash as substitute for sand. To ensure its application, the material or the mix should qualify hydro-chemical requirements for a compacted liner. It is also important to understand the long-term performance and compatibility of fly ash-bentonite mix. Such studies are not reported in the literature and specifically for Indian fly ashes.

Hydraulic conductivity is the most important parameter of soil used as hydraulic and contaminant barriers in waste containment facility. Studies have explored the adequacy of bentonite-sand mix as liner material due to its low permeability (Tripathi and Viswanadham, 2012; Meier and Shackelford, 2017; Mukherjee and Mishra, 2019, 2020; Wang et al., 2021). The potential use of bentonite-fly ash mixes to use as landfill liners has been explained by previous researchers ( Mollamahmutoğlu and Yilmaz, 2001; Prashanth et al., 2001; Younus and Sreedeep, 2012a). According to United States Environmental Protection Agency (USEPA), the hydraulic conductivity of liners should be less than $10^{-9}$ m/s. The determination of bentonite or bentonite-fly ash mix hydraulic conductivity is time consuming

and complex. The complexity is mostly associated with the reactive or swelling nature of bentonite when it interacts with water or leachate, development of diffused double layer (DDL), and the chemical compatibility of bentonite and fly ash. During the initial phase of an unfilled landfill, the liner may be exposed to water interaction under minimal overburden stress acting on it. This condition may result in the free swelling of the liner layer. As the overburden stress increases, the swelling may get progressively restricted. Such constant-volume or free-swelling condition (Cui et al., 2008a,b; Dafalla et al., 2015; Weerasinghe et al., 2021) would impact the hydraulic conductivity of compacted liner.

Hettiaratchi et al. (1999) investigated the compressive strength, tensile strength, flexibility, cracking potential of different fly ash-bentonite composites and found majority of them suitable for liner materials. However, majority of these studies suggest to explore the heavy metal retention capacities of fly ash-bentonite composites as future scope to have a holistic understanding of the material as liner material. Deka and Sekharan (2017) conducted batch adsorption tests on Indian fly ash-bentonite samples based on 1:1 ratio of the two material and the model contaminant was chosen as lead ($Pb^{2+}$). However, no previous studies take into account the changes in $Pb^{2+}$ adsorption for different fly ash-bentonite ration, adsorption kinetics and do not juxtapose the results with sand-bentonite mixes.

General procedure of adsorption studies in batch experiments necessitates the initial pH to be controlled (Li and Li, 2001; Huang et al., 2011; Hong et al., 2016; Liu et al., 2016; Kumar et al., 2019). In majority of these studies, the pH is controlled at 5 to simulate the pH of leachate in field conditions (Rowe, 1995; Lo, 1996; Li and Li, 2000). The adsorption capacity of adsorbent obtained from batch studies at this initial controlled pH would give us the minimum or representative contaminant removal, predominantly based on adsorption phenomenon. However, contaminant retention is governed by both adsorption and precipitation, typically at higher pH (Liu et al., 2016; Deka and Sekharan, 2017). At uncontrolled pH, typically higher than 5.5, precipitation of heavy metal ($Pb^{2+}$) would be dominant followed by adsorption of the adsorbate as the pH of the solution decreases. The pH of the adsorbent in field will be different based on its mineralogy. Typically, for reactive material such as bentonite and bentonite-based composites the range would be at 8-12 (Li and Li, 2001; Liu et al., 2016; Tahervand and Jalali, 2017). There is a need to understand the impact of constant and variable pH conditions on the adsorption characteristics of bentonite-fly ash mixes.

The fly ash inclusion in bentonite decreased the Atterberg limits, optimum moisture content (OMC) while increased the maximum dry density (MDD), which further makes it suitable as a liner material (Singh et al., 2015; Sun et al., 2019). However, these studies do not compare in detail the strength efficacy of bentonite-fly ash mixes against conventionally used bentonite-sand mixes. Also, the compressive strength of contrasting fly ash (i.e., class C and class F) mixed with bentonite was not comparatively investigated. The effect of pH and electrical conductivity (EC) of bentonite-fly ash mixes on compressive strength has also not been investigated in the literature. This is relevant as these easily measurable electrochemical properties are directly dependent on the unique mineralogical content of the mixes. For instance, pH is a direct indication of the CaO content of a fly ash (Antoni et al., 2016) and can even vary within its individual class. Furthermore, a detailed study on its microstructure and the consequent effect of strength characteristics of bentonite-fly ash mixes is lacking in literature. Along with strength, the volumetric shrinkage of the bentonite-fly ash mixes needs specific attention. A highly plastic soil is bound to shrink more (Mitchell et al., 2005; Tripathy et al., 2014b; Barreto, 2019) and can result in cracks.

## 1.2 Motivation and broad objective of this study

A need to understand the hydraulic conductivity and contaminant retention characteristics of different bentonite-fly ash mixes and maximizing the utility of waste material like fly ash in environmentally sensitive waste containment projects has motivated this study. As stated above, there are different knowledge gaps existing for adopting bentonite-fly ash liners compared to bentonite-sand mix. With this in view, the proposed study purports to perform a detailed hydro-chemical evaluation of bentonite-fly ash mix.

There are two main objectives that have resulted in the origin of this research work. (1) exploring the application of alternate materials as compacted backfills in waste containment, and (2) maximizing the utility of waste material like fly ash for geoenvironmental projects. For meeting both objectives, it is essential to determine the hydro-chemical characteristics of soil and its mixes. However, flow-through low permeable backfills are complex and time-consuming, mainly due to the reactivity of expansive soil in the presence of water and fly ash. Therefore, this study demonstrates the utility of accelerated physical modeling (geotechnical centrifuge) as against the conventional methods for obtaining hydraulic conductivity of low permeable swelling bentonite-fly ash mix.

Another objective is to explore contaminant retention behavior of bentonite and bentonite-fly ash mixes. Based on these analyses, an appropriate bentonite-fly ash mix satisfying the hydro-chemical requirement of the liner was examined. The mix so obtained was also investigated for the long-term performance assessment to make sure that fly ash-bentonite interaction will not result in an undesirable effect. Additional objectives include determining of volumetric shrinkage characteristics and strength of bentonite-fly ash mixes.

## 1.3 Organization of the thesis

The thesis is organized into nine chapters. Chapter 1 gives a general overview of the thesis, the motivation behind this research work, and its relevance for the geoenvironment. Chapter 2 reviews the literature comprehensively on the background research and identifies the research gaps. The main objective and scopes of the study are listed in this chapter. Chapter 3 deals with the characterization of used materials and the details of the methodologies adopted in this study to meet the research objectives. Chapter 4 describes the development of an experimental setup for performing the volumetric shrinkage curve (VSC). Balloon method was used for the evaluation of the soil shrinkage characteristics curve (SSCC), and a predictive model was developed for the determination of (SSCC) for the highly expansive soils. Chapter 5 demonstrates an in-house developed permeability setup for B, B-FA and B-S mixes. This chapter further details the centrifuge setup for determining the low hydraulic conductivity of highly expansive soils like B in short duration of time. The chapter also deals with the hydraulic characteristics associated with long-term interaction. Chapter 6 presents the adsorption characteristics of Barmer bentonite for its application in waste containment application. Also, the effect of the liquid to solid ratio on the adsorption behavior of B was evaluated. This chapter also presents the effect of a buffering agent used to adjust the pH in the adsorption process on the adsorption capacity. Chapter 7 demonstrates the contaminant retention characteristics of B-FA mixes and B-S mixes under controlled and uncontrolled pH environments. The results show the advantage of B-FA mixes for the contaminant retention over the B-S mixes for the same proportion. Also, this chapter includes the effect of B-FA interaction with time on its contaminant retention capacity taking into account its practical application in the long-term. Chapter 8 evaluated the mechanical performance and microstructural characterization of B-FA mixes and B-S mixes. Chapter 9 lists the conclusions and major findings of this study. The limitations and future work of the study are also presented in the chapter.

# 2

# Literature Review

## General

An understanding on the utility of fly ash bentonite mixes in geoenvironmental applications is essential for proposing it as alternate material for hydro-chemical barrier in landfills liner in place of sand bentonite mixes. Focus has been laid on studies related to the determination of long term hydraulic characteristics of fly ash, bentonite and their mixes to access the reactivity of the materials. A comparative study was done with the established materials for liner, sand bentonite mixes. Hydraulic characteristics of the fly ash bentonite mixes and sand bentonite mixes were evaluated under normal laboratory condition 1g and at Ng condition using geotechnical centrifuge. Further contaminant retention characteristics of fly ash, bentonite and its various mixes were reviewed. To simulate the actual field scenario for the retention characteristics of fly ash, bentonite and mixes, review was also focus on the column study.

## 2.1 Flow characteristics of fly ash and expansive soil

Abeele (1986) studied the permeability of bentonite silt ratio for its effective utilization in landfill liner application by conducting consolidation test. The study indicates that the permeability is inversely proportional to the square of the bentonite silt ratio. The hydraulic conductivity decreased as the compaction pressure increased. The hydraulic conductivity could be expressed as a function of void ratio. A strong relationship exists between the void ratio and $\log(\sigma)$ for each bentonite ratio.

Cowland and Leung (1991) performed both field and laboratory testing to study the performance of bentonite amended weather granite landfill liner. The field investigation was carried out on both flat and sloping ground. The study indicates that bentonite content of around 5-7% was found to be adequate in reducing the hydraulic conductivity of completely weathered granite (CWG) to $10^{-11}$ m/s. Both water and leachate was used as the permeant in the field permeability test. The permeability was found to lie between $10^{-11}$ m/s and $10^{-6}$ to $10^{-12}$ m/s. Laboratory permeability test on the CWG has given decreasing value of the coefficient of permeability with increase in bentonite content.

Gleason et al. (1997) studied the performance of calcium and sodium bentonite for the application in soil- bentonite landfill liner and cover, geosynthetic clay liners (GCLs) and cement bentonite mixtures for vertical cutoff wall. In case of hydraulic conductivity, three times more calcium bentonite was required for the reducing the hydraulic conductivity to about $10^{-9}$ m/s than the sodium bentonite. Again, the hydraulic conductivity of sand bentonite mixture increased when permeated with $CaCl_2$ solution. All the thin bentonite layers (simulating the use of GCL) has given the hydraulic conductivity less than $10^{-9}$ m/s. Sodium bentonite was found to be approximately 10 times less permeable with tap water than calcium bentonite.

Ghosh and Subbarao (1998)studied the effect of fly ash stabilized with lime and gypsum on the hydraulic conductivity and leachability. The effect of moulding water content, lime content, gypsum content, curing period and flow period on the hydraulic conductivity was investigated in detail. From, the study, it was found that the addition of lime to fly ash reduced the hydraulic conductivity. Again gypsum, in the presence of lime, helps to decrease hydraulic conductivity even further. It made the matrix more stable and enhanced the pozzolanic reaction. Hydraulic conductivity was less on wet side of optimum. For all the mixes of fly ash, lime and gypsum there was a reduction in hydraulic conductivity with an increase in curing period. The concentrations of As, Cd, Cr, Cu, Fe, Hg, Mg, Ni, Pb and Zn in the effluent from the stabilized mixes was below threshold limits acceptable for ground water.

Li and Li (2000) demonstrated the effect of wet dry cycles on plasticity and swelling characteristics of bentonite by conducting various tests. Three different types of liquid were used for the experimental investigation. The hydraulic conductivity of the geosynthetic clay liner (GCL) was also studied for these liquid for various wetting cycles. The study indicates

that the plasticity of the bentonite decreased for increasing wet- dry cycles when tap water and $CaCl_2$ was used as a wetting liquid. On the other hand, the plasticity characteristics of the bentonite increased when deionized and tap water was used for wetting. The hydraulic conductivity was found to be less for few cycles of wetting, but gradually increased as the cycle increased.

Palmer et al. (2000) conducted laboratory and field hydraulic conductivity test on class F fly ash, class C fly ash, sand and bottom ash for its use in waste containment liners. The study revealed that mixture of class F and C ashes combined with a course aggregate (e.g. bottom ash) could be compacted to achieve hydraulic conductivity near or below $10^{-9}$ m/s at compaction water content above OMC.

Prashanth et al. (2001) studied the use of pozzolanic fly ash as a hydraulic barrier in landfill. The behavior of three different fly ashes collected from different sources and having different physico-chemical properties wre investigated in this study. Various geotechnical properties like shrinkage, compaction, permeability, consolidation and strength have been determined. From the study, it was clear that fly ash had a very low shrinkage and compacted fly ash undergo very little volume change. The pozzolanic fly ash was found to develop good strength with time even without the addition of lime. As the fly ash consists of silt size particles, it exhibits low hydraulic conductivity. However, pozzolanic fly ashes with lime content exhibit low permeability on curing because the formation of gel compounds which block the pores.

Cokca and Yilmaz (2004) investigated the fly ash mixed with bentonite as a liner material. Type C fly ash was collected from Soma thermal power plant in Turkey. Falling head permeability test was performed using oedometer. The hydraulic conductivity of fly ash mix with 10% bentonite was found to be within the acceptable limit for liner design ($10^{-9}$ m/s).

Daniels et al. (2004) investigated the effects of soil-bentonite mixture for hydraulic conductivity and retention of lead from the solution. The study indicates that the hydraulic conductivity of soil- bentonite mixture (96% soil and 4% bentonite by weight) was found to be $1\times10^{-10}$ m/s. Acid extraction and SEM/EDXS analysis were carried out to study the sorption of lead by soil-bentonite mixture.

Phani Kumar and Sharma (2004) noted that the hydraulic conductivity of expansive soil-fly ash mix decreased with an increase in expansive soil content. The study indicates that

the plasticity characteristics of expansive soil was reduced by addition of fly ash content. Again increase in fly ash content decreased the liquid limit and increased the plastic limit of the expansive soil. It was found that the free swell index of expansive soils could be effectively reduced up to about 50% by addition of 20% fly ash.

Yeo et al. (2005) studied the consolidation and hydraulic conductivity of various backfill materials used in soil-bentonite vertical cut off wall. Different percentage of sand and bentonite were used for preparing the mixtures. The coefficient of consolidation (Cv) was found to decrease with increase in backfill- fine content or backfill-bentonite content. It was found that more than 40% of fine was required in the back fill to achieve the hydraulic conductivity of $10^{-9}$ m/s when the backfill contained only low- plasticity clay. Again, when the backfill consists of clean, coarse-grained materials, a significant amount of dry bentonite (5% in this study) might be required to achieve a hydraulic conductivity of $10^{-9}$m/s.

Prakash and Sridharan (2009) have studied the permeability of different coal ashes and found to be in the range of silts. The permeability of class C fly ash was found to be less than that of class F fly ashes, and its permeability was found to decrease with time.

Heineck et al. (2010) studied the effect of bentonite proportion on the hydraulic conductivity of bottom ash, fly ash and compacted sand by using flexible wall permeameter. The particle morphology was studied based on thin section micrographs. The proportion of bentonite used in the study was taken 0, 3, 6, 9, and 18%. The study indicates that there was only a marginal reduction in hydraulic conductivity ($1.78\times10^{-6}$ m/s to $1.39\times10^{-7}$ m/s for bottom ash and from $5.67\times10^{-6}$ m/s to $1.12\times10^{-7}$m/s for fly ash) of bottom ash and fly ash on addition of bentonite. Hydraulic conductivity reduction was achieved only when bentonite was added to the sand (from $3.17\times10^{-5}$ m/s to $5.15\times10^{-10}$ m/s). Due to the solid particles of the sand and longitudinal contact between them, the hydraulic conductivity of sand bentonite mixture was less whereas, ash had angular and porous particles with puncturing contact points. The elevated cation concentration in the pore water was an important aspect for high hydraulic conductivity of ash bentonite mixtures. The cation exchange decreased the swelling capacity of bentonite and thus increased the hydraulic conductivity of the mixture.

Yeheyis et al. (2010) studied the use of coal fly ash and fly ash-bentonite mixtures as a barrier material for mine waste. The fly ash used in this study was of class C fly ash and the bentonite was of Na-montmorillonite type. The permeant used was acid mine drainage.

The results of this study suggest that the addition of 10% bentonite to coal fly ash reduced the hydraulic conductivity of coal fly ash to less than $1\times10^{-9}$ m/s.

Amadi (2011) determined the hydraulic conductivity of lateritic soil and fly ash mix. Soil mix was prepared at 0, 5, 10, 15 and 20% fly ash content compacted at 2% wet of OMC compacted using modified Proctor method. Class C fly ash was taken for the study and it was found that hydraulic conductivity decrease with increase in fly ash content up to 10% due to increase in fines in the mixture. Above 10%, the hydraulic conductivity was found to increase again.

Sivapullaiah and Baig (2011) have investigated the hydraulic conductivity of two class F fly ashes of Indian origin using falling head method. Lime was added to the fly ash up to 10%. The hydraulic conductivity of fly ash was found to decrease with increase in lime content.

Alam et al. (2012) studied the seepage and geotechnical properties of fly ash mixed with bentonite for its use in various engineering applications. In their investigation it was found that bentonite can be used as stabilizing material for the fly ash, as fly ash is cohesion less material and having very low compressive and shear strength. The strength was found to increase by adding low cost cohesive materials such as lime and clayey soil. It was also observed that 20% bentonite-fly ash mix is an optimum mix that can be safely used as a subgrade material of pavements and as cover or liner at waste disposal sites.

## 2.2 Contaminant retention characteristics of fly ash

The usefulness of fly ash as a low cost adsorbent has been studied by a lot of researchers all over the world. Fly ash has been extensively used for the removal of heavy metals from the waste water due to its physical and chemical properties. More over the alkaline nature of fly ash makes it good neutralizing agent.

Nhan et al. (1996) studied the hydraulic and contaminant barrier properties of coal fly ash by using synthetic municipal solid waste (MSW) leachate. The ability of the barrier material to attenuate metal ion contaminants was investigated in this study. The study indicates that the hydraulic conductivity of the barrier remains constant at the beginning and then showed a long term linear increase with the leachate volume. The metals carried by the leachate was reduced due to precipitation in the barrier material. The contaminant metals were precipitated in the barrier as either hydroxide or carbon depending upon the

solubility constants of the two solid species.

Pandian et al. (1996) conducted laboratory experiments to study the effectiveness of fly ash for retention of heavy metals. The effect of fly ash types and pH on the retention of heavy metals have been investigated in this study. The study indicates that fly ash contains lead ions through the formation of lead hydroxide which gets precipitated in the pore volume and at the surface of fly ash. It also retained lead ions by adsorption on to the surface sites of silica, alumina and iron oxide. Again, the retention of lead ions by fly ash increase with the increase in initial pH of the solution. It was found from this study that fly ash containing high amount of calcium retains more lead ions than low calcium fly ash. The fly ash was found to retain lead ions permanently when the leachate pH was between 3.5 and 10. Fly ash however released lead ions at very low and very high pH.

Ayala et al. (1998) investigated that adsorption of Cd and Cu by fly ash. The effect of initial metal concentrations, pH, contact time, grain size and ionic strength were investigated in this study. The retention of metals by the fly ash gets decreased as the pH of initial solution decreased. The presence of high ionic strength or appreciable quantities of calcium and chloride did not have significant effect on the removal of Cd and Cu by fly ash. The removal of metals increased as the grain size decreased.

Gupta and Torres (1998) studied the removal of heavy metals like Cu, Pb and Zinc from waste water effluent using fly ash collected from Indian River Power Plant, Millsoboro, DE. The treatment of the effluent with the fly ash has significantly reduced the amounts of the heavy metals. The toxicity level of the effluent could be alleviated.

Piekos and Paslawska (1999) studied the characteristics of fly ash in retention of fluoride. Experiments were conducted on various concentrations of fluoride ions to see the uptake of fluoride ions by the fly ash. It was seen in this study that retention of fluoride ions by the fly ash is initially low up to about 24 hours but it gradually increased dealing to almost complete retention at 120 to 144 hrs. The study showed a double mechanism in the retention of fluoride ions by fly ash, one is chemical binding by calcium hydroxide and the other is physical sorption by residual carbon particles.

Poulose et al. (2000) studied centrifugal modelling of moisture migration in silty soils for understanding the complex behaviour of transport of solute in soil strata. The centrifuge was rotated at a value of 33.33, 50, 75g for three prototypes for 5.2, 10.42 and 17.36 days. In this study the modelled both sample length as well as time. For this, they used 2, 3

and 4.5 m long prototypes of silty soil and compacted statically. For centrifuge modelling, they prepared a sample of the same soil with sample length 60 mm which was 33.33 times smaller than 2 m prototype. And in this way, they calculated the N value for centrifugation. Similarly, for 3 m and 4.5 m prototype N was 50 and 75 respectively. They also modelled the time of water flow by dividing $N^2$ to the time of water flow in the prototype. A graph was plotted between prototype depths versus moisture migration after centrifugation. The results have shown that the modelling of model technique and advection properties of solute can be studied in the centrifuge. It is also shown that as the degree of saturation increases advection decreases. This is because when the soil is already highly saturated, there are very little pores to be filled.

Lin and Chang (2001) studied the effect of fly ash on the removal of Cu(II)from aqueous solution. The fly ash used in this study was obtained from China steel corporation (Kaohsiung, Taiwan). The study investigated the effect of carbon fraction of fly ash on the removal of Cu(II). The fly ash containing different carbon fractions were prepared by thermal decarbonation in the laboratory. The equilibrium concentration of Cu(II) was found to decrease with increasing adsorbent dosage and carbon fraction.

Mollamahmutoğlu and Yilmaz (2001) studied the potential use of bentonite fly ash mixes for the effective use as hydraulic barrier for different contaminant. Fly ash was added with bentonite at 5% to 30% by weight. Tests were conducted on pure fly ash and fly ash bentonite mixes (Permeability, triaxial tests, unconfined compression and consolidation) to discuss the potential use of bentonite fly ash mix as a landfill cover material. The results of permeability test show that 20% bentonite fly ash mix can serve the purpose of land fill cover both under acidic and basic condition. Bentonite fly ash mixes can minimize collapse in case of flooding as their collapse potential is far less than the required (5%).

Singh and Gupta (2001) have determined the hydraulic conductivity of different silty soils of varying compaction state at 1g as well as Ng using a geotechnical centrifuge. Samples were centrifuged at different g-values and hydraulic conductivity was measured using falling head permeability test. Hydraulic conductivity was measured using the oedometer falling head test also. Scaling relationship for hydraulic conductivity was given by

Rao et al. (2002) investigated that the removal of $Cr^{6+}$ and $Ni^{2+}$ from aqueous solution using raw bagasse fly ash from sugar mill and coal fly ash from thermal power plant. The effect of hydrogen ion concentration, contact time, sorbent dose, initial concentration of

adsorbate and adsorbent and the particle size on the uptake of $Cr^{6+}$ and $Ni^{2+}$ was investigated in this study using batch experiment. The optimum pH for removal of $Cr^{6+}$ and $Ni^{2+}$ by the fly ash was found to be 6 and 8 respectively. The effect of contact time on the rate of uptake of $Cr^{2+}$ and $Ni^{2+}$ was found to be rapid, having maximum adsorption within the first hour of contact time. After that adsorption was very slow and saturation attained within 1.5 to 2 hr for both the metal. Again, the rate of uptake of $Cr^{6+}$ and $Ni^{2+}$ was found to increase with the increase in adsorbent dose. The adsorption efficiency of both the bagasse of fly ashes was found to decrease with the increase in initial concentration of the metals. The uptake of metals was found to increase with the decrease in particle size due to greater surface area.

Rio and Delebarre (2003) discussed the removal of mercury from aqueous solution using two different types of fly ash produced located in the Northeast and Southeast of France. The kinetic studies of the two types of fly ash indicate that the equilibrium adsorption had reached within 72 hr for both the fly ashes. Again, the rate of adsorption was faster and the steady state removal was higher for the sulfo-calcic fly ashes than for silico- aluminous fly ashes for any value of pH of the aqueous solution. The adsorption capacities for the sulfo-calcic fly ash was found to be 5 mg/g, whereas for sillico- aluminous fly ash, the adsorption capacities was found to be 3.2 mg/g.

Weng and Huang (2004) investigated the adsorption of Zn(II)ions from aqueous solution by using fly ash. The fly ash used in this study was collected from Delmarva Power plant in Wilmington, DE. Batch adsorption experiments was conducted to study the sorption of Zn(II) by the fly ash. The study indicates that the amount of Zn(II) ions adsorbed gets increased with the increase in fly ash content and pH of solution. Again, the adsorption of Zn(II) was found to increase with the decrease in ionic strength for a particular value of pH of the solution. The Langmuir adsorption isotherm model was used to study the adsorption of Zn(II) ion on the fly ash.

Cho et al. (2005) studied the adsorption of heavy metals (Zn, Pb, Cd, and Cu) from aqueous solution using fly ash as a low cost adsorbent. The fly ash used in this study was collected from a bituminous coal- burning plant of Korea Electric Power Corporation, Boryung, Korea and was categorized as class F fly ash. The adsorption characteristics of fly ash was studied under different pH, heavy metals concentrations and fly ash dosages using both isotherm and kinetic studies. In this study, the heavy was found to be adsorbed very

rapidly (within 20 min). The equilibrium time for the zinc was found to be 2 hours, while the other metals apart from zinc, it was 3 hr. the precipitation of the metals on fly ash was found to be higher for high pH. The adsorption data were fitted using Freundlich isotherm.

Pehlivan et al. (2006) studied the effectiveness of fly ash in the removal of copper and zinc from aqueous solution using the batch sorption studies. The fly ash was obtained from a sugar industry, produced by burning of young brown coal. Batch kinetics and isotherm studies were conducted to determine the adsorption capacities of sorbents. The effect of contact time, pH, sorbent dose and initial concentration of adsorbate on the adsorption were studied. The adsorption of the metals was found to increase with the increase in contact time and it reaches equilibrium within an hour. The adsorption of the metals by the fly ash was found to decrease with decrease in pH of the initial solution. Maximum sorption of both metals was found to be between pH 5 and 4 for the fly ash. Again the adsorption of both metals was found to increase with the increase in adsorbent dosage and the increase in initial concentration of the metal ions. The adsorption data were found to fit very well with Langmuir and Freundlich models.

Alinnor (2007) investigated the adsorption of $Pb^{2+}$ and $Cu^{2+}$ from aqueous solution by fly ash collected from Nigeria Coal Corporation. Batch adsorption study was carried out to see the adsorption of the metals. The effect of contact time, pH and temperature on the removal of these metals was investigated. Lead and copper was adsorbed onto the fly ash very rapidly within 20 min, and the equilibrium was achieved within two hours. The retention of metals gets increased with an increase in pH. There was a decrease in uptake of the metals with the increase in temperature.

Papandreou et al. (2007) studied the adsorption of copper and cadmium from aqueous solution on pellets made from class C fly ash, collected from Megalopolis power plants in southern Greece. For investigation fly ash was shaped in to pellets, having diameter 3-8 mm with high porosity and very good mechanical strength. The effect of agitation rate, equilibrium time, pH and initial metal concentration were investigated in this study. The adsorption of both metal was found to increase with an increase in pH with 100% sorption at pH above 9. The adsorption capacities of pellets was found to increase with an increase in initial metal concentration. Again, the adsorption of copper by the pellets was found to be higher than cadmium ion. This study indicates that the pellets could be used for adsorption of copper (20.92 mg/g) and cadmium (18.98, and could be used for their removal from

aqueous solution at ambient temperature.

Hsu et al. (2008) used raw fly ash for the adsorption of $Cu^{2+}$ from waste water. The effect of pH, adsorbent does and effect of temperature on adsorption was studied. The fly ash was found to remove $Cu^{2+}$ from the waste water effectively. Again, the raw fly ash was found to be more effective in removing $Cu^{2+}$ from the waste water than the modified fly ash.

Visa et al. (2010) studied the removal of heavy metals from aqueous solution using fly ash collected from Romania and modified with NaOH-2N. The heavy metals used for this study were $Cd^{2+}$, $Cu^{2+}$ and $Ni^{2+}$. Batch adsorption study was conducted to determine retention property of the fly ash. The effect of contact time was found to be around 30 min or less for single metal ion solution. The second order kinetic study was done and the experimental results were fitted with Langmuir isotherm model. The adsorption efficiency of copper was found to be more than the other metals used in this study.

## 2.3 Centrifuge modelling studies for mass transfer

Arulanandan et al. (1988) studied the time for pollute transport in geotechnical centrifuge. The study discussed about scaling laws, physical aspects of modelling, testing procedure that is to be adopted. Four silica samples with different heights and different water levels was used for centrifugation at 25g, 33.3g, 37.5g, and 50g. The water level was different in each of these samples to ensure that same pressure was acting on all samples while centrifugation. The study adopted modeling of models and ensured that the scaling laws for time was valid. It was found that advection and dispersion could be simulated but adsorption cannot be simulated successfully.

Esposito (2000) discussed about LNAPL migration in Dutch dune sand in unsaturated conditions. Moisture profile curves for different g-levels was simulated successfully. The samples were tested at 20g and 30g on 2 types of sand with different porosities to examine the effect of porosity on migration of LNAPL in unsaturated sand. There was good agreement of LNAPL transport at different g-levels and modelling of models was properly validated. It is to be noticed that distribution of plume is very large in loose soil which shows the density dependence on flow of contaminant.

Pantazidou et al. (2000) studied the migration of Dense Non Aqueous Phase Liquid (DNAPL) in saturated soils using geotechnical centrifuge. The DNAPL migration was stud-

ied using modelling of models technique. In this study two DNAPL solutions n-butyl phthalate (BP), Freon 113 (F113) were considered. Sand-size and silt size glass beds were used for experimentation. Centrifuge results were compared with predictions of a numerical model to further support the usefulness of centrifuge in simulating DNAPL migration in sub-surface. It was observed that the transport patterns of DNAPL in both sand bed and silt bed was almost similar and hence concluded that capillary pressure is not a barrier for migration of DNAPL. Low density and high viscosity DNAPL displaces water in steady and stable manner while high density and low viscosity DNAPL displaces the soil in unstable manner.

Singh and Gupta (2000) studied the hydraulic conductivity of different silty soils of varying compaction states at 1g and Ng state using a geotechnical centrifuge. Samples were centrifuged at different g-levels and hydraulic conductivity was measured using falling head permeability test. Hydraulic conductivity was determined by using oedometer falling head test, conventional falling head tests and consolidation tests ($k=c_v\ m_v\ \gamma_w$) at 1g condition. It was observed that permeability in centrifuge was N times more than that at 1g condition, where N is the amount by which acceleration due to gravity is enhanced in centrifuge modeling.

Singh and Gupta (2001) studied the hydraulic conductivity of silty sand and clayey soil in a geotechnical centrifuge. They studied the effect of sample length and time of centrifugation on hydraulic conductivity. They took different sample lengths and tested at different N values and found that with an increase in sample length hydraulic conductivity decreases and to avoid the scaling errors they suggested the sample length should be less than 10% of the effective radius of the centrifuge. And hydraulic conductivity k as a function of the unit weight of permeant increases with increase in centrifugal acceleration N. Hydraulic conductivity of the soil sample depends upon the initial orientation of soil fabric and the rearrangement of individual soil fabric due to the moulding water content. And an increase in centrifugal acceleration does not alter the orientation of soil fabric it only increases the discharge of permeant by increasing its unit weight.

Thusyanthan and Madabhushi (2003) found that defining the scaling law of permeability and seepage flow velocities were often confusing. Darcys permeability is defined as the rate

of fluid flow through a porous media is proportional to the potential energy gradient.

$$v = i * k \tag{2.1}$$

Where v is the velocity of discharge, k is the constant called Darcys permeability, and i is hydraulic gradient

$$i = \frac{\delta(H)}{\delta(L)} \tag{2.2}$$

Timms and Hendry (2008) conducted the experiment on column tests and stated that it seems to be impractical when the solute transport time is very long. A geotechnical centrifuge served this purpose. The main objective of this research was to develop centrifugation technique to describe the transport of a simple solution in low permeable clay rich media. Effort was made to compare the test results with conventional laboratory tests and field observations which was not done before. In-situ exchange capacity and exchange coefficients were compared with values determined by standard batch techniques. A 52mm × 33mm sample core was rotated in centrifuge for 90 days at 330-g to model the migration of saline pore water (0.5M Nacl) under in-situ conditions through a 17-m thick layer for about 24000 years.

Kererata et al. (2013) studied centrifuge modelling of LNAPL migration through sandy soil for checking the effectiveness of remediation technology (constructing barrier walls) under flow and no flow conditions. Modelling was done at 30g to simulate 80 days of migration of contaminant in soil. Soil-cement walls were used as contaminant barriers. Results show that flow of LNAPL was deeper and faster than flow of water. It was suggested to have a depth of barrier wall 1.5m for no water flow condition and 2.5m for flow for effective control of contaminant migration.

Pasha et al. (2013) investigated the effect of soil fabric on the migration of contaminant in unsaturated soil. Centrifuge tests were done on two unconsolidated soils with different moisture contents and a soil consolidated due to its own weight at 50g. Model set up was rotated in geotechnical centrifuge in two phases. For unconsolidated soils, centrifuge was rotated for few minutes and for consolidated sample it was rotated for 119 minutes to ensure consolidation. In phase 2, the LNAPL was released into the model at a rate 19.8 $m^3/m$ (prototype). After the experimentation the samples were collected for calculating

moisture and contaminant content. It was observed that for LNAPL migration in unconsolidated soils, the plume was narrow and widely spread at saturated zone. In consolidated zone the plume spreads over a large area in unsaturated zone as the void ratio was less. The LNAPL which reached saturated zone was reasonably very less. The contamination pattern was not similar for the three tests. Test results indicate that at a same time for a same soil sample with three different soil fabric, the contaminant phases were different (mobile, immobile, residual). Hence it was concluded that while determining the contaminant migration through unsaturated soil it is important to have thorough investigation of geological site.

## 2.4 The unconfined compressive strength of liner materials

Sridharan et al. (1997) have investigated the effect of varying fly ash content on the the strength of black cotton soil. For their study, they used two types of fly ash and found that only reactive fly ash can increase the unconfined compressive strength. This is due to the presence of base-soluble silica which makes fly ashes reactive. The base-soluble silica reacts with the free lime present in fly ashes in the presence of water and produces cementitious compounds, leading to the development of strength. It is observed from this study that the small amount of fly ash should have decreased the immediate unconfined compressive strength of black cotton soil. This is because the pozzolanic reaction is a time-dependent process and fly ash not undergoing the pozzolanic reaction behaves just like silt. It has been found that the pozzolanic compounds formed to bind the soil particles and enhance the strength and fly ashes without pozzolanic compound just behave like silt and it disturbs the soil matrix and decreases the strength. And In the absence of pozzolanic reactions, fly ash behaves just like silt, and can only decrease the unconfined strength of soil with increasing fly ash content. From this, they concluded that pozzolanic reaction is the triggering factor in enhancing the strength and it reduces the cohesive strength of soil due to the addition of fly ash.

Al-Yaqout and Townsend (2001) have investigated the feasibility of using gatch sand as a liner material for waste materials in arid regions. It has been found that gatch sand is considered a low-permeable soil when compacted at optimum moisture content and modified maximum dry density. Further, it was noted that adding bentonite to gatch decreases

permeability by one magnitude compared to natural permeability. It is observed from this study that wet of optimum achieve a lower permeability than compacting at dry of optimum moisture content with the same density. It is observed from this study that permeability increases after the wetting and drying cycles on the gatch sands for both laboratory and field cases. A 90 cm thick gatch liner compacted in four layers and a 60cm thick gatch cover that consists of three layers has been recommended for Kuwaiti landfill.

Cokca and Yilmaz (2004) have studied the feasibility of utilizing class C fly ash and pulverized rubber chips with bentonite as a liner material. They found hydraulic conductivity increased with decreasing bentonite percentage and by increasing rubber percentage and vice versa. And the unconfined strength of mix governed by the hydration of pozzolanic compound present in fly ash during curation. And the curing period is a major factor affecting the hardening of fly ash.

Phani Kumar and Sharma (2004) considered the significance of fly ash as an additive in improving the engineering properties of expansive soil. They found that by increasing fly ash content in the mix, its maximum dry density is decreasing which leads to an increase in hydraulic conductivity of soil fly ash mix. They also conducted unconfined compressive strength on all the mixes with the variation in fly ash content, they found that the undrained shear strength decreased with increase in water content for all percentage of fly ash mix and undrained shear strength increased with increase in fly ash content at a particular water content. This was due to an increase in maximum dry density with increase in fly ash content.

Sivapullaiah and Lakshmikanthay (2005) have investigated the feasibility of using lime stabilized illite as a liner material for waste materials. In this study, the amount of illite and bentonite were chosen to be 80% and 20% respectively by weight. It was found that the addition of bentonite increases the cation exchange capacity and decreases the permeability without affecting the compaction and volume change behaviour and also it increases the plasticity index and decreases the shrinkage limit. It was found that the unconfined compressive strength of illite increases on the addition of bentonite and also found that the hydraulic conductivity of illite decreases without increasing the compressibility.

Dash and Hussain (2012) studied the effect of adding lime to the properties of a mixture of montmorillonite rich expansive soil and silica-rich non-expansive soil. They found that due to adding lime DDL thickness reduced due to which liquid limit decreases hence plastic

limit and plasticity index increases. Due to the formation of calcium silica hydrate and calcium aluminium hydrate, the unconfined compressive strength of the mix increased up to a certain point after that strength of soil reduced because of formation of excess silica gel which is a porous material and reduced the strength.

Tripathi and Viswanadham (2012) used sand bentonite mixture with different composition to find a suitable composition for satisfying liner criteria. They found that by adding bentonite to sand its compressive strength increase and the saturated hydraulic conductivity decreases.

Younus and Sreedeep (2012a) investigated the utility of fly ash-bentonite mixes for application in landfill liner. The objective of the study was to maximize the utility of class F fly ash in a waste containment facility. Hydraulic conductivity and unconfined compressive strength test was determined for different percentage of fly ash-bentonite mixes. The study recommended that a maximum of 70% by weight of class F fly ash can be used with bentonite in compacted clay liners. They compacted the mix at both dry and wet side of the OMC and they found strength and hydraulic conductivity of mix at dry side of the OMC higher than wet side. And by increasing fly ash content OMC reduced and it also reduced the volume change tendency of the mix. The study also concluded that bentonite and fly ash could not be used alone in landfill liner construction.

## 2.5 Critical appraisal on gaps in findings

The reviewed literature indicates that the flow and contaminant transport characteristics is important for project related to waste containment where materials like fly ash, expansive soil and its mixes has a lots of potential in the construction of liner and covers (hydraulic and contaminant barriers). There are several studies on the hydraulic conductivity of the fly ash and expansive soil. It was observed that the range of hydraulic conductivity of fly ash is in the range of silt, and hydraulic conductivity of class C fly ash is less than the class F fly ash. In all these studies it was assumed that the soil and fly ash mix is fully saturated. There are not many studies that investigate the hydraulic conductivity of bentonite-fly ash mix, especially for Indian fly ashes.

Another important geoenvironmental characteristics is the contaminant retention property of fly ash, which plays a major role in the retention of heavy metals. Reviewed literature shows that heavy metals like $Cu^{2+}$, $Pb^{2+}$, $Cd^{2+}$, $Hg^{2+}$, $Ni^{2+}$, $Zn^{2+}$ etc. can be successfully

removed from the waste water using fly ash. This makes fly ash an excellent material in combination with low permeable material (expansive soil) for waste containment liner construction. However, there are not many studies that reports contaminant retention characteristics of expansive soil-fly ash mixes. The influence of different sources of fly ashes on contaminant retention property also needs to be understood in detail.

## 2.6 Objective and scope of the work

The critical appraisal of the reviewed literature shows that geoenvironmental characterization have not been performed extensively on fly ash and its mix with expansive soil. Such characterization is required for its utility in waste containment projects. With this in view, the main objectives of this research work is (1) to explore the utility of bentonite-fly ash mixes in waste containment liners and covers instead of bentonite-sand mixes (2) maximizing the utility of waste material like fly ash for waste containment projects. Following are the different scope of the study to achieve these objectives:

* Development of a predictive model for the soil shrinkage characteristic curve of high plastic soils and B-FA mixes.
* Optimize the B-FA mix with the objective of maximizing FA utility and satisfying the hydraulic requirements of waste containment liners.
* Study the effect of long-term interaction of B-FA on hydraulic conductivity to assure the serviceability aspect when it is used as a landfill liner material.
* Exploring the utility and validity of geotechnical centrifuge for assessing permeability of low permeable water-reactive swelling B and B-FA mixes.
* Evaluating pH dependent and long-term interaction impact on contaminant retention characteristics of B, B-FA and B-S mixes.
* To study the mechanical performance of B-FA mixes and their comparison with that of the B-S mixes and its microstructural characterization.

# 3

# Materials and its Characterization

## General

This chapter contains the details of the materilas used in the present research work. The materials were subjected to different physical, chemical, mineralogical, and geotechnical characterization which were presented in following section.

## 3.1 Materials used in the present study

Five commercially available bentonites majorly sourced from the Barmer district in the state of Rajasthan, India, were chosen for the present study (Fig. 3.1). Bentonite was selected based on the variation in their plasticity and clay fraction present in it. The raw fly ashes (FAs) samples were collected from the National Thermal Power Corporation (NTPC) Limited situated in different parts of India. The sources and the designation of these fly ashes and bentonites are presented in Table 3.1. Locally available construction sand as an established material for the construction of landfill liner was also taken to compare the performance of B-FAs mixes with that of B-S mixes.

## 3.2 Characterization of geomaterials

The basic physical and geotechnical properties of the bentonites and FAs were investigated using standard laboratory procedures (guidelines provided in ASTM Standard). The results of the physical and geotechnical properties of FAs and sand are presented in Table 3.2, while Table 3.3 summarizes the results of all bentonites. The chemical composition of oxides of the FAs and bentonites is depicted in Table 3.4. Also, Table 3.5 presents the Atterberg limits,

pH, electrical conductivity, and compaction characteristics of B-FA and B-S mixes and their designations.

Table 3.1: List of geomaterials used in the present study

| Material | Designation | Source |
|---|---|---|
| Bentonite -1 | B-1 | Commercially available |
| Bentonite -2 | B-2 | Commercially available |
| Bentonite -3 | B-3 | Commercially available |
| Bentonite -4 | B-4 | Commercially available |
| Barmer bentonite | B/BX | Commercially available |
| Farakka fly ash | FFA | NTPC, Farakka, West Bengal, India |
| Neyveli fly ash | NFA | Neyveli Lignite Corporation, Tamil Nadu |
| Badarpur fly ash | BFA | NTPC Badarpur, New Delhi |
| Pond ash | PA | NTPC Singrauli, Uttar Pradesh |
| Sand | S | Locally available construction sand |

NTPC- National Thermal Power Corporation

Table 3.2: Physical properties and classification of the fly ash and sand used in this study

| Properties | Material | | | | |
|---|---|---|---|---|---|
| | FFA | NFA | BFA | PA | S |
| Specific gravity | 2.16 | 2.64 | 2.20 | 2.20 | 2.65 |
| Particle size distribution (%) | | | | | |
| Coarse sand (4.75-2 mm) | 0 | 0 | 0 | 0 | 0 |
| Medium sand (2-0.425 mm) | 0 | 3 | 0 | 0 | 52 |
| Fine sand (0.425-0.075 mm) | 24 | 55 | 8 | 36 | 48 |
| Silt (0.075-0.002 mm) | 74 | 42 | 88 | 61 | 0 |
| Clay (< 0.002 mm) | 2 | 0 | 4 | 3 | 0 |
| Atterbergs limits (%) | | | | | |
| Liquid limit | - | - | - | - | - |
| Plastic limit | - | - | - | - | - |
| Shrinkage limit | - | - | - | - | - |
| Plastic index | - | - | - | - | - |
| USCS classification | - | - | - | - | - |
| MDD (kN.m-3) | 13.8 | 14.9 | 12.1 | 12.3 | - |
| OMC (%) | 19.33 | 22.25 | 30 | 26 | - |
| Free swell index (%) | - | - | - | - | - |
| SSA (m2/g) - EGME Method | 12.59 | 13.24 | 11.54 | 10.45 | - |
| CEC (meq/100 g) | 1.89 | 10.04 | 1.44 | 0.99 | - |
| pH (L/S= 20) | 10.5 | 12.45 | 8.45 | 8.52 | - |
| Classification (ASTM C-618) | F | C | F | F | - |

Fly ashes used in the present study were not hazardous as toxic elements were not reported in X-Ray Fluorescence spectra. The grain-size distribution of the parent materials was conducted as per guidelines of ASTM D422-63 (ASTM, 2007a). Bentonites constitutes

of more than 95% finer materials, having 52-65% clay particles below 2$\mu$m in average diameter. Both sand and fly-ashes exhibit poorly graded grain size distribution. The specific gravity and Atterberg limits of the parent material and mixtures were determined as per ASTM D854-92 (ASTM, 1994) and ASTM D4318 (ASTM, 2010), respectively. The Atterberg limits for all mixtures are given in Table 3.5 The maximum dry density (MDD) and optimum moisture content (OMC) were evaluated as per guidelines of ASTM D698 12 (ASTM, 2012). The MDD of the FAs used in the current study varied with the class type. The MDD of Class F fly ash typically is lower than that of B, while Class C fly ash had a much higher value in magnitude. Class C fly ash i.e., NFA showed highest MDD than all other parent materials due to its inherent high pH (i.e., 11.5), which enables a face-to-face arrangement of particles in presence of water (Ghobadi et al., 2014). The OMC and MDD of the mixes studied in the current study are tabulated in Table 3.5. The chemical oxides composition of bentonite and fly ash was determined using X-ray fluorescence (XRF) (AXIOS, PANalytical, Malvern, UK) and the results are presented in Table 3.4. The total specific surface area (SSA) of bentonite and fly ash was determined using the ethylene glycol monoethyl ether (EGME) retention procedure (Cerato and Lutenegger, 2002) with three repetitions, and the results are listed in Table 3.2. The CEC was determined by following an ammonium replacement method (Chapman, 1965).

A known mass (25 g) of oven-dried sample was washed thoroughly in 250 mL of 1 M ammonium acetate solution at pH 7.0 in an orbital shaker for 4 h and allowed to stand overnight (Muurinen, 2011). The supernatant solution was separated by centrifuge at 3,000 rpm for 10 min for the determination of exchangeable cation concentration. The concentrations of individual major cations (i.e., $Na^+$, $Ca^{2+}$, $K^+$, and $Mg^{2+}$) in the extracted solution were determined using a flame photometer and atomic absorption spectroscopy (AAS) (Varian, model: spectra AA - 55B). The flame photometer works on the principle of ionization of alkali metal salt upon contact with a nonluminous flame. These ions emit a characteristic wavelength (color) for which the intensity is proportional to the concentration of element in the solution. The emitted wavelengths are detected by a photocell and converted into voltage. The concentration of ions in the solution is measured using a calibration chart by knowing the voltage. AAS relies on the principle of adsorption of electromagnetic radiation through a sample. The method uses the Beer-Lambert law to relate the measured absorbance and the absorbance through a standard solution of the same

element. The total CEC was determined from the summation of all the individual cations. The average CEC obtained from the three trials is presented in Table 3.2.

Table 3.3: Basic geotechnical properties of bentonites used in the study

| Properties | Materials | | | | |
|---|---|---|---|---|---|
| | B1 | B2 | B3 | B4 | B/BX |
| Specific gravity (Gs) | 2.84 | 2.88 | 2.87 | 2.86 | 2.88 |
| Particle size distribution (%) | | | | | |
| Coarse sand (4.75-2 mm) | 0 | 0 | 0 | 0 | 0 |
| Medium sand (2-.425 mm) | 0 | 0 | 0 | 0 | 0 |
| Fine sand (.425-.075 mm) | 5 | 2 | 0 | 2 | 5 |
| Silt (.075-.002 mm) | 31 | 43 | 48 | 41 | 30 |
| Clay (<.002 mm) | 64 | 55 | 52 | 57 | 65 |
| Atterberg limit (%) | | | | | |
| Liquid limit | 300 | 310 | 450 | 244 | 300 |
| Plastic limit | 53 | 48 | 54 | 61 | 43 |
| Plastic index | 247 | 262 | 396 | 183 | 257 |
| MDD (kN.m-3) | 12.4 | 13.9 | 13.6 | 11.5 | 13.5 |
| OMC (%) | 37.5 | 28.89 | 33.16 | 49.24 | 33.2 |
| Free swell index (%) | 980 | 1433 | 1700 | 1600 | 686 |
| SSA (m2/g) -EGME method | 260 | 244 | 428 | 215 | 450 |
| CEC (meq/100g) | 6.29 | 15.66 | 38.18 | 23.41 | 54 |
| pH (L/S= 20) | 9.25 | 9.15 | 9.65 | 9.75 | 9.50 |
| Classification (USCS) | CH | CH | CH | CH | CH |

Table 3.4: Chemical composition of the materials used in this study

| Oxides (%) | FFA | NFA | BFA | PA | B1 | B2 | B3 | B4 | B/BX |
|---|---|---|---|---|---|---|---|---|---|
| $SiO_2$ | 46.47 | 30.10 | 67.8 | 52.2 | 51.68 | 57.04 | 57.51 | 58.54 | 52.23 |
| $Al_2O_3$ | 27.49 | 28.80 | 12.50 | 30.5 | 17.07 | 13.45 | 13.07 | 14.56 | 19.06 |
| $Fe_2O_3$ | 1.06 | 2.40 | 3.80 | 2.6 | 2.03 | 6.9 | 9.02 | 9.54 | 15.6 |
| MnO | 2.93 | 0.04 | 1.20 | 0.06 | 0.05 | 0.076 | 0.098 | 0.121 | 0.54 |
| CaO | 2.84 | 18.73 | 3.90 | 0.08 | 0.52 | 0.51 | 1.12 | 0.61 | 1.39 |
| MgO | 0.06 | 2.24 | 2.50 | 1.20 | 1.95 | 0.12 | 0.14 | 0.12 | 1.32 |
| $Na_2O$ | 0.56 | 0.50 | 1.30 | 0.12 | 2.36 | 2.21 | 2.23 | 2.20 | 2.82 |
| $K_2O$ | 0.84 | 0.04 | 1.80 | 0.13 | 0.60 | 0.58 | 0.22 | 0.69 | 1.44 |
| $TiO_2$ | 6.58 | 1.75 | 0.70 | 3.80 | 1.94 | 1.52 | 1.67 | 2.26 | 2.76 |
| $P_2O_5$ | 5.20 | 0.02 | 0.80 | 0.12 | 0.05 | 0.01 | 0.035 | 0.034 | 0.09 |
| LOI | 6.17 | 5.07 | 4.7 | 85.3 | 22.69 | 20.4 | 18.5 | 21.6 | 13.11 |
| pH | 9.25 | 10.58 | 8.50 | 6.60 | 9.25 | 9.50 | 9.75 | 9.32 | 9.24 |
| CEC (meq/100g) | 1.85 | 9.04 | 1.44 | 0.99 | 20.45 | 15.66 | 38.18 | 23.41 | 53.66 |

X-Ray Diffraction (XRD) was conducted using (Rigaku, Model, Micromax-007HF) on all parent materials to understand their mineralogy. The step size, 2theeta range, and scan speed was kept at 0.02° , (3 - 70°) and (20° 2theeta/min), respectively, and obtained XRD

response was analyzed using Match software. For XRD analysis, air-dried soil samples were taken, mixed uniformly using pedestal and sieved through 75-micron IS sieve. The XRD of the parent materials are presented in Fig. 3.2. The XRD pattern of B revealed montmorillonite as the predominant mineral, followed by Kaolinite, Illite, and Quartz. For FA, the peaks correspond primarily to Mullite and Quartz minerals, followed by Hematite and Aragonite (Millero et al., 2001; Gimsing and Borggaard, 2007). Mullite typically exhibits low fracture toughness and low strength, while Quartz is a stable mineral that primarily imparts strength to the material. Sand is entirely composed of inert quartz.

The surface morphology of the sorbents was obtained using field emission scanning electron microscopy (FESEM)-EDX (Zeiss Sigma, Oberkochen, Germany). The surface photo micrograph of the bare geo-materials is depicted in the Fig. 3.3. All four FAs showed the presence of spherical particles called the cenospheres, which are generally deemed to be hollow and contain embedded spherical particles of varying smaller sizes (Fernández-Jiménez et al., 2005). B has flaky clay particles, which are mostly dispersed and have an average diameter less than 2 microns. The structures observed confirm the presence of montmorillonite mineral (Mitchell et al., 2005). FESEM images of sand particles reveal the presence of incompressible solid particles, which are angular and rough-edged.The elemental composition of the parent materials was evaluated through the FESEM-EDX analysis. Prior to the analysis soil samples were dried in the oven at 60$^{o}$C. It was crushed into powdered form using a pestle and sieved through 75-$\mu$m Indian Standard (IS) sieve and mounted on aluminum stubs over doublesided carbon tape followed by double gold coating using a sputter coater (Quorum, SC7620, Quorum Technologies, Lewes, UK and Edwards, RV3, Czech Republic) prior to the analysis. The same procedure was adopted for the soil samples after post experiment, to see the variation in the elemental composition. The elemental composition of the soil samples used in this study is depicted in Fig. 3.4.

Fourier-transform infrared spectroscopy (FTIR) spectral analysis was conducted to study the functional group of the geo-materials used in the present study. Fourier transform infrared (FTIR) spectra were obtained using the KBr pellet method at room temperature (PerkinElmer, Spectrum Two, Waltham, MA). The samples were uniformly mixed with KBr in a 100: 1 ratio. The analysis was performed over the entire range of wave number (400 - 4,000 cm$^{-1}$) with 20 consecutive scans at 4.0 cm-1 resolution by transmittance mode. Similar procedure was conducted to observe the alteration in the functional group for the soil

samples collected after post experiment. Figure 3.5 dipicts the FTIR spectra of the parent soil samples. For the shake of bravity, only barmer bentonite FTIR spectra was presented for the bentonites. pH and EC of the samples were tested by using a pH meter and electrical conductivity meter (systronics, India), respectively.

Table 3.5: Atterberg limits, pH, electrical conductivity and compaction characteristics of B-FA and B-S mixes

| B (%) | Fly ash (%) | Designation | LL (WL) % | PL(WP) % | pH | Ec (ms.cm-1) | MDD (kN.m-3) | OMC (%) |
|---|---|---|---|---|---|---|---|---|
| 70 | 30 | B-FFA30 | 196 | 29 | 10.00 | 1.35 | 14.22 | 27.05 |
| 50 | FFA 50 | B-FFA50 | 149 | 25 | 10.15 | 1.07 | 14.68 | 23.00 |
| 30 | 70 | B-FFA70 | 93 | 21 | 10.30 | 0.83 | 14.78 | 19.00 |
| 70 | 30 | B-NFA30 | 156 | 38 | 10.50 | 1.69 | 14.15 | 29.25 |
| 50 | NFA 50 | B-NFA50 | 97 | 35 | 10.75 | 1.62 | 14.75 | 26.75 |
| 30 | 70 | B-NFA70 | 65 | 32 | 10.95 | 1.56 | 14.85 | 25.75 |
| 70 | 30 | B-BFA30 | 225 | 33 | 9.65 | 1.34 | 14.10 | 29.01 |
| 50 | BFA 50 | B-BFA50 | 174 | 29 | 9.45 | 1.03 | 14.29 | 25.82 |
| 30 | 70 | B-BFA70 | 101 | 26 | 9.05 | 0.70 | 14.23 | 24.71 |
| 70 | 30 | B-PA30 | 212 | 30 | 9.75 | 1.27 | 13.98 | 26.18 |
| 50 | PA 50 | B-PA50 | 150 | 27 | 9.80 | 0.99 | 14.20 | 23.97 |
| 30 | 70 | B-PA70 | 93 | 24 | 9.56 | 0.64 | 14.08 | 21.48 |
| 70 | 30 | B-S30 | 165 | 35 | 9.25 | 1.20 | 15.17 | 25.00 |
| 50 | S 50 | B-S50 | 126 | 27 | 9.00 | 0.95 | 16.48 | 20.00 |
| 30 | 30 | B-S70 | 78 | 23 | 8.75 | 0.52 | 17.57 | 16.87 |

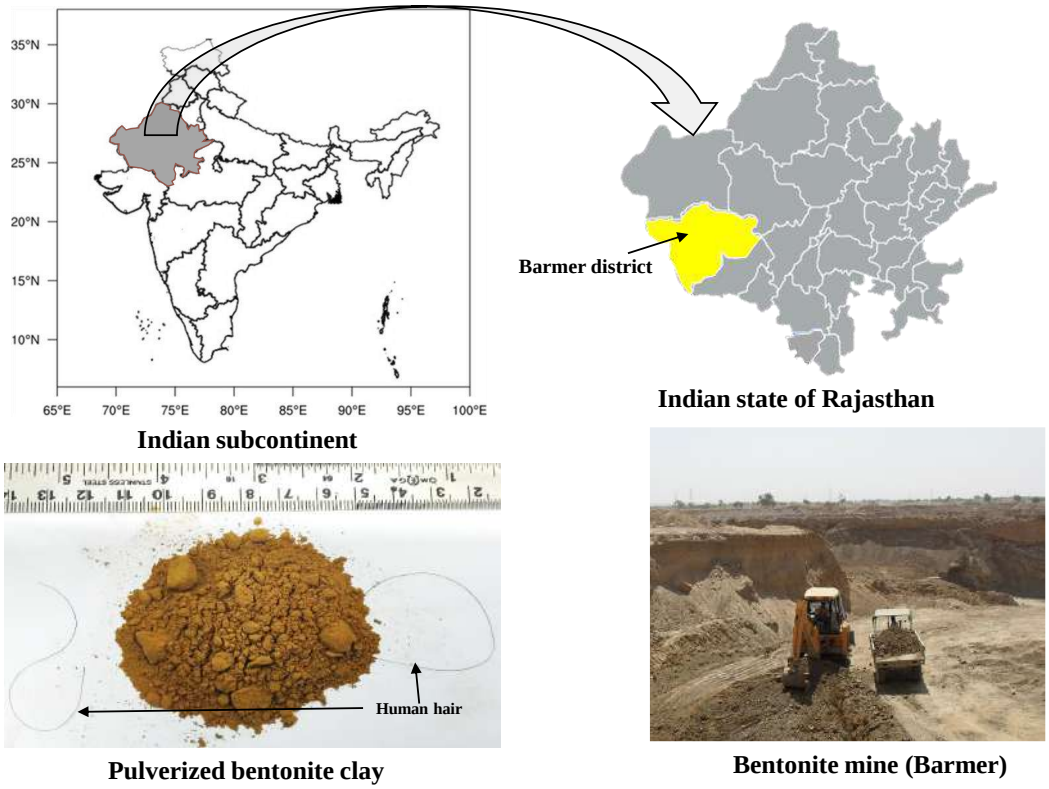


Figure 3.1: Source and location of bentonite used in the study

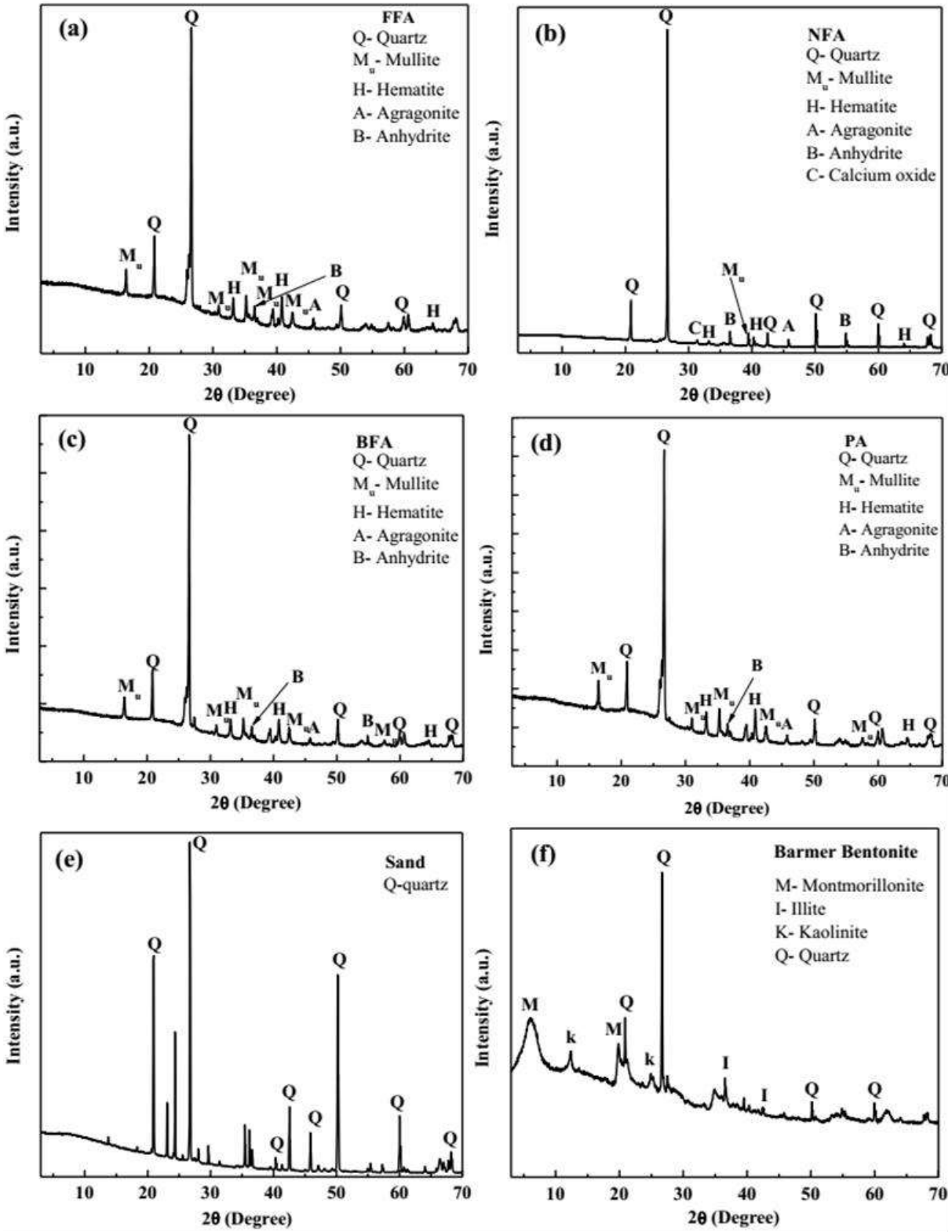


Figure 3.2: X-ray diffraction of parent geo-materials used in the study

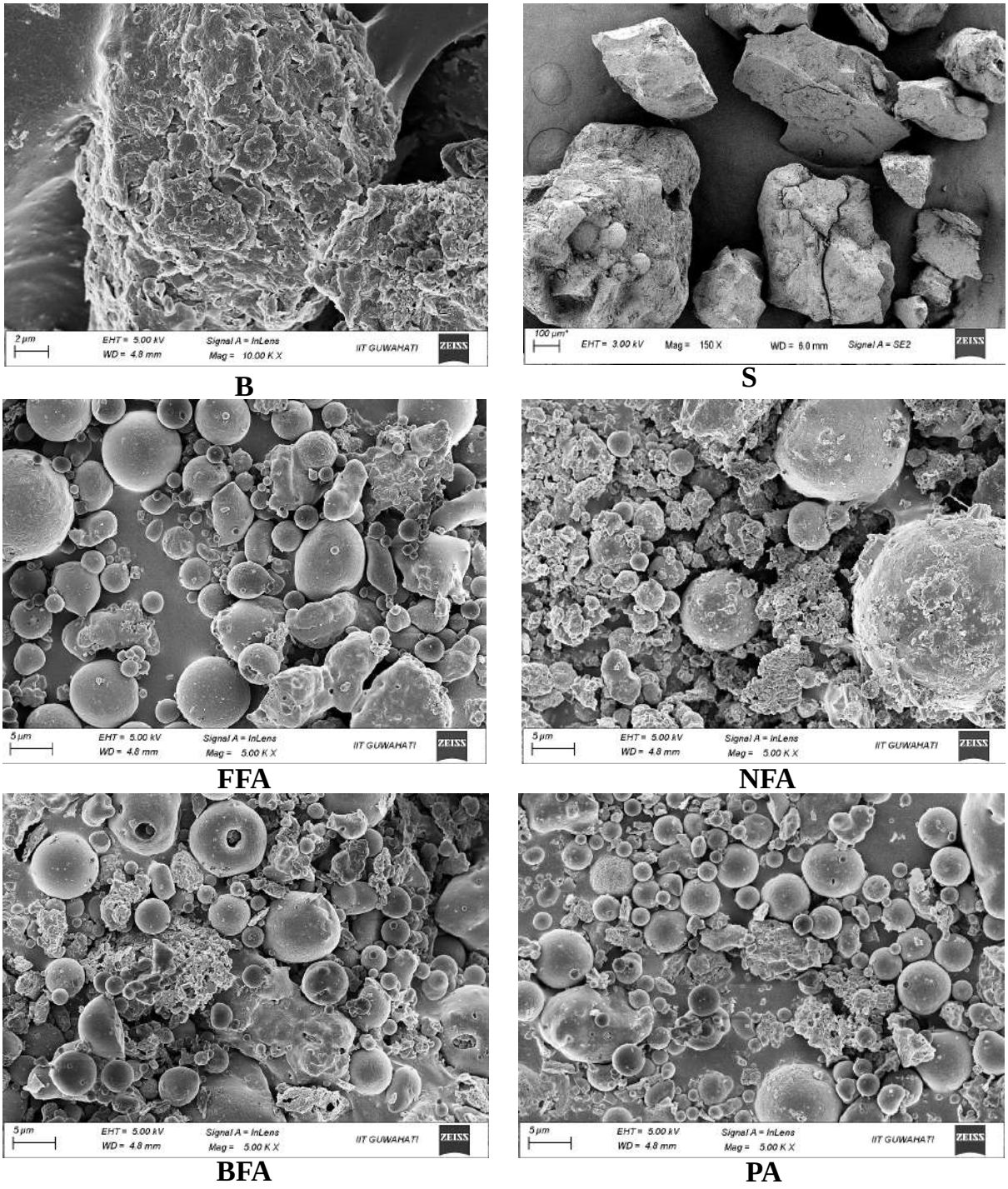


Figure 3.3: Fesem surface morphology of the geomaterials used in the present study

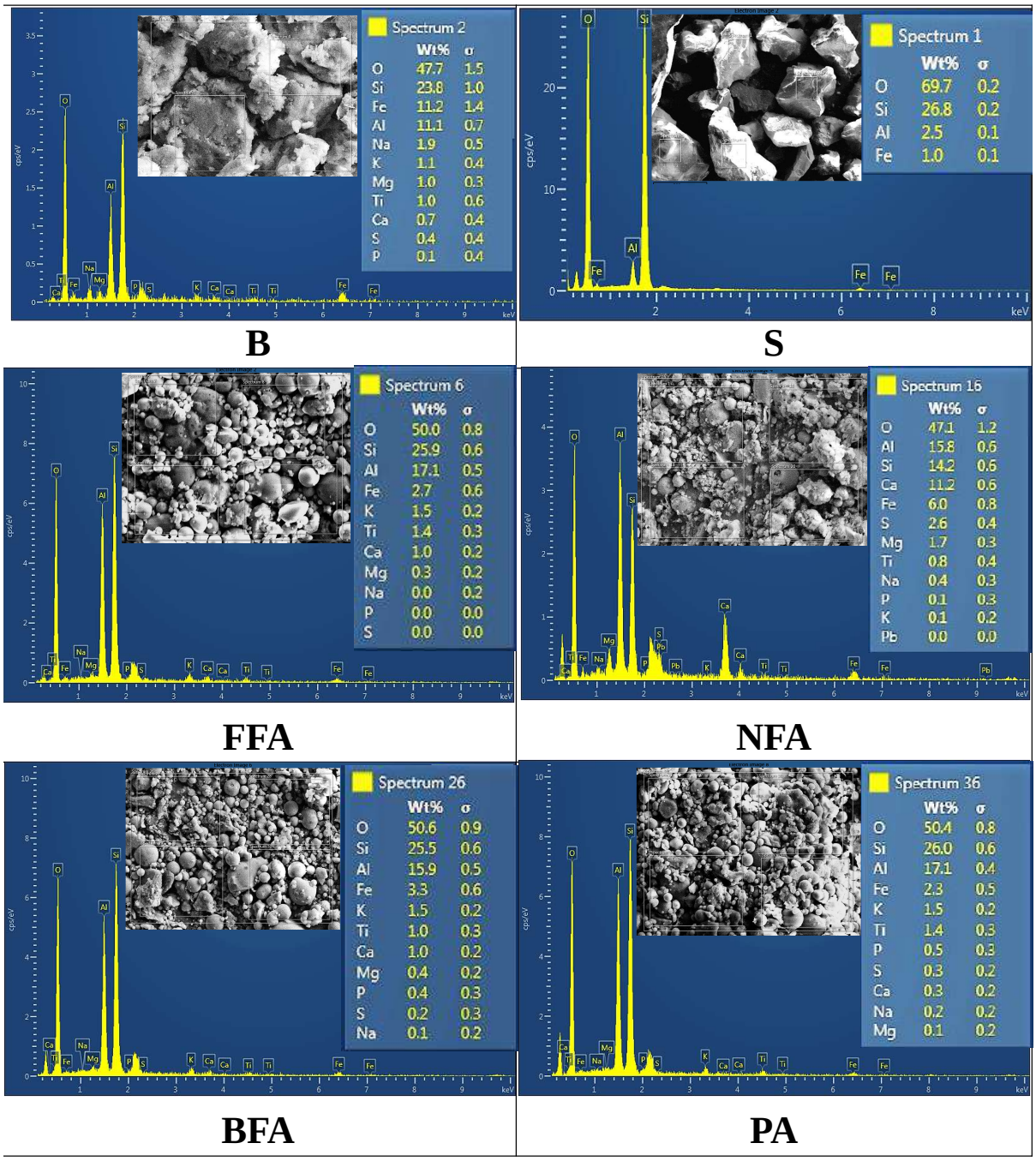


Figure 3.4: EDX spectra of the geomaterials used in the present study

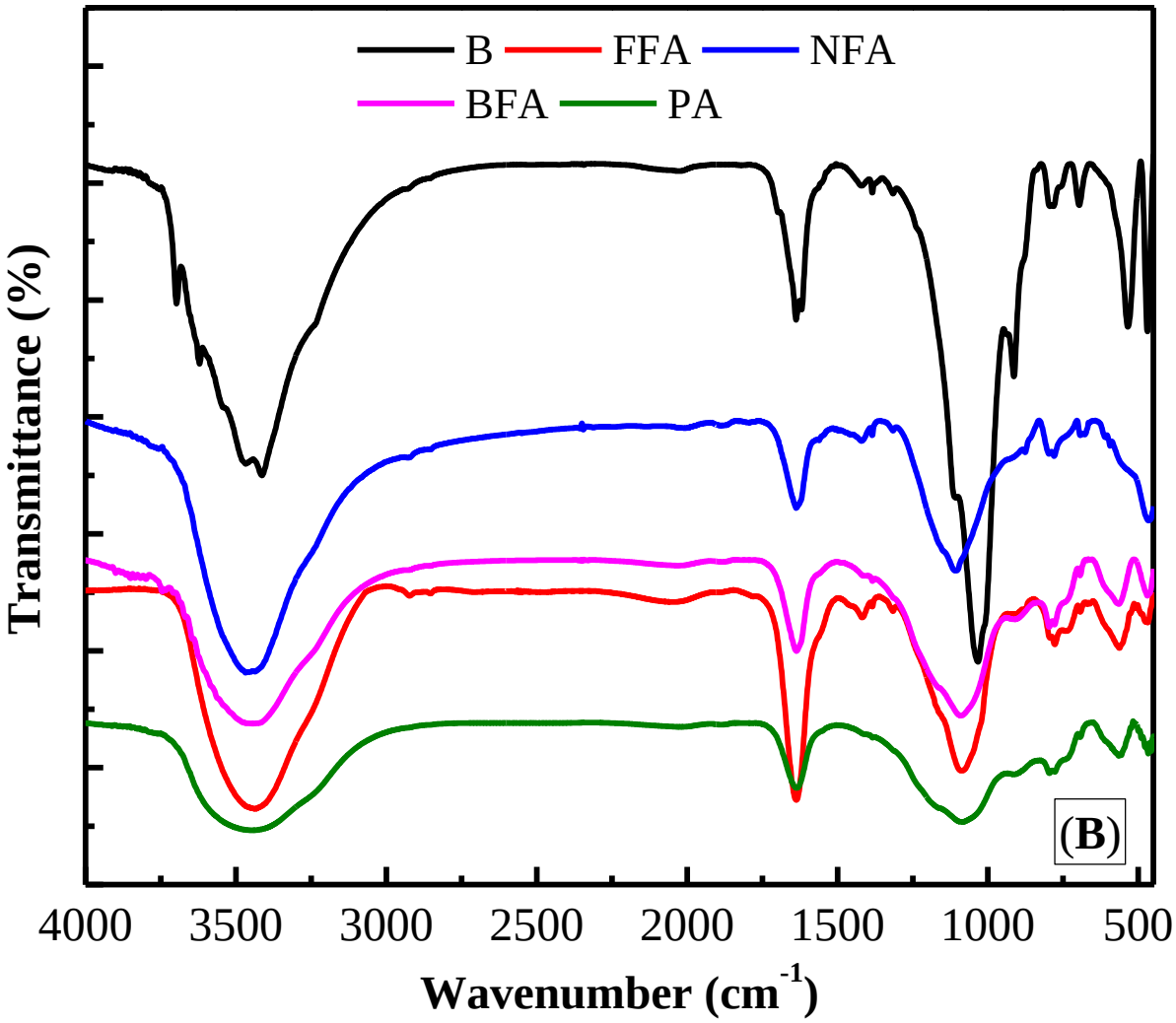


Figure 3.5: FTIR spectra of geomaterials used in the present study

# 4

# Predictive Model for Soil Shrinkage Characteristic Curve of High Plastic Soils

## General

This chapter deals with the measurement of soil shrinkage characteristic curve (SSCC) of soils. The main objective was to understand the characteristics of SSCC of different plastic soils and evaluate the SSCC models reported in the literature based on measured curves. It must be noted that the measurement of SSCC is time consuming and cumbersome. Therefore, SSCC has been quantified and correlated with plasticity characteristics for the varying range of plasticity considered in this study. The shrinkage limit determined from mercury displacement method was compared with those obtained from SSCC. The SSCC is invariably necessary while defining water retention characteristics of unsaturated plastic soil. It was essential to understand the air entry point on SSCC to verify its relationship with shrinkage limit. This is mainly due to the fact that soil is treated to be fully saturated till the moisture content reaches shrinkage limit. This chapter is mainly divided into three parts. In the first part, the robustness of the balloon method for SSCC measurement is demonstrated. Secondly, the impact of plastic index (PI) on important SSCC parameters such as void ratio ($e_0$), water content at air entry ($w_{AE}$) and shrinkage limit ($w_s$) are discussed. Finally, a predictive model for SSCC is developed based on easily measurable PI of the soil, followed by its validation.

## 4.1 Background

Soil shrinkage characteristic curve (SSCC) is a key constitutive relationship between hydraulic state variable, gravimetric water content ($w$) and volumetric state variable, void ratio ($e$) representing drying of a soil sample from fully saturated to completely dry state under zero external stress (Chen and Lu, 2018). SSCC is mandatory for determining soil-water characteristic curve (SWCC) and modelling water transport in soils susceptible to significant volume change under hydraulic loading (Garnier et al., 1997; Boivin et al., 2006; Cornelis et al., 2006a; Wijaya et al., 2015; Prakash et al., 2020a,b). Apart from hydraulic characteristics, SSCC is also used for the assessment of soil compaction (Boivin et al., 2006) and determination of soil mechanical properties (Baumgartl and Köck, 2004). The measurement of SSCC involves the simultaneous measurement of pore volume (in terms of $e$) with reduction in $w$ of a saturated soil sample subjected to air drying. Various methodologies are employed for the determination of SSCC such as core method (Berndt and Coughlan, 1977) for undisturbed soil, paraffin coated method (Lauritzen and Stewart, 1942; Tripathy et al., 2014b) for individual soil clods, and balloon method (Tariq and Durnford 1993b) for disturbed soil. Paraffin coated method and balloon method measures the volume of the soil sample using Archimedes principle. Cornelis et al. (2006a) demonstrated that balloon method and paraffin method exhibited similar results. Also, the effectiveness of the balloon method for determining SSCC of highly expansive soils was reported by Barman and Mishra (2022). Recently, methods based on laser beam and imaging techniques were employed for studying soil shrinkage (Abou Najm, 2009; Lu and Kaya, 2013; Sanchez et al., 2013; Dong and Lu, 2017; Amenuvor et al., 2020). Amenuvor et al. (2020) verified the SSCC measured by image based method with the balloon method and found satisfactory agreement in results.

Irrespective of the methods used for developing SSCC, it is apparent that the procedure is time consuming, tedious and cumbersome for highly plastic clays due to the slow drying process. For example, obtaining SSCC for a highly plastic bentonite using balloon method (Tariq and Durnford, 1993b) would necessitate not less than 30 days. Further, a lot of care need to be taken for a reliable measurement of volume without inducing cracking in the soil sample. For this purpose, a very low drying rate has to be maintained, which makes it time intensive. In this context, it is desirable to estimate the SSCC from easily mea-

surable soil properties such as plasticity index (PI). While there are numerous models for representation of a continuous SSCC (e.g. McGarry and Malafant, 1987; Kim et al., 1992; Tariq and Durnford, 1993a; Braudeau et al., 1999; Chertkov, 2000; Fredlund et al., 2002; Chertkov, 2003; Peng and Horn, 2005; Cornelis et al., 2006b; Mbonimpa et al., 2006; Lu et al., 2017; Chen and Lu, 2018), a few studies have attempted to estimate SSCC from commonly measured physical properties of soil (Crescimanno and Provenzano, 1999; Chertkov, 2000, 2003; Mbonimpa et al., 2006).

Crescimanno and Provenzano (1999) provided regression equations for estimation of the parameters in the three straight line model (McGarry and Malafant, 1987) using clay content. However, the three straight line model (McGarry and Malafant, 1987) cannot be used to generalize the SSCC for soils as it cannot describe the zero shrinkage zone of the SSCC (Cornelis et al., 2006a) as well as the curvature (ref. Fig. 4.1), after the soil begins to desaturate. In general, SSCC comprises of four different phases, which include structural, normal, residual and the zero shrinkage phases (Bensallam et al., 2012). During structural shrinkage phase, the reduction in volume of the soil samples is smaller than the volume of the water extracted from the soil. The decrease in volume in structural phase is mainly due to water extraction present in macro pores of the soil without considerably reducing the total volume of bulk soil. (Cornelis et al., 2006a; Peng and Horn, 2013). However, this phase is not captured for the clayey soils (Chertkov, 2003). Chertkov (2000, 2003) linked the SSCC of clays with its microstructure and pore size distribution. This study outlined the mechanism of soil water interaction, volume change and interrelation between pore structure and shrinkage characteristic of the soil. But the study cannot be used to estimate SSCC readily, since the knowledge of microstructure and pore size distribution of soil requires intensive instrumentation, which are not routine procedures in geotechnical engineering. Mbonimpa et al. (2006) proposed an equations for SSCC with two fitting parameter in terms of e and soil suction. For the estimation of SSCC, the two fitting parameters were correlated with shrinkage limit($w_S$) and liquid limit($w_L$). However, routine measurement of SSCC are done in terms of e and w. To verify the proposed form of equation by Mbonimpa et al. (2006), measurement of SWCC is mandatory. It may be noted that a reliable determination of SWCC of a high volume change soil necessitates the prior knowledge of SSCC.

Plasticity characteristics of soil is a predominant parameter that influences the soil shrink-

age. A highly plastic soil is bound to shrink more (Mitchell et al., 2005; Tripathy et al., 2014b; Barreto, 2019). For a soil with high water content as the initial state, the shrinkage property is entirely dependent on soil type and mineralogy. Plasticity characteristics can adequately capture both these aspects (soil type and mineralogy). Therefore, plasticity characteristics can be correlated with SSCC. The objectives of this study are twofold (a) investigate the impact of plasticity characteristics on SSCC and (b) formulate a predictive model for SSCC based on easily measurable soil properties, which are missing in the literature for high plastic clays. Four bentonites and nine bentonite-fly ash mixes were used to represent soils with wide range of plasticity. The study demonstrates that the important characteristics of measured SSCC, the minimum void ratio ($e_0$), the water content at air entry ($w_{AE}$) and the shrinkage limit ($w_S$) correlates well with the plasticity index (PI). The predictive model for SSCC was developed in this study by correlating the parameters of SSCC model by Fredlund et al. (2002) (minimum void ratio ($a_{sh} = e_0$) and ($c_{sh}$) to easily measurable PI. The accuracy of the proposed predictive model was evaluated using an independent data set of bentonite, its mixes with fly ash and literature data. It is noted that the proposed model can estimate the SSCC with reasonable accuracy in majority of the cases.

The SSCC is parameterized using Fredlund et al. (2002) model as shown in Eq. 4.1.

## 4.2 Methodology for SSCC determination

A typical SSCC for non-structured plastic soil as depicted in Fig. 4.1 consists of three stages, (1) normal shrinkage (2) residual shrinkage and (3) zero shrinkage (Cornelis et al., 2006a; Fredlund and Fredlund, 2020). Normal or proportional shrinkage zone, represents the drying stage from a fully saturated state. Upon drying, bulk water is removed from the soil and hence the volume change (shrinkage) is same as the amount of water lost from the soil. Upon further drying, when water is removed from the largest pores, soil becomes unsaturated and air start to enter these pores. This zone is known as residual shrinkage zone and the decrement in soil volume at this stage is less than the volume of water lost from the soil. Finally, in the zero shrinkage, soil particles achieve their most compact state under zero external stress and no further change in soil volume is observed upon further drying. This stage is depicted by a flat horizontal line in Fig. 4.1. Apart from the frequently observed three stages in SSCC, a fourth stage known as structural shrinkage can occur before the normal shrinkage. This stage is likely to be observed for undisturbed samples

containing well defined structural aggregates due to biological activities such as plant roots or insect worms (Cornelis et al., 2006a). This study used balloon method of Tariq and

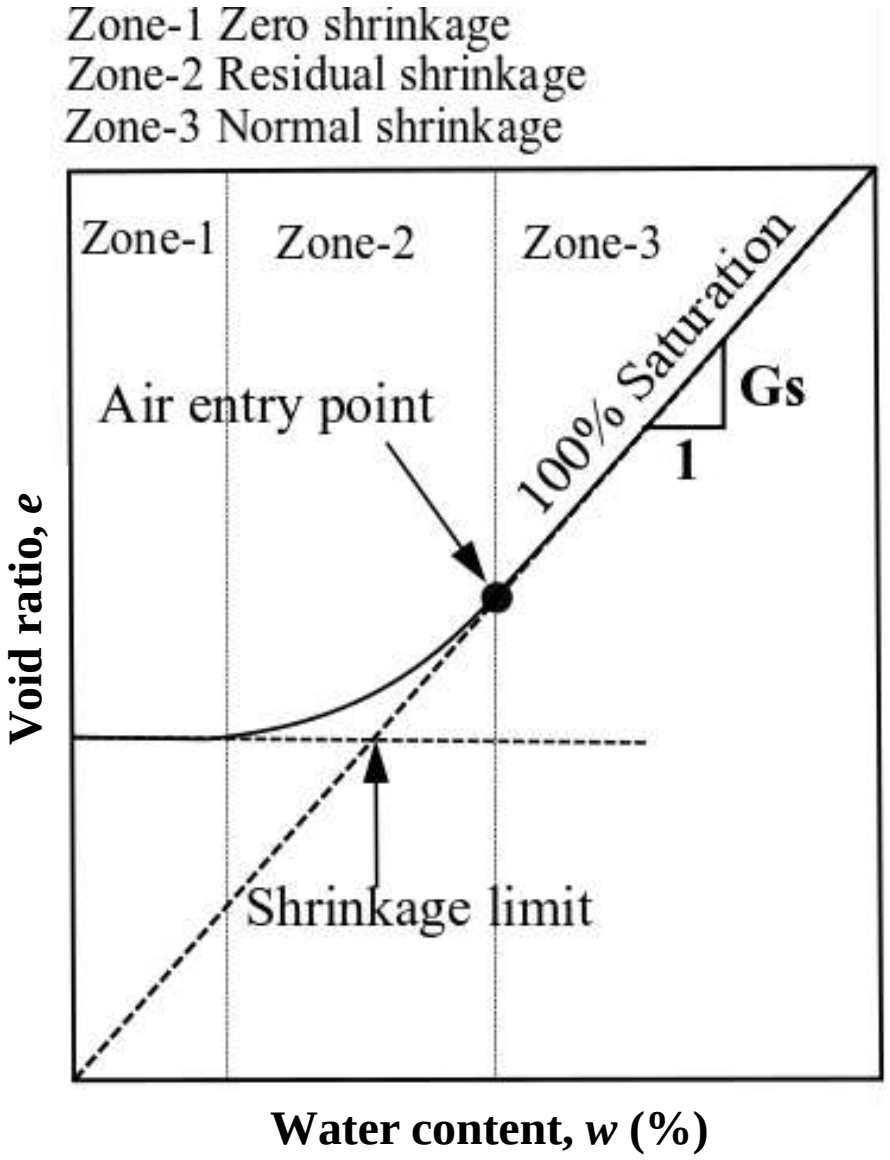


Figure 4.1: Details of a typical SSCC for non-structured soil

Durnford (1993b) for the determination of SSCC. For this purpose, an in-house facility was fabricated as shown in Fig. 4.2a and schematic details in Fig. 4.2b. Samples with w approximately 1.2 times the liquid limit ($w_L$) was prepared by mixing distilled water with the air dried sample. The mixed samples were packed in a polythene and thereafter placed in a desiccator for one week to achieve uniform moisture distribution. This is necessary to allow complete maturation of the sample and ensure 100 % saturation before the start of the drying process. The samples were then placed in prophylactic rubber balloon in three

layers and tamped for nearly 10 minutes per layer to expel out any entrapped air bubbles according to ASTM 4943 (2008b). The rubber balloon used in this study have sufficient tensile strength (30 MPa) and can be stretched up to 8 times from its initial state (PIACT, 1980). Sufficient care was taken for the sample preparation to avoid any damage of the balloon. Further, no damage was noticed during tamping to remove entrapped air bubble from the soil sample. The same procedure was adopted by Barman and Mishra, (2022) for determining SSCC of highly expansive soil. The rubber balloon was connected to a hard rubber cork fitted with an inlet and outlet pipe along with valves. Inlet pipe was connected to an air pump (a simple aquarium pump was used), which propels air over the sample for drying. The air circulating inside the balloon was allowed to escape through the outlet pipe by maintaining both the valves open during the drying process. The air flow over the sample was kept very low (50-150 liter/hour) to prevent the development of cracks during drying. At initial stage of drying, flow rate was kept 50 liter/hour where the chances of cracking was high. The flow rate was increased in stages and kept constant till it reached a value of 150 liter/hour corresponding to residual shrinkage zone (less shrinkage). Keeping in view the durability aspect of the balloon, it was proposed to complete the testing within 30 days. Krisdani et al. (2008) have reported that drying rate have no impact on shrinkage curve. In this manner, the soil sample was subjected to three-dimensional drying by detaching the balloon from the soil sample. This was achieved by maintaining a pressure gradient between inlet and outlet, which causes the balloon to inflate and thereby resulting in homogenous drying.

Duration for the complete drying process varied from 15 days for low plastic soils and up to 30 days for highly plastic soil samples. Drying period for the test may be reduced by increasing the air flow rate but a rapid drying rate may also induce cracking in high plastic soils. The cracks may then induce errors in the calculation of $e$. For calculation of $e$ and $w$ of the sample during drying, weight and volume were measured at regular intervals of time (8-12h). For the measurement of volume, inlet valve was closed and thereafter a minimal suction was applied through the outlet valve using a surgical suction pump. The purpose of applying suction was to remove the air surrounding the sample in the balloon. The outlet valve was closed after the rubber balloon collapses completely and engulf the sample.

With the provision of hanging hook, the rubber balloon with sample enclosed in it was lowered into a beaker partially filled with water. The volume of the sample was calculated

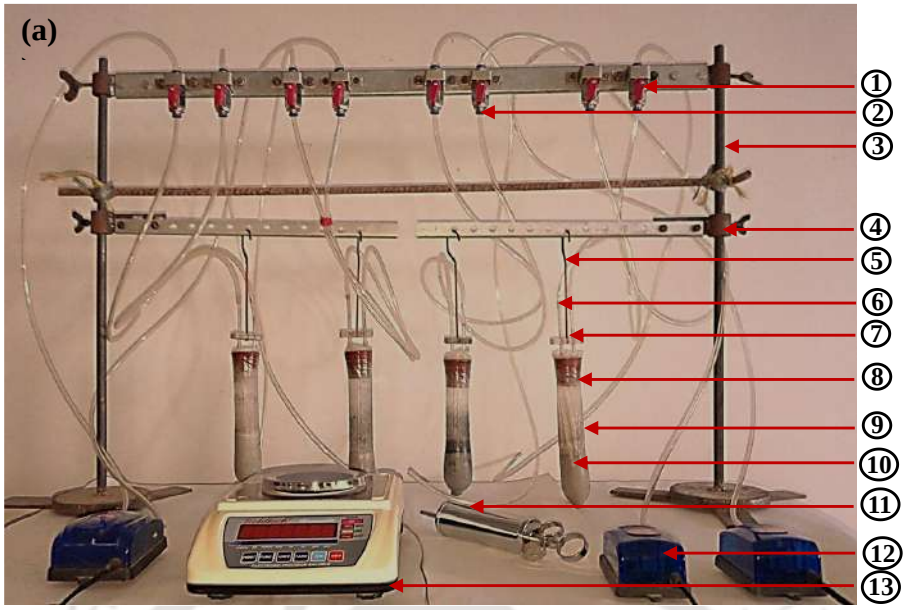


**1**. Inlet valve **2**. Outlet valve **3.** Stand **4.** Movable Screw **5.** Hanging rod **6.** Inlet pipe **7.** Outlet pipe **8.** Rubber cork **9.** Rubber balloon **10.** Soil sample 11. Hand operated suction pump **12.** Aquarium air pump.**13.** Electronic balance

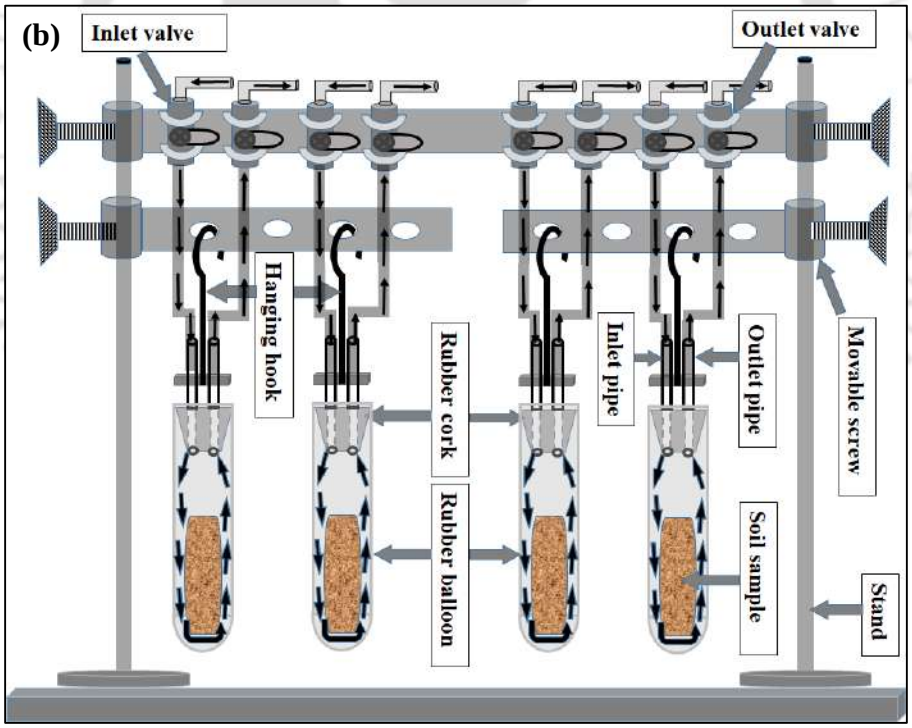


Figure 4.2: In-house fabricated experimental set up of (a) balloon method (Tariq and Durnford, 1993b) and (b) Schematic diagram for measurement of SSCC

by measuring the increase in weight of water. Air drying was continued until the measured sample volume became constant. At this stage of constant volume, water content present in the soil sample is lower than the shrinkage limit of the soil sample. It is known that

below the shrinkage limit, there is negligible reduction in the volume of the soil sample with change in water content. Therefore, the volume of soil samples corresponding to the last reading of the air dried state is considered same as oven-dried state. Subsequently, the sample was removed from the balloon and oven dried at 105$^o$C for computing $w$ at each preceding step of the volume measurement. The schematic diagram representing the step-by-step procedure is depicted in Fig. 4.3.

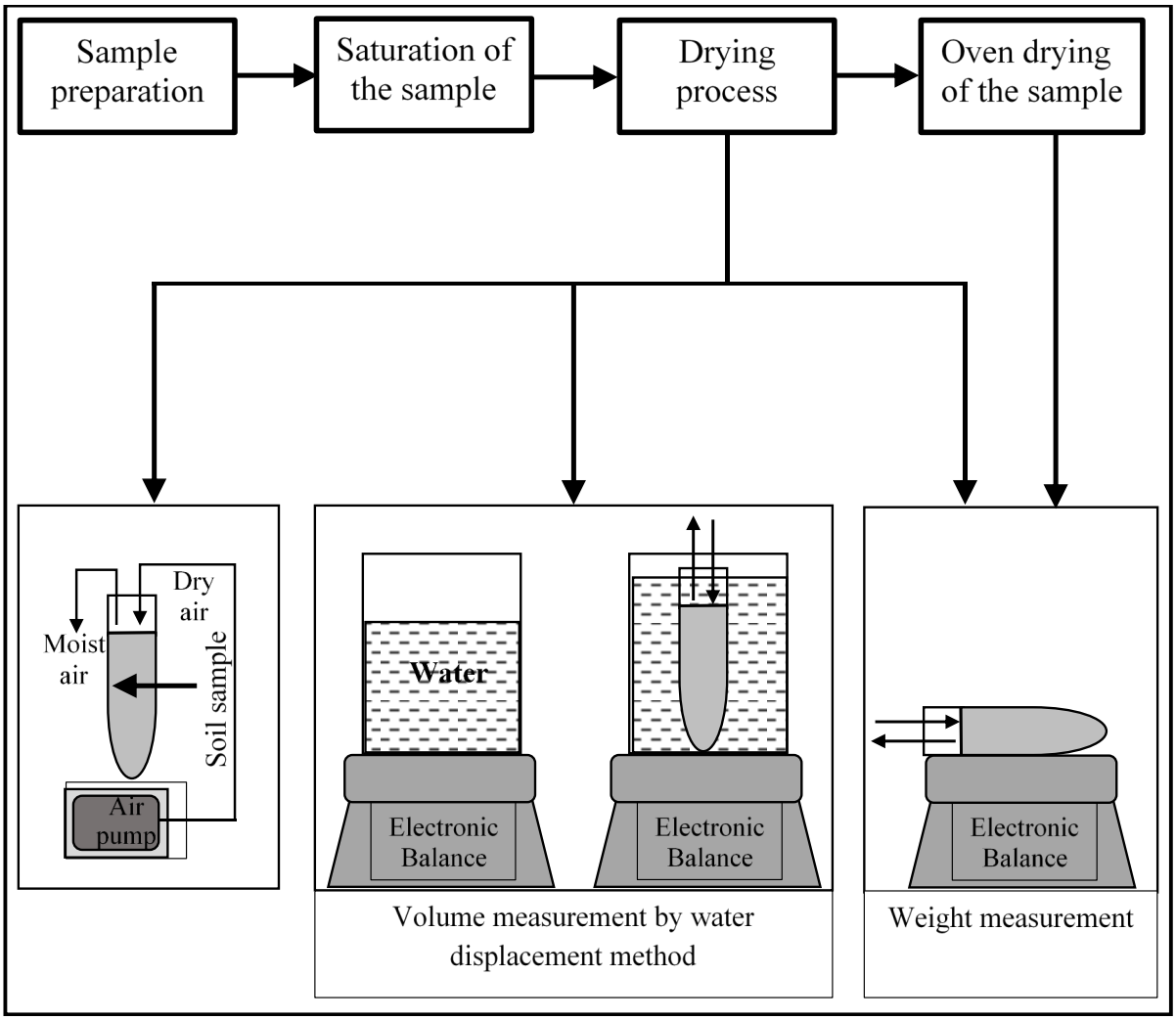


Figure 4.3: Schematic outline of the balloon method for the measurement of SSCC

### 4.2.1 Validity of the balloon method for the determination of SSCC

The validity and effectiveness of the balloon method to determine the SSCC has been reported in the past studies (Cornelis et al., 2006a; Stewart et al., 2012; Saha and Sekharan, 2021; Sharanya et al., 2021; Barman and Mishra, 2022). The balloon method was also used as the reference method to validate the data of SSCC obtained from newly proposed

methods. Amenuvor et al. (2020) validated the SSCC measured by image based technique with the balloon method and found satisfactory agreement in results. Mishra et al. (2019) reported that balloon method is better amongst the measurement technique for soil volume measurement. Gapak et al. (2017) highlighted that selection of rubber balloon (size and uniformity in dimension) and volume of the soil sample used for measurement plays an important role in the accuracy of balloon method. To take this into account, sufficient volume of the soil sample should be taken (decided by trial and error experiments) so that the minimum volume in the residual shrinkage zone is greater than 10 $cm^3$. In this study, initial volume of the slurry soil sample was taken approximately 90 $cm^3$ while the minimum volume of the soil sample was observed to be greater than 12 $cm^3$.

The error in volume measurement associated with the distortion of the soil sample during the initial stage (slurry state) of drying process is mainly caused by two reasons: (a) upper cross-section of the slurry soil sample placed in balloon would be large enough. This occurs mainly due to non-uniform size of the balloon (Fig.6 of Gapak et al., 2017), (b) tension in the rubber membrane during suction application due to self-weight of the soil sample. This prevents the rubber membrane from encompassing and assuming the shape of the soil sample. To alleviate these errors, a uniform size balloon was used in the present study. The issue of tension in the membrane was taken care by placing the balloon filled with the soil sample on a horizontal surface while applying vacuum. The sticking of the soil samples on the walls of the balloon was minimized by using prophylactic balloon, which was lubricated. These additional steps minimize the errors associated with the volume change measurement of high water content soil sample using balloon method.

## 4.3 Results and discussion

This section is divided into three parts. In the first part, the robustness of the balloon method for SSCC measurement is demonstrated. Secondly, the impact of PI on important SSCC parameters such as $e_0$, $w_{AE}$ and $w_S$ are discussed. Finally, a predictive model for SSCC is developed based on easily measurable PI of the soil, followed by its validation.

### 4.3.1 Balloon method for measuring SSCC of highly plastic soils

For verifying the robustness of the balloon method for measuring SSCC, three trials on two bentonites B1 and B3 having PI of 247 % and 396 % (ref. Table 3.3), respectively, were performed. The aforementioned bentonites were chosen specifically to check the suitability

of the balloon method for highly plastic soils. Fig. 4.4 presents the obtained results in terms of $e$ versus $w$ as well as degree of saturation (S) versus $w$. It can be observed from Fig. 4.4 that the SSCC obtained for the three trials match very well, indicating the repeatability of the test procedure. To check the effect of initial w on SSCC, trial test samples were prepared at varying initial w. For B3, it can be observed that for initial w greater than the $w_L$ (450 %), the SSCCs of saturated samples follow the same drying path. The results were similar for B1 with a $w_L$ of 300 %. However for the sample prepared at initial $w$ of 150 % i.e. half the $w_L$ of B1, a marginal deviation in the desaturation was observed initially.

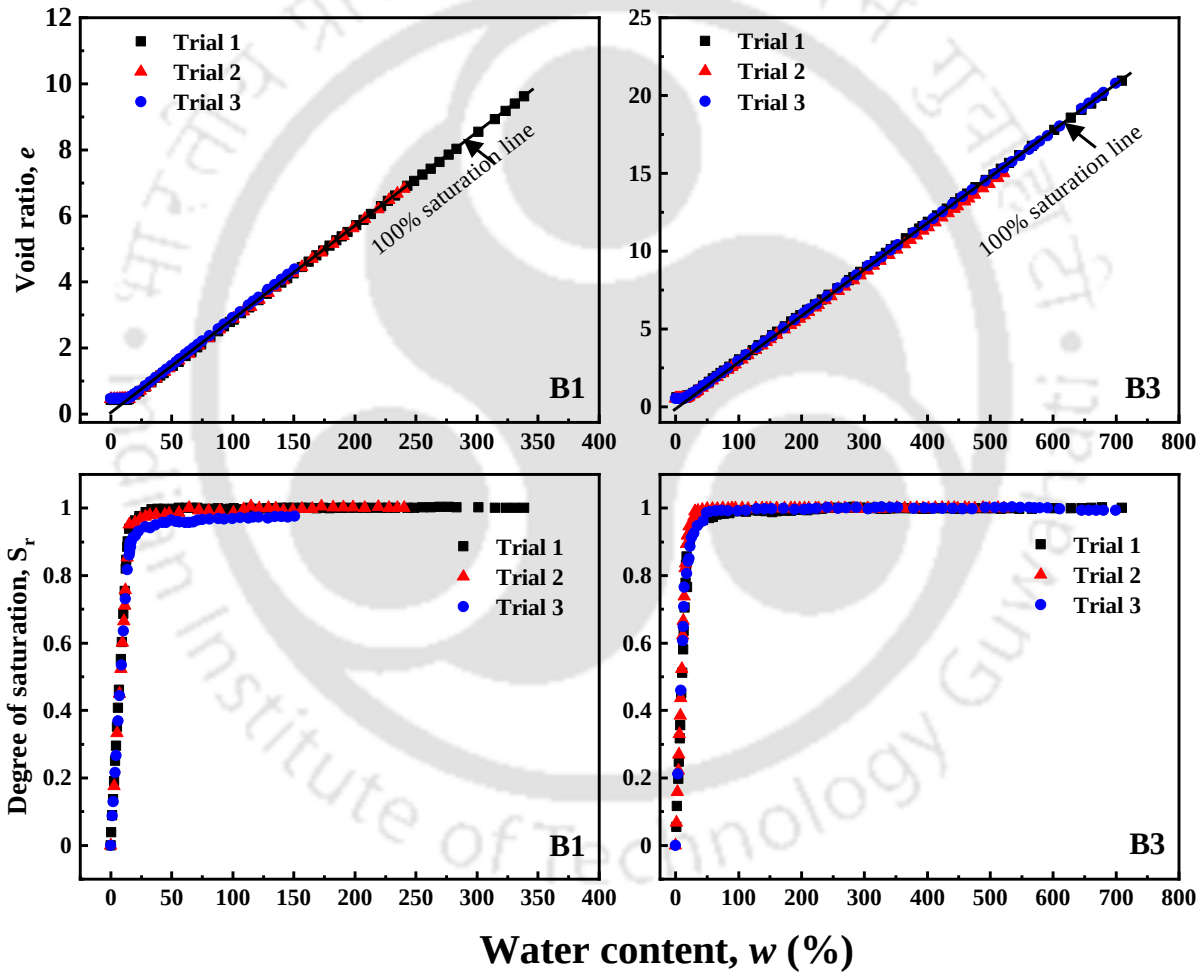


Figure 4.4: Repeatability of the volumetric shrinkage test for three different trials

This may be due to the entrapped air bubbles during sample preparation due to lower w. Upon further drying, the SSCC merged with the SSCCs of other two trials. This observation implies that maintaining initial $w$ close to $w_L$ helps to expel any entrapped air easily by simple tamping. The aforementioned results demonstrate the robustness of the fabricated

experimental balloon method for measuring the SSCC with high repeatability. Cornelis et al. (2006a) have reported that balloon method provides a good agreement with the paraffin wax method for SSCC determination. Balloon method offers an additional advantage that the whole SSCC is obtained using a single soil specimen whereas the paraffin wax method requires separate samples corresponding to the number of data points required. It can be noted from Fig. 4.4 that there is no structural shrinkage phase for the measured SSCC. This is mainly due to the remolding of fine-grained soil (considered as non-structured soil). Previous literature reported that for the non-structured soil, structural shrinkage phase is absent (Chertkov, 2003; Cornelis et al., 2006a). The structural phase of SSCC is applicable for the structured soils, which comprises large inter-aggregate pores and channels caused by the natural factors like worms and roots (Cornelis et al., 2006a; Peng and Horn, 2013).

### 4.3.2 Impact of plasticity on SSCC

It is evident from the past studies that PI can effectively represent soil properties such as mineralogy, swelling behavior, water retention and strength (Lu and Likos 2004; Klopp et al. 2019). Highly plastic soils undergo high volumetric change during drying, which preserves its saturation at low $w$ (Fityus and Buzzi, 2009; Tripathy et al., 2014b). From these studies, it is apparent that PI can represent the shrinkage behavior of soil and forms the physical basis for correlating SSCC with plasticity characteristics. In addition, this section specifically studies the impact of plasticity on SSCC. Figure 4.5 presents the measured SSCCs for various bentonites (4) and it mixes (9) with fly ash. It can be noted that the e at slurry state for bentonites is high in comparison to the mixes. The reason for this is due to the high $w_L$ of bentonites. From Fig. 4.5, it can be observed that it is difficult to differentiate among the various SSCCs visually. Also, no clear distinction could be made among the saturation, desaturation or residual zones, hence the impact of plasticity on key SSCC parameters such as $e_0$, $w_{AE}$ and $w_S$ is not evident from the figure. For deciphering the impact of plasticity on SSCC, e was normalized with maximum void ratio ($e_{max}$) observed at the slurry state. The resulting SSCCs in terms of normalized void ratio ($e/e_{max}$) and $w$ (log scale) are shown in Fig. 4.6. It can be easily observed that the resulting SSCCs are now visually distinct. However, $e_{max}$ cannot be treated as a soil property as it will depend on the $w$ of slurry state. Hence, any observation or conclusion based on Fig. 4.6 would be misleading. Therefore, $e$ at $w_L$ ($e_L$ ) was further explored for normalizing $e$. The accuracy of void ratio at liquid limit is dependent on corresponding liquid limit determination of the soil samples. The liquid

limit of the soil depends on the method (cone penetration method or percussion method) chosen and on the equilibrium time for the maturation of the soil sample as reported by Bharat et al. (2020).

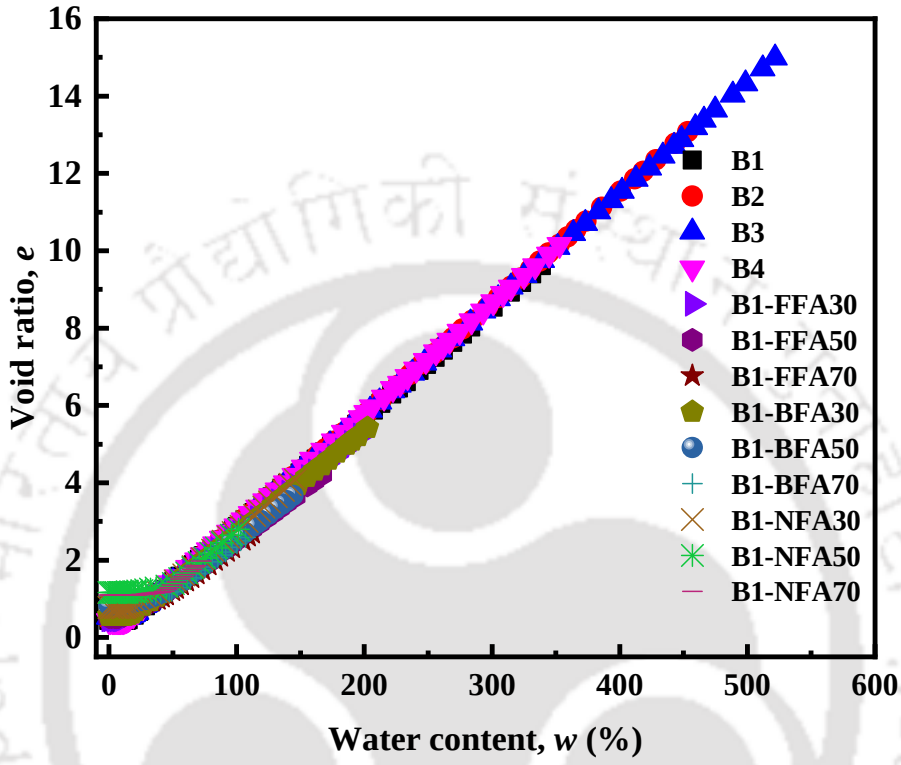


Figure 4.5: Variation of void ratio versus water content for wide range of plasticity

In this study, liquid limit of the soil samples was evaluated using well-established percussion method only. Prior to determination of the liquid limit, soil samples were mixed with water and kept for one week for complete maturation of the soil samples to avoid any aging effect on the liquid limit of the soil samples (Bharat et al., 2020). The choice of normalizing void ratio with $e_L$ is appealing since it is an inherent soil property. Also, the $w$ was also normalized with respect to $w_L$ and the resulting SSCCs are presented in Fig. 4.7. It can be observed that the normalized SSCCs are distinct and the impact of plasticity on SSCC is explicit. The impact of PI on three SSCC parameters $e_0$, $w_{AE}$ and $w_S$ is quantified in the following sections.

### 4.3.3 Impact of plasticity index (PI) on minimum void ratio ($e_0$)

Void ratio at zero shrinkage $e_0$ i.e. the stage where soil sample ceases to shrink, represents the minimum e possible under natural drying condition corresponding to zero external

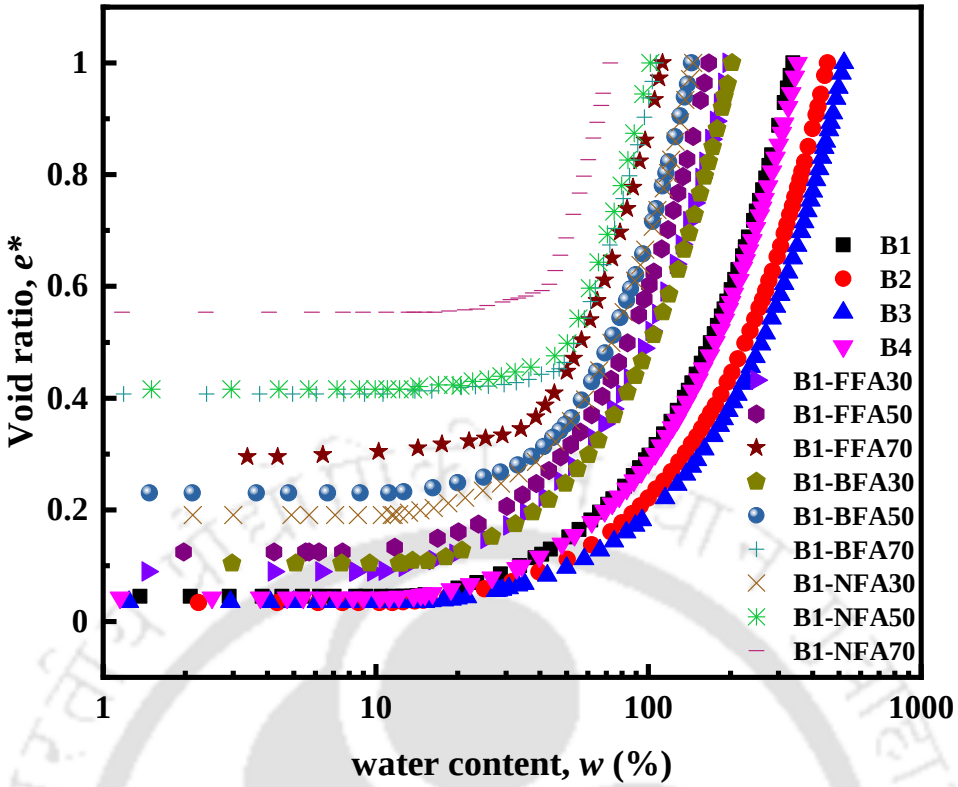


Figure 4.6: Comparison of e* (=$e/e_{max}$ ) versus $w$ response of all samples

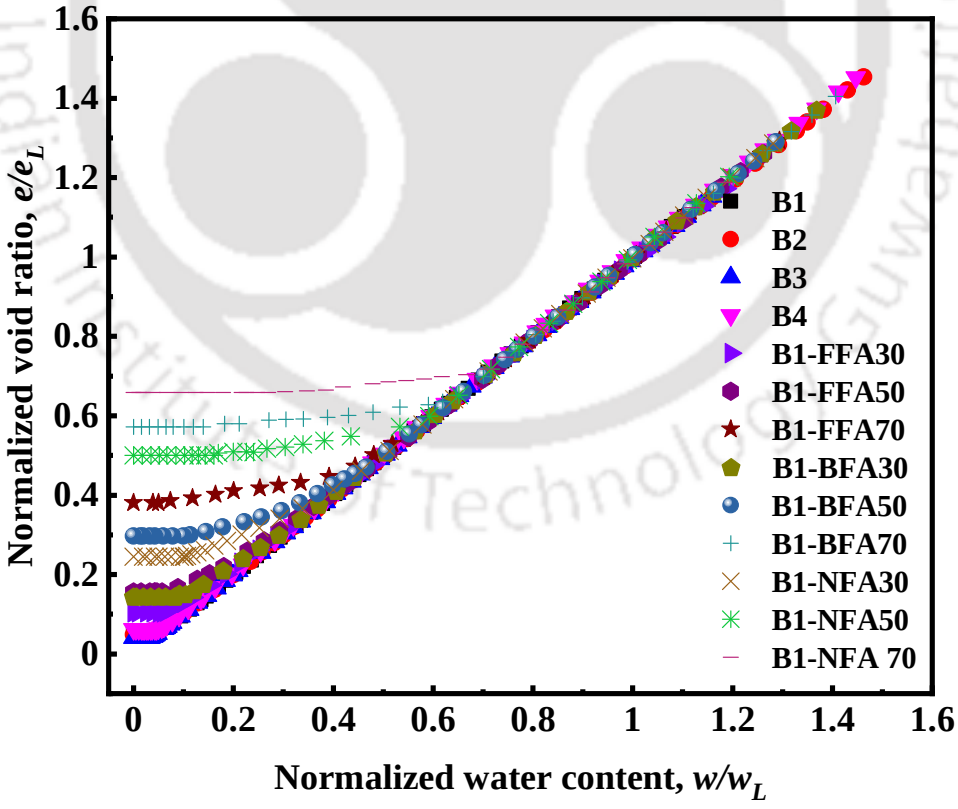


Figure 4.7: Variation of $e/e_L$ versus $w/w_L$ for all soil samples

stress. It is one of the most important parameters associated with the SSCC. On comparison among a particular bentonite and its mixes in Table 4.1, it can be observed that $e_0$ is minimum for the bentonites. For example, the $e_0$ is 0.43 for bentonite B1. Upon addition of fly ashes in various proportions it can be noted that the $e_0$ varies in the range from 0.47 to 1.16.

This is not unexpected since addition of non-plastic slit size (fly ash) particles to the bentonite leads to an increment in void size. For a particular $w$, suction developed in silt size particles is lower than clays resulting in less shrinkage. This results in a higher $e_0$ for the mixes in comparison with bentonites. The same trend can also be explained in terms of PI as the mixes exhibit a lower PI than bentonites. In Table 4.1, it can also be noted that for the same proportion of mixes with various fly ashes, higher $e_0$ was observed for the mixes with class C fly ash (NFA). For example for B1-FFA30, B1-BFA30 and B1-NFA30, the observed $e_0$ is 0.47, 0.57 and 0.78, respectively. Similar trend was observed for the mixes with other proportions. This is mainly due to the self-cementation property exhibited by Class C NFA fly ash, which is attributed to the higher calcium content in the form of calcium oxide (CaO).

Table 4.1: SSCC parameters for all soil samples

| Sample | $PI$ | $W_L$ | $W_S$ | $W_{AE}$ (%) | $W_L - W_{AE}$ | $e_{AE}$ | $e_0$ |
|---|---|---|---|---|---|---|---|
| B1 | 247 | 300 | 13.16 | 28 | 272 | 0.81 | 0.43 |
| B2 | 262 | 310 | 13.18 | 28.5 | 281.5 | 0.82 | 0.44 |
| B3 | 396 | 450 | 12.24 | 28 | 422 | 0.83 | 0.53 |
| B4 | 183 | 244 | 10.65 | 26.62 | 217.38 | 0.8 | 0.44 |
| B1-FFA30 | 134 | 166 | 16.5 | 53.34 | 112.66 | 1.45 | 0.47 |
| B1-FFA50 | 106 | 132 | 25.4 | 51.92 | 80.08 | 1.33 | 0.52 |
| B1-FFA70 | 63 | 87 | 34.5 | 45 | 42 | 1.1 | 0.8 |
| B1-BFA30 | 114 | 148 | 26.43 | 49.58 | 98.42 | 1.34 | 0.57 |
| B1-BFA50 | 82 | 112 | 38.75 | 52.22 | 59.78 | 1.34 | 0.85 |
| B1-BFA70 | 48 | 76 | 40.87 | 49.09 | 26.91 | 1.2 | 1.05 |
| B1-NFA30 | 87 | 120 | 19.5 | 45.65 | 74.35 | 1.31 | 0.77 |
| B1-NFA50 | 55 | 85 | 30.35 | 50.34 | 34.66 | 1.39 | 1.16 |
| B1-NFA70 | 34 | 61 | 39.92 | 43.24 | 17.76 | 1.19 | 1.09 |

During drying under zero stress condition, the cementation behavior counteracts the shrinkage due to loss of water resulting in higher $e_0$. The same behavior is also reflected in

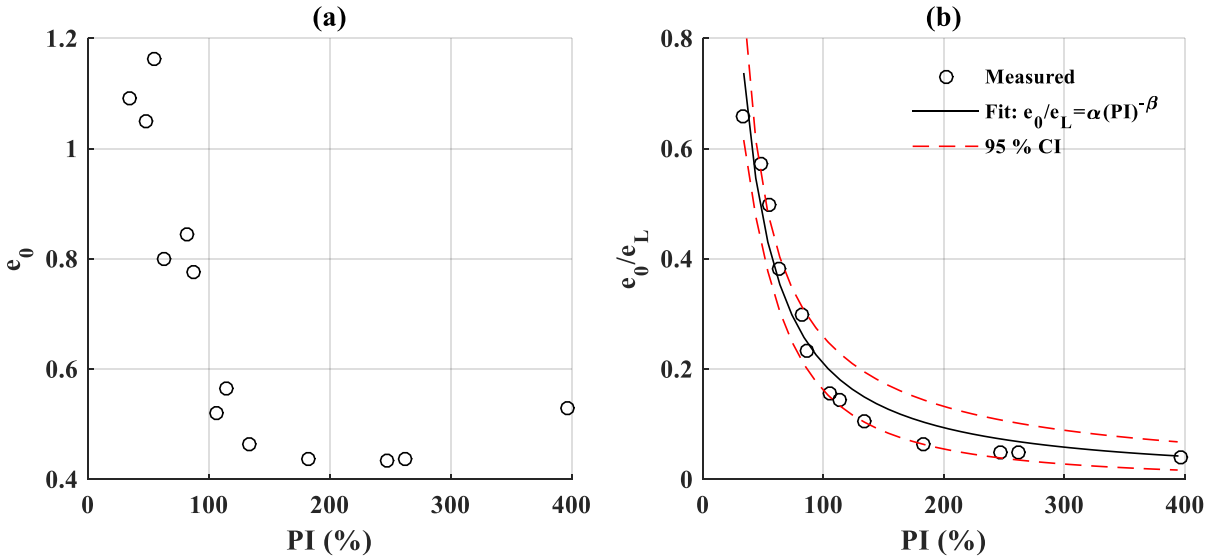


Figure 4.8: Variation of (a) minimum void ratio ($e_0$), (b) normalized $e_0$ ($e_0/e_L$) with plasticity index ($PI$)

the variation of $e_0$ with PI. This implies that although the primary reason for the variation in $e_0$ could be chemical in nature at microscopic level, the same is reflected in the macroscopic response such as PI. Hence, the PI can be considered as an important index property, which can be correlated with $e_0$ as presented in Fig. 4.8 (a). It is noted that there is no conclusive trend of $e_0$ with PI. For example, B1-BFA (ref. Table 4.1) with PI of 48 % exhibits an $e_0$ of 1.05 where as B1-NFA50 with PI of 55 % has an $e_0$ of 1.16. Also the bentonite B3 with a PI of 396 % has an $e_0$ of 0.53, higher than all other bentonites despite having the maximum PI. For an unambiguous comparison, normalized void ratio $e_0/e_L$ was plotted as a function of PI as shown in Fig.4.8(b). The resulting trend can be viewed as conclusive. A power equation $e_0/e_L = \alpha(PI)^{(-\beta)}$ with parameters $\alpha$ and $\beta$ equal to 44.1 and 1.2, respectively was found to capture the relationship satisfactorily (coefficient of determination ($R^2$ ) of 0.95) and the same will be further utilized to develop a predictive model for SSCC in the subsequent section.

### 4.3.4 Impact of plasticity index (PI) at air entry

Air entry is the starting point of residual shrinkage zone from where the desaturation of soil sample initiates. This results in a lower volume reduction of the soil in comparison to the volume of the water lost from the sample. As depicted in Fig. 4.9, air entry point is considered as the point on the SSCC where saturation S falls below 100 % in the S versus $w$ and $e$ versus $w$ plots. The observed air entry characteristics in terms of void ratio at air

entry ($e_{AE}$) and water content at air entry ($w_{AE}$) for all the soil samples are listed in Table 4.1. It can be observed that $e_{AE}$ for bentonites (0.80-0.83) is significantly lower than the mixes (1.10-1.45). The bentonites exhibit a very high shrinkage thereby maintaining full saturation even at a very low $w$. This is in accordance with the results reported in the literature (Fityus and Buzzi, 2009; Tripathy et al., 2014b). On addition of fly ash to bentonites, the PI and the shrinkage reduces. Hence, early desaturation is expected resulting in higher $e_{AE}$ and $w_{AE}$ for the mixes (ref. Table 4.1). However, in Table 4.1 it should also be noted that an increasing fly ash content results in marginal decrease in $e_{AE}$.

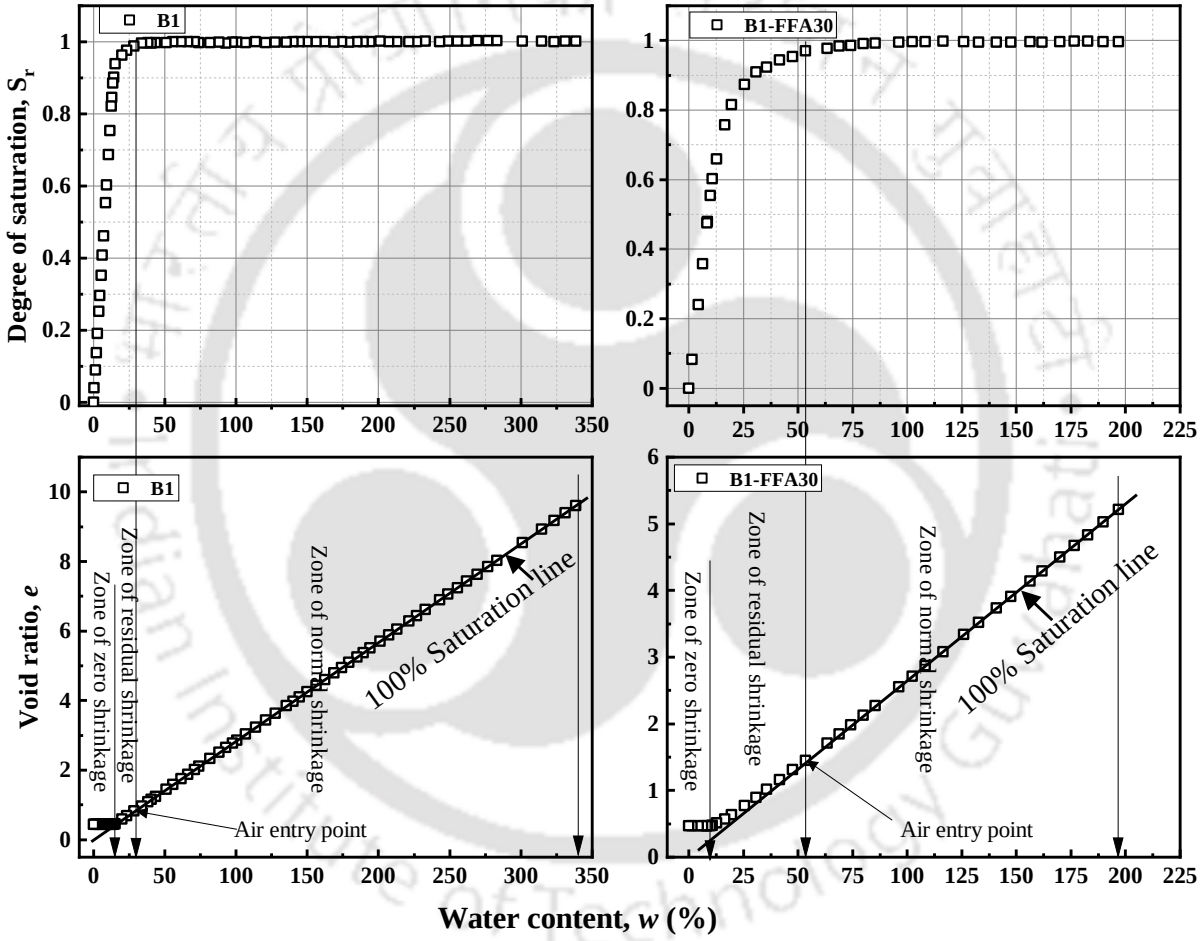


Figure 4.9: Determination of air entry point in conjunction with degree of saturation

Figure 4.9 shows three different zones (normal, residual and zero shrinkage zones) of the SSCCs. There is negligible variation in void ratio with water content in the zero shrinkage zone where the volume of soil samples ceases to reduce. Based on the observed results, volume change between air dried (when ceases to shrink) and oven dried state for the high plastic bentonites were found to be 0.45% and even less for B-FAs mixes. Less than 0.5% change in the volume was assumed to be negligible in this study. This observation

is similar to those reported in the literature for high water content samples undergoing shrinkage under drying (zero stress condition) (Montes-h et al., 2003; Zhang et al., 2019a; Tan et al., 2020; Barman and Mishra, 2022). The observation is different from Lu et al. (2017), which reported variation in void ratio in the zero shrinkage zone. Lu et al. (2017) have determined volumetric shrinkage based on the concept of suction stress and the elastic modulus function. This may be mostly applicable for unsaturated stiff soil exhibiting elastic properties and is different from the present study (plastic response of initial high water content samples).

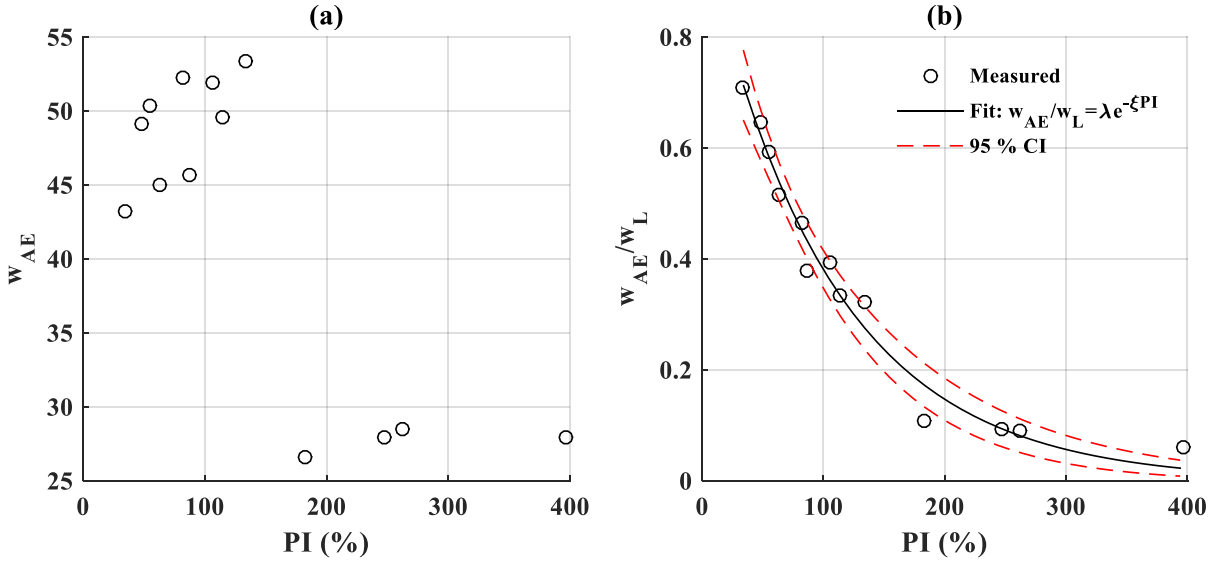


Figure 4.10: Variation of water content at air entry ($w_{AE}$) with plasticity index ($PI$)

The results of $w_{AE}$ are plotted as a function of PI as presented in Fig. 4.10 (a). The result indicates that there is no unique trend, which implies that $w_{AE}$ cannot be directly correlated with PI. The width of normal shrinkage zone defined by $w_L$-$w_{AE}$ (ref. Fig.4.1 and Table 4.1) is however found to decrease consistently with decrement in PI. Therefore, it is expected that the sample should desaturate earlier upon decrement of PI. However, this trend may not directly translate to $w_{AE}$ (ref. Fig. 4.10 (a)) as the starting point of SSCC varies with plasticity. Therefore, $w_{AE}$ was normalized with the corresponding $w_L$ as shown in Fig. 4.10 (b). It can be observed that the$w_{AE}$ follows a definite (and expected) trend with PI. An exponential decay form of equation $w_{AE}/w_L = \lambda exp(-\xi PI)$ was found to satisfactorily represent the observed trend. The coefficient of determination $R^2$ for the fit is 0.97 and the parameter values $\lambda$ and $\xi$ are 0.99 and 0.1, respectively. This equation will be quite handy for directly estimating $w_{AE}$ by knowing easily measurable soil parameter PI.

### 4.3.5 Impact on shrinkage limit ($w_S$)

Shrinkage limit ($w_S$ ) depicts the end of residual zone beyond which the loss of water does not translate to any further decrement in soil volume. A highly plastic fine-grained soil is expected to have a lower $w_S$. As expected, Table 4.1 indicates that $w_S$ for bentonites is lower than that of the mixes with fly ash. However, similar to the observation made in previous two subsections, $w_S$ cannot be directly correlated with PI unless all the curves are normalized with respect to their starting points ($e_L$,$w_L$). Fig. 4.11 presents the non-normalized and normalized $w_S$ as a function of PI. It can be noted that the variation of normalized shrinkage limit ($w_S/w_L$) exhibits a more conclusive trend.

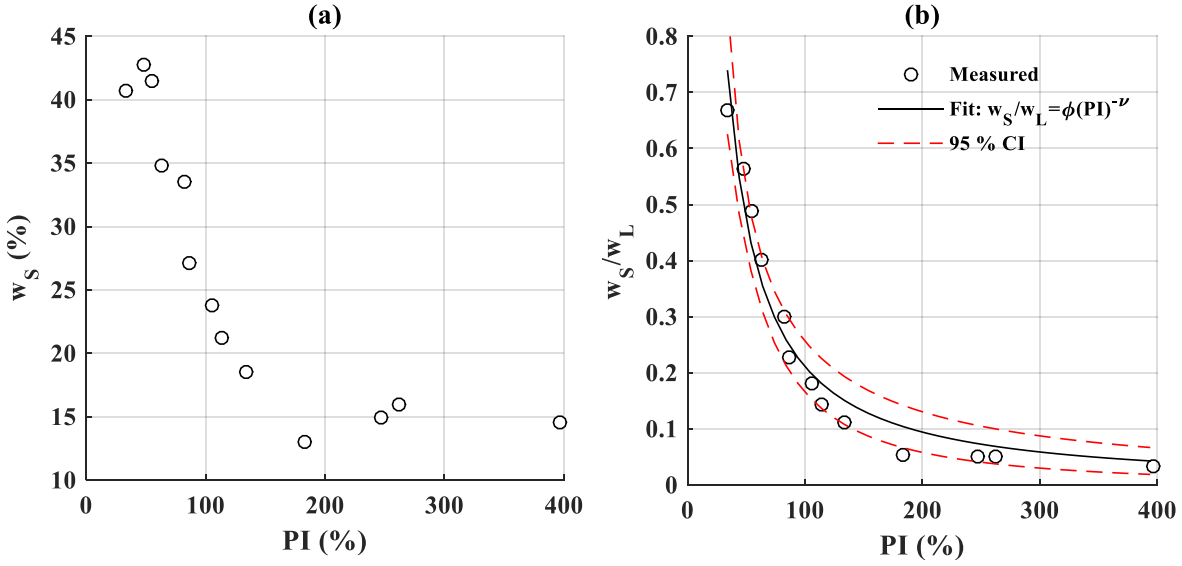


Figure 4.11: Variation of shrinkage limit ($w_s$) with plasticity index ($PI$)

A power equation $w_S/w_L=\phi(PI)^{-\nu}$ was found to satisfactorily capture the exhibited trend. The parameters $\phi$ and $\nu$ are equal to 44.1 and 1.2, respectively with $R^2$ value of 0.95.

In order to verify the effectiveness of balloon method for measuring the SSCC for highly plastic soils, the $w_S$ determined from the measured SSCC was compared with those obtained from mercury displacement method (ASTM D 427, (2007b)). Three trials were conducted for measuring $w_S$ from mercury displacement method and the average of the results were compared with $w_S$ determined from the SSCC using the tangent method proposed by Marinho (1994) (Fig. 4.12). From Fig. 4.12, the $w_S$ is identified as the point of intersection of the two tangents drawn from the zero shrinkage and the normal shrinkage portion of the SSCC. The $w_S$ determined using both the methods are compared in Fig.4.13. It can

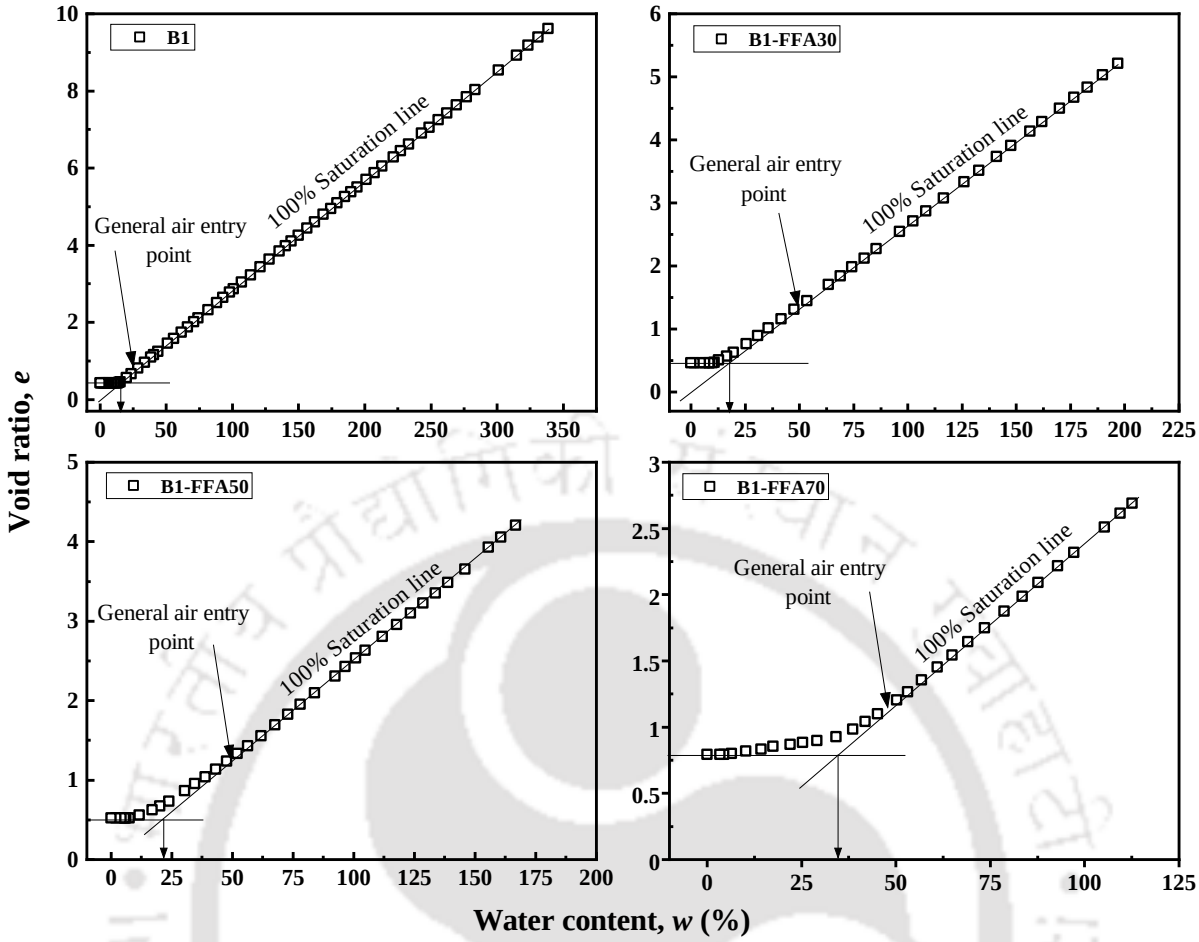


Figure 4.12: Determination of shrinkage limit and general air entry point from SSCC

be observed that the data obtained from SSCC is in close agreement with the mercury displacement method. This demonstrates the efficiency of balloon method for successfully capturing shrinkage characteristics of soil with wide range of plasticity. It can also be noted that from Fig. 4.12 that there is a reduction in the void ratio beyond the shrinkage limit with decreasing water content of the soil samples.

### 4.3.6 Predictive model for SSCC

In this section an empirical predictive model was developed for the estimation of SSCC based on easily measurable PI of the soil. The SSCC is parameterized using Fredlund et al. (2002) model as shown in Eq. 4.1.

$$e(w) = a_{sh}\left[\frac{w^{c_{sh}}}{b_{sh}^{c_{sh}}} + 1\right]^{1/c_{sh}} \tag{4.1}$$

where, the parameter $a_{sh}$= minimum void ratio; $b_{sh}$= slope of the line of tangency and $c_{sh}$ represents the curvature of the SSCC. The Fredlund et al. (2002) model fitted to the

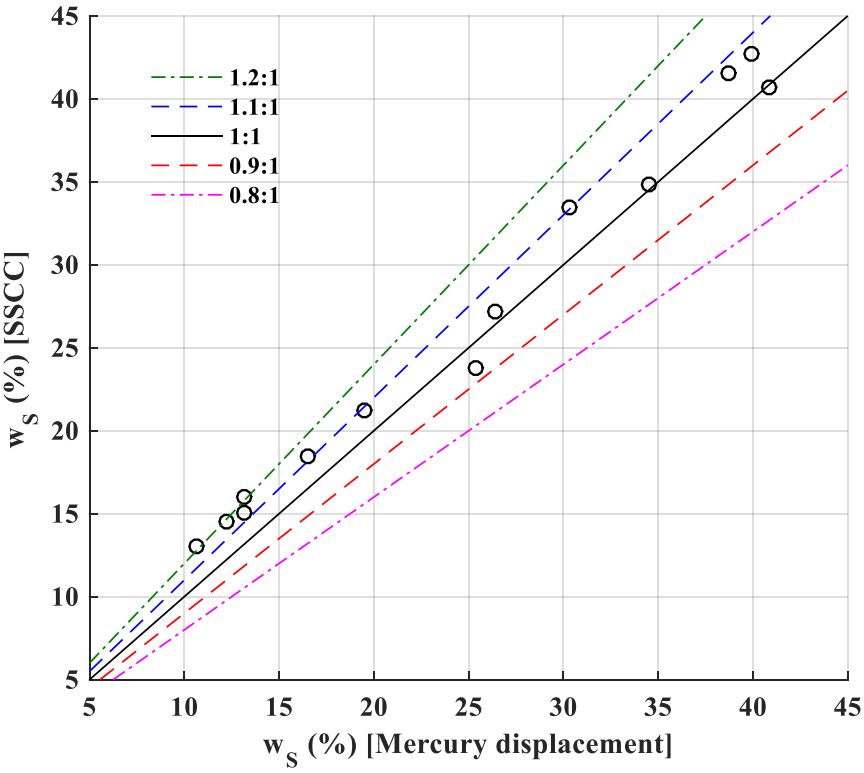


Figure 4.13: Comparison of shrinkage limit obtained from SSCC and mercury method

experimental results of SSCC is shown in Fig. 4.14 for selected samples. It can be easily observed that the Fredlund et al. (2002) model can efficiently represent the measured SSCC. All the samples followed similar trends and are not presented here for the sake of brevity. The parameters corresponding to each of the fit are summarized in Table 4.2.

As already observed in Fig. 4.8(b), it was noted that a power curve can be used to represent the variation of $a_{sh}/e_L$ with PI. The same is also presented in Fig. 4.15a and Eq. 4.2.

$$a_{sh}/e_L = \alpha(PI)^{-\beta} \tag{4.2}$$

Making use of basic relationships, $e_L = w_L G_s$, Eq. 4.2 can be rewritten as :

$$a_{sh} = w_L G_s\left[\alpha(PI)^{-\beta}\right] \tag{4.3}$$

For the dataset used in this study, the parameters $\alpha$ and $\beta$ were found to be 44.1 and 1.2, respectively. The parameter $b_{sh}$ is equal to $a_{sh}/G_s$ based on Fredlund et al. (2002) model and hence can be calculated from the estimated $a_{sh}$ in Eq. 4.3. For estimation of curvature parameter $c_{sh}$, various combinations of correlation with liquid limit, plastic limit, and plasticity index were explored. It was found that the power equation similar to Eq. 4.2

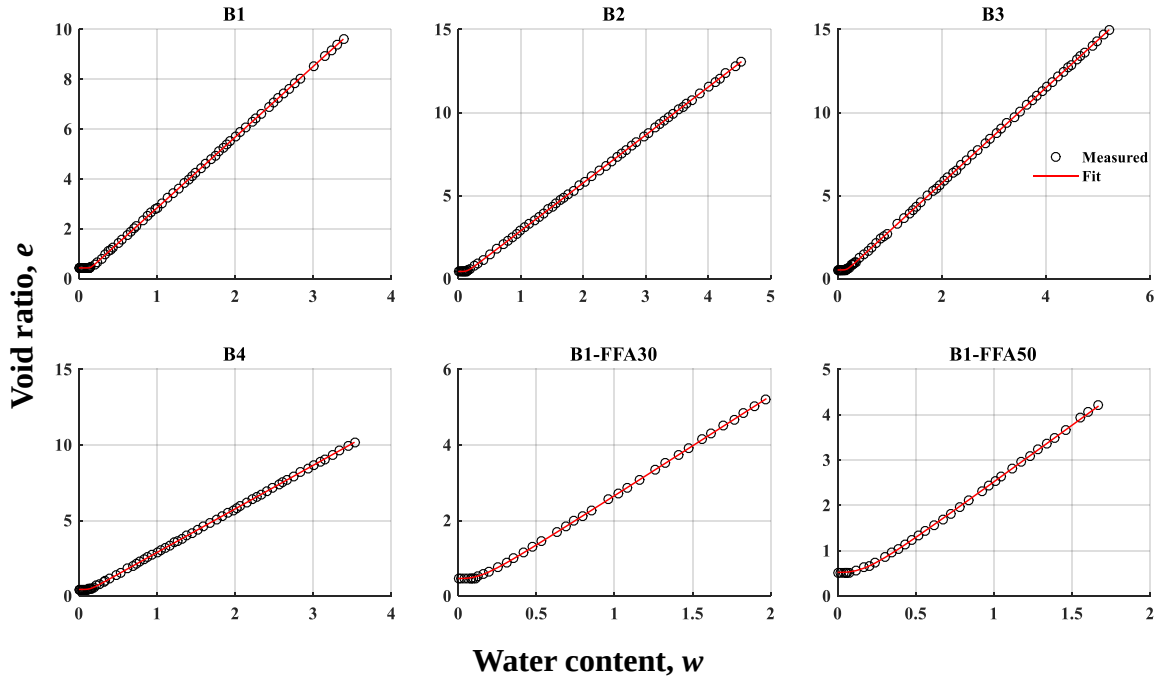


Figure 4.14: Fredlund et al., 2002 model fitted to the measured SSCC for bentonites and its mixes

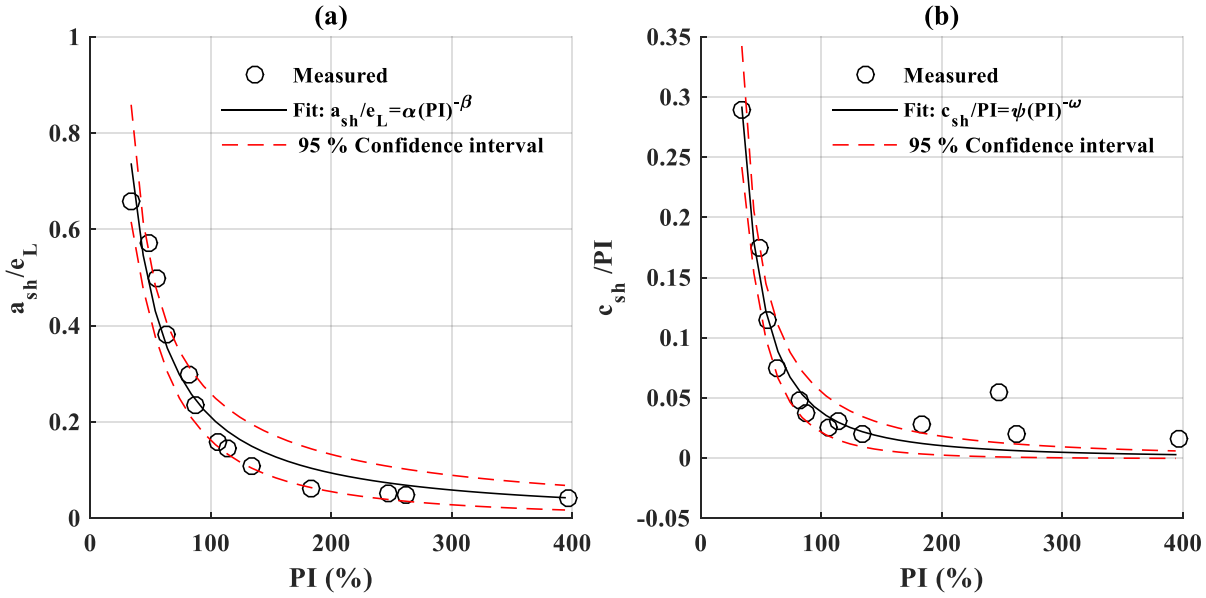


Figure 4.15: Fredlund et al., 2002 model fitted to the measured SSCC for bentonites and its mixes

was found to be adequate ($R^2$=0.95), as shown in Fig. 4.15 b and given by Eq. 4.4.

$$c_{sh} = PI[\,\psi(PI)^{-\omega}] \tag{4.4}$$

Table 4.2: The details of Fredlund et al., 2002 model fitted to SSCC.

| Sample | $a_{sh}$ | $b_{sh}$ | $c_{sh}$ | $W_l$ | $W_p$ | $PI$ | $G_s^*$ | $G_s^\#$ |
|---|---|---|---|---|---|---|---|---|
| B1 | 0.43 | 0.15 | 13.35 | 300 | 53 | 247 | 2.84 | 2.84 |
| B2 | 0.44 | 0.16 | 5.07 | 310 | 48 | 262 | 2.88 | 2.88 |
| B3 | 0.53 | 0.19 | 6.48 | 450 | 54 | 396 | 2.87 | 2.87 |
| B4 | 0.44 | 0.16 | 5.08 | 244 | 61 | 183 | 2.86 | 2.88 |
| B1-FFA30 | 0.47 | 0.18 | 2.68 | 166 | 32 | 134 | - | 2.65 |
| B1-FFA50 | 0.52 | 0.21 | 2.74 | 132 | 26 | 106 | - | 2.51 |
| B1-FFA70 | 0.79 | 0.34 | 4.71 | 87 | 24 | 63 | - | 2.37 |
| B1-BFA30 | 0.57 | 0.21 | 3.53 | 148 | 34 | 114 | - | 2.67 |
| B1-BFA50 | 0.85 | 0.34 | 3.96 | 112 | 30 | 82 | - | 2.54 |
| B1-BFA70 | 1.05 | 0.44 | 8.38 | 76 | 28 | 48 | - | 2.41 |
| B1-NFA30 | 0.78 | 0.29 | 3.21 | 120 | 33 | 87 | - | 2.77 |
| B1-NFA50 | 1.16 | 0.43 | 6.29 | 85 | 30 | 55 | - | 2.74 |
| B1-NFA70 | 1.09 | 0.41 | 9.84 | 61 | 27 | 34 | - | 2.71 |
| BX | 0.40 | 0.14 | 9.32 | 300 | 43 | 257 | - | 2.88 |
| BX-FFA30 | 0.42 | 0.16 | 2.62 | 196 | 29 | 167 | - | 2.66 |
| BX-FFA50 | 0.57 | 0.23 | 3.15 | 149 | 22 | 127 | - | 2.52 |
| BX-FFA70 | 0.76 | 0.32 | 5.17 | 93 | 20 | 73 | - | 2.37 |
| BX-NFA30 | 0.52 | 0.19 | 3.73 | 156 | 38 | 118 | - | 2.79 |
| BX-NFA50 | 0.73 | 0.27 | 3.80 | 97 | 35 | 62 | - | 2.75 |
| BX-NFA70 | 0.86 | 0.32 | 9.64 | 65 | 32 | 33 | - | 2.71 |

Note: $--$ denotes that the data was not needed hence not calculated, $G_s^*$ denotes measured specific gravity and $G_s^\# = a_{sh}/b_{sh}$

where $\psi$,$\omega$ for this dataset were found to be 227.6 and 1.9, respectively. Substituting Eq. 4.2 and Eq. 4.4 in Eq. 4.1, the predictive model for SSCC can be represented by Eq. 4.5. The predictive model is a function of easily measurable soil properties PI and $G_s$.

$$e(w) = w_L G_s[\alpha(PI)^{-\beta}][\frac{w^{PI[\psi(PI^{-\omega})]}}{(w_L[\alpha(PI)^{-\beta}])^{PI[\psi(PI^{-\omega})]}}]^{\frac{1}{PI[\psi(PI^{-\omega})]}} \tag{4.5}$$

Table 4.3: Parameters of the predictive model for SSCC.

| Parameter | Value |
|---|---|
| $\alpha$ | 44.1 |
| $\beta$ | 1.2 |
| $\psi$ | 227.6 |
| $\omega$ | 1.9 |

The parameters $\alpha$, $\beta$, $\psi$ and $\omega$, from the present study, is summarized in Table 4.3. In

addition to the measured results from this study, an attempt was made to further investigate the generality of the proposed equation using the data set reported in Wijaya et al. (2015). Figs. 4.16(a) and 4.16 (b) presents the measured data in this study along with the dataset of Wijaya et al. (2015) fitted with Eq. 4.2 and Eq. 4.4, respectively. For the parameter $a_{Sh}$, it can be observed that the proposed power form of equation fits reasonably well to the dataset in Wijaya et al. (2015) with $R^2 = 0.68$. Also, at high PI, it can be noted that the trend line from both datasets converges. However, for the $c_{Sh}$ parameter the fit for the Wijaya et al. (2015) data was not found to be representative with a poor $R^2$ value of 0.13. It can be noted that the database in Wijaya et al. (2015) included only a few soils with higher PIs. The maximum PI reported was 66 % only whereas the current study contains soils with plasticity up to 396 %. Also, the parameters used in this study are exclusively for soil drying from slurry state under zero external stress, whereas the database reported in Wijaya et al. (2015) also contains soils with different initial states. Although the observation limits the generality of the proposed form of Eq. 4.4 for the parameter $c_{sh}$, it can still be used effectively to predict the SSCC of highly plastic soils, as shown in the next section.

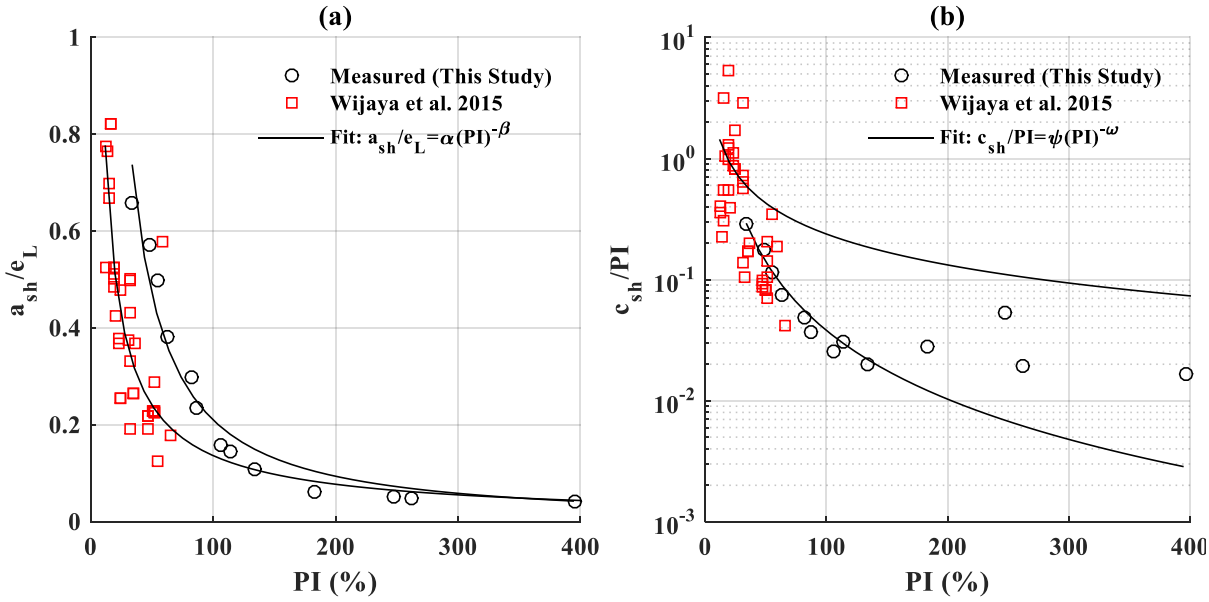


Figure 4.16: Verification of the proposed equation on the dataset reported by Wijaya et al., 2015 for parameter (a) minimum void ratio($a_{sh}$) (b) curvature parameter ($c_{sh}$)

### 4.3.7 Validation of the proposed predictive model for SSCC

The validation of the proposed model (Eq. 4.5) for the estimation of SSCC is presented in Figs. 4.17, 4.18a, and 4.18b, which consists of predicted and measured SSCCs. The root

mean squared error (RMSE) and coefficient of correlation ($R^2$) between the measured and predicted curve are also presented. It can be noted that the predicted SSCC based on PI and $G_s$ are in close agreement with the measured results. The Fig. 4.18a shows the validation of the estimation model using an independent data set of Barmer bentonite (BX) and its six mixes (ref. Table 4.2). It can be noted that apart from the two mixes, i.e., BX-BFA70 and BX-NFA70, the predicted results matches well with the measured data.

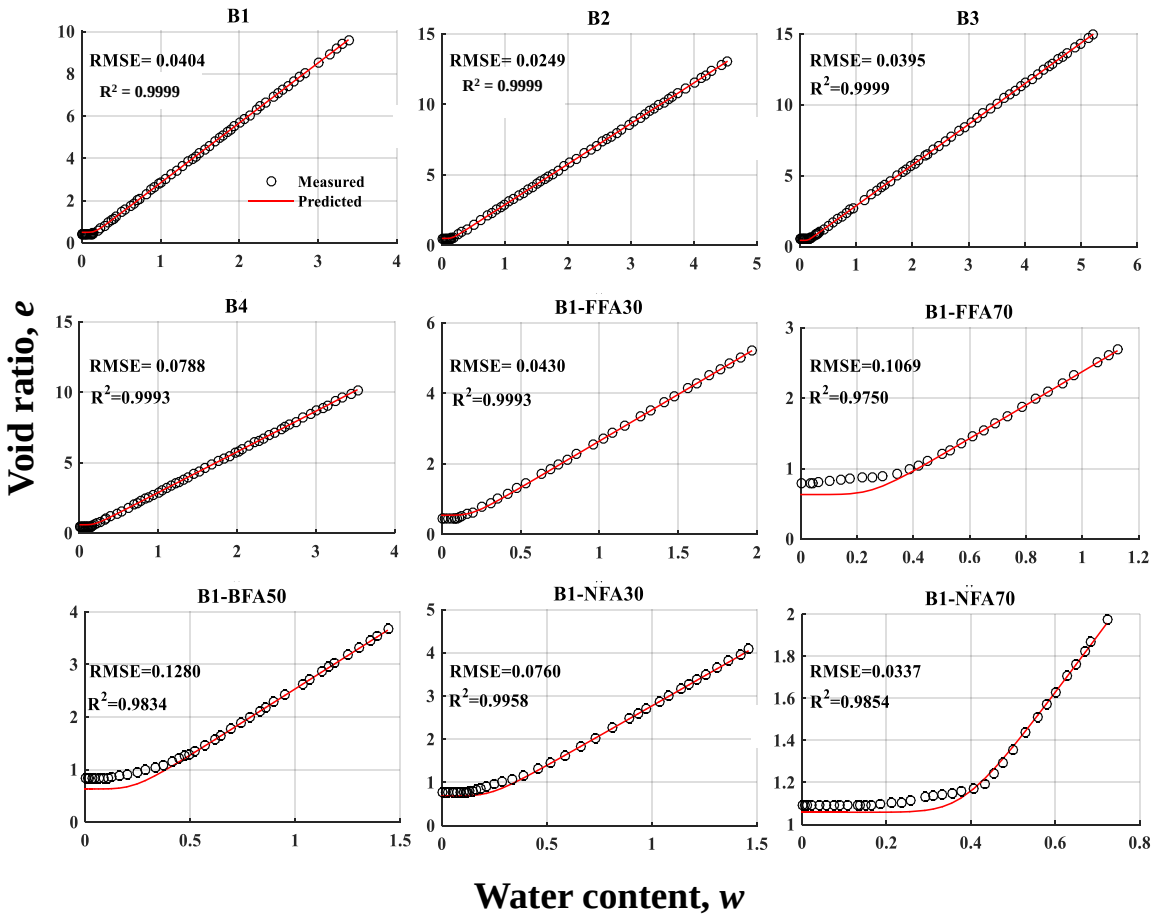


Figure 4.17: Predicted SSCC for bentonite and its mixes

Figure 4.18b presents the validation of proposed model based on the experimental data sets of SSCC for bentonites obtained from different literatures (Tripathy et al., 2014b; Gapak et al., 2017; Barman and Mishra, 2022). The model fits fairly well with the experimental data of SSCC from diverse literature with $R^2$ close to 0.99. This indicates that the predictive accuracy of the model is better for the soils with higher PI. As the plasticity decreases, the predictability of SSCC below shrinkage limit also decreases (after desaturation). It may be noted that the volumetric shrinkage curve is mostly needed for high plastic soils.

For low to moderate plasticity, volumetric shrinkage curves are generally not used for determining SWCC. Fig. 4.19 compares the predicted parameters $a_{sh}$ and $c_{sh}$ with the measured ones for all the 20 SSCCs used in this study. It can be noted that majority of the estimated values are well within ± 20 % of the measured values. For $c_{sh}$ parameter, most of the values are also well within ± 20 % error band. It should be noted that the sensitivity of the SSCC on $c_{sh}$ parameter is relatively low (Fredlund et al., 2002; Wijaya et al., 2015). Further, Fredlund et al. (2002) observes that for the representation of SSCC, $a_{sh}$ is the most critical parameter.

The instructions for using the predictive model are summarized as follows. For a given high plastic soil, the basic properties such as PI and $G_s$ needs to be determined. The SSCC can be estimated by using Eq. 4.5 based on the known values of PI, $G_s$ and the parameters ($\alpha$,$\beta$,$\psi$,$\omega$) listed in Table 4.3. It is highly recommended to generate some experimental data for verifying the accuracy of the SSCC model before actual application. In the absence of experimental data, the above method may be adopted as it is. The estimation procedure is advantageous because it is quick and relatively easy as compared to the time consuming and cumbersome actual measurements of SSCC.

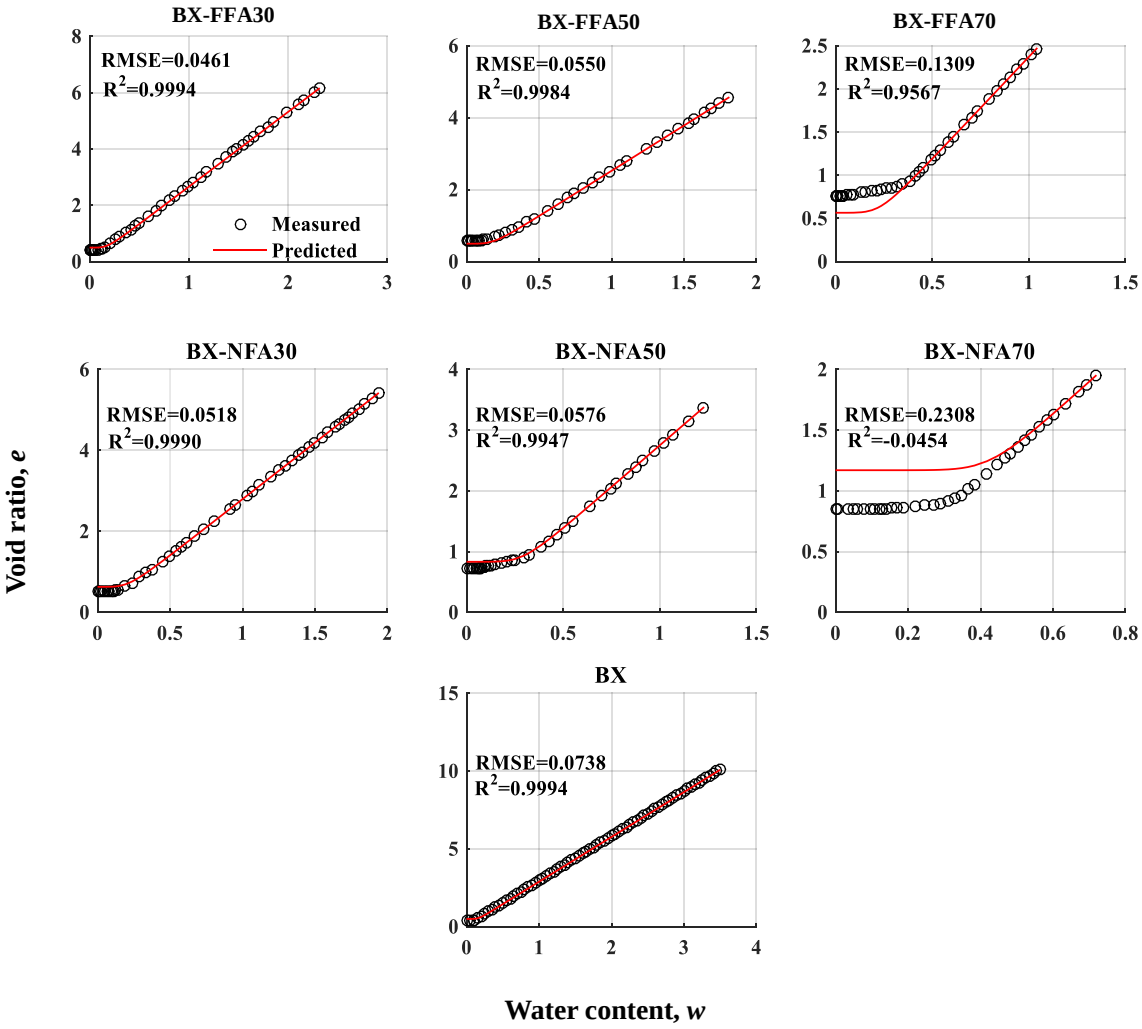


(a) Validation of SSCC predictive model using independent data set of Barmer bentonite (BX) and its six mixes

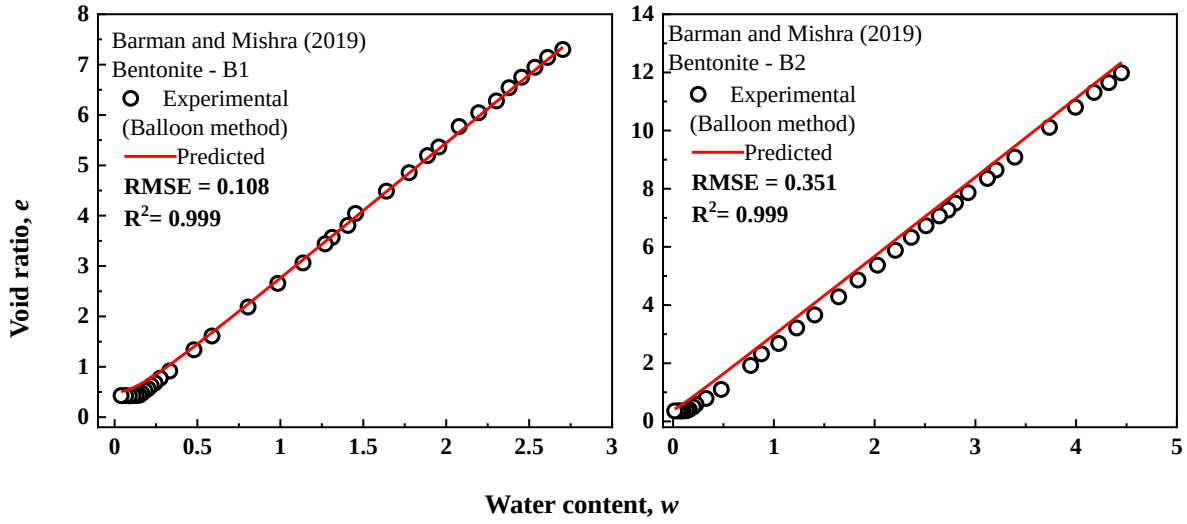


(b) Validation of SSCC predictive model using independent data set of bentonites from literature

Figure 4.18

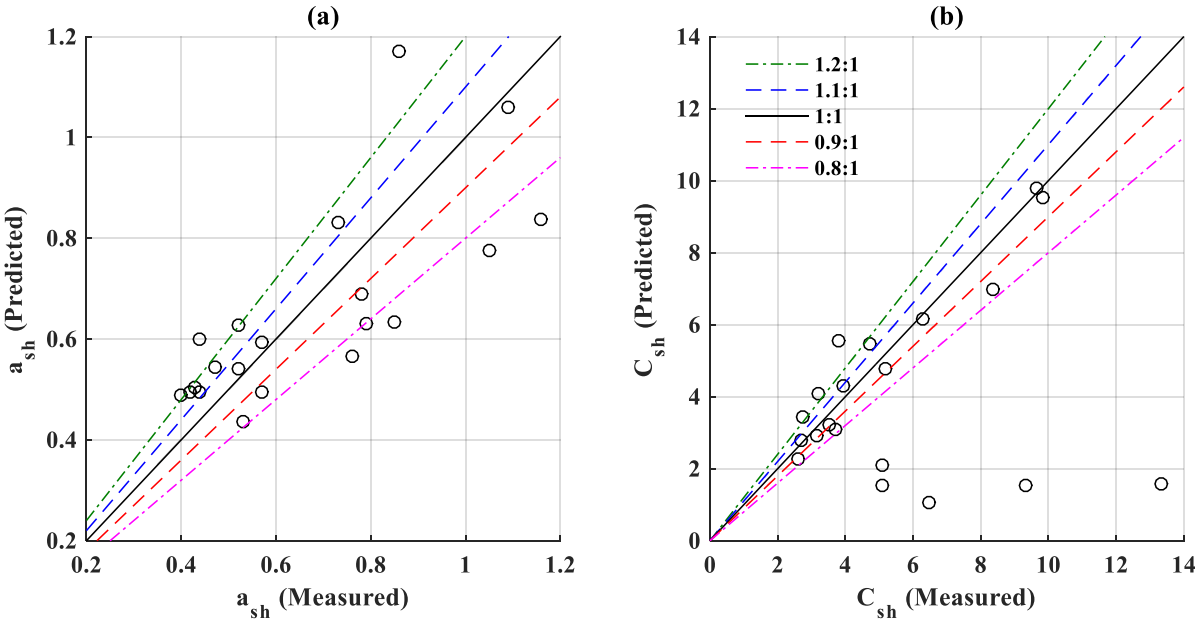


Figure 4.19: Measured and predicted Fredlund et al., 2002 model parameters (a) $a_{sh}$ (b) $c_{sh}$

## 4.4 Summary

A predictive model was developed in this study for estimating SSCC of high plastic soils using an easily measurable index property, plasticity index (PI). The study recommends initial water content of the soil samples close to liquid limit ($w_L$) for measuring SSCC for easy expulsion of entrapped air by simple tamping. The shrinkage limit ($w_S$) determined using mercury displacement method and SSCC were found to be in close agreement demonstrating the efficiency of balloon method for successfully capturing shrinkage characteristic curve of soil with wide range of plasticity. The normalized SSCCs in terms of e/$e_L$ and w/$w_L$ was distinct and revealed the impact of plasticity on shrinkage characteristics, where $e_L$ is the void ratio at $w_L$. It was found that the key parameters of SSCC; the minimum void ratio at zero shrinkage ($e_o$), water content at air entry ($w_{AE}$) and the $w_S$, when normalized with $e_L$ and $w_L$ (e/$e_L$, $w_{AE}/w_L$, $w_S/w_L$) correlates well with easily measurable PI. The air entry characteristics defined in terms of void ratio at air entry ($e_{AE}$) and $w_{AE}$ was found to be higher for low plastic soils due to early desaturation. The $e_o/e_L$ and $w_S/w_L$ showed an inverse power relationship whereas $w_{AE}/w_L$ followed an exponential decay with PI. It was noted that the predictive model did not fare well for low plastic soils. Further studies are needed to improve the predictability of the proposed model for determining shrinkage characteristics of soils with low to moderate plasticity.

# 5

# Hydraulic Conductivity of B-FA and B-S Mixes

## General

Compacted bentonite-sand (B-S) and bentonite-fly ash (B-FA) are established combinations for the construction of landfill liners. This study determined the upper and lower bounds of equilibrium hydraulic conductivity ($k_{eq}$) of amended bentonite under extended duration of flow. The $k_{eq}$ for constant volume flow condition differed from free swelling condition by more than two orders of magnitude due to the difference in geomaterial interaction, microstructural changes, and mineralization. Considering constant volume and free swelling condition, B-FA mix with class F and class C fulfilled the hydraulic conductivity criterion up to 70 % and 30 % amendment, respectively. The higher $k_{eq}$ observed for the B mixed with class C FA was attributed to the formation of porous calcium aluminium silicate hydrate gel and ettringite needle type minerals. The time taken to achieve equilibrium was inversely related to $k_{eq}$ by a power relationship. The data from this study were used to propose empirical relationships for estimating $k_{eq}$ (long-term) based on k obtained at 48 hours (short-term), plasticity and geomaterial type. The study reveals that FA can be used as an alternate for S as amendment material and $k_{eq}$ based on free swelling condition should be used for designing the liner.

## 5.1 Hydraulic conductivity variation in compacted B-FA mixes under constant volume and free swelling flow conditions

### 5.1.1 Background

Hazardous and municipal solid waste management requires engineered landfills (Fleming and Rowe, 2004), which constitutes three primary layers, viz. the liner, waste, and final cover (Ng et al., 2019). The liner underlying the waste limits the leachate seeping into the groundwater table (Ali et al., 2016). A typical engineered liner constitutes compacted fine-grained soil that satisfies the criteria of minimal hydraulic conductivity of $1 \times 10^{-9}$ m/s (USEPA, 1989; Younus and Sreedeep, 2012a). Based on the guidelines stated in the literature, the minimum unconfined compressive strength (UCS) should be greater than 200 kPa for the material used as low permeable barrier layer in landfill liners (Daniel et al., 1984; Daniel and Benson, 1990; Yong, 2000). Bentonite (B) was used to construct a liner layer adhering to both the permeability and strength criterion (Marcial et al., 2002; Meier and Shackelford, 2017). Due to high specific surface area, B is also an ideal retention medium there by limiting the migration of contaminants to groundwater (Sharma et al., 2021). However, the compacted clay liner constructed with only B is susceptible to high swelling, shrinkage cracks, poor compressive strength, high compressibility and uneconomical for mass utilization (Daniel and Benson, 1990; Gilbert et al., 1996; Komine and Ogata, 2003; Budihardjo et al., 2021).

To improve the performance of B, cohesionless geomaterials or natural soils were mixed with B for compacted low permeable layer construction (EPA/ 530-SW-86-007-F, 1987; LFE10; Meier and Shackelford, 2017; Nguyen et al., 2019). Sand (S) was considered as an established geomaterial followed by fly ash (FA) and suitable natural soil for amending B (Blatz et al., 2002; Komine and Ogata, 2003; Phani Kumar and Sharma, 2004; Tripathy et al., 2004; Younus and Sreedeep, 2012a,b; Agus et al., 2013; Tripathy et al., 2017). Apart from improving the mechanical properties of B, the partial replacement by cohesionless material makes the compacted liner construction more workable and economical without compromising the primary hydraulic conductivity requirement (EPA/ 530-SW-86-007-F, 1987; LFE10; Sobti and Singh, 2017; Arifin and Sambelum, 2019). Though S is relatively inert, it

is exhaustive in nature, a costly construction material, and its mining has negative effects on river dredging (de Leeuw et al., 2010; Meng et al., 2018). On the contrary, FA is found in abundance (a by-product of thermal power plants) (Yao et al., 2014). However, FA is a reactive material and may impact the characteristics of amended B with time.

Hydraulic conductivity of B is dependent on the void ratio and diffused double layer (DDL) formation (Tripathy et al., 2014a; Ren et al., 2016; Schanz et al., 2018). Upon interaction with water, B, which constitute primarily of montmorillonite minerals, swells due to the formation of the DDL between individual flaky clay particles (Katti et al., 2015). The void ratio of clay upon interaction with water is dependent on the overburden pressure to which it is subjected (Olgun and Yıldız, 2010). For instance, if the overburden pressure is higher than the swell pressure of the clay, no swelling can occur (Tu and Vanapalli, 2016). In the field, the clay, or the clay- geomaterials mix is generally compacted at dry of optimum moisture content (OMC) or at OMC. Typically, at that state, the soil is partially saturated, and upon interaction, there is an associated volume change due to swelling. In practice, the overlying layers and wastes impose an overburden pressure on the clay liner. During the initial phase of an unfilled landfill, the liner may be exposed to water interaction under minimal overburden stress acting on it. This condition may result in the free swelling of the liner layer. As the overburden stress increases, the swelling may get progressively restricted. Such constant volume or free swelling condition (Cui et al., 2008b,a; Dafalla et al., 2015; Weerasinghe et al., 2021) would impact the hydraulic conductivity (k) of compacted liner.

A sudden rise in the groundwater table can also expose the unfilled landfill liner to excessive water leading to free swell conditions (Chen et al., 2017). Recently, Feng et al. (2019) reported the operational failure of an unfilled landfill cell in Shanghai, China, due to a sudden rise in the water table. Cui et al. (2008a) investigated the change in k for B-S mixes under constant-volume and free-swell conditions and found a contrasting change in k. For free swell conditions, the hydraulic conductivity increases by order of one. This is important as it could drastically increase leachate migration downwards. In the case of bentonite-fly ash (B-FA) mixes, the change in k due to constant volume and free swelling flow condition has not been investigated. Moreover, FA is pozzolanic in nature and induces additional mineralization or even aggregation with the clay matrix. The degree of mineralization will vary with respect to the type of FA (whether Class C or Class F). This can further change the k of the B-FA mixes. Thus, for ensuring proper compatibility of geomaterials,

it is necessary to investigate the time-dependent variation of k of B-FA mixes, considering changes in mineralogy, morphology and swelling restrictions.

This study measures the equilibrium saturated hydraulic conductivity ($k_{eq}$) from falling head test for an extended duration of 90 days for different compacted B-S and B-FA (class F and class C) mixes. The measurement was done under constant volume (completely restricted) condition and free swelling (swelling to its full potential) condition to establish the possible lower and upper bounds of $k_{eq}$, respectively, using an in-house hydraulic conductivity test setup that conforms to falling head test (ASTM, 2015). Based on the observations, the impact of varying percentages of S, class F, and class C FA on $k_{eq}$ of amended bentonite obtained from long term measurements was investigated. The microstructural and mineralogical changes associated with the long term flow interaction and its impact on $k_{eq}$ was investigated. The relationship of keq with short-term saturated hydraulic conductivity (48 hours), plasticity and geomaterial type was determined. While proposing B-FA mix as a low permeable barrier of municipal and hazardous landfill liner, it is important to study any undesirable effect of FA on the hydraulic performance of the barrier. The long-term hydraulic behaviour observed in this study would help to rule out any undesirable changes, if any, that can preclude B-FA mix an alternate material in liner construction.

### 5.1.2 Specimen preparation and test plan

The original materials B, S, FA, the mixes B-FA and B-S were subjected to hydraulic conductivity test. For preparing the mix, the geomaterial (FA or S) was uniformly dry mixed with B at a weight percentage of 30, 50 and 70 based on previous literature (Deka et al., 2015; Deka and Sekharan, 2017). Appropriate amount of distilled water was added to achieve optimum moisture content (OMC) of the respective mix. These samples were transferred to an air tight plastic bag, stored in desiccator placed inside a humidity-temperature-controlled room (for at least 48 hours) for achieving moisture equilibrium (Ng and Yung, 2008). Further, the homogeneous samples were statically compacted at respective OMC and MDD in a specially designed PVC mould for performing falling head hydraulic conductivity test. The details of the PVC mould that facilitate controlled swelling is explained later section. Compaction characteristics (i.e., OMC and MDD) for all parent materials, B-FA mixes, and B-S mixes are presented in Fig. 5.1. The MDD and OMC of B are 1.36 g/cm$^3$ and 33%, respectively. A similar observation for the MDD and OMC of B was found in the previous studies (Zhang et al., 2012; Fattah and Al-Lami, 2016; Thyagaraj and Soujanya, 2017; Kale

et al., 2021). The inclusion of both FAs in B gradually increases the MDD by 8.5% at 70:30 (FA: B) mix.

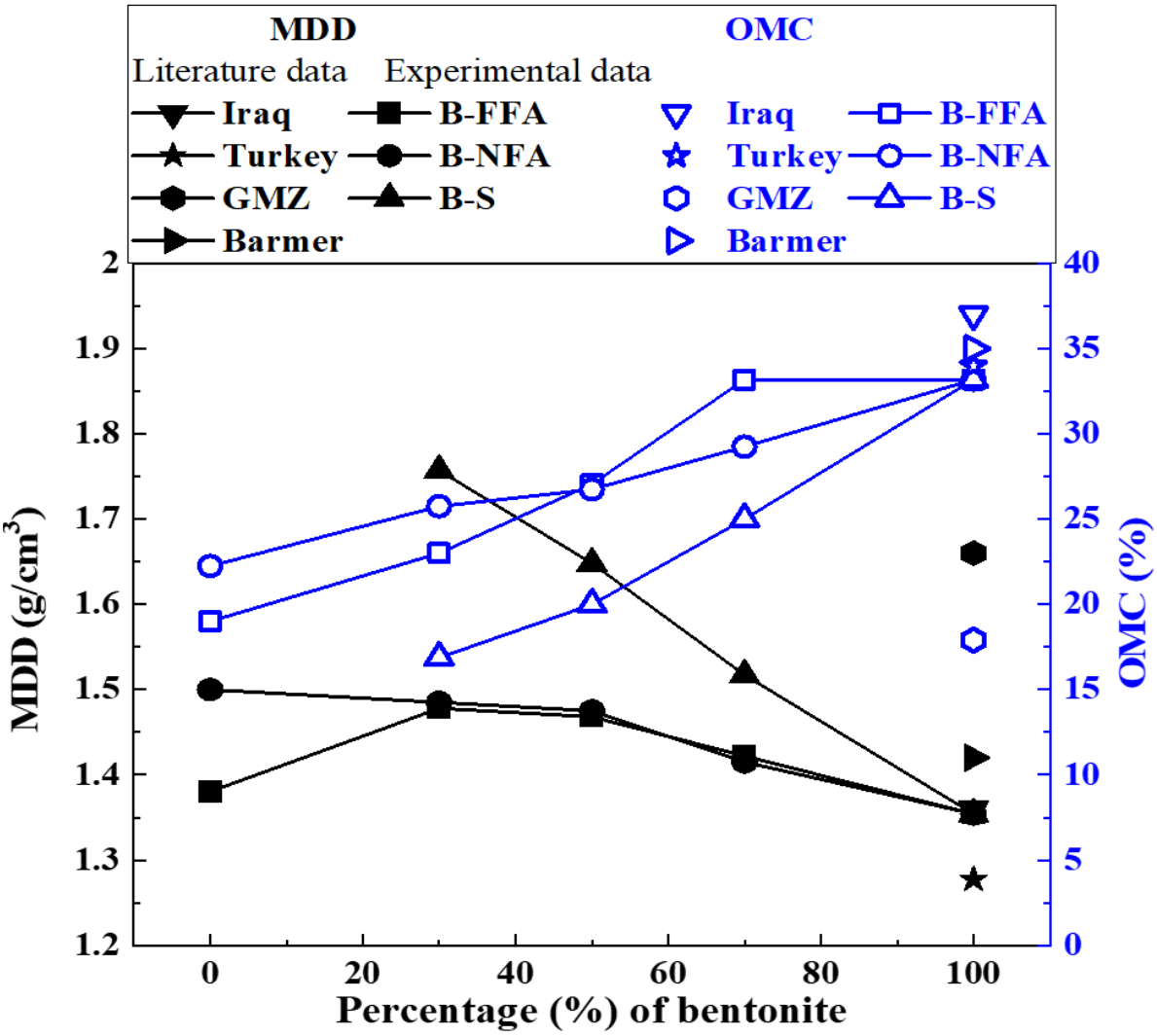


Figure 5.1: Compaction characteristics of B, B-FA, and B-S mixes

It may be due to a reduction in repulsive electrostatic force between negatively charged bentonite clay particles upon inclusion of fly ash particles (Binal, 2016). On the other hand, OMC decreases rapidly with FA inclusion. This is expected because when a high plastic bentonite is replaced with cohesionless FA, the overall water holding capacity of the B-FA mix reduces (Deka and Sekharan, 2020). The inclusion of S in B-S mixes result in an increase of MDD as compared to B-FA mixes. The pores present between the S particles are filled with fine B particles that make the mix denser. Depending on the test condition (constant volume and free-swelling), the ultimate compaction state gets altered due to flow of water during k measurement. The k was measured daily up to 90 days as this

was considered to be a sufficient time for any possible geomaterial interaction (pozzolanic activity and/or change in DDL) to cease (Deka et al., 2015).

### 5.1.3 Hydraulic conductivity test setup

Laboratory k tests on clay can be performed with either rigid-wall or flexible-wall permeameters (Chapuis, 2004; ASTM, 2015, 2016). Rigid-wall permeameters are generally cheaper than flexible-wall devices and have been employed for measuring the k of B in a controlled compacted state (Chapuis et al., 2019). Depending on its density, B exhibits extremely low k in the order of $1\times 10^{-10}$ to $1\times 10^{-12}$ m/s. For attaining full saturation for flexible permeameter (having a 1:1 size ratio), excess time is required. There is also a possibility of uneven swelling during measurements in a conventional flexible wall permeameter. A modified rigid-wall permeability test set-up with a smaller soil sample was developed by Younus and Sreedeep (2012a) to minimize the saturation time and uneven swelling. In the current study, a new rigid-wall permeability test setup modified after Younus and Sreedeep (2012a) was developed, which could measure the k corresponding to both one-dimensional free swelling and constant volume condition. A schematic diagram of the hydraulic conductivity apparatus is shown in Fig. 5.2. The thickness and diameter of the compacted soil used in this set-up are 10 and 60 mm, respectively. Transparent hydraulic conductivity mould made from polymethyl methacrylate (Perspex material), as shown in Fig. 5.2, hosted the compacted soil specimen. Just after compaction, deaired and deionized water was applied to the specimen through the porous stone. The mould has one nozzle at the top and bottom for permitting the flow of water under constant volume and free swell condition. Variable falling head was provided in the inlet, and k was calculated according to the provisions stated in ASTM (2015).

In the case of the constant volume condition, a vertical movable screw rod attached to the upper porous plate was adjusted for preventing swelling (Fig. 5.2). The arrangement maintains a constant volume of the soil throughout the testing period. For free swelling condition, the movable screw rod was kept 0.5 cm above the upper porous plate as shown in Fig. 5.3 (stage 1). During flow of water, the soil sample was allowed to swell uniformly in one-dimension (due to rigid walls of the mould) until the porous plate touches the bottom of the screw rod (stage 2 in Fig. 5.3). The screw rod was raised in equal and small increments until full swelling was achieved as shown in stages 3 and 4 (Fig. 5.3). This procedure was suggested based on the trial and error experiments conducted prior to actual testing. In the

absence of this procedure, a non-uniform swelling was noted due to the adhesion between soil and the mould at the boundary, which can result in improper determination of k.

Figure 5.3 further depicts the progressive decrease in the free swell conditions of B-FA samples as the percentage of FA increases. A maximum of 15 days was required for full swelling depending on the clay or clay mix considered. Thereafter, the k was measured as a function of time based on equation (5.1) for the falling head test (ASTM, 2015).

$$k = \frac{aL}{At} ln(\frac{h_1}{h_2}) \tag{5.1}$$

where a is the stand pipe area, L is the final length of the soil specimen, A is the cross-sectional soil area, t is the time for inducing head change from h1 to h2 (h1>h2). All tests were conducted at room temperature (27 ± 2 °C), and the hydraulic conductivity data reported was based on the average of the three replicates. Following ASTM (2015) guidelines, equilibrium hydraulic conductivity ($k_{eq}$) was obtained when the subsequent values were within ±10% of the average of the last three measurements. For free swell condition, it was noted that the soil specimen dissociated from the bottom porous plate when the flow occurred from bottom to top. This would induce error in the determination of k. Hence, the flow direction was considered from top to bottom in the case of free swell condition. The k of sand was measured by constant head method and falling head method was adopted for FA.

### 5.1.4 Temporal variation of hydraulic conductivity of parent materials

Figure 5.4 presents the temporal variation of k for different parent materials from initiation of tests to the stage where equilibrium hydraulic conductivity ($k_{eq}$) is achieved. For S and FA, k tests were done only under constant volume conditions as they do not exhibit any swelling. In case of B (Fig. 5.4a), the constant volume condition considerably reduced the magnitude of k by an order or more. For the constant volume condition, the initial k was much lower (i.e., $4.5 \times 10^{-12}$ m/s) than that of the free-swelling condition (i.e., $2.8 \times 10^{-10}$ m/s). As the flow of water occurs under constant volume condition, the swelling is restricted, which alter the pore space and undergoes further densification. Hence, the flow paths within the voids get further reduced. This results in lower k under controlled volume condition compared to free swell condition. In the case of free swell conditions, the volume expansion lead to an increase in the void ratio ($e$).

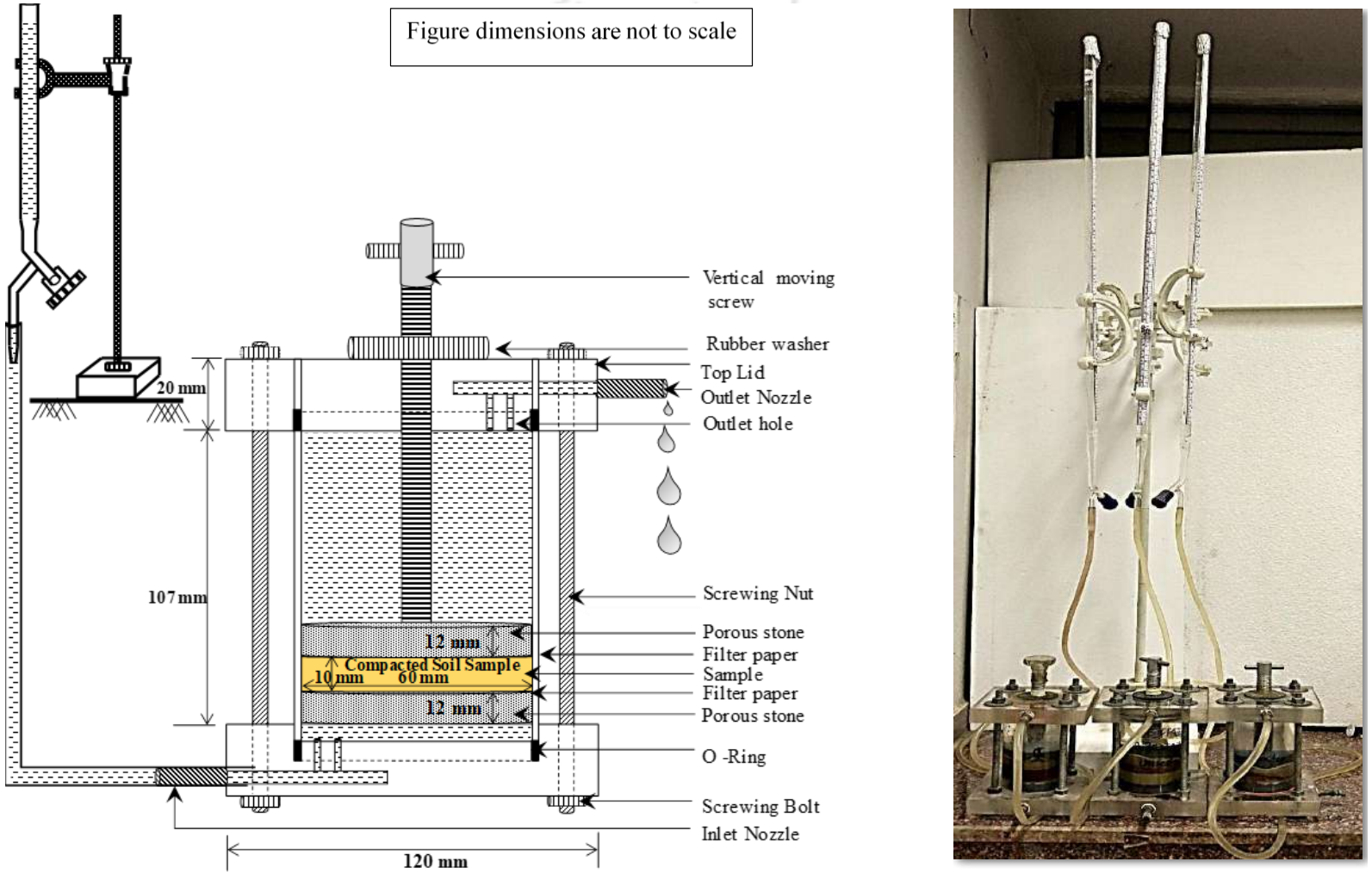


Figure 5.2: (a) Schematic diagram and (b) Pictorial view of in house developed hydraulic conductivity setup

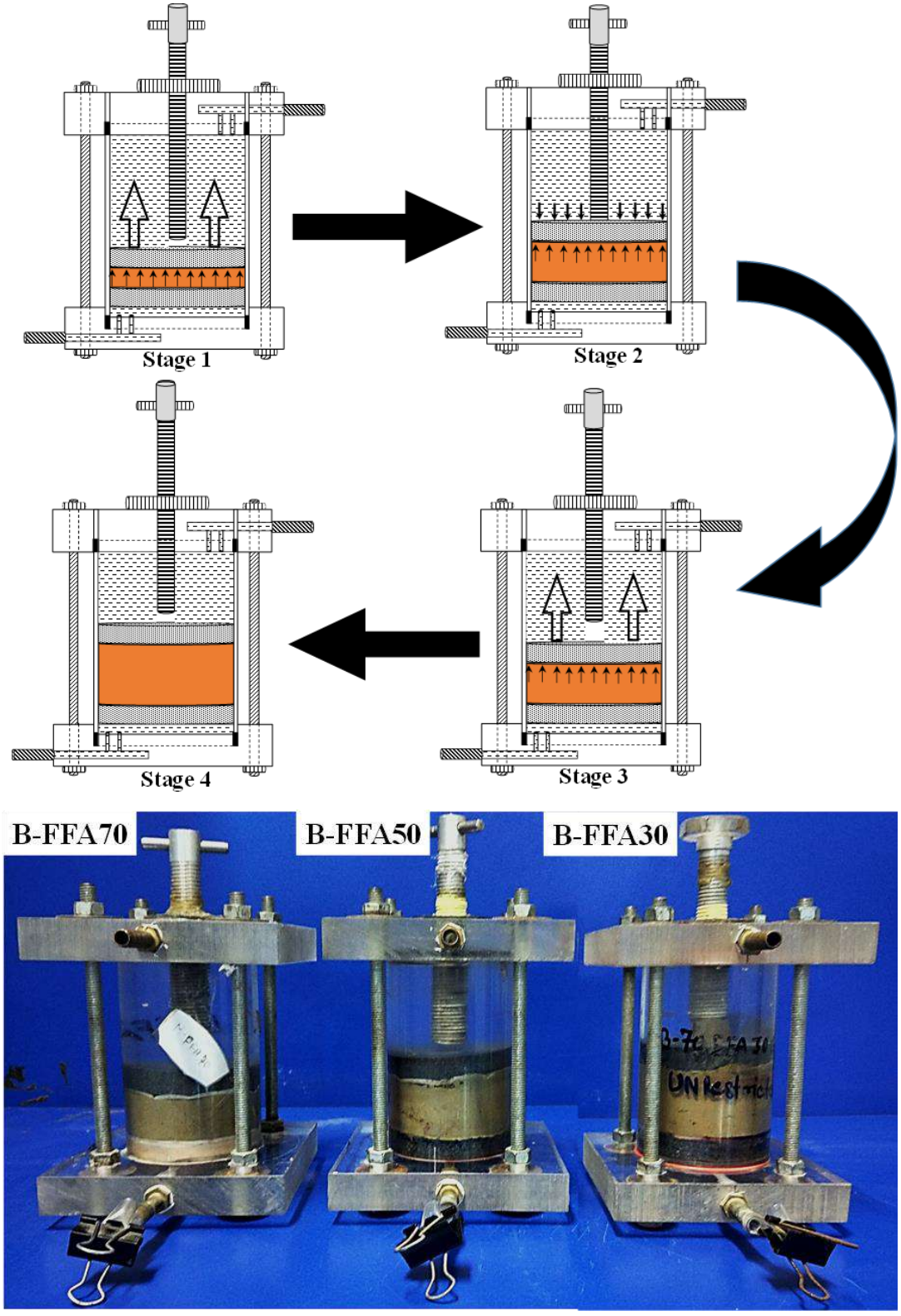


Figure 5.3: Schematic and pictorial view of B-FA mixes subjected to hydraulic conductivity measurement under free swelling condition

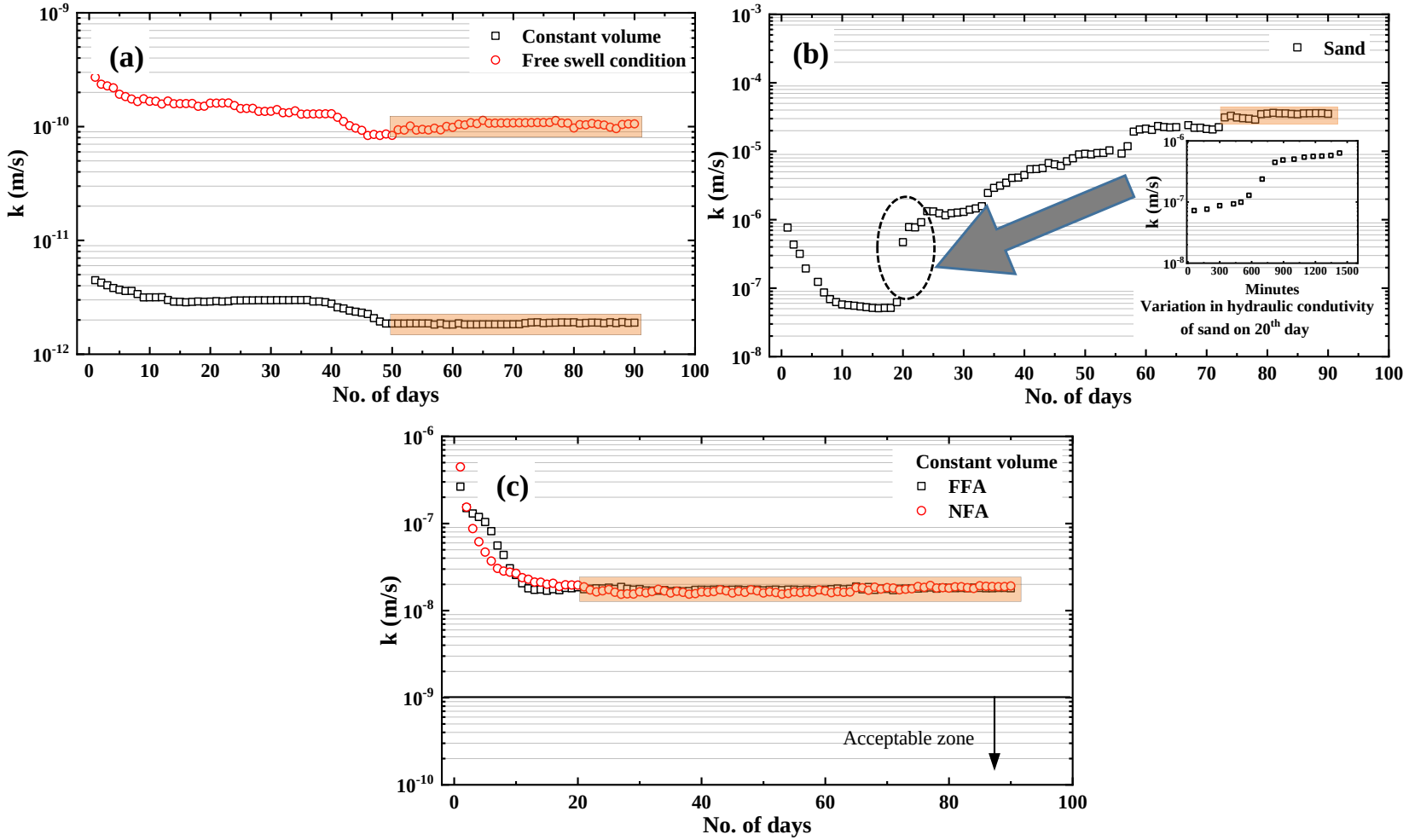


Figure 5.4: Temporal variation of hydraulic conductivity of parent geomaterials (a) B, (b) S, and (c) FAs

As k is directly proportional to e in case of clays (Mesri and Olson, 1971), it can be inferred that the magnitude of k will be higher than the constant volume condition. The temporal variation of k of bentonite for constant volume and free swell condition indicates progressive decrease in k with time and reaching a constant value equal to $k_{eq}$. The variation in k value prolongs for sufficient duration before it reaches $k_{eq}$. This is mainly due to the combined influence of (a) changes in the pore structure due to time dependent swelling phenomenon, and (b) achieving complete saturation. The influence of both these factors ceases beyond a certain time duration and k tends to a constant $k_{eq}$.

For a reactive material (swelling upon hydration) like B, the changes that happens within the pore structure will depend upon the swelling conditions (free swell, limited swell or constant volume). Since swelling is a time dependent phenomenon (long duration), this would induce changes in pore structure with time even though the saturation would have happened much earlier. This would result in changes in k with time and is a function of swelling. For both conditions, the equilibrium value ($k_{eq}$) was obtained at around 50 days for B. However, the measurement time was extended till 90 days to ensure that there are no further deviations from $k_{eq}$. In all the cases, the variation was negligible beyond 50 days. This clearly highlights the need for extended duration hydraulic conductivity test for reactive soils like B.

In the case of FA (Fig. 5.4c), pozzolanic reactivity leads to the progressive formation of calcium silicates hydrates (C-S-H) or calcium alumio-silicate hydrates (C-A-S-H) which leads to dense formation within the FA matrix (Fang and Zhang, 2020). FA reaches keq within 24 days as the pozzolanic activity ceases (Garg et al., 2020; Simatupang et al., 2020). A similar decreasing trend of hydraulic conductivity with elapsed time for the fly ashes was also reported by Pal and Ghosh (2013). The k for sands (Fig. 5.4b), decreases with elapsed time initially which might be attributed to particle rearrangement of sand because of seepage forces. The k variation was found to be less than 10% at around 17 to 20 days. However, after 20 days, the k increased exponentially by three orders of magnitude from 5 $\times 10^{-8}$ m/s to 3.5 $\times 10^{-5}$ m/s. This can be attributed to progressive saturation due to the expulsion of dissolved air from 85% to 100%. Such a trend was also reported by Chapuis et al. (2019) on sand with similar particle size distribution. This may also be attributed to the loss of fines held between coarser particles after complete saturation causing easy flow path. Generally, long-term $k_{eq}$ is not determined for swelling and non-swelling geomaterials

for majority of the flow test results reported in the literature. The results shown in this section is indicates the necessity of long-term flow monitoring required for determining $k_{eq}$, specifically for projects related to waste management.

### 5.1.5 Effects of fly ash class on keq of B-FA mixes

Figure 5.5 presents the temporal variation of k for both constant volume and free swell conditions of the bentonite-fly ash (B-FA) mixes. Similar to B, the k decreases with time until $k_{eq}$ is attained for all the B-FA mixes. The temporal variation in k for the B mixes can be attributed to the combined influence of (a) changes in the pore structure due to time dependent swelling phenomenon, (b) the formation of any reactive products within the pore space, and (c) achieving complete saturation. The formation of reactive products within the pores is also a time dependent process. Therefore, it is invariably necessary to perform long-term flow measurements to study whether there is any undesirable influence on k when two reactive materials are mixed together. Thus, the time required to achieve keq is dependent on the mix, class of FA and swelling condition. In constant volume cases, both Class C (NFA) and Class F (FFA) show a similar trend in the variation of $k_{eq}$, which increases with FA percentage. This can be discussed based on the arrangement of flaky B particles and spherical FA particles within the soil matrix. It was observed from the FESEM images (Fig. 5.6) that FA particles are sandwiched between flaky B particles at a lower amendment rate. On the contrary, B particles are sandwiched between the FA particles at a higher amendment rate (70%). This arrangement can be idealized based on the three-dimensional schematic diagram given in Fig. 5.6. At a lower amendment rate, the k of the mix is dependent primarily on the k of parent bentonite (refer Fig.5.4). However, at 70% FA amendment, the k is dependent on the flow channels between FA and B particles.

From Fig. 5.5, it can be further observed that B-NFA mixes exhibit higher keq than B-FFA for the same amendment rate. This can be discussed based on the high Ca content of the NFA (refer to table 2) that would suppress the formation of DDL. It also results in agglomeration of the B particles due to reactivity between FA and B forming ettringite minerals (Shizong et al., 1995). This was verified by conducting hydraulic conductivity experiments on bentonite-lime mixes at different lime amendment rates (refer Appendix Fig. A). Lime was mixed with bentonite at an amendment rate of 3%, 6%, and 10%. It is observed that $k_{eq}$ increases progressively by a magnitude of three orders with lime amendment from 3% to10%. At 3% lime content, the $k_{eq}$ was $1.8 \times 10^{-11}$ m/s, which was equivalent to $k_{eq}$ for

B-FFA mix at 70% amendment rate (Fig. 5.5a). Incidentally, the parent FFA has a lime content of around 3% (Table 3.4), which indicates that lime content in FA may influence $k_{eq}$. Nevertheless, in constant volume cases, all mixes with FFA amendment fulfil the minimum k criterion for landfill liners ($< 1 \times 10^{-9}$ m/s according to USEPA, 1989).

Under free swell conditions, the effect of percentage amendment on $k_{eq}$ is negligible for FFA (Fig. 5.5a), and all values fall within the acceptable limit of k ($< 1 \times 10^{-9}$ m/s) (Daniel, 1984; USEPA, 1989; Daniel and Benson, 1990; Yong, 2000). The $k_{eq}$ was attained at almost the same time for B-FFA mixes under free swell condition. This indicates that for B-FFA mixes, the swelling phenomenon was instrumental in decreasing k with time as compared to the contribution of any pozzolanic activity induced by FFA. For class C NFA under free swell condition, the $k_{eq}$ was attained early at about 25 days for high FA amendment rate (i.e. 50% and 70%). This indicates that upon completion of the pozzolanic activity, there will be limited changes in k associated with swelling and hence approaches keq. However, at low FA amendment rate of 30%, the $k_{eq}$ was obtained at around 61 days indicating that progressive swelling would play a dominant role in reaching an equilibrium flow condition. From the above discussion, it can be inferred that the maximum replacement (amendment) possible for Class C FA was 30% considering the $k_{eq}$ from constant volume and free swell condition. However, for Class F FA, the maximum replacement can be up to 70% for the compacted layer of landfill liner.

For completeness(USEPA, 1989), Figs. 5.7a and 5.7b presents the temporal variation of k of B-S mixes for constant volume and free swell condition. For constant volume condition, there is a gradual decrease in k by more than one order for all three B-S mixes. In comparison to B-FFA, the variation from initial k to $k_{eq}$ was high for B-S mixes. This is expected as sand particles are much coarser than FFA particles (Table 3.2). The $k_{eq}$ for both B-S mixes and B-FFA mixes at 30 and 50% amendment shows comparable magnitude. For B-FFA mix at 70% amendment, the k was higher than the B-S mix for the same proportion. This can be attributed to the marginal pozzolanic activity which resulted in the suppression of swelling. The time required to achieve $k_{eq}$ in case of B-S mix at constant volume condition was around 60 days for all amendment rate. In comparison to B-NFA mixes, the $k_{eq}$ of B-S mixes is lower in magnitude by at least one order. In the case of the free swell condition, the time required for achieving $k_{eq}$ is much faster (around 45 days) compared to the constant volume condition (around 60 days).

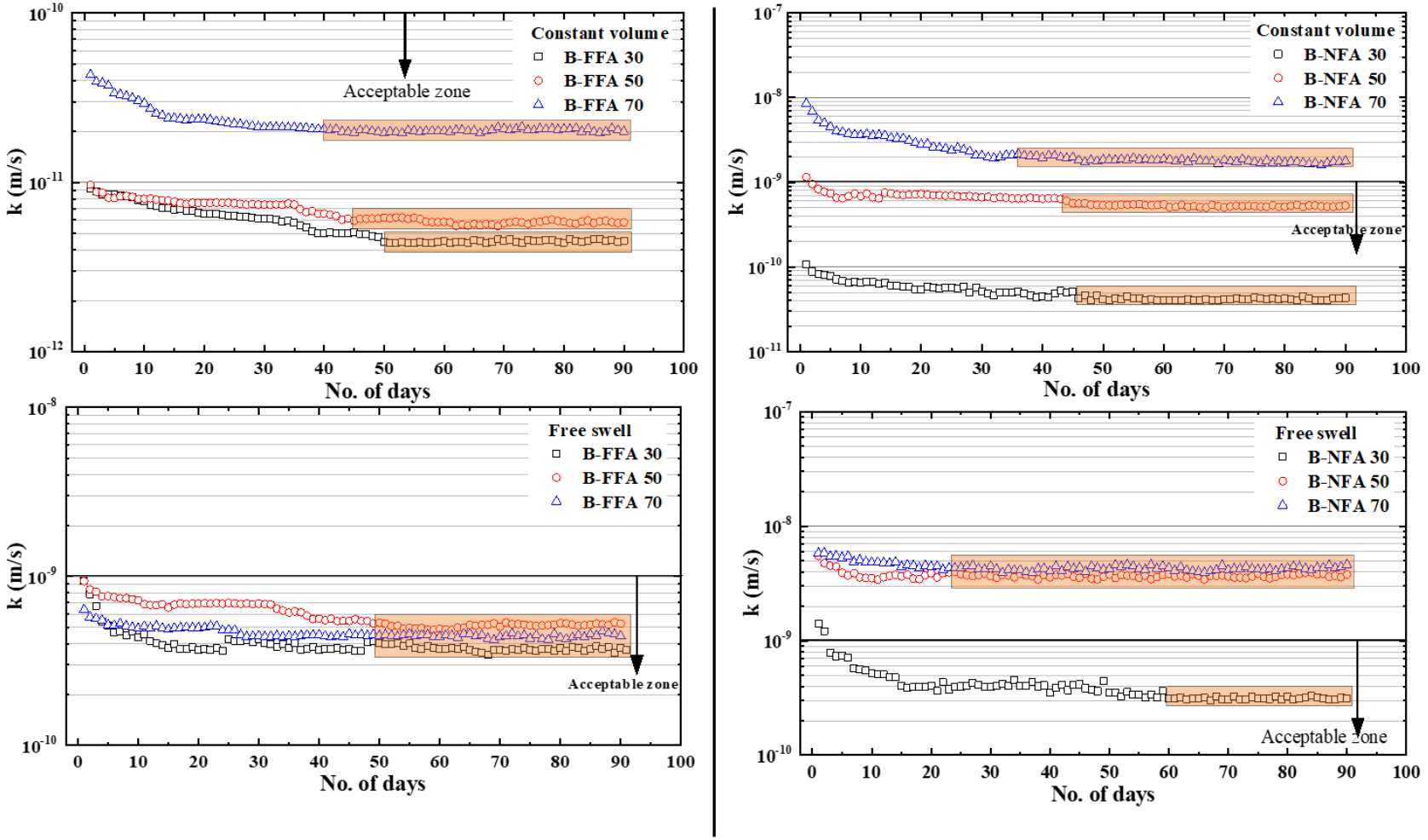


Figure 5.5: Effect of FA class (class C and class F) on hydraulic conductivity of B-FA mixes under constant volume and free swell condition for (a) FFA and (b) NFA

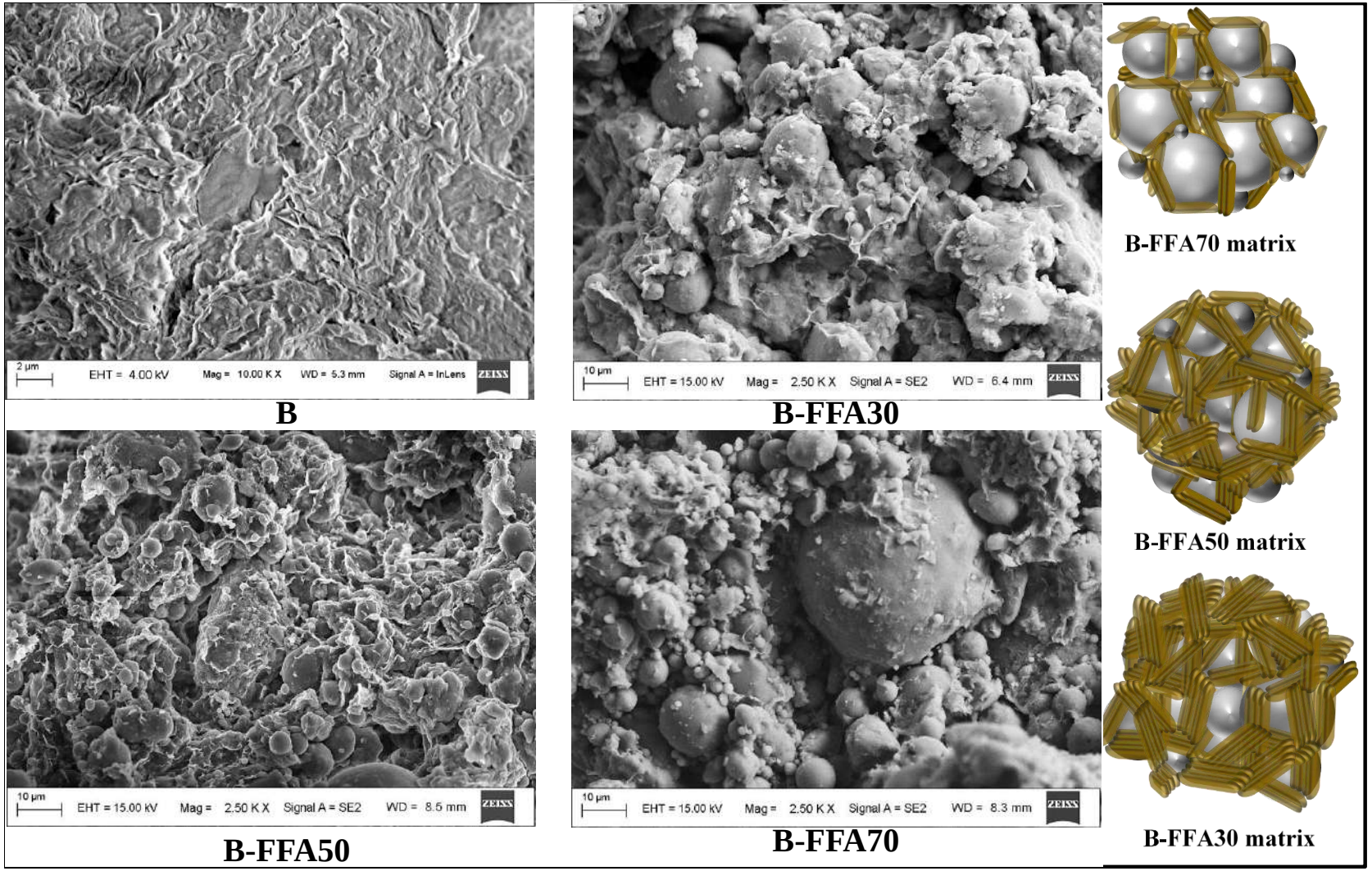


Figure 5.6: FESEM images of bentonite and its mixes in compacted state and schematic diagram of B-FFA mixes

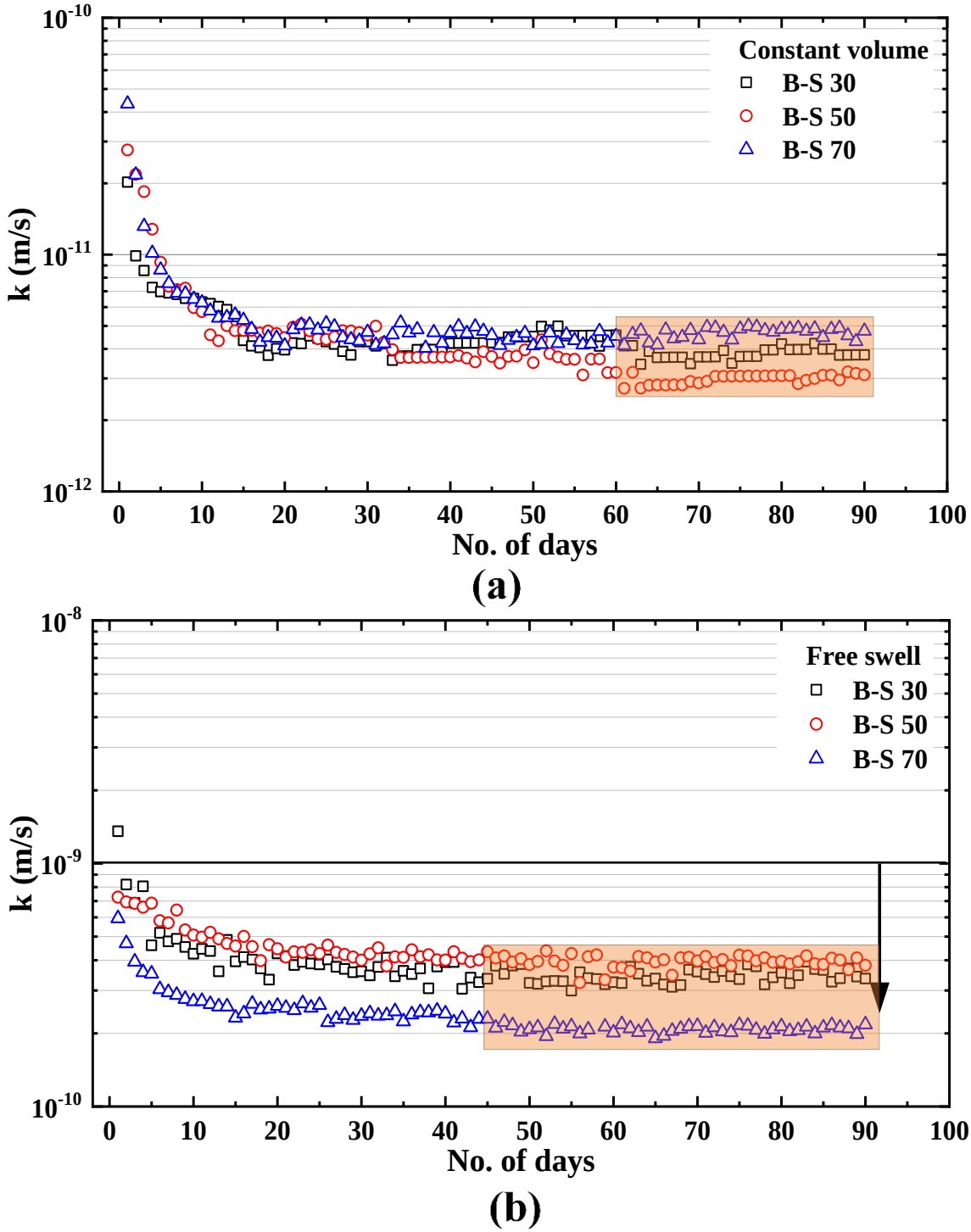


Figure 5.7: Temporal variation of hydraulic conductivity of B-S mixes under (a) constant volume and (b) free swell condition.

For free swell conditions, the pore structural changes associated with swelling was achieved much faster as compared to the constant volume case. Regardless of the amendment rate, $k_{eq}$ of B-S mixes was found to be equivalent to B-FFA mixes for free swell condition. This implies that Class F fly ash is a suitable material to replace S as an amendment material for

liner construction considering the k criterion, different swelling conditions and reactivity. The above observations highlight the importance of measuring k for extended duration of time under both constant volume and free swell condition considering the class of FA before using it in the field for liner construction.

### 5.1.6 Correlation of $k_{eq}$ with $k_{48}$, equilibrium time, and plasticity index

Figure 5.8a shows the variation of $k_{eq}$ with equilibrium time ($t_{eq}$) correlated using a power relationship represented by Eq. 5.2.

$$k_{eq} = 2804 t_{eq}^{-8.4} \tag{5.2}$$

The time $t_{eq}$ is inversely related to $k_{eq}$ with $R^2$ value of 0.86. There are not many studies that deals with keq and equilibrium time, specifically for B and B bases mixes. However, this empirical relationship is only valid for the specimen thickness considered in this study and for the sample compacted at OMC-MDD state. It can be inferred from the results that equilibrium time can be even more than a month. Hence, it will be beneficial if a correlation can be developed to estimate the $k_{eq}$ based on some initial value of k. Therefore, keq was correlated to hydraulic conductivity recorded at 48 hours ($k_{48}$) as shown in Figs. 5.8b and 5.8c, respectively for constant volume and free swelling condition. Two simple power equations represented by Eqs. 5.3 and 5.4 corresponding to constant volume and free swelling conditions, respectively, were fitted to the data points with $R^2 > 0.89$.

$$k_{eq} = 0.56 k_{48}^{1.02} \tag{5.3}$$

$$k_{eq} = 9.93 k_{48}^{1.14} \tag{5.4}$$

Figure 5.8d presents the $k_{eq}$ variation with a plasticity index (PI) of B, B-FA, B-S and B-lime mixes. It can be observed that the $k_{eq}$ decreases from $8.7 \times 10^{-9}$ to $3.8 \times 10^{-12}$ m/s with a corresponding increase in PI from 30 % to 130 %. This trend is consistent with the previous studies (Benson et al., 1994; Benson and Trast, 1995; Phani Kumar and Sharma, 2004; Pal and Ghosh, 2013; Mechleb et al., 2014). Only a marginal decrement from $3.8 \times 10^{-12}$ to $1.9 \times 10^{-12}$ m/s was noted for further increase in PI from 130 to 253. This trend was mainly applicable for the amendment percentage less than 50% in B (Table 3.5), where the amended material was sandwiched between B particles as depicted in Fig. 5.6.

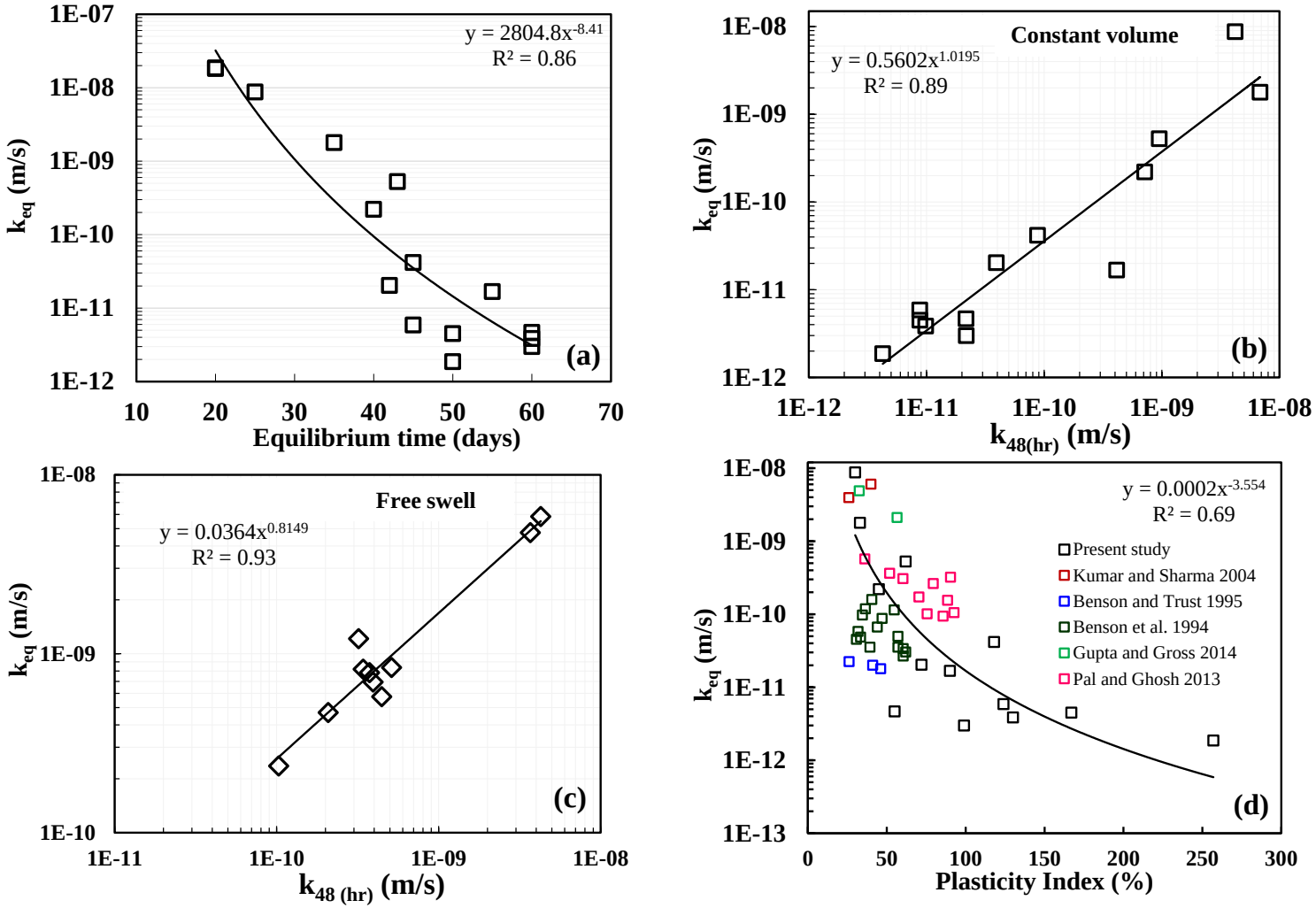


Figure 5.8: Correlation between $k_{eq}$ with (a) $t_{eq}$, (b) $k_{48}$ (hr) under constant volume (c) $k_{48}$ (hr) under free swell, and (d) Plasticity index

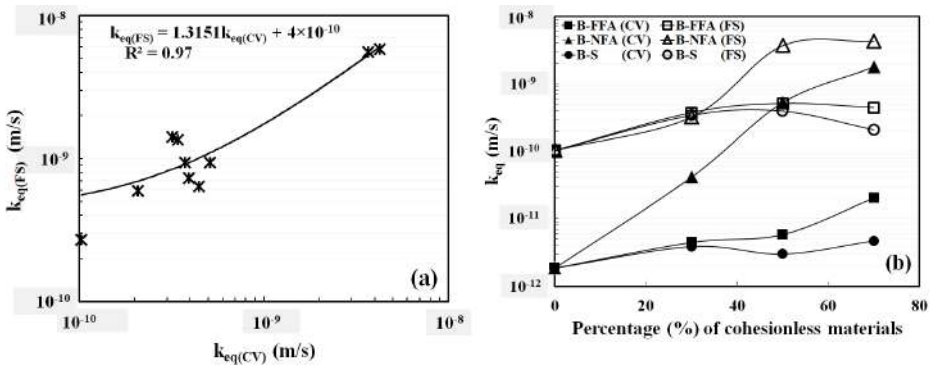


Figure 5.9: Correlation between free swell and constant volume equilibrium hydraulic conductivity ($k_{eq}$) and (b) variation of $k_{eq}$ with percentage amendment of cohesionless materials

It can be concluded that at lower amendment rate, k is governed by the B clay particles especially for the constant volume condition. An empirical power relationship was observed (Eq. 5.5) and presented in the figure incorporating test data from the current study.

$$k_{eq} = 0.00024PI^{-3.55} \tag{5.5}$$

Previous researchers have developed several correlations to predict k with the plasticity index (Mechleb et al., 2014; Dolinar, 2009; Zeng et al., 2020). However, most of the correlations are based on natural soils or clay with relatively low plasticity with duration of measurements $<$ 10 days. The advantage of the relationship presented in this study is that the estimated $k_{eq}$ correspond to long duration flow experiments. However, the empirical equations 2 to 4 are valid only for B, B -mixes with FA, S, lime and correspond to OMC-MDD compaction state. Figure 5.9a presents the variation of $k_{eq}$ corresponding to constant volume state ($k_{eq(CV)}$) with that of free swell state ($k_{eq(FS)}$). Conceptually, $k_{eq(CV)}$ and $k_{eq(FS)}$ represents the lowest and highest possible k that can be expected when the swelling B mixes is used in landfill liner. A simple exponential correlation between $k_{eq(FS)}$ and $k_{eq(CV)}$ is represented by Eq. 5.6 with $R^2$ =0.97.

$$k_{eq(FS)} = 1.32k_{eq(CV)} + 4.0 \times 10^{-10} \tag{5.6}$$

The implication of this relationship is that it provides a simple approach to estimate the $k_{eq(FS)}$ foreseeable in field conditions due to swelling (upon no overburden) during the construction and waste placement phase from the known value of $k_{eq(CV)}$. It may be noted that

$k_{eq(CV)}$ measured under controlled volume using rigid wall permeameter is relatively cheap, easy-to-conduct, and popular test in literature (Daniel et al., 1985; Bowders Jr and Daniel, 1987; Mollamahmutoğlu and Yilmaz, 2001; Chapuis, 2004; Ahn and Jo, 2009; Chapuis, 2012; Chapuis et al., 2019; Luo et al., 2020; Xu et al., 2020). There are not many results in the literature that deals with k variation with swelling wherein no confining stress is applied, unlike the flexible permeameter approach (Daniel et al., 1984; Daniel, 1994; Samingan et al., 2003; Benson and Yesiller, 2016). Figure 5.9b presents the variation in keq with percentage of cohesionless material amendment (30 50, 70) corresponding to both constant volume and free swell states, considering all mixes. Comparing $k_{eq(CV)}$ and $k_{eq(FS)}$ at a certain percentage finer, the possible range of $k_{eq}$ expected in field conditions can be assessed. For instance, in the liner mix with a percentage amendment of 50%, the range of k for B-NFA is less than one order of magnitude. However, at the same percentage, $k_{eq}$ differs by more than 2 order for B amended with class F FA. The observed variability of B-FFA mixes imply that it is imperative to consider $k_{eq(FS)}$ (maximum value) for designing the liner. Consideration of $k_{eq(CV)}$ for determining the liner layer thickness may lead to non-conservative design in the case of Class F FA.

### 5.1.7 Microstructure analysis of B-FA mixes

Figure 5.10 shows the FESEM micrographs of B-FFA and B-NFA mixes after the long-term k test. Under the constant volume and free swell condition, the surface morphology showed marked changes in terms of mineral formation and inter-particle void spaces. For B-FFA, the inter particle voids between spherical FA particles and flaky clay particles vary with swelling condition. Under constant volume condition, B-FFA exhibit micro void spaces (0.56 $\mu$m to 1.2 $\mu$m) with a relatively smaller flow channel than that of free swell conditions. Thus, the relatively larger void spaces between B and FFA in case of free swell conditions (1.67 $\mu$m to 3.95 $\mu$m) results in higher keq than that of constant volume condition. Regardless of B content in B-FFA mixes, the flow paths around the B-FA particles (highlighted in yellow in Fig. 5.10) were higher in free swell condition than those observed in constant volume state. This similarity in flow path size may be an indicator as to why the keq did not show any marked difference in magnitude, regardless of bentonite content in B-FFA for free swell condition. This change in pore space and flow channel was even more evident for B-NFA mixes, wherein the free swell condition resulted in pore space ranging from 2.86 $\mu$m to 9.25 $\mu$m.

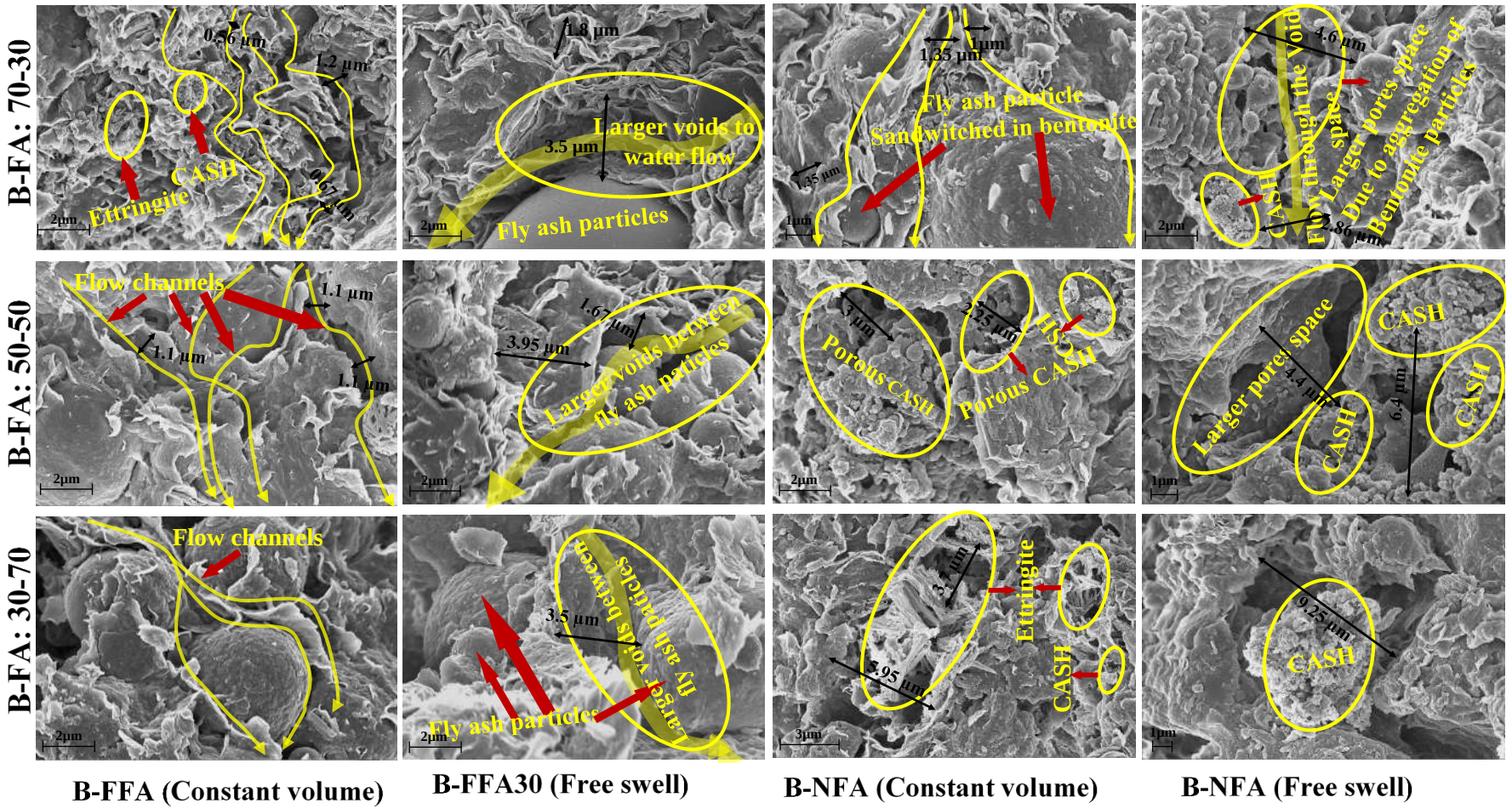


Figure 5.10: FESEM micrograph of B-FAs mixes under constant volume and free swell condition after 90 days water flow test

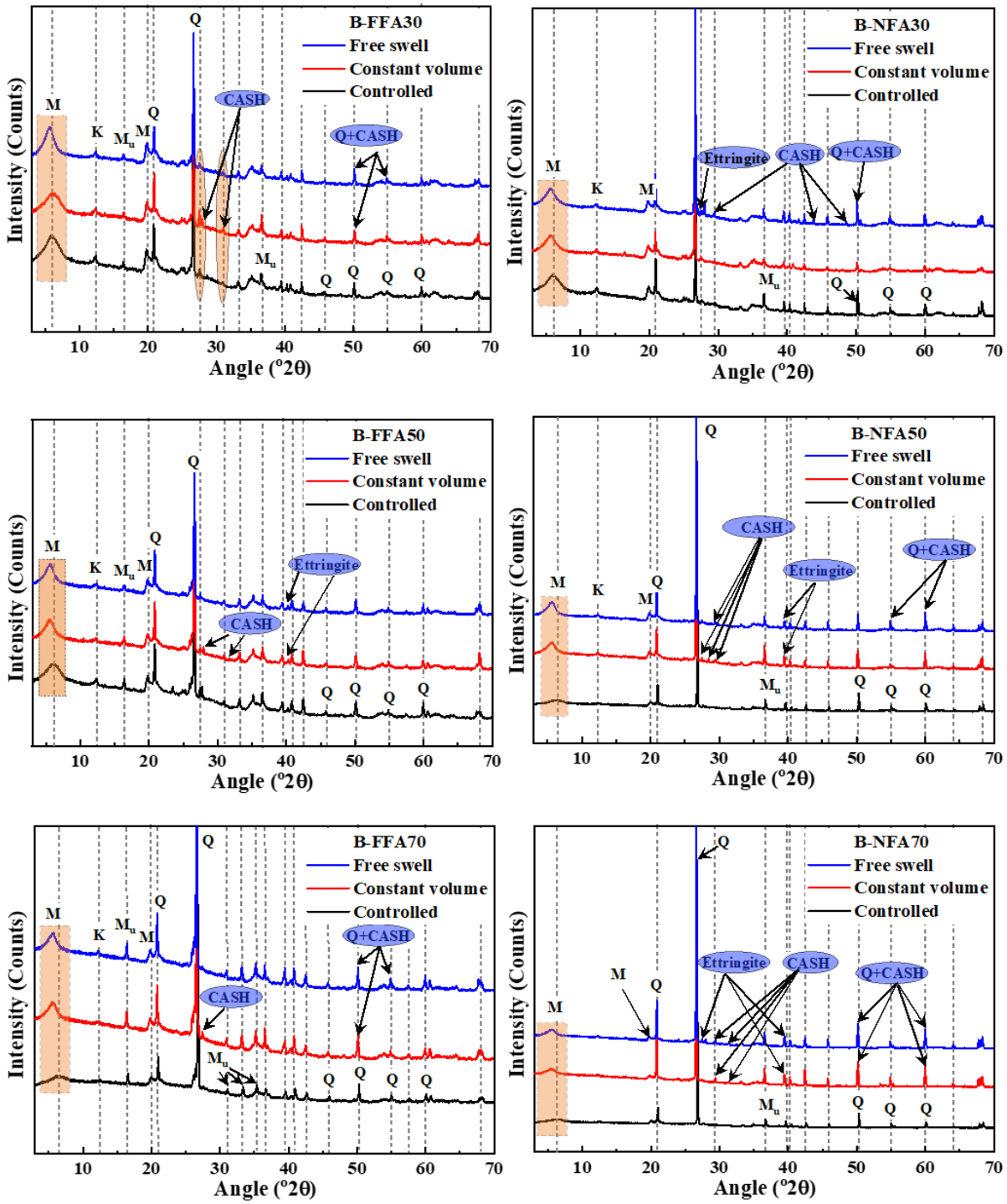


Figure 5.11: XRD pattern of B-FA mixes of control and after 90 days of water flow under constant volume and free swell condition

Moreover, the higher $k_{eq}$ observed for the B-NFA mixes can be attributed to the formation of porous CASH gel and ettringite needle-type mineral (Shizong et al., 1995). Aggregation of the B particle due to ettringite and CASH formation provides a less torturous path for water flow, ultimately increasing the $k_{eq}$ (Nalbantoglu and Tuncer, 2001). In case of B-FFA

mixes no aggregation of the bentonite particle was found up to 50% FFA mix (refer Fig. 5.10).

Figure 5.11 shows the XRD spectra of B-FFA and B-NFA mixes for air-dried mixed samples (control) and after the completion of long-term flow test (both constant volume and free swell). XRD spectra are generally used to verify the formation of gel like formation in a porous material (Garbev et al., 2008; Li et al., 2019). Peaks of C-A-S-H in the spectra at constant volume and free swell conditions indicated that these minerals are formed due to the interaction of B with FA during the tests, which resulted in keq variation. Furthermore, peaks corresponding to ettringite minerals were detected in B-NFA mixes regardless of mixing ratio, while only a slight peak was detected for B-FFA 50. It can be noted that for all the mixes under constant volume and free swell conditions, the peak depicting montmorillonite clay mineral shifted to a lower value of $2\theta^o$ as compared to control. This change in peak position was mainly attributed to the complete saturation of the samples, which changes the interlayer spacing (2:1 unit spacing) of the bentonite particles.

Figure 5.12 presents the FTIR spectra of B-FFA, and B-NFA mixes for air-dried samples (control) and after the completion of long-term flow test (both constant volume and free swell). The quantitative measure of the pozzolanic reaction of a material can also be confirmed by the shift of FTIR peaks, both in terms of peak intensity and change in peak wave number (Geng et al., 2017). The transmittance band in the range 1100 $cm^{-1}$ to 900 $cm^{-1}$ is related to the asymmetric stretching vibration of Si-O-T (Abdalqader et al., 2016). The presence of a band near the wavenumber of 795 $cm^{-1}$ is indicative of the symmetric and asymmetric vibration due to the Al-OH band in $Al(OH)_6$ octahedral structure of FA. Moreover, a reduction in the peak intensity near the wavenumber of 795 $cm^{-1}$ is a strong indicator for the formation of CASH gel. Furthermore, a shift near 470 $cm^{-1}$ wavenumbers confirms the involvement of Si-O-Si in the formation of CASH in B-FA mixes. The formation of CASH minerals was also evident based on the widening of the transmittance band near the wavenumber 3640 $cm^{-1}$ (Kapeluszna et al., 2017). It is revealed from the FTIR spectra that the highest change in peak intensity in the functional groups occurred for NFA, indicating its pozzolanic reactivity. As -OH peak intensity decreases significantly and shifts in wavenumber, it is a clear indication that pozzolanic reactions have occurred, resulting in minerals such as CASH and ettringite.

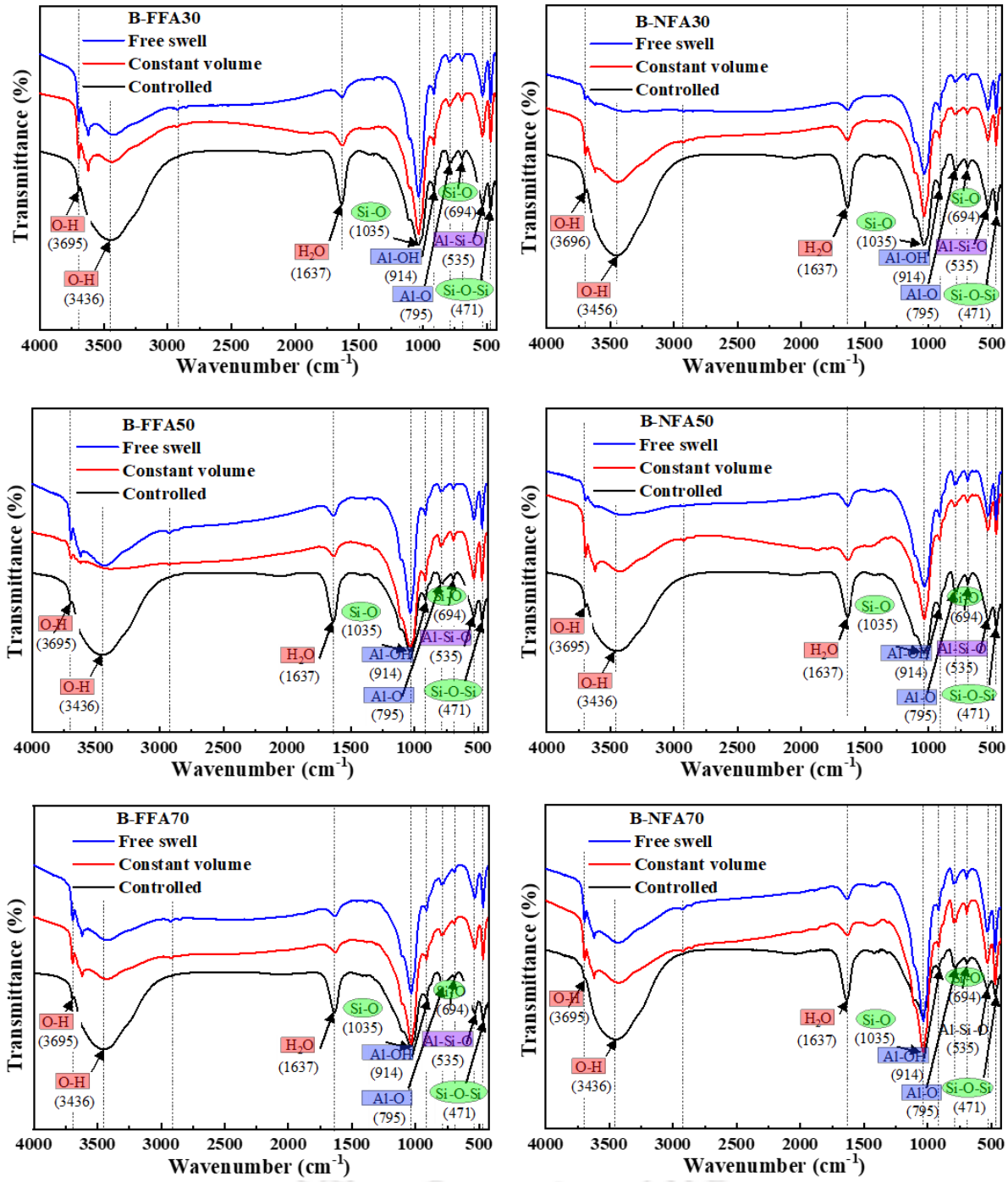


Figure 5.12: FTIR spectroscopy of B-FA mixes of control and after 90 days of water flow under constant volume and free swell condition

## 5.2 Variation of hydraulic conductivity with time of interaction between B and FA

It is hypothesized that the long-term interaction between B and FA may induce changes in the pore structure and result in k variation. This is mainly due to the fact that both B and

FA are reactive materials capable of altering the microstructure, diffuse double layer development and hence the flow/ contaminant retention characteristics of the mixes. Therefore, it is necessary to understand whether there will be an increase in k or decrease in contaminant retention characteristics due to long-term interaction that would disqualify the mix for its application in liner construction. This section essentially deals with the impact of long-term interaction of different B-FA mixes on $k_{eq}$ . Different B-FA mixes designated in Table 3.5 was compacted at OMC+2%-MDD, packed in polythene cover and stored in a desiccator maintained at relative humidity more than 90 % for required interaction time ranging from 0, 6, 12, 24, 36 and 48 months. Efforts were made to minimize moisture loss and shrinkage using the dessicator maintainted at relative humidity more than 90%. For verification, moisture content was determined from trial samples at the end of interaction time. It was noted that a maximum difference in moisture content was noted for the sample corresponding to 48 months and was less than 1%. The mix subjected to k measurement immediately after compaction (after moisture maturation as stated in section 5.2.1) is considered as no interaction. The k measurement of each samples was performed up to 90 days under both constant volume and free swell condition as stated in section 5.3.2. For every interaction time and swelling conditions, three identical samples were tested and an additional sample kept for moisture content determination.

The repeatability of the k measurements with different interaction time is presented in Fig. 5.13 for selected samples. It is noted that the observations were fairly repeatable and similar trends were observed for all other samples. For sake of brevity, the repeatability of other samples are not presented here. Figures 5.14 to 5.21 presents the k variation with time for all B-FA mixes subjected to different interaction time, constant volume and free swell conditions. Since the results are repeatable, only one k variation with time curve is presented for each sample. This was needed for comparing the results with more clarity. It can be noted from all the figures that there is a decrease in k with time and attains a constant value which is considered to be the equilibrium value (as discussed in section 5.2.1). This trend of k variation with time is identical for all interaction times and for both constant volume and free swell conditions. However, a marginal deviation of this trend was noted for class C NFA for higher interaction time and the mix constituting 70 % FA. The final equilibrium k value was obtained from all the results (as stated in section 5.3.2) and tabulated in Tables 5.1 and 5.2 for constant volume and free swelling condition,

respectively.

The variation of $k_{eq}$ with interaction time for B-FA mixes corresponding to constant volume and free swelling condition is shown in Figs. 5.22 and 5.23, respectively. Considering constant volume condition, it can be noted that except one case of B-NFA mix, all the B-FA mixes qualify the hydraulic conductivity criterion for liners and covers, when the mix is restricted to 50% FA. For 70% FA, the class C NFA was found to exhibit k $10^{-9}$ m/s. However, it is noteworthy that all class F FA qualified the k criterion even at 70% FA in the mix. Under free-swell condition, even the 50% FA mix was not suitable for class C NFA. For all other FAs, the equilibrium k was found to be $10^{-9}$ m/s.

The results of $k_{eq}$ for all the B-FA mixes and interaction time was plotted together for constant volume and free swell condition. Unlike for zero time interaction (Fig. 5.24) there is no clear relationship between free-swell and constant volume $k_{eq}$. This figure can be considered as a final summary of all the results pertaining to the k of B-FA mixes. The k of constant volume condition is at least one order of magnitude less than the free swell condition. Except for class C FA, all other samples qualify k criterion. For free-swell condition majority of the NFA samples exceeded k of $10^{-9}$ m/s. Overall, class C FA should be used with proper caution in the case of liner and cover construction whereas class F FA qualifies the k criterion satisfactorily under most of the condition (interaction time and swelling) investigated in this study.

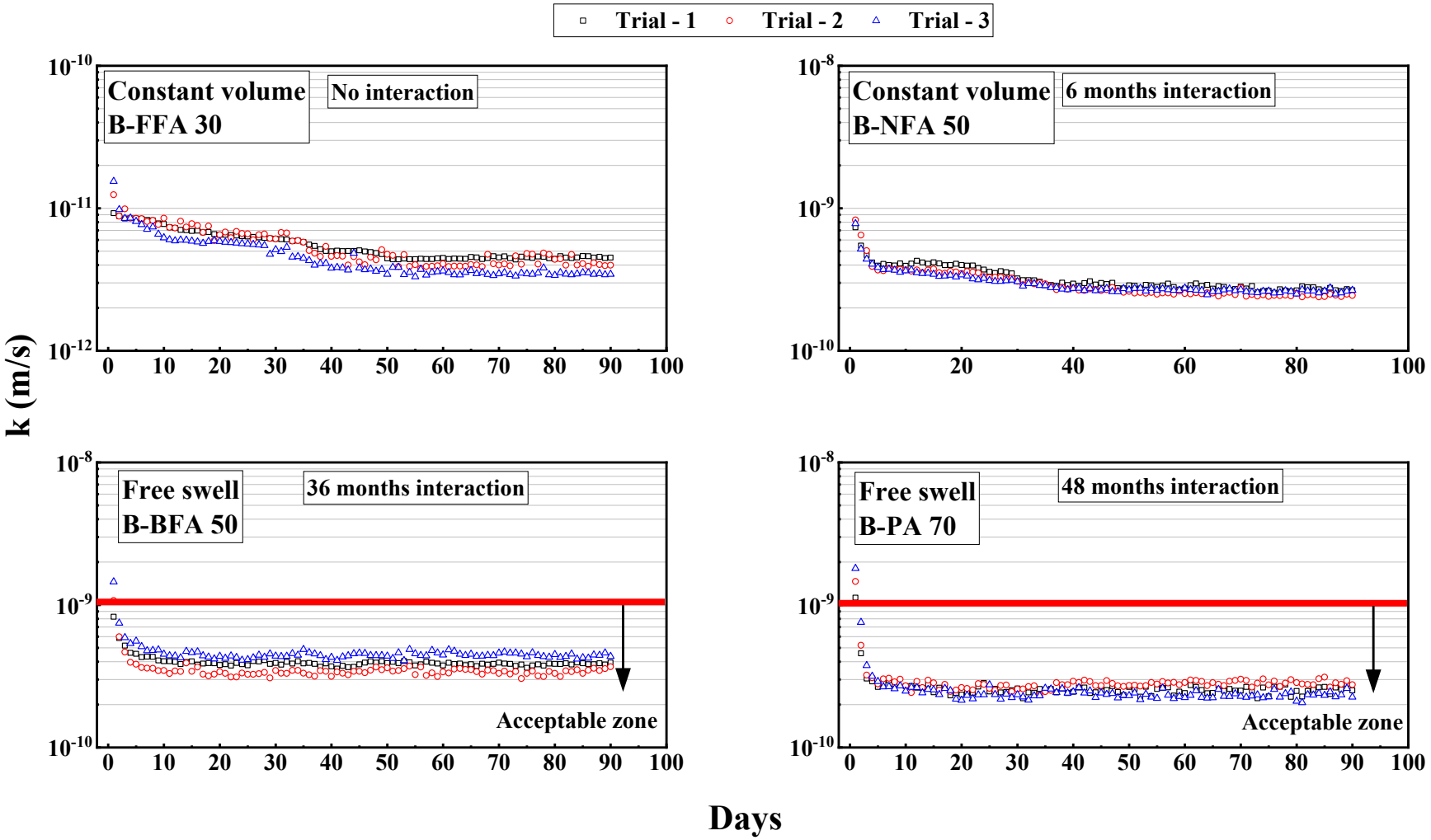


Figure 5.13: Repeatability of the test results for different interaction time and different mixes of B-FA under constant volume and free swell conditions

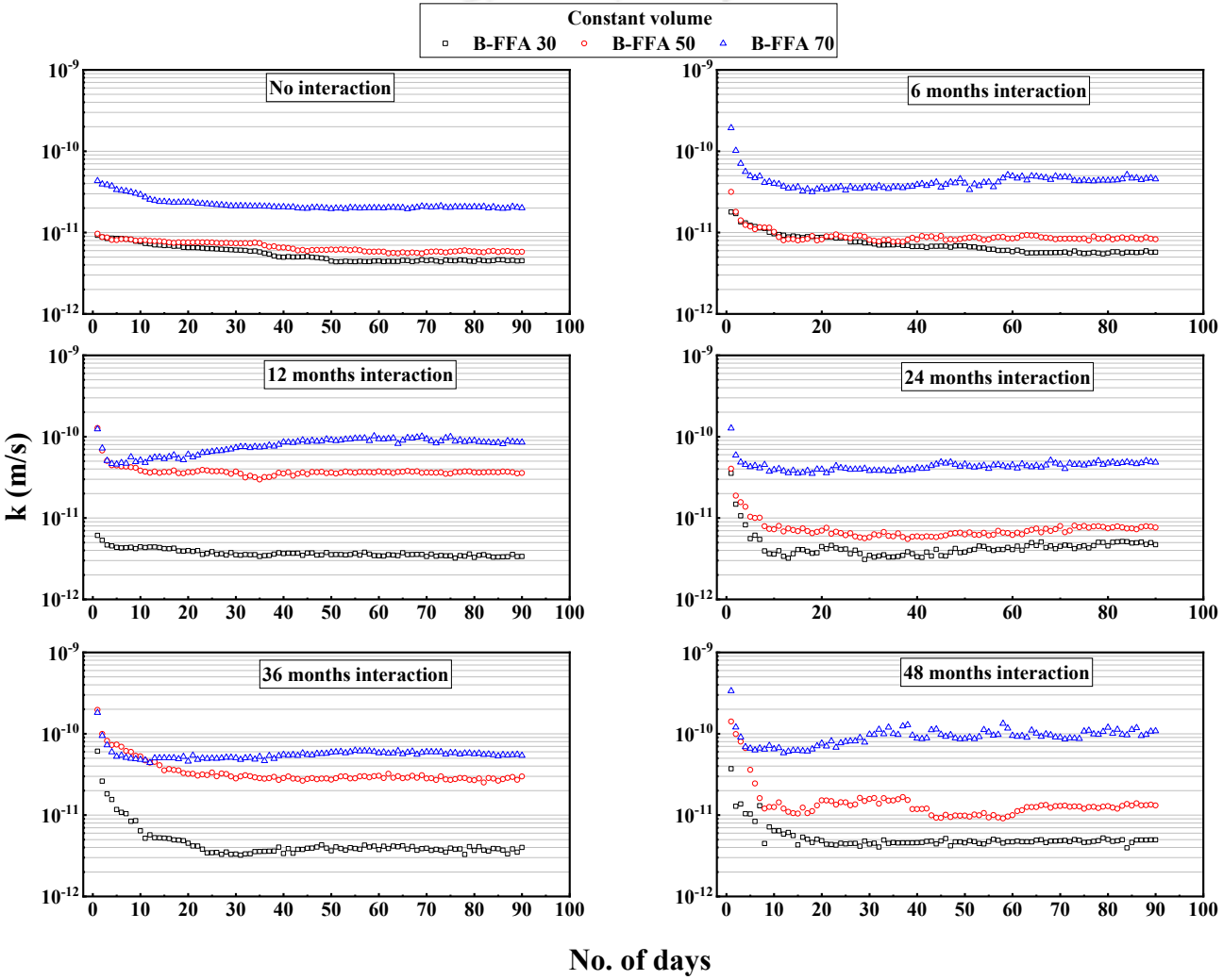


Figure 5.14: Variation in hydraulic conductivity with interaction time of B-FFA mixes under constant volume conditions

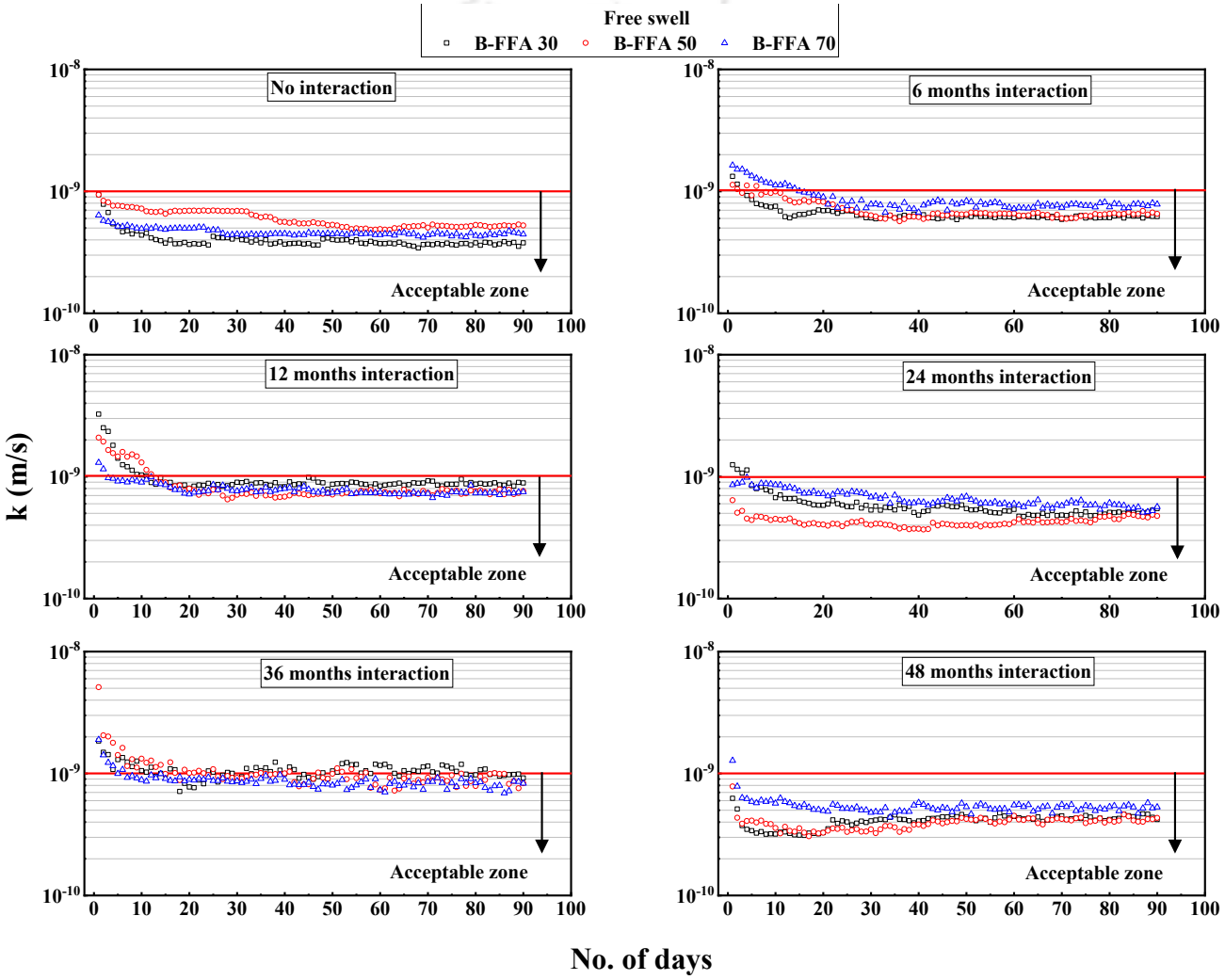


Figure 5.15: Variation in hydraulic conductivity with interaction time of B-FFA mixes under free swelling conditions

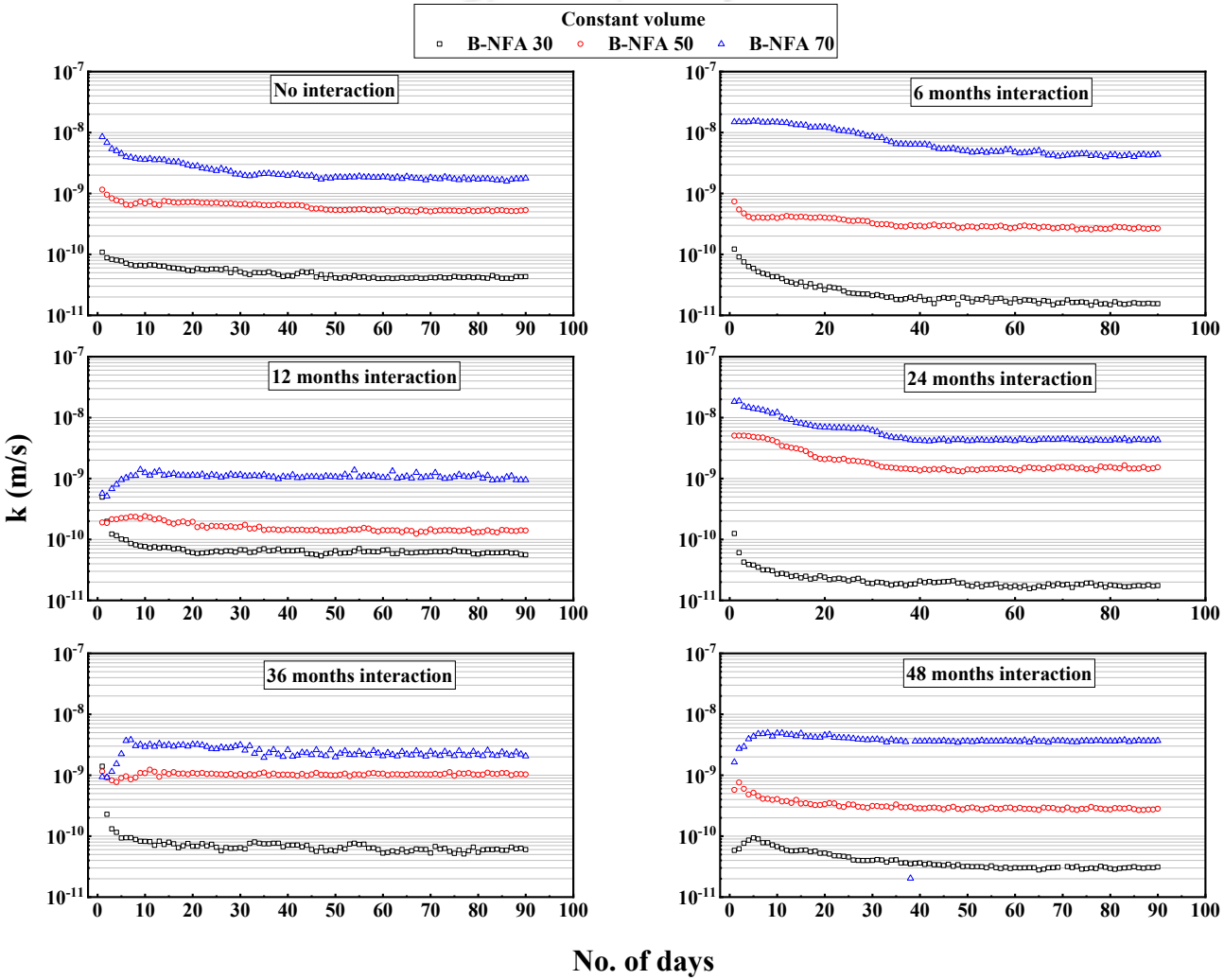


Figure 5.16: Variation in hydraulic conductivity with interaction time of B-NFA mixes under constant volume conditions

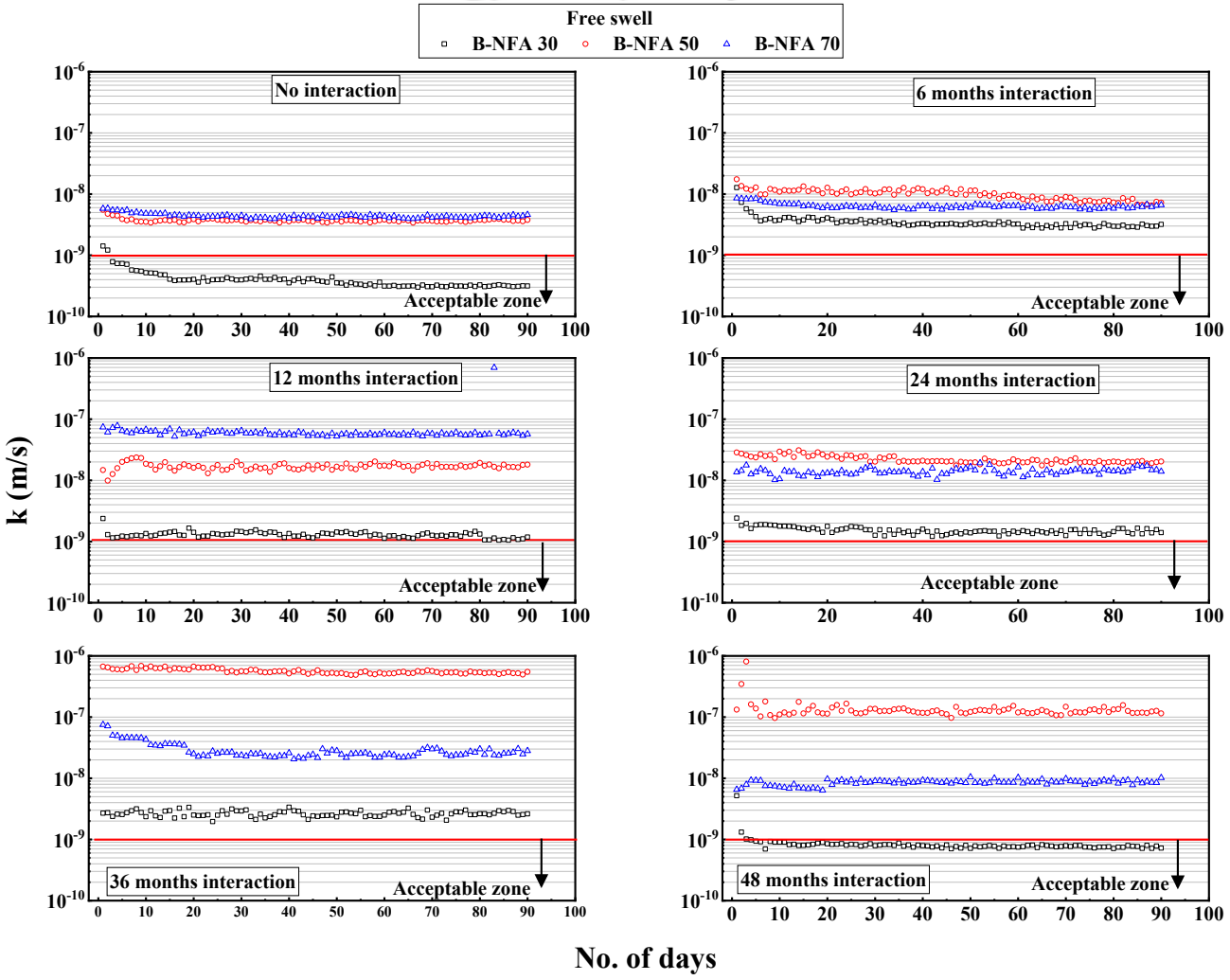


Figure 5.17: Variation in hydraulic conductivity with interaction time of B-NFA mixes under free swelling conditions

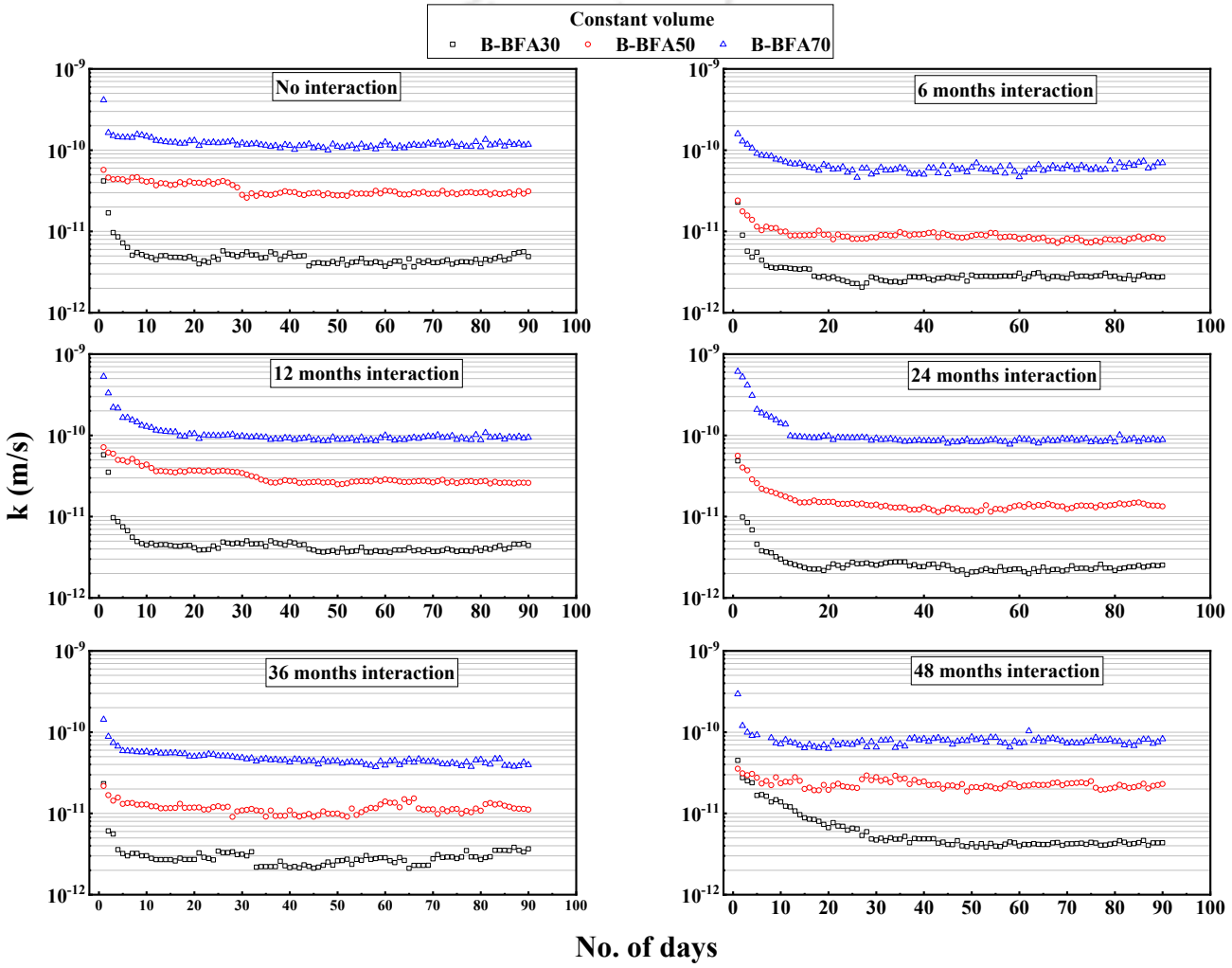


Figure 5.18: Variation in hydraulic conductivity with interaction time of B-BFA mixes under constant volume conditions

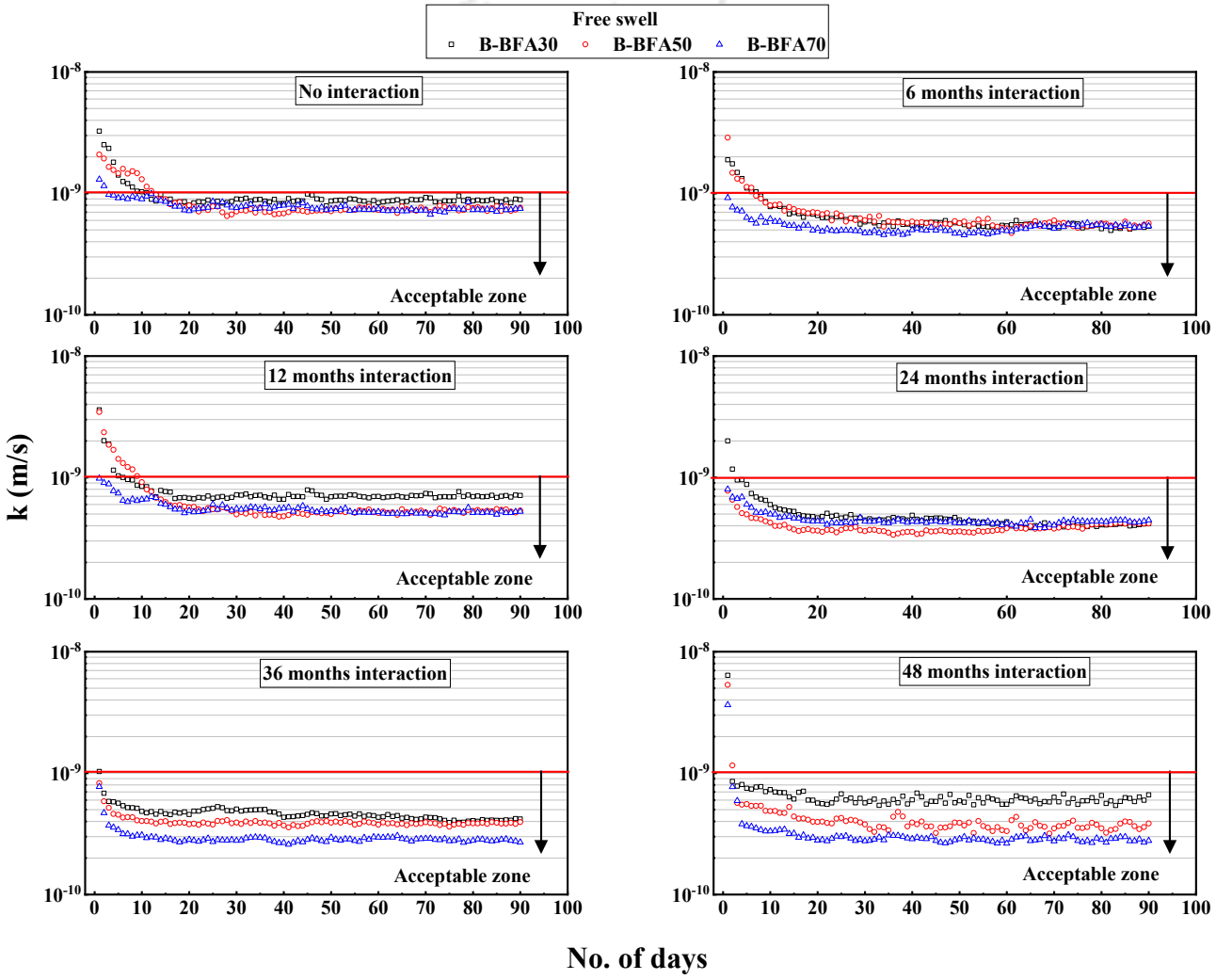


Figure 5.19: Variation in hydraulic conductivity with interaction time of B-BFA mixes under free swelling conditions

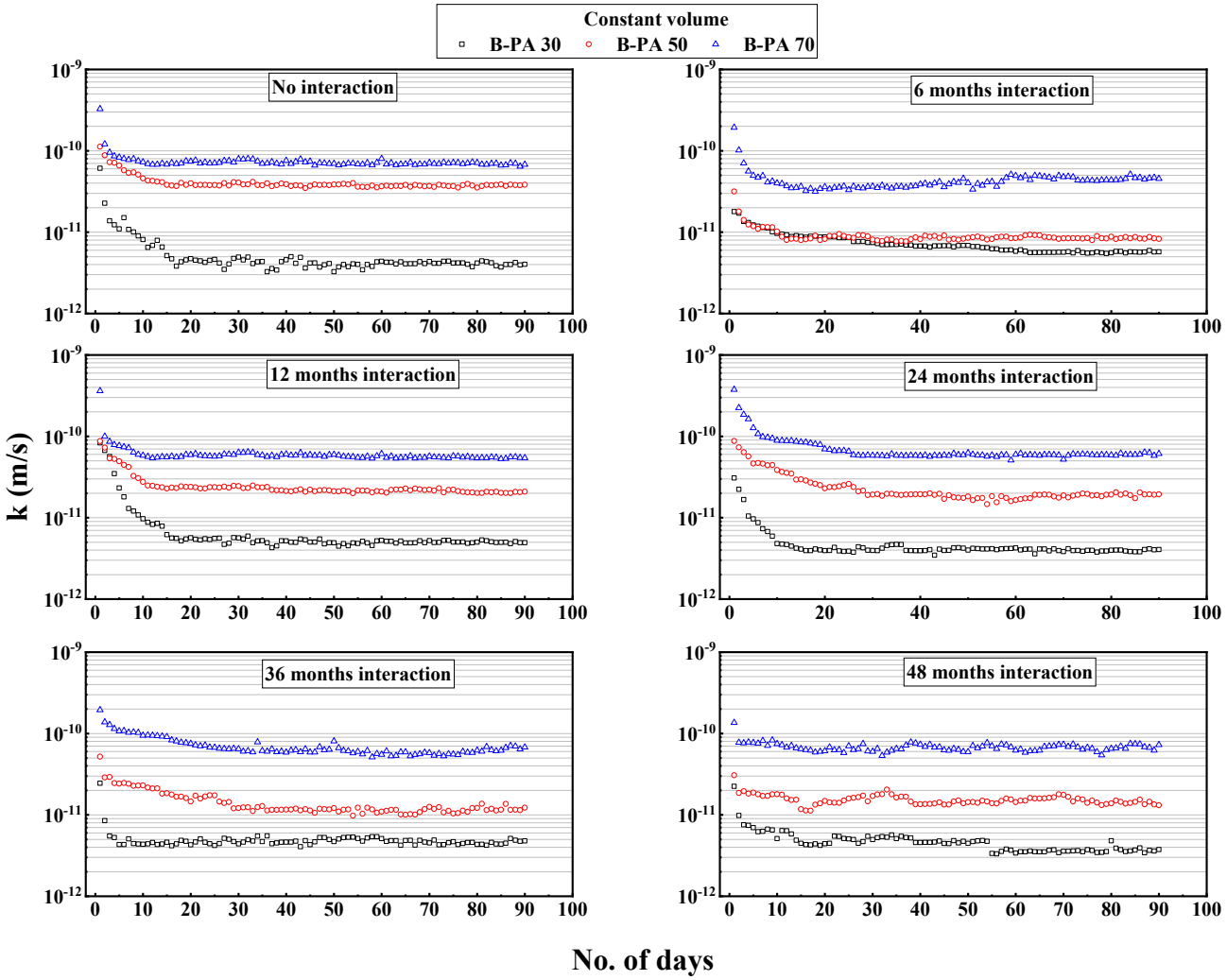


Figure 5.20: Variation in hydraulic conductivity with interaction time of B-PA mixes under constant volume conditions

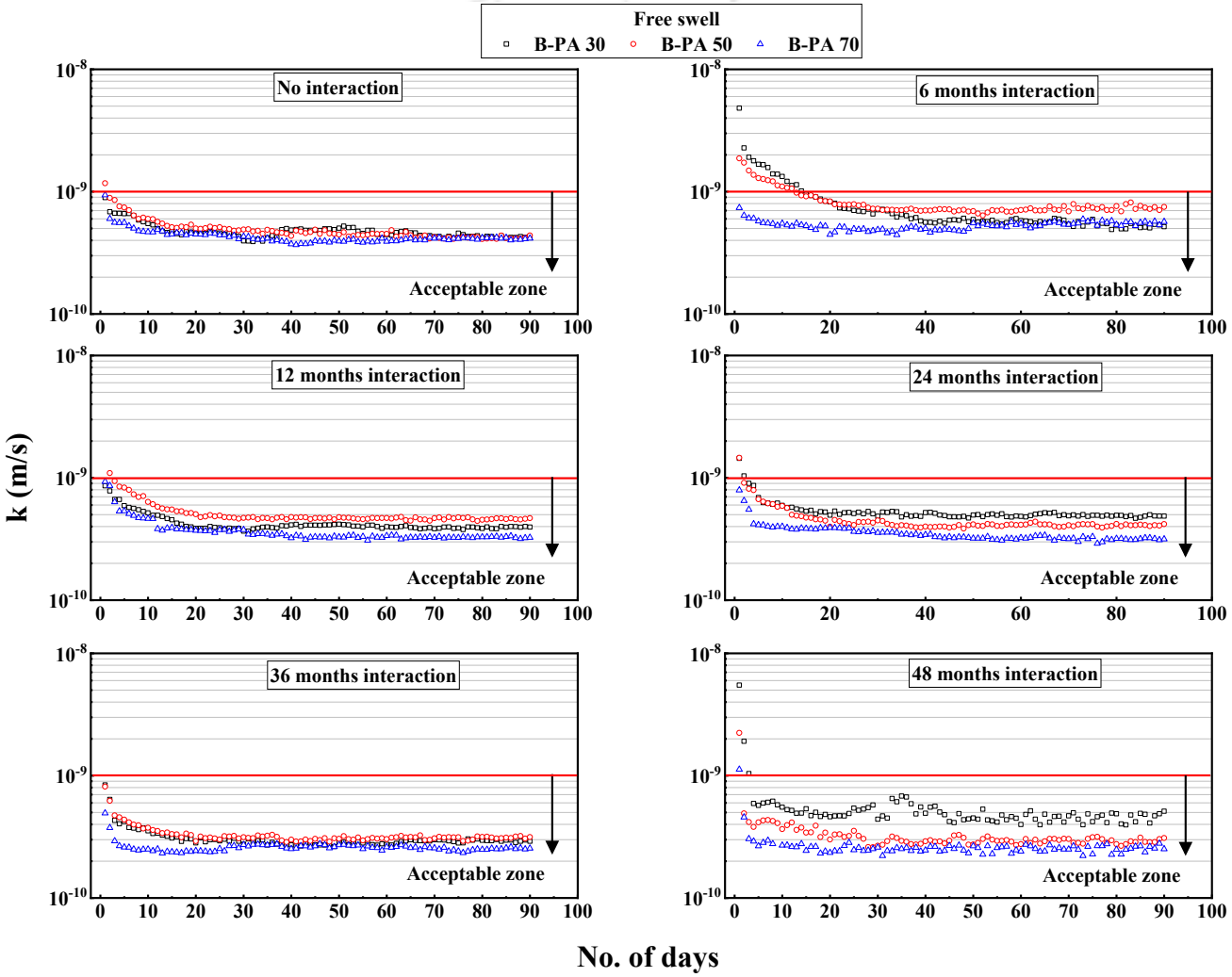


Figure 5.21: Variation in hydraulic conductivity with interaction time of B-PA mixes under free swelling conditions

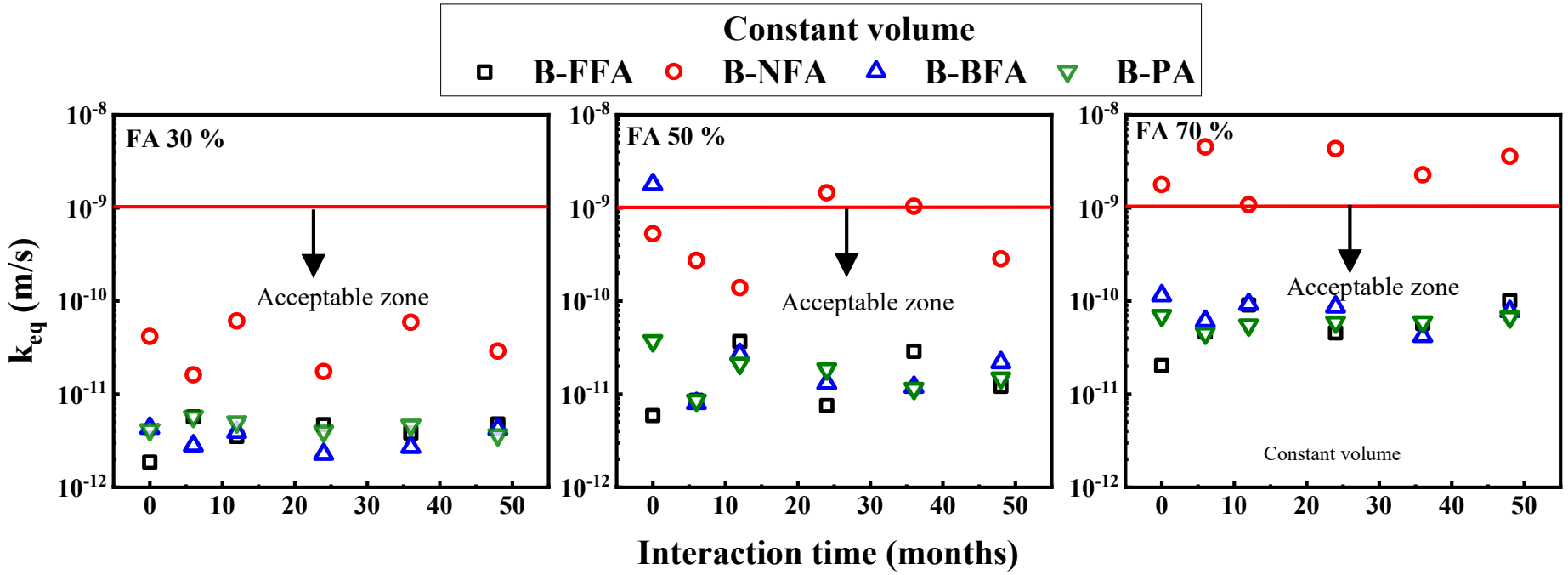


Figure 5.22: Variation of $k^{eq}$ with interaction time for B-FA mixes corresponding to constant volume condition

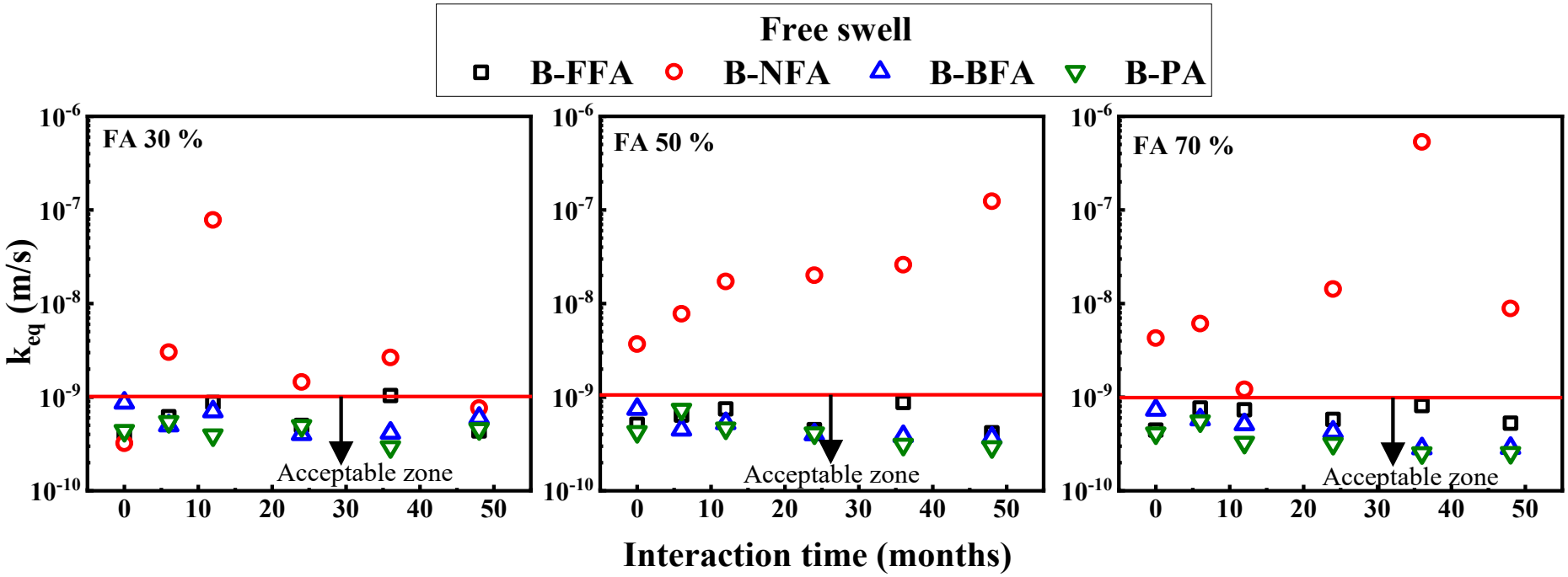


Figure 5.23: Variation of $k^{eq}$ with interaction time for B-FA mixes corresponding to free swell condition

Table 5.1: $k_{eq}$ (in m/s) of B-FA mixes corresponding to different interaction time and constant volume condition

| Sample | Interaction time (in months) | | | | | |
|---|---|---|---|---|---|---|
| | 0 | 6 | 12 | 24 | 36 | 48 |
| B-FFA 30 | 1.86E-12 | 5.68E-12 | 3.50E-12 | 4.70E-12 | 3.81E-12 | 4.77E-12 |
| B-FFA 50 | 5.87E-12 | 8.56E-12 | 3.66E-11 | 7.51E-12 | 2.88E-11 | 1.21E-11 |
| B-FFA70 | 2.03E-11 | 4.63E-11 | 9.07E-11 | 4.55E-11 | 5.73E-11 | 1.01E-10 |
| B-NFA 30 | 4.16E-11 | 1.61E-11 | 6.11E-11 | 1.75E-11 | 5.92E-11 | 2.89E-11 |
| B-NFA 50 | 5.26E-10 | 2.73E-10 | 1.39E-10 | 1.45E-09 | 1.04E-09 | 2.83E-10 |
| B-NFA 70 | 1.78E-09 | 4.52E-09 | 1.08E-09 | 4.32E-09 | 2.26E-09 | 3.56E-09 |
| B-BFA 30 | 4.32E-12 | 2.80E-12 | 3.92E-12 | 2.28E-12 | 2.70E-12 | 4.22E-12 |
| B-BFA 50 | 1.79E-09 | 7.98E-12 | 2.68E-11 | 1.31E-11 | 1.19E-11 | 2.19E-11 |
| B-BFA 70 | 1.15E-10 | 6.12E-11 | 9.26E-11 | 8.68E-11 | 4.19E-11 | 7.77E-11 |
| B-PA 30 | 4.11E-12 | 5.72E-12 | 4.99E-12 | 3.97E-12 | 4.58E-12 | 3.63E-12 |
| B-PA50 | 3.72E-11 | 8.56E-12 | 2.13E-11 | 1.86E-11 | 1.15E-11 | 1.48E-11 |
| B-PA70 | 6.96E-11 | 4.48E-11 | 5.51E-11 | 5.90E-11 | 5.95E-11 | 6.69E-11 |

Table 5.2: $k_{eq}$ (in m/s) of B-FA mixes corresponding to different interaction time and free swelling condition

| Sample | Interaction time (in months) | | | | | |
|---|---|---|---|---|---|---|
| | 0 | 6 | 12 | 24 | 36 | 48 |
| B-FFA 30 | 3.74E-10 | 6.16E-10 | 8.76E-10 | 4.98E-10 | 1.04E-09 | 4.34E-10 |
| B-FFA 50 | 5.12E-10 | 6.41E-10 | 7.46E-10 | 4.48E-10 | 8.78E-10 | 4.17E-10 |
| B-FFA70 | 4.45E-10 | 7.66E-10 | 7.33E-10 | 5.78E-10 | 8.13E-10 | 5.26E-10 |
| B-NFA 30 | 3.21E-10 | 3.02E-09 | 7.83E-08 | 1.45E-09 | 2.66E-09 | 7.65E-10 |
| B-NFA 50 | 3.68E-09 | 7.78E-09 | 1.72E-08 | 2.01E-08 | 5.33E-07 | 1.24E-07 |
| B-NFA 70 | 4.27E-09 | 6.10E-09 | 1.21E-09 | 1.43E-08 | 2.60E-08 | 8.84E-09 |
| B-BFA 30 | 8.74E-10 | 4.98E-10 | 7.02E-10 | 4.02E-10 | 4.17E-10 | 6.02E-10 |
| B-BFA 50 | 7.46E-10 | 4.48E-10 | 5.27E-10 | 4.01E-10 | 3.84E-10 | 3.68E-10 |
| B-BFA 70 | 7.33E-10 | 5.78E-10 | 5.13E-10 | 4.27E-10 | 2.84E-10 | 2.86E-10 |
| B-PA 30 | 4.36E-10 | 5.44E-10 | 3.92E-10 | 4.93E-10 | 2.93E-10 | 4.56E-10 |
| B-PA50 | 4.26E-10 | 7.34E-10 | 4.63E-10 | 4.11E-10 | 3.11E-10 | 2.93E-10 |
| B-PA70 | 4.11E-10 | 5.52E-10 | 3.27E-10 | 3.18E-10 | 2.53E-10 | 2.54E-10 |

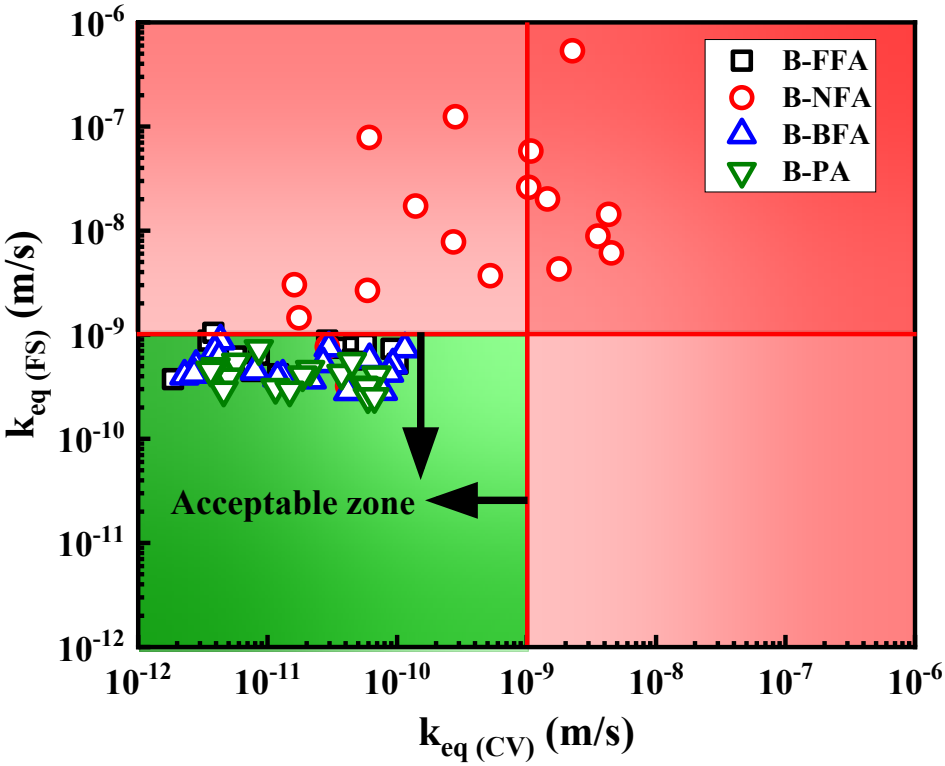


Figure 5.24: Relationship between $k_{eq}$ constant volume and $k_{eq}$ free swelling for all mixes and interaction time

## 5.3 Accelerated physical modelling for determining hydraulic conductivity of hydraulic barriers

### 5.3.1 Background

As stated in the previous previous section of this chapter $k_{sat}$ is one of the most important engineering properties crucial in seepage, settlement, and stability of earthen structures (Sivapullaiah et al., 2000). Compacted clay liners constructed from low permeable soils like bentonites, black cotton soil or other local clays have low $k_{sat}$ ($< 10^{-9}$ m/s). Due to this, the determination of hydraulic conductivity of bentonite or bentonite-based mixes (mixed with sand or fly ash) is highly time consuming. This is further complicated by the reactive or swelling nature of bentonite when it interacts with water or leachate. One of the implications is the change in $k_{sat}$ with time due to change in pore structure associated with swelling till it reaches an equilibrium state. Therefore, it is important to monitor $k_{sat}$ variations for long duration of time till it reaches an equilibrium value (refer section 5.2). However, there are only a few studies that investigate the $k_{sat}$ variation with time

for bentonite-fly ash mix. According to the results presented in the section 5.2, the time taken for $k_{sat}$ measurements under ambient laboratory condition ranged from 20 to 60 days. There is a need to explore alternate methods to reduce the time duration for $k_{sat}$ measurements specifically for low permeable swelling soils.

Accelerated physical modelling using geotechnical centrifuge is an established methodology for reducing the time taken for $k_{sat}$ measurement, and at the same time simulating actual field condition (Arulanandan et al., 1988). One of the major advantages of using a centrifuge is that the unit discharge (Darcys velocity) in a centrifuge model tested at N times earths gravitational acceleration (g) is N times the unit discharge in the prototype (Singh and Gupta, 2000; Thusyanthan and Madabhushi, 2003; Sharma and Samarasekera, 2007). Therefore, the time taken for flow test can be considerably reduced in geotechnical centrifuge. However, it is not explicit from the literature whether the scaling laws are truly applicable for highly reactive swelling soils. Therefore, this study explores the utility of geotechnical centrifuge for determining the $k_{sat}$ of bentonite-fly ash (B-FA) mixes in comparison with sand-bentonite (B-S) mixes.

### 5.3.2 Methodology for hydraulic conductivity determination using geotechnical centrifuge

For $k_{sat}$ measurement in a centrifuge, a new setup was fabricated having an inner diameter of 11 cm and height 7 cm shown in Figs. 5.25 and 5.26. A small transparent tube (perspex glass) was attached on the top of the set up to note the fall in head precisely during the test. As bentonite swell during its interaction with water, arrangements were made to restrict the swelling during the test. All the mixes were prepared at OMC and MDD and compacted statically. The sample diameter was kept 11 cm and height was 0.65 cm, to avoid the influence of increased gravity on $k_{sat}$ measurement. Details of the geotechnical centrifuge used in this study are presented in Table 5.3. There are two sets of measurements considered. For the first set, the $k_{sat}$ of all mixes was measured after 24 hours of compaction (samples were kept in a desiccator). This was done to ensure minimal interaction of mixes. .For the second set of samples, mixes were prepared at their respective OMC and MDD and kept in a sealed bag for 6 months. It is expected that FA causes pozzolanic reaction with bentonite due to the minerals present in it (ref. Fig. 3.2). This may cause alteration in the pore structure and result in $k_{sat}$ changes with time.

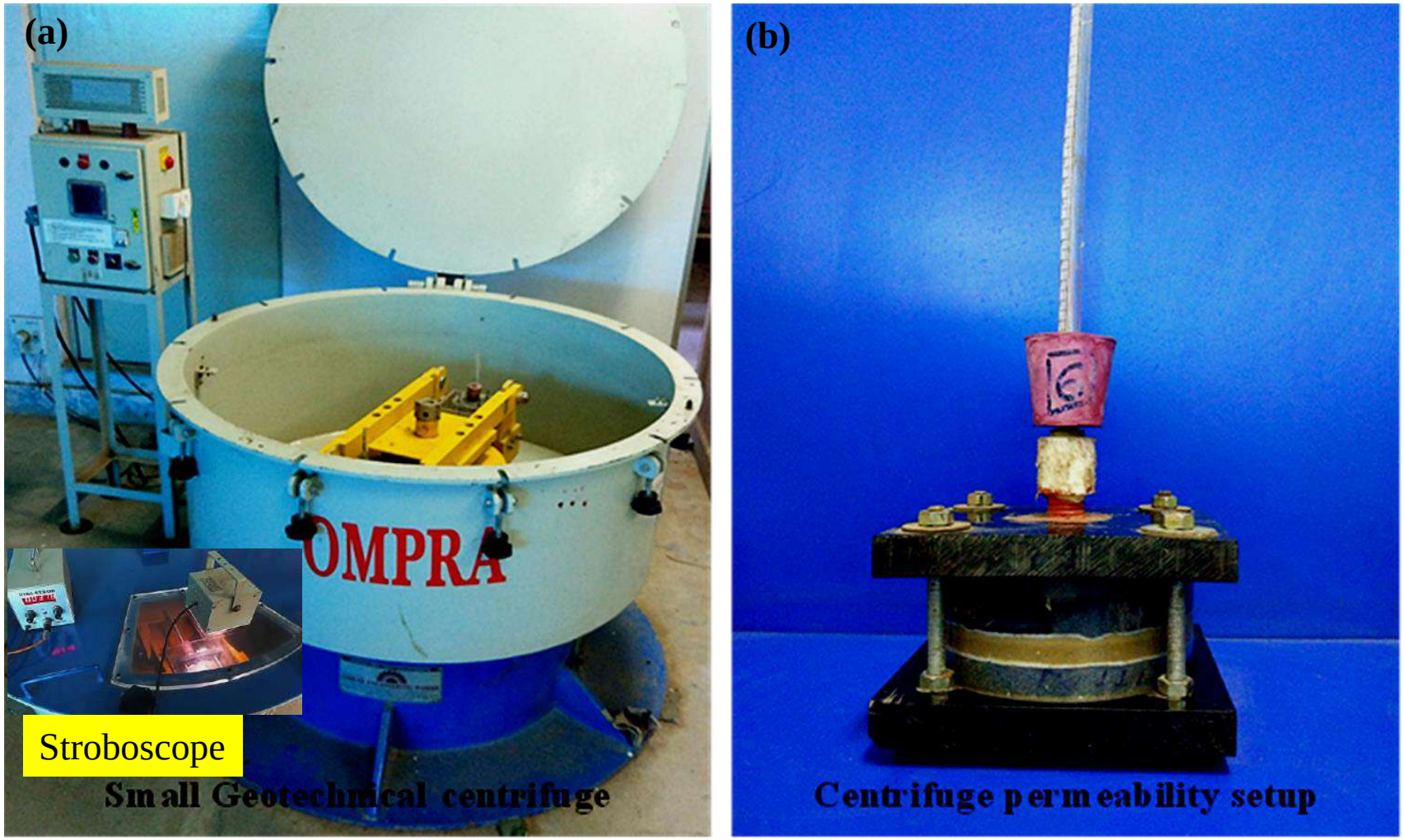


Figure 5.25: (a) Pictorial view of small geotechnical centrifuge (b) Pictorial view centrifuge permeability set up

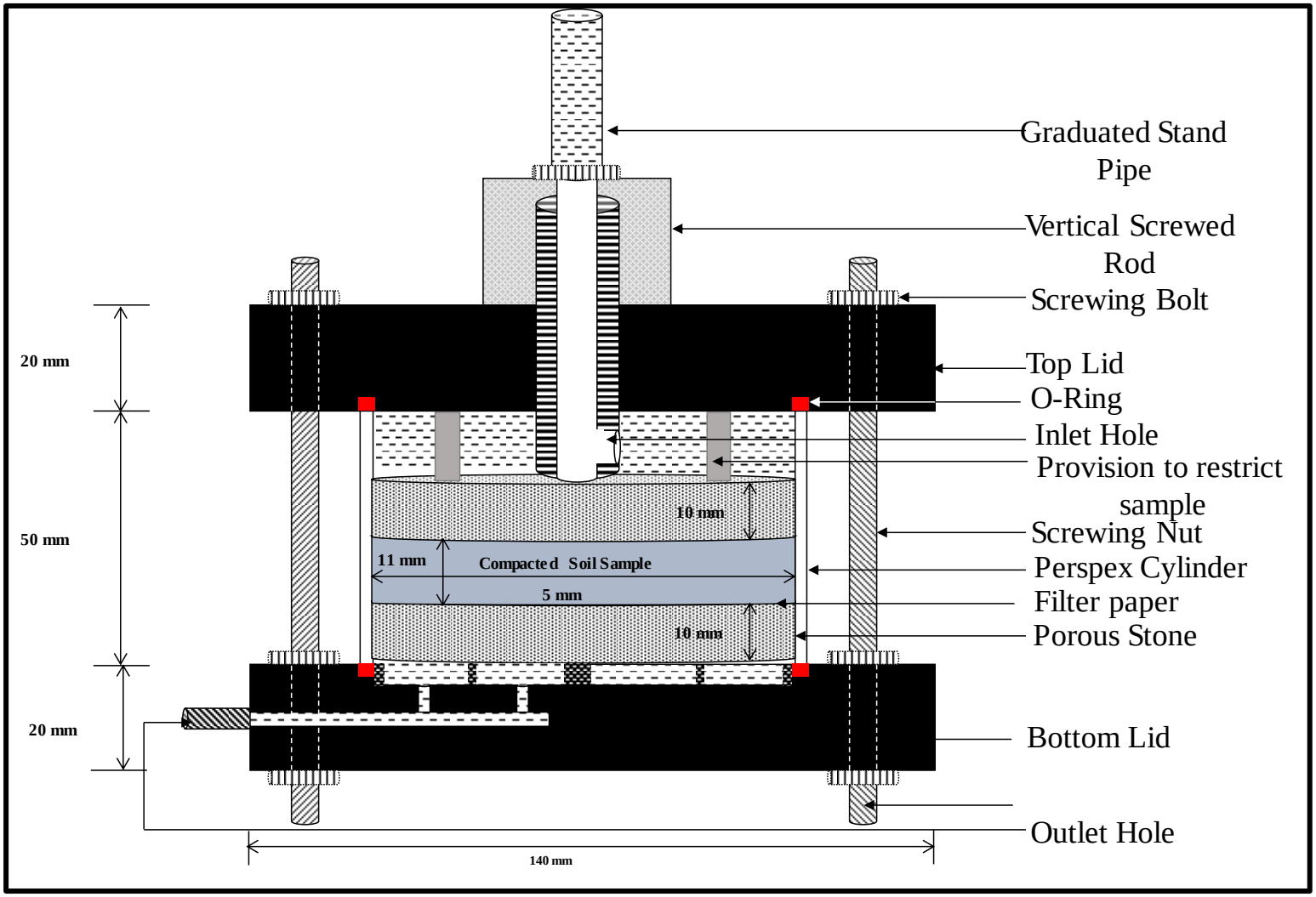


Figure 5.26: Schematic diagram of centrifuge hydraulic conductivity set up

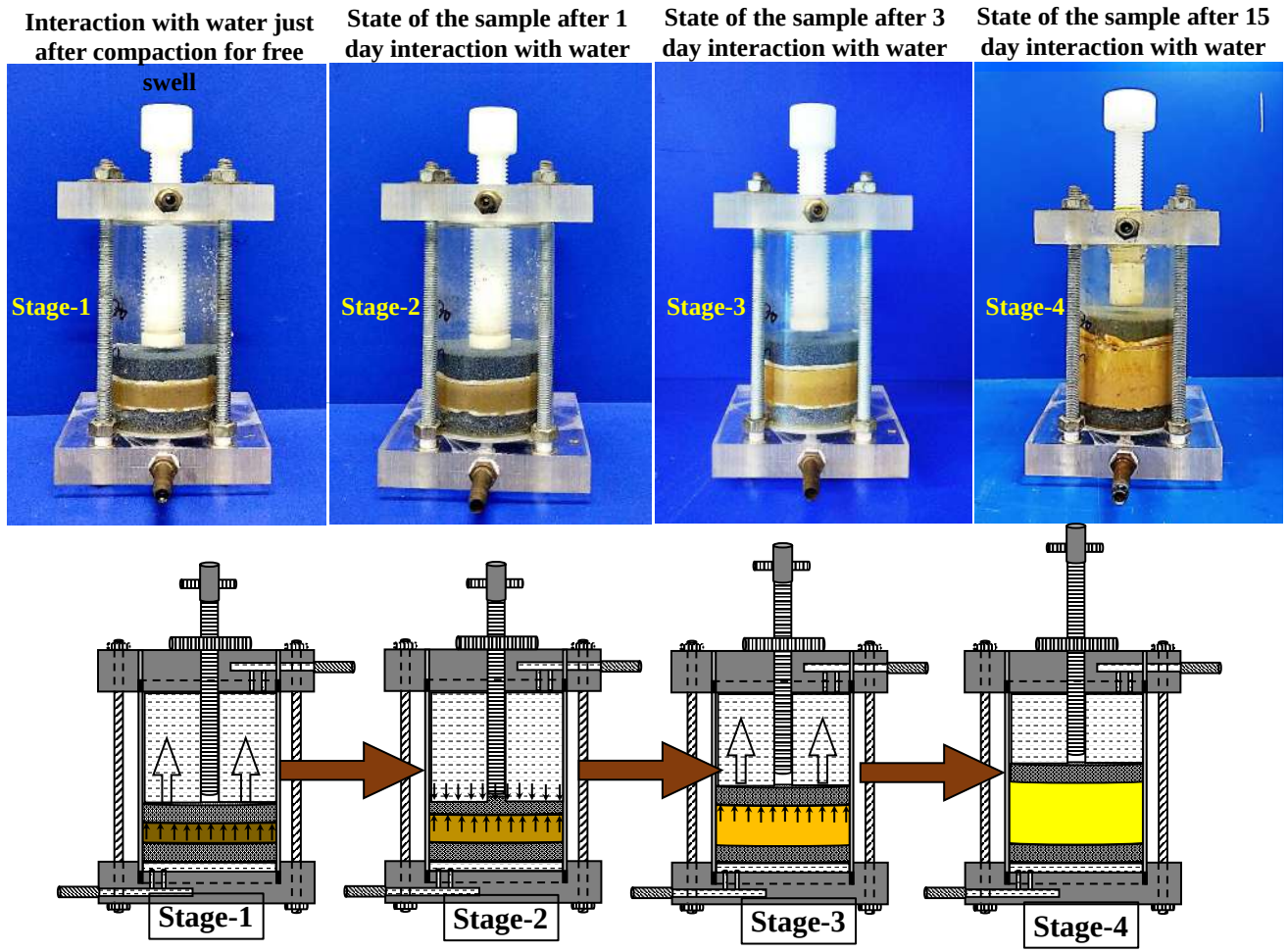


Figure 5.27: Pictorial view of different stages for the uniform free swelling and the mechanism for the uniform free swelling of bentonite for the evaluation of unrestricted hydraulic conductivity (1g)

The setup with compacted sample was placed in the centrifuge as shown in Fig. 5.25a with an initial water height of 32 cm on the surface of the soil for all samples. Each sample was centrifuged at a g level of 25, 50,100 and 150 until the measured $k_{sat}$ exhibited a constant value (equilibrium). The falling head readings were taken during the centrifuge flight using a specially designed light setup (stroboscope) provided by the manufacturer as shown in Fig. 5.25a. Fig. 5.27 shows the different stages of swelling mechanism of the bentonite and its pictorial view to the carry out its hydraulic conductivity under free swelling conditions at 1g environment.

From Darcys law (v=ki), discharge velocity of soil model in the centrifuge ($v_m$) is directly proportional to hydraulic gradient ($i_m$) and expressed as Eq. 5.7 and presented equation below, where $k_m$ is the saturated hydraulic conductivity of model in the centrifuge.

$$v_m = i_m * k_m \tag{5.7}$$

The increase in discharge velocity due to an increase in g level is either due to an increase in hydraulic gradient ($i_m$) or due to an increase in the coefficient of hydraulic conductivity ($k_m$) (Thusyanthan and Madabhushi, 2003). In this study, it is considered that hydraulic conductivity increases by following the literature (Singh and Gupta, 2000, 2001). The hydraulic gradient ($i_m$) is a dimensionless quantity, and hence assumed to be not affected by centrifugal acceleration. The increase in hydraulic conductivity due to an increase in g level can be described by the relationship between hydraulic conductivity (k) and gravitational acceleration (g) i.e.

$$k = \frac{K\rho g}{\mu} \tag{5.8}$$

where, K is the intrinsic hydraulic conductivity, $\rho$ is the fluid density, $\mu$ is the absolute viscosity of the fluid.

Table 5.3: Details of the centrifuge used in this study

| Type | Swinging bucket Beam |
|---|---|
| Pay Load (kg) | 2 |
| Maximum Outer Radius (m) | 0.51 |
| Maximum Centrifugation (RPM) | 700 |
| Maximum Acceleration (g) | 252 |

This indicates that the hydraulic conductivity depends on the fundamental fluid properties, the strength of acceleration field, and the intrinsic hydraulic conductivity (K), which is a property of the porous medium only. Therefore, it is possible to express

$$k_m = N * k_p \tag{5.9}$$

where $k_m$ is the hydraulic conductivity of soil in the centrifuge model, $k_p$ is the hydraulic conductivity of the same state of soil at 1 g condition and N is the level by which g is enhanced in geotechnical centrifuge (Ng model). The scaling relationship for hydraulic conductivity is already established in the literature (Singh and Gupta, 2000; Thusyanthan and Madabhushi, 2003; Sharma and Samarasekera, 2007). A brief description of the same is stated below.

The hydraulic conductivity of the soil can be expressed by the Eq. 5.8. Therfore, hydraulic conductivity for model and prototype can be written as Eqs. 5.10 and 5.11

$$k_m = \frac{K\rho g_m}{\mu} \tag{5.10}$$

$$k_p = \frac{K\rho g_p}{\mu} \tag{5.11}$$

$$\frac{k_m}{k_p} = \frac{\frac{K\rho g_m}{\mu}}{\frac{K\rho g_p}{\mu}} \tag{5.12}$$

Sicne, the gravitation field acting on the model in the centrifuge is N times the prototype

Therefore,

$$\frac{k_m}{k_p} = \frac{g_m}{g_p} = N \tag{5.13}$$

$$\frac{k_m}{k_p} = N \tag{5.14}$$

$$k_m = N * k_p \tag{5.15}$$

In this study, the hydraulic conductivity of bentonite (B), B-FA and B-S at different proportion were determined in geotechnical centrifuge. All the mixes were compacted statically at OMC and MDD with degree of saturation less than 100%. The samples were first cen-

trifuged at 25g and it took approximately 40 hours to achieve constant $k_{sat}$. Subsequently, the samples were centrifuged at 50g, 100g and 150g and ksat was determined as a function of time to ensure constant value. For calculating $k_{sat}$, the falling head equation (Eq. 5.1) was found appropriate as suggested by Singh and Gupta; Singh and Gupta (2000; 2001) and Sharma and Samarasekera (2007).

### 5.3.3 Hydraulic conductivity measured in geotechnical centrifuge

Before measuring $k_{sat}$, trial tests were performed to measure moisture migration in the soil sample and understand the increase in degree of saturation with time. This was important to know the approximate centrifugation time corresponding to each Ng level required to achieve close to 100% degree of saturation. The Fig. 5.28 shows the relationship between centrifugation time and degree of saturation. Only the results of B (use short form), B-FFA70 and B-FFA30 is shown, and all other samples followed similar trend. From the figure, it can be seen that the degree of saturation of bentonite (with lowest $k_{sat}$) increased from its initial value of 84.7% at OMC to 100% in 30 hours at 25g. For B-FFA30 full saturation was achieved in 30 hours and for B-FFA70 (relatively higher $k_{sat}$ due to low bentonite content) the time taken for full saturation was 10 hours.

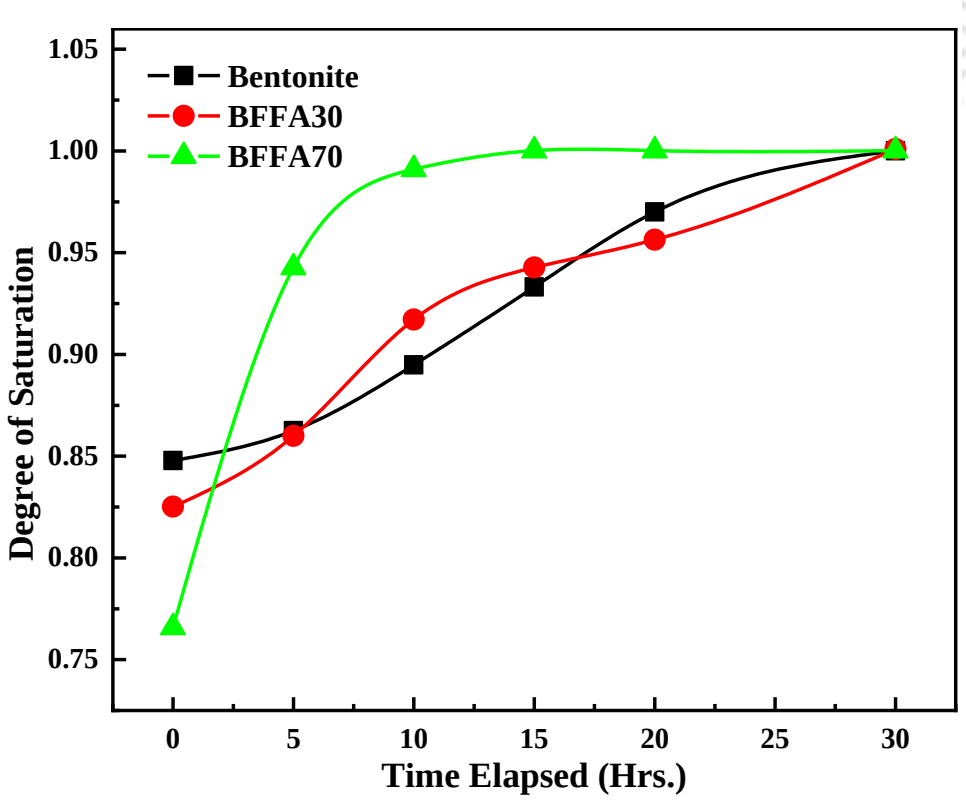


Figure 5.28: Variation of degree of saturation with elapsed time

Figure 5.29 represents the centrifuge hydraulic conductivity of B at different levels of centrifugation. Similar to 1g test, the $k_{sat}$ was measured in the centrifuge corresponding to both constant volume and free swelling condition. For constant volume condition, the $k_{sat}$ initially decreased and after 40 hours of centrifugation, it achieved a nearly constant value with very minimal changes up to 90 hours. It was found that at 25g, $k_{sat}$ decreased even after 30 hours (the time taken for full saturation). The reason behind this may be the time taken for the pore structure readjustment associated with the complete formation of diffused double layers (DDL). After complete development of DDL, the $k_{sat}$ becomes nearly constant. Subsequently, when the same specimen was centrifuged at higher centrifugal acceleration i.e. at 50, 100 and 150g, $k_{sat}$ was constant at every g level, which indicates that there are no further changes in the pore space. With increase in g level, the $k_{sat}$ increases as expected.

Figures 5.30 to 5.32 shows the $k_{sat}$ variation of B-FFA30, B-FFA50 and B-FFA70 respectively, for the samples with 24 hours and 180 days interaction time. For all the B-FFA mixes bentonite swells along with the formation of DDL, which blocks the pores and reduces $k_{sat}$. With decrease in bentonite content, such a closure of pores do not occur, thereby increasing $k_{sat}$ (Ranganatham, 1961; Kenney et al., 1992; Benson et al., 1999; Mitchell et al., 2005; Mishra et al., 2009; Ören et al., 2011). For low bentonite content, $k_{sat}$ is controlled by the coarser fraction of the mix (in this case FFA) and when bentonite content is more than the voids in FFA, $k_{sat}$ is controlled by bentonite (Sivapullaiah et al., 2000). For 180 days interaction period, all three B-FFA mixes exhibited the same trend as discussed above. In all the cases there is not much difference in $k_{sat}$ due to the interaction period. The ksat of 180 days samples in B-FFA30, B-FFA50 and B-FFA70 with respect to $k_{sat}$ of 24 hours samples increased 1.3, 1.4 and 1.6 times respectively, which is negligible for a parameter like $k_{sat}$. It is worth noting that all the $k_{sat}$ values are well within the hydraulic conductivity criterion of liners. These results indicate the validity of B- FA compatibility as a liner material.

Figures 5.33 to 5.35 shows the $k_{sat}$ variation of B-NFA30, B-NFA50 and B-NFA70 with 24 hours and 180 days interaction period. In the case of B-NFA30, there is a huge difference in $k_{sat}$ values due to interaction period. On the other hand, in B-NFA50, $k_{sat}$ values for samples with 24 hours interaction period, increased continuously from starting of the centrifugation. This might be due to the presence of $Ca^{2+}$ ions (37% CaO) in NFA, which reduced the thickness of DDL in bentonite over time and resulted in an increase in $k_{sat}$. The other

reason may be the formation of CSH and CAH gel which will bind the clay lumps. This will lead to the flocculation of particles of mixes, which would further depend on curing period. Due to this reason $k_{sat}$ increased over time and after certain period it becomes constant (Cokca and Yilmaz, 2004). For samples with 180 days interaction, there is no such increase in $k_{sat}$ with time. Due to high $k_{sat}$ of B-NFA70 it was not possible to conduct the test at higher g.

Figures 5.36 to 5.38 shows the $k_{sat}$ variation of B-S30, B-S50 and B-S70 respectively at different g level. Bentonite present in the mix controls the ksat. Due to this reason, $k_{sat}$ for both B-S30 and bentonite are almost similar. With a decrease in bentonite content, ksat increased for B-S50 and B-S70. This variation in $k_{sat}$ of sand-bentonite mixes is found to be in good agreement with the results of Kenney et al. (1992), Tripathi and Viswanadham (2012). Figures 5.29 to 5.38 shows the variation of $k_{sat}$ of all mixes obtained corresponding to different levels of centrifugal acceleration. A linear fit was applied to determine $k_{sat}$ corresponding to 1g by extrapolating the measured $k_{sat}$ at different g level. The results obtained for $k_{sat}$ at 1g are summarized in Table 5.4.

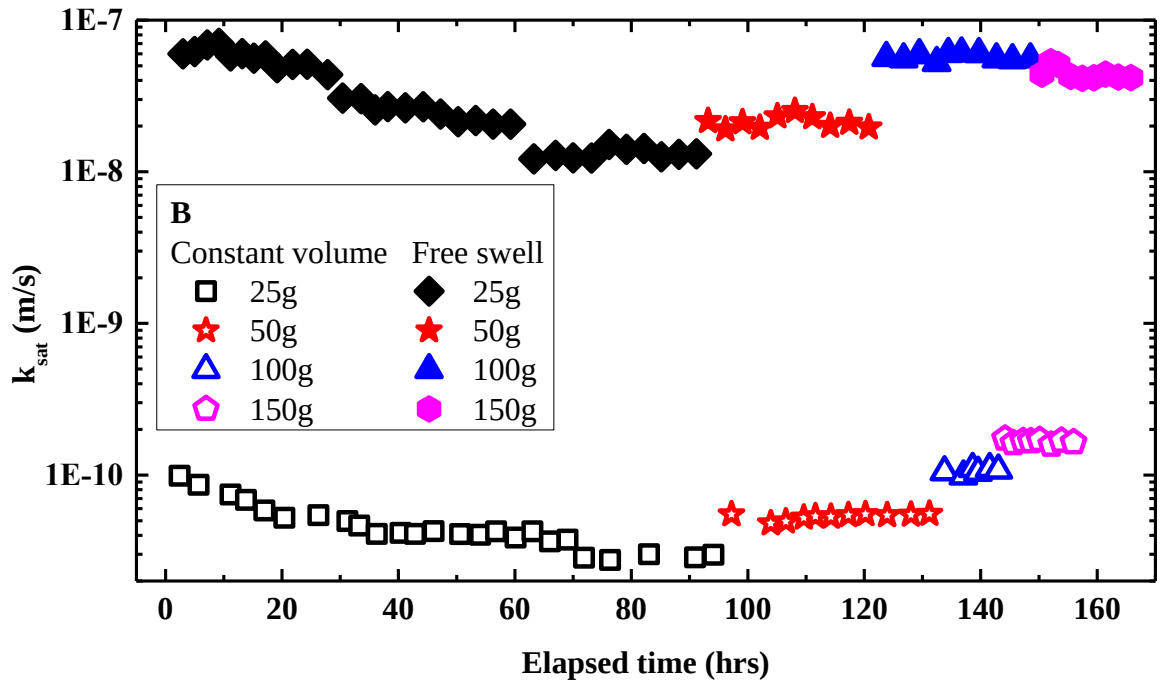


Figure 5.29: The long term saturated hydraulic conductivity of bentonite under constant volume and free swelling conditions at different g level

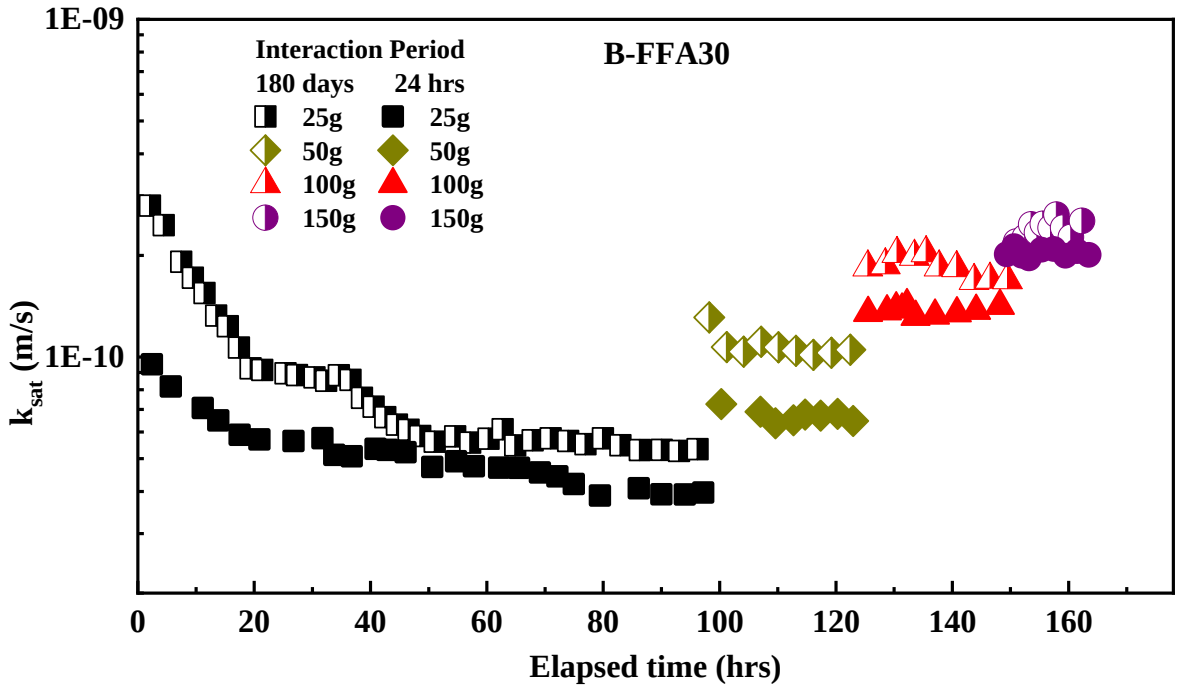


Figure 5.30: Saturated hydraulic conductivity of B-FFA30 at different g with interaction periods

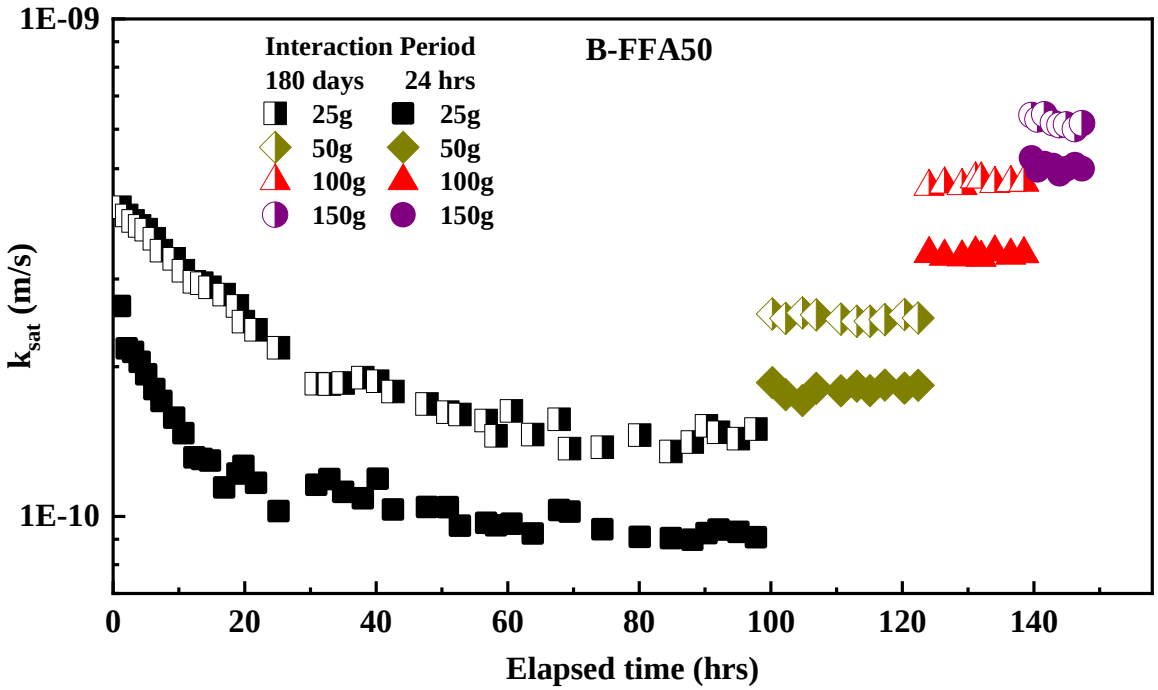


Figure 5.31: Saturated hydraulic conductivity of B-FFA50 at different g with interaction periods

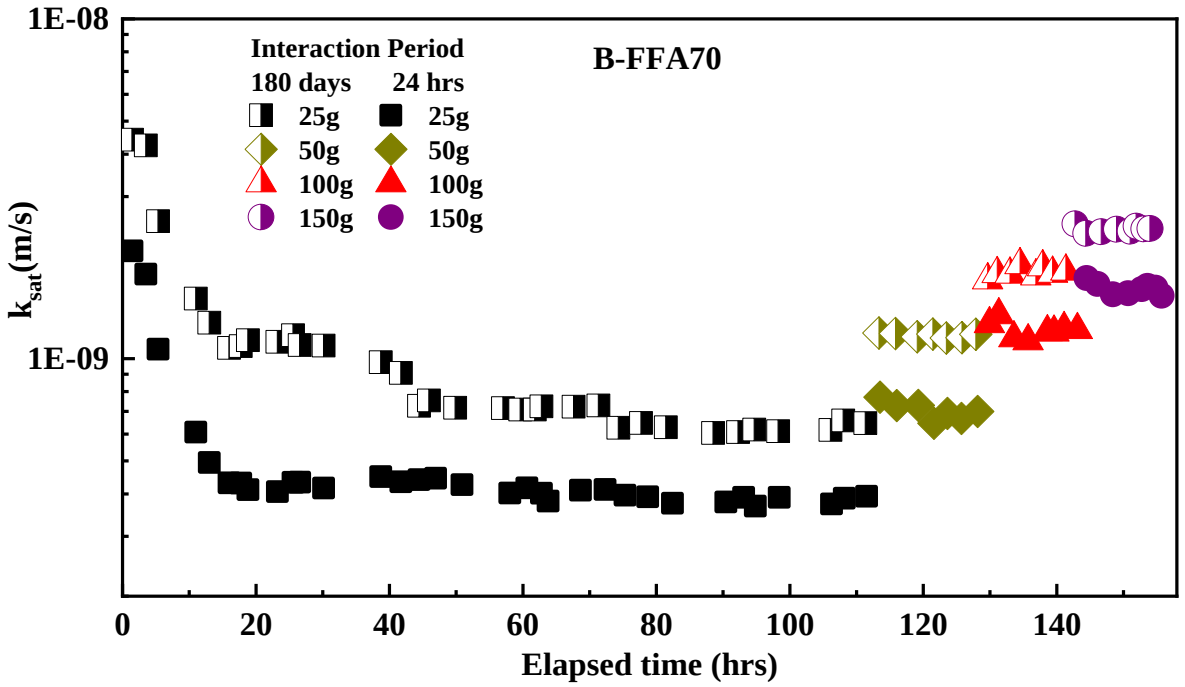


Figure 5.32: Saturated hydraulic conductivity of B-FFA70 at different g with interaction

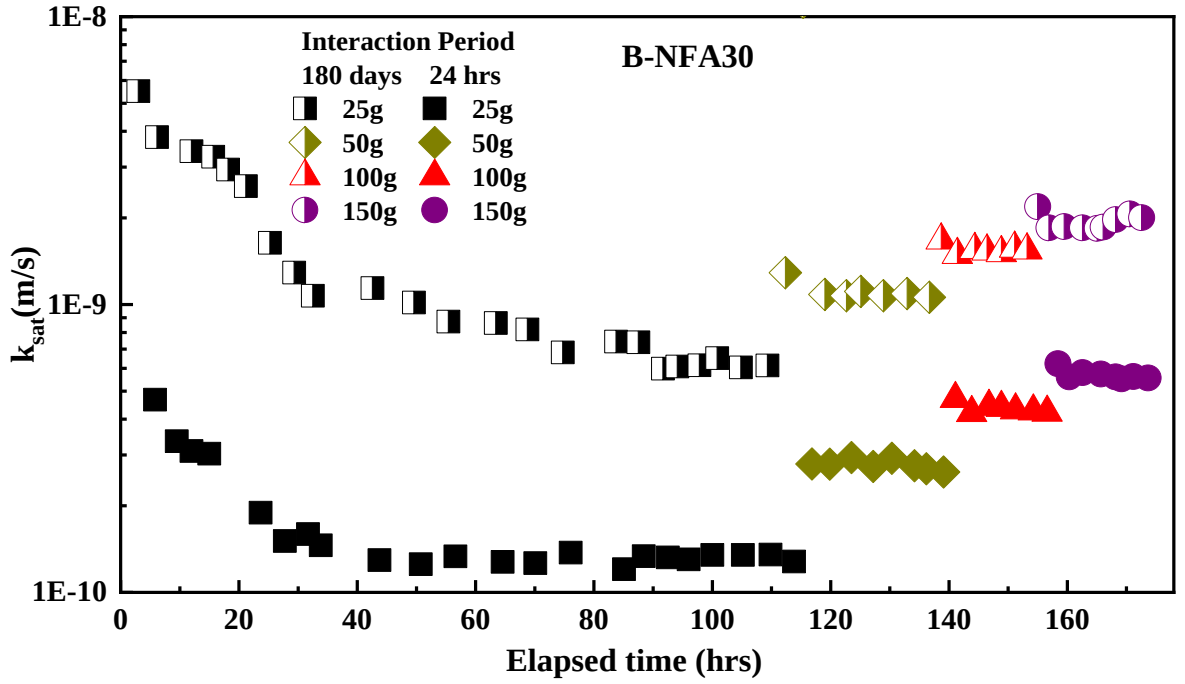


Figure 5.33: Saturated hydraulic conductivity of B-NFA30 at different g with interaction

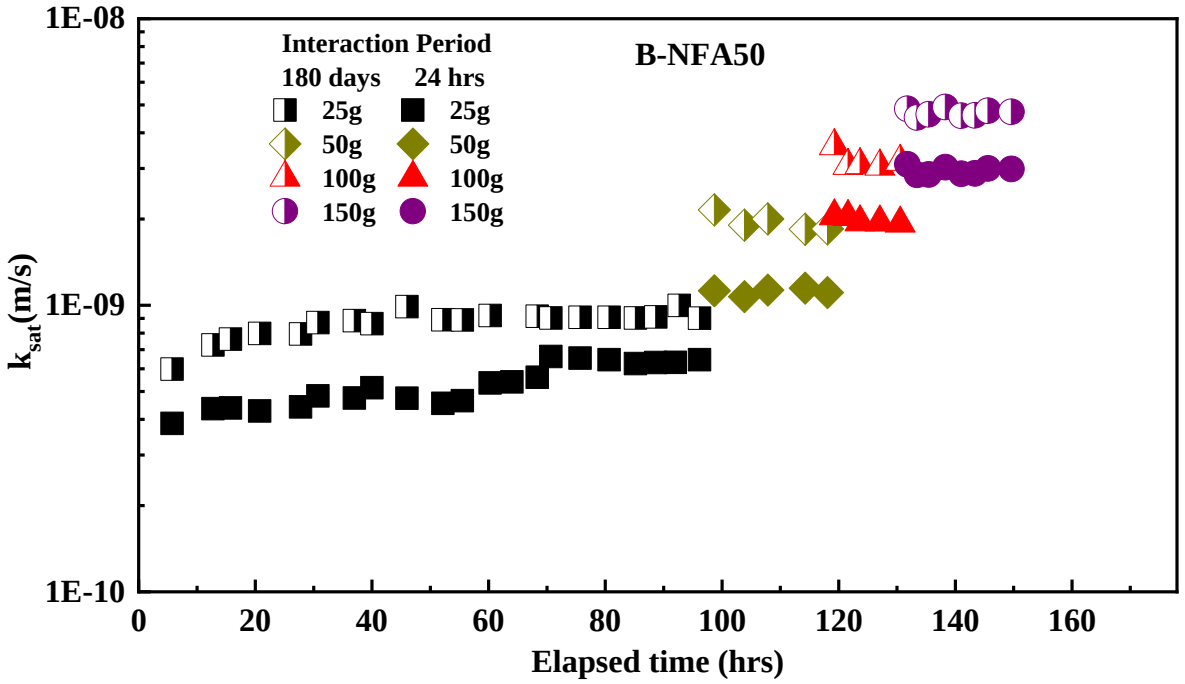


Figure 5.34: Saturated hydraulic conductivity of B-NFA50 at different g with interaction

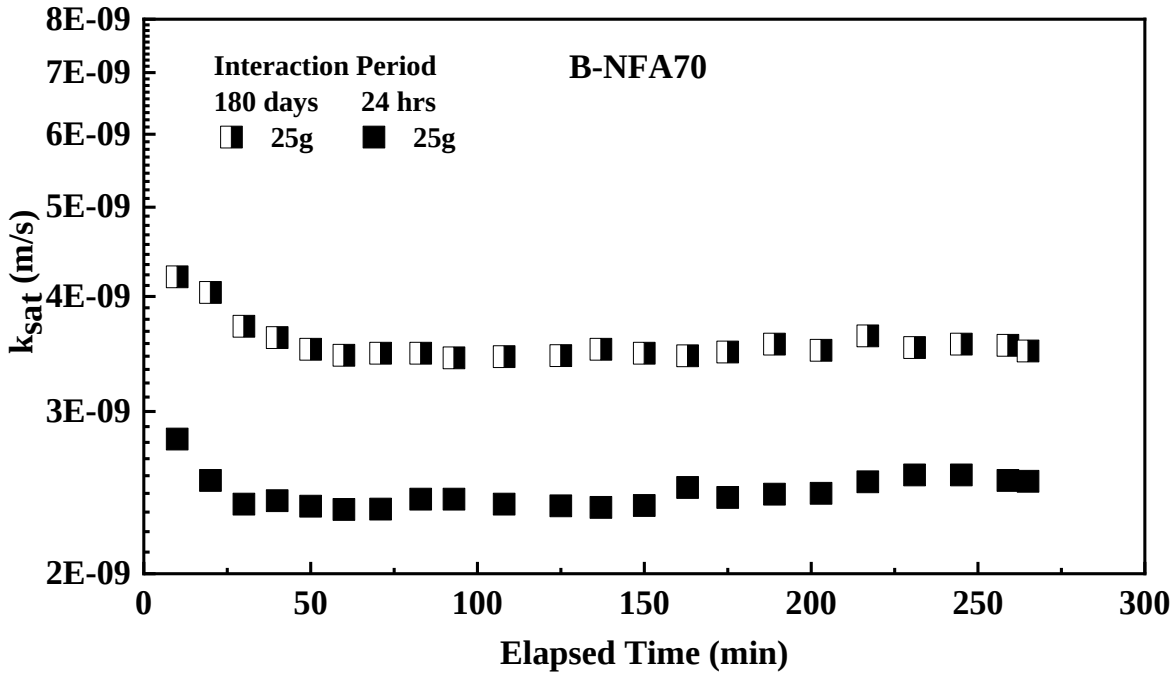


Figure 5.35: Saturated hydraulic conductivity of B-NFA70 at different g with interaction

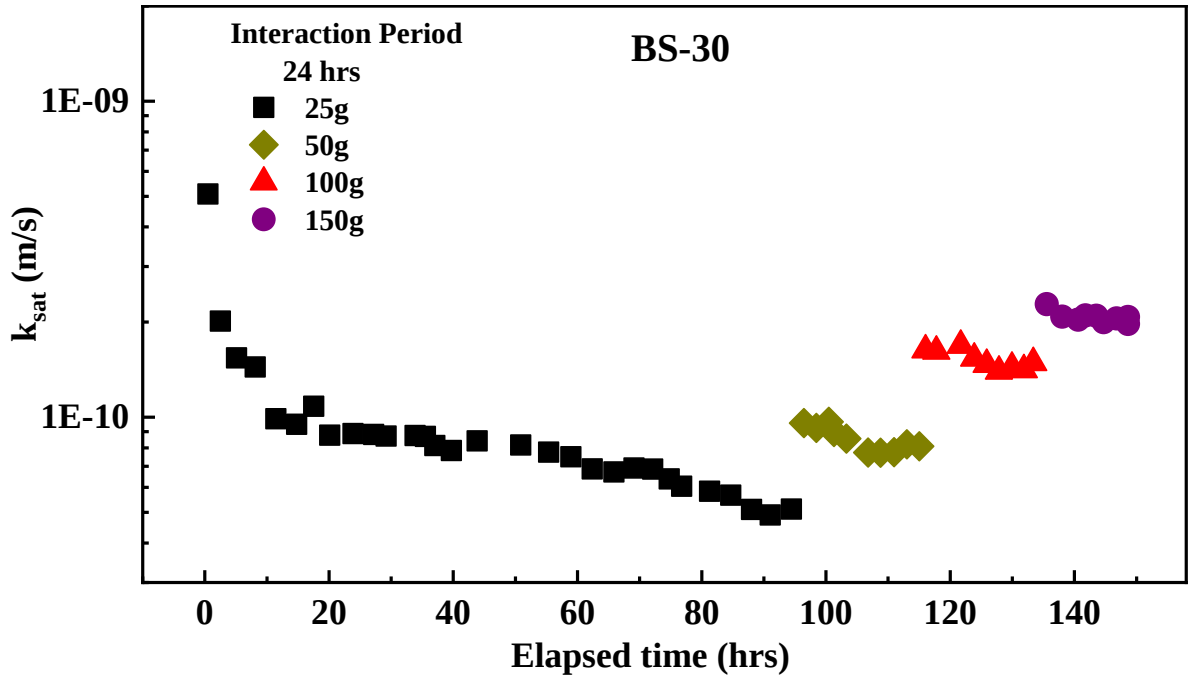


Figure 5.36: Saturated hydraulic conductivity of BS-30 at different g

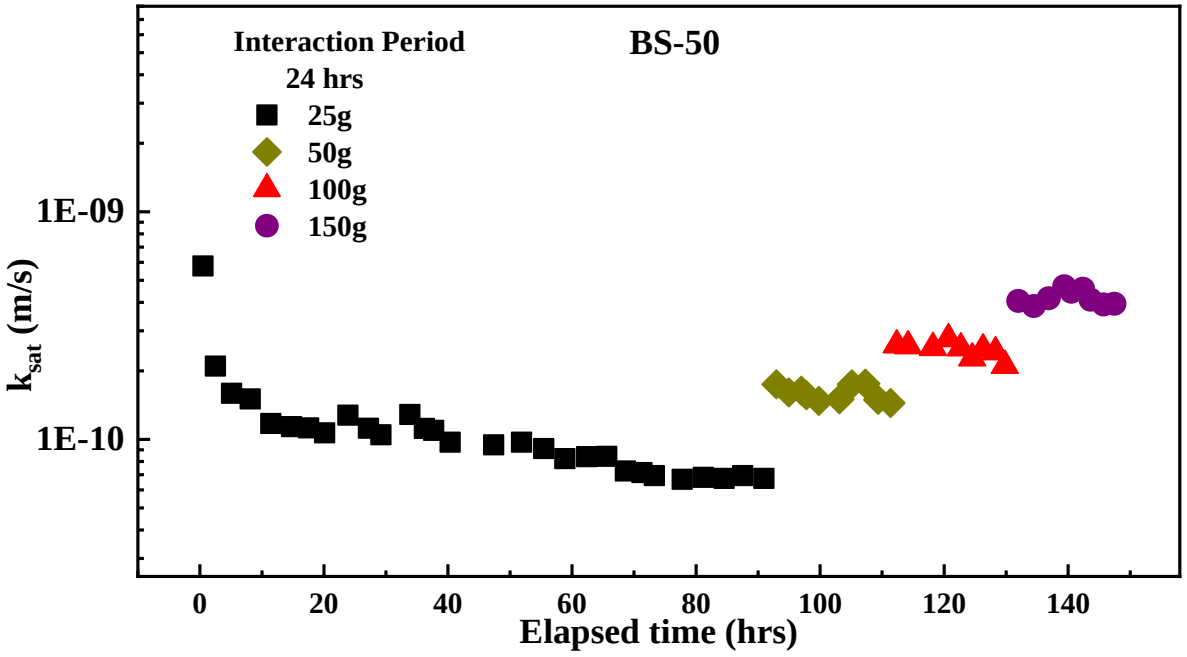


Figure 5.37: Saturated hydraulic conductivity of BS-50 at different g

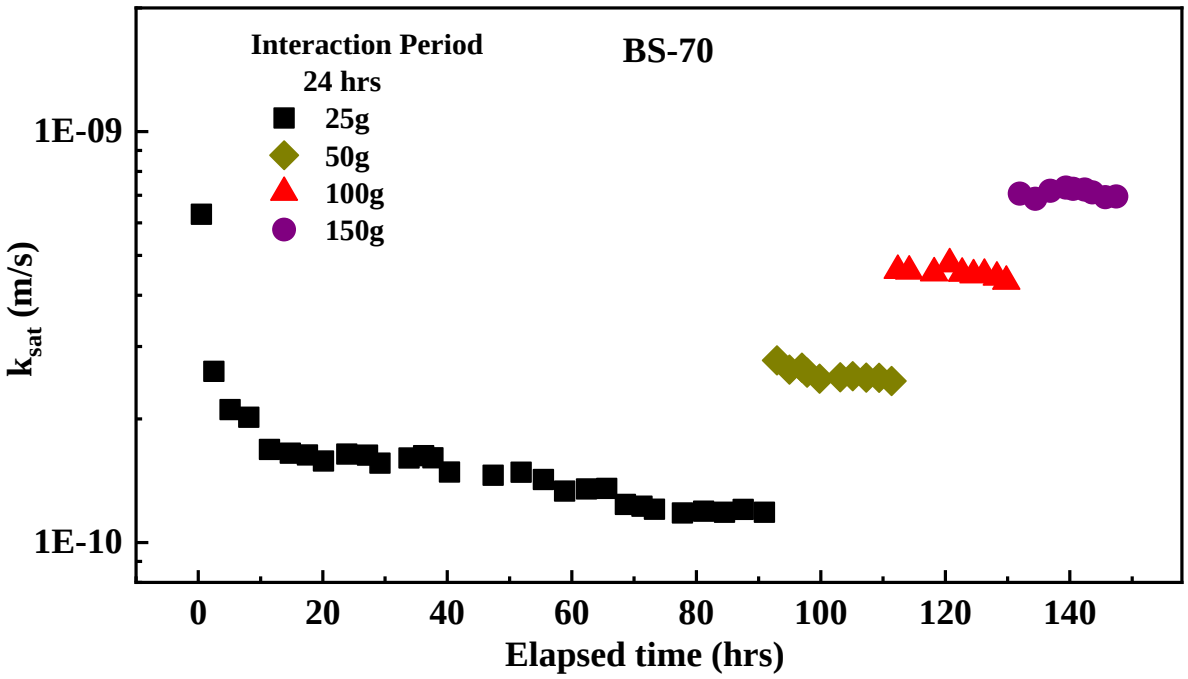


Figure 5.38: Saturated hydraulic conductivity of BS-70 at different g

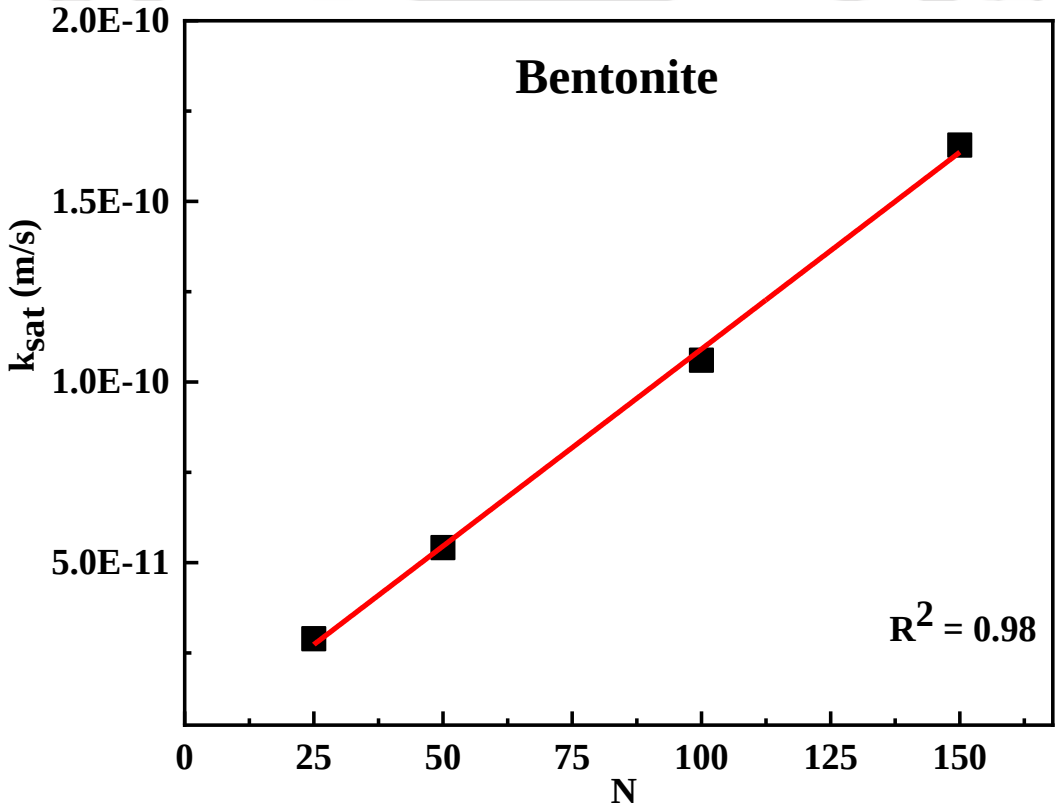


Figure 5.39: Linear fitting of ksat for Bentonite determined at different g

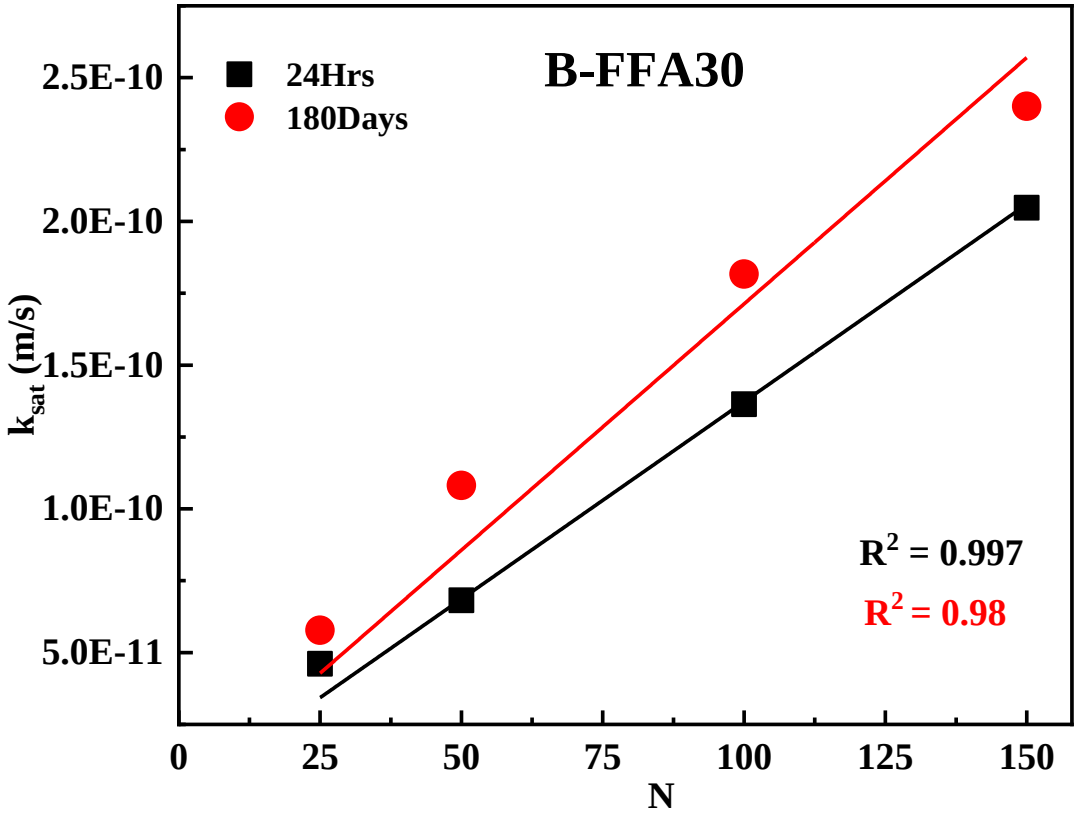


Figure 5.40: Linear fitting of ksat for B-FFA30 for 24Hrs and 180 days interaction

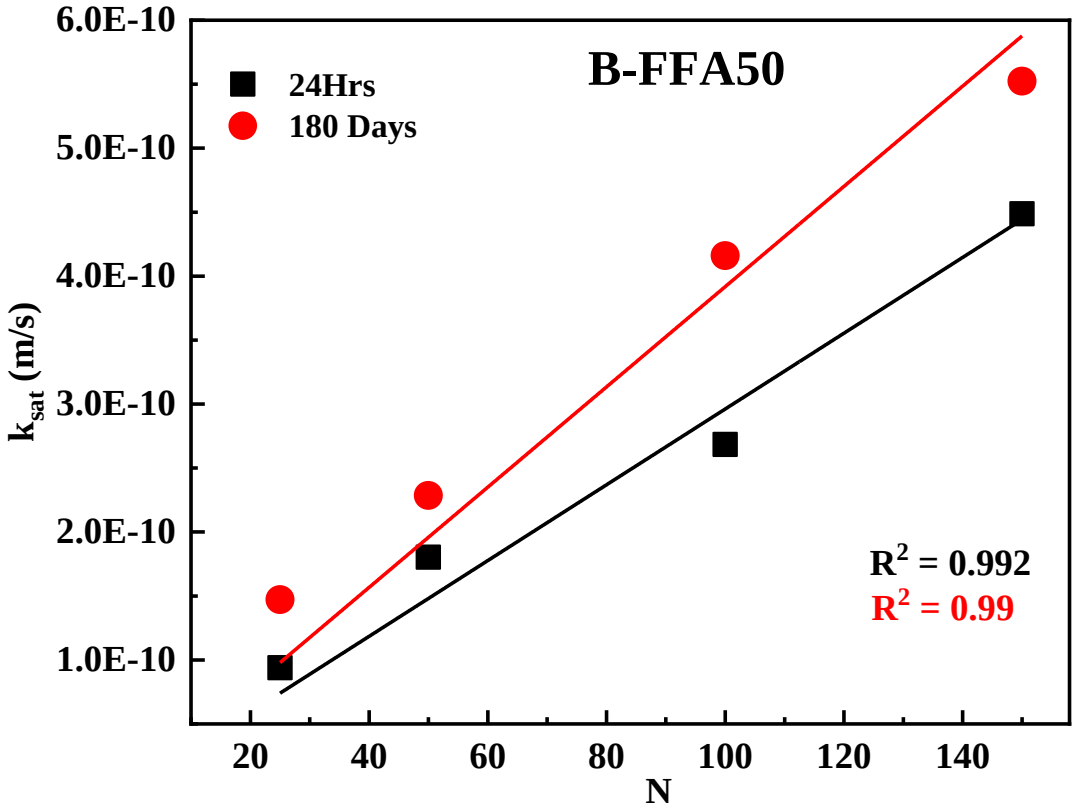


Figure 5.41: Linear fitting of ksat for B-FFA50 for 24Hrs and 180 days interaction

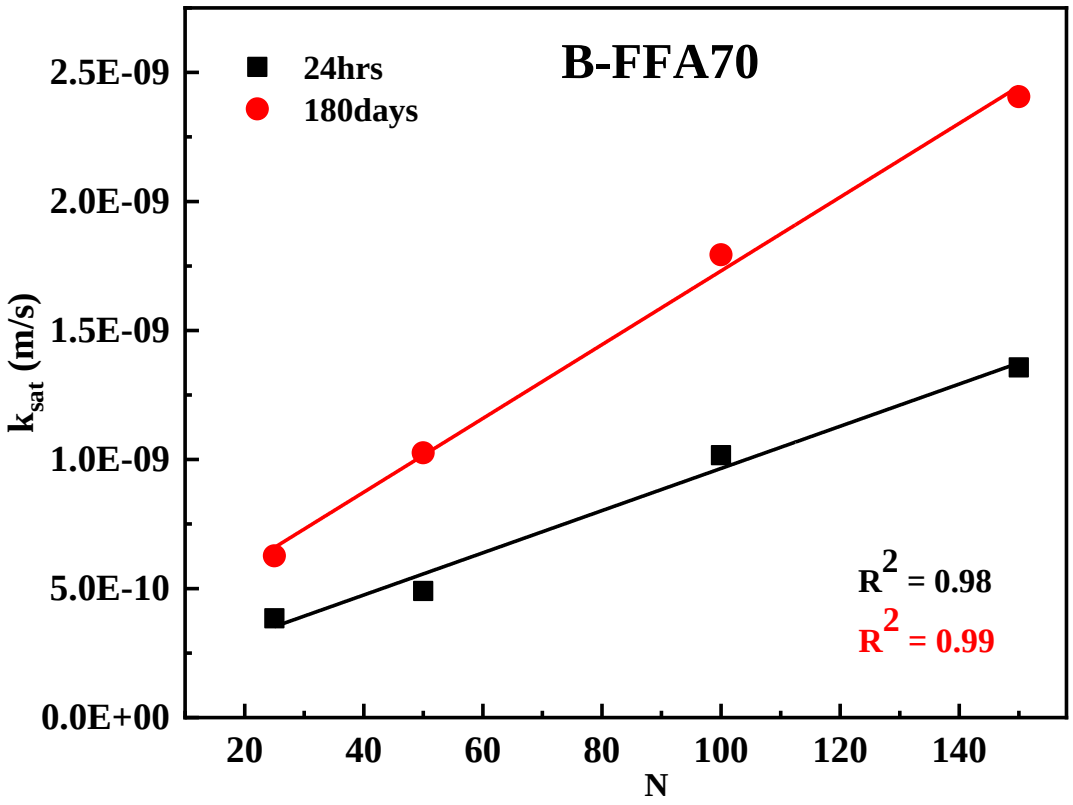


Figure 5.42: 5.42Linear fitting of keq for B-FFA70 for 24Hrs and 180 days interaction

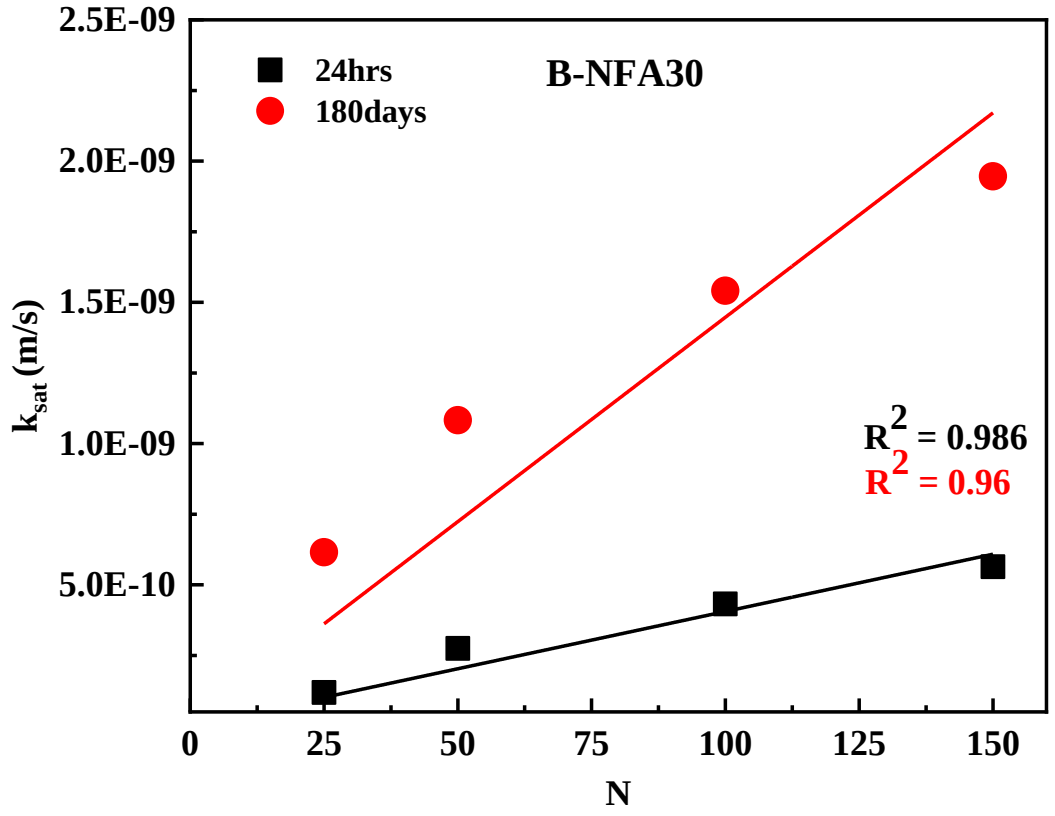


Figure 5.43: Linear fitting of $k_{eq}$ for B-NFA30 for 24Hrs and 180 days interaction

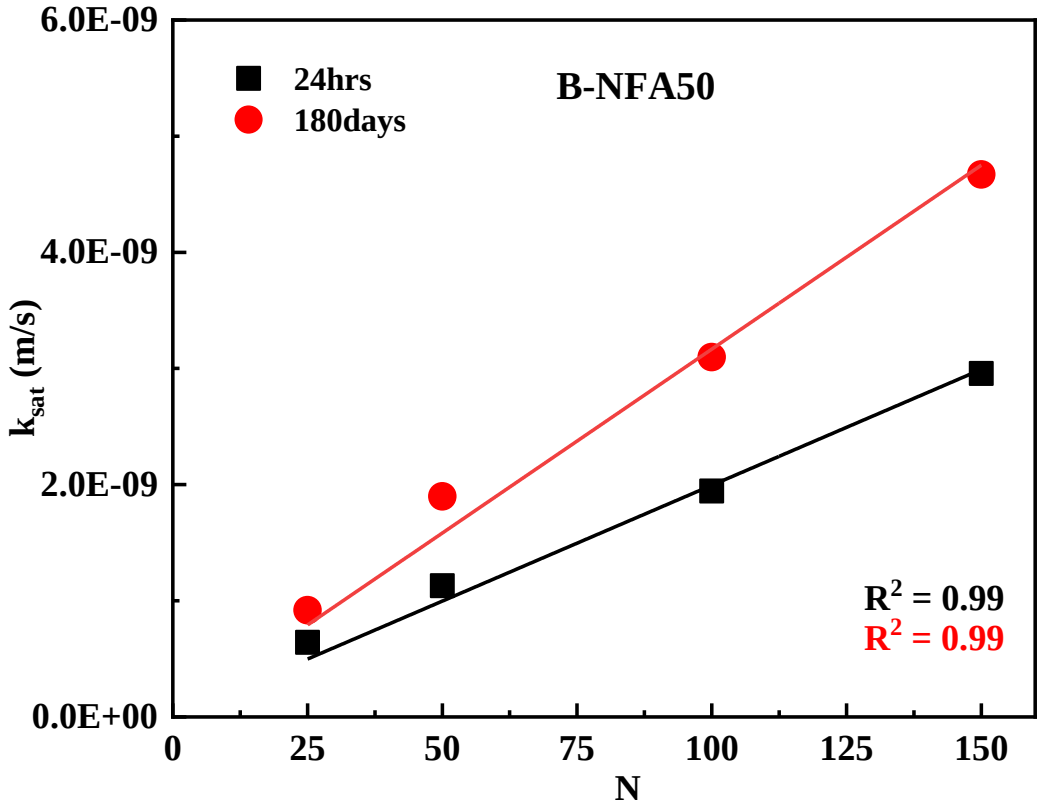


Figure 5.44: Linear fitting of $k_{sat}$ for B-NFA50 for 24Hrs and 180 days interaction

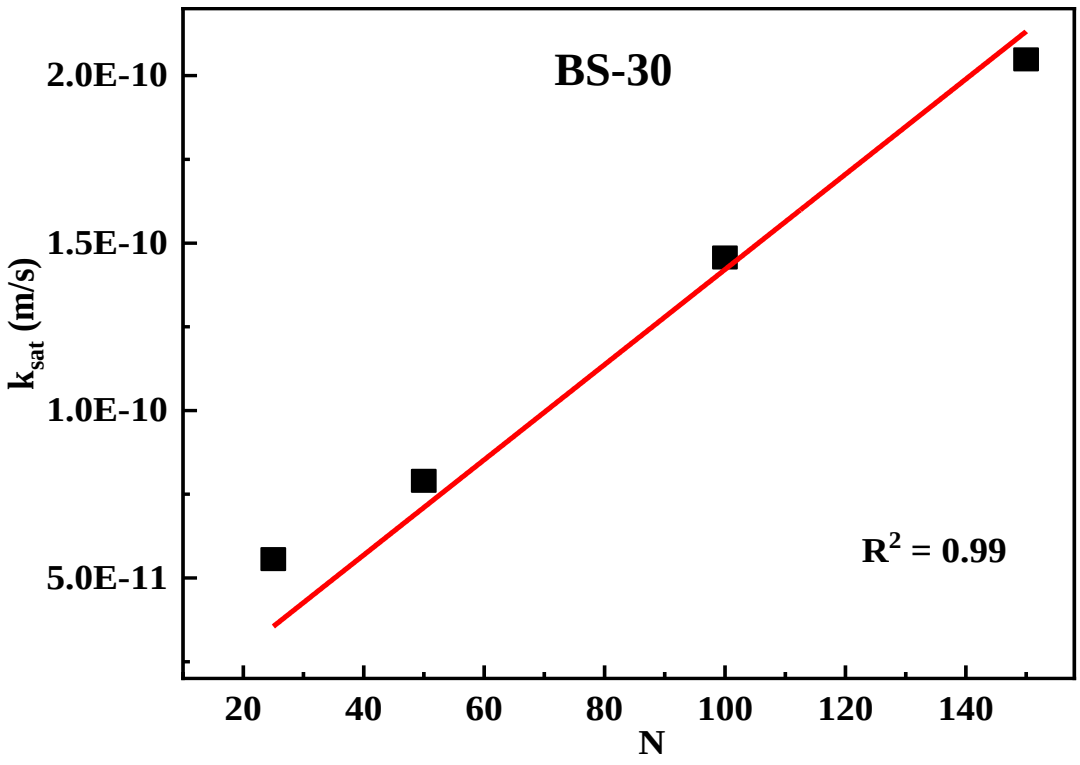


Figure 5.45: Linear fitting of $k_{sat}$ for BS-30 at different g

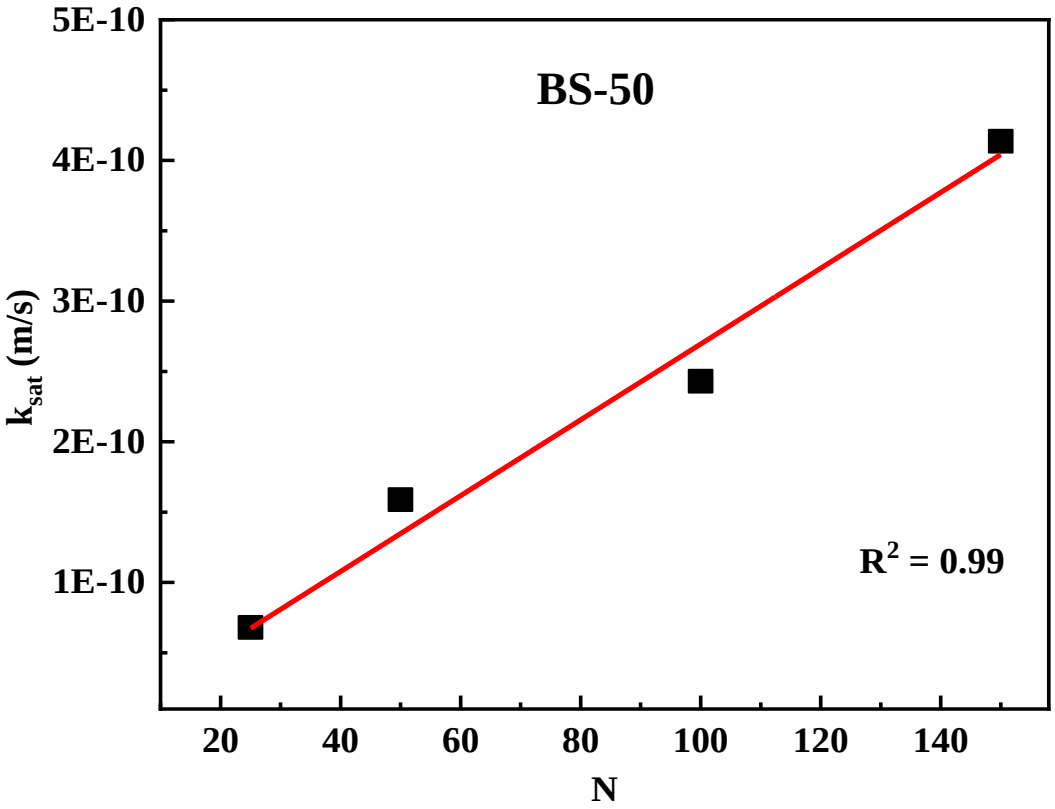


Figure 5.46: Linear fitting of $k_{sat}$ for SB-50 at different g

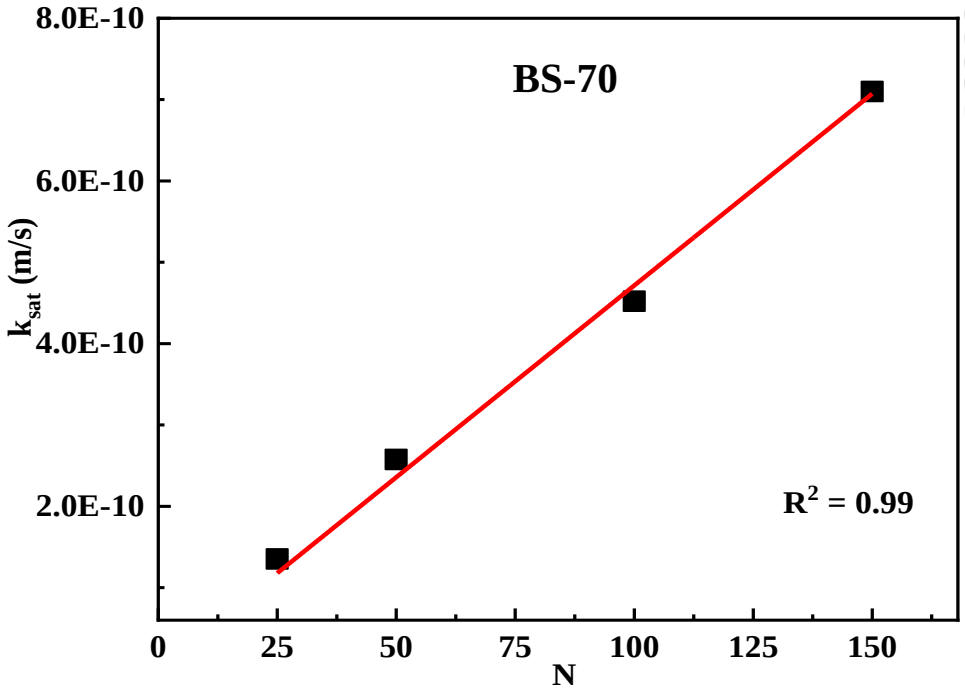


Figure 5.47: Linear fitting of $k_{sat}$ for SB-70 at different g

Table 5.4 shows the $k_{sat}$ of different mixes corresponding to 1g, which was determined

by extrapolating the results of different g level. These 1g values obtained from geotechnical centrifuge were further compared with the $k_{sat}$ measured at 1g (as reported in section 5.2 of this chapter). The comparisons are listed in Table 5.5. For ease of comparison, the results were plotted in Figure 5.48 for both interaction time. It can be noted that majority of the data is well within 20% variation, which can be considered better for widely varying parameter like $k_{sat}$. It is demonstrated that geotechnical centrifuge can be effectively utilized for determining $k_{sat}$ of swelling soils in relatively less time duration.

Table 5.4: Derived hydraulic conductivity from centrifuge tests corresponding to 1g.

| Mixes | Centrifuge $k_{sat}$ at 1g | |
|---|---|---|
| | 24 Hrs. | 180 Days |
| B-FFA30 | 1.37E-12 | 1.71E-12 |
| B-FFA50 | 2.96E-12 | 3.92E-12 |
| B-FFA70 | 9.53E-12 | 1.70E-11 |
| B-NFA30 | 4.05E-12 | 1.45E-11 |
| B-NFA50 | 2.05E-11 | 3.28E-11 |
| B-NFA70 | 2.43E-09 | 3.51E-09 |
| B | 1.09E-12 | |
| BS30 | 1.42E-12 | |
| BS50 | 2.70E-12 | |
| BS70 | 4.71E-12 | |

Table 5.5: Comparison of saturated hydraulic conductivity measured using centrifuge and laboratory falling head permeameter

| Mixes | $k_{sat}$ at 1g | | | |
|---|---|---|---|---|
| | Centrifuge $k_{sat}$ (m/s) | | Falling head $k_{sat}$ (m/s) | |
| | 24 Hrs. | 180 Days | 24 Hrs. | 180 Days |
| B-FFA30 | 1.37E-12 | 1.71E-12 | 4.52E-12 | 5.73E-12 |
| B-FFA50 | 2.96E-12 | 3.92E-12 | 5.75E-12 | 8.45E-12 |
| B-FFA70 | 9.525E-12 | 1.704E-11 | 2.1E-11 | 4.65E-11 |
| B-NFA30 | 8.05E-12 | 1.45E-11 | 4.31E-11 | 1.55E-11 |
| B-NFA50 | 4.05E-11 | 3.28E-11 | 5.25E-10 | 2.63E-10 |
| B-NFA70 | 2.43E-09 | 3.51E-09 | 1.72E-9 | 4.31E-9 |
| B | 1.091E-12 | | 1.89E-12 | |
| BS30 | 1.421E-12 | | 4.72E-12 | |
| BS50 | 2.695E-12 | | 4.25E-12 | |
| BS70 | 4.714E-12 | | 4.72E-12 | |

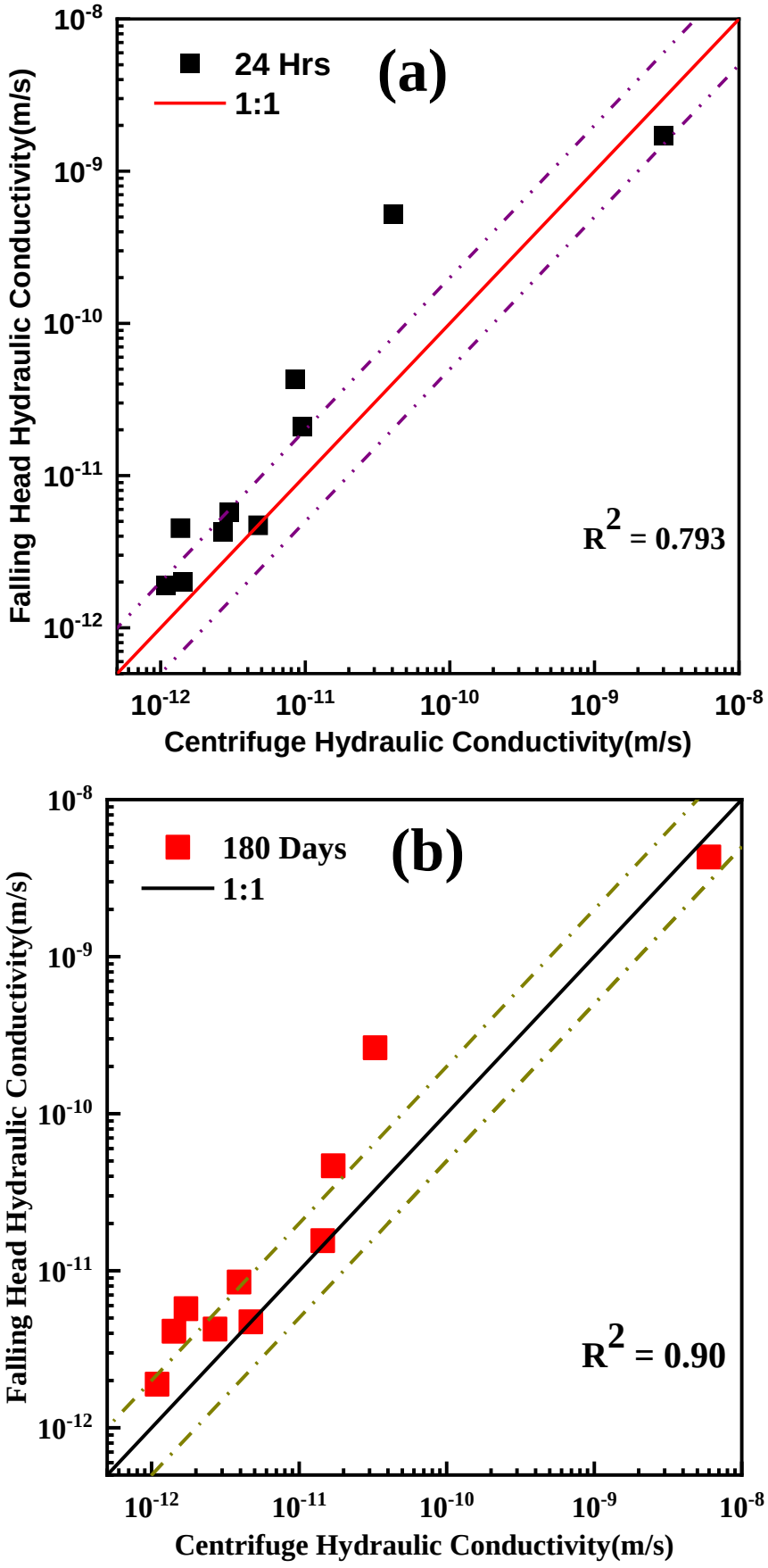


Figure 5.48: Centrifuge hydraulic conductivity vs. Falling head hydraulic conductivity (a) with no interaction time and (b) with 6 month interaction period

## 5.4 Summary

This study investigates the hydraulic conductivity (k) of compacted bentonite-fly ash (B-FA), and bentonite-sand (B-S) mixes under constant volume (swelling restricted) and free-swell (no restriction) conditions. The compatibility of B-FA mixes was assessed based on equilibrium hydraulic conductivity ($k_{eq}$) by performing a series of 26 hydraulic conductivity tests for a period of 90 days. The influence of FA type (class C and F) and amendment percentage (30%, 50 %, and 70 %) on the $k_{eq}$ of B-FA mixes were studied in conjuncture with B-S mixes for constant volume and free swell cases. Additionally, the microstructure and spectral properties of the compacted B-FA mixes before and after the long-term water flow test were investigated to interpret the measured $k_{eq}$. The equilibrium time taken for $k_{eq}$ is dependent on the mix, class of FA and swelling restriction. The results from the study reveal the importance of long-term flow test for reactive geomaterials used in waste management projects in order to determine permeability values for design. Class C FA exhibit higher k than class F for B-FA mixes, which was mainly attributed to the presence of relatively high Ca content. Hence, class F FA with less Ca content is recommended for B amendment as it fulfils hydraulic conductivity criterion for both constant volume and free swell conditions. This criterion is fulfilled up to 70% amendment rate for class F FA.

Measurement of hydraulic conductivity in the conventional falling head method for low permeable liner material, is extremely time-consuming and a tedious task. To counter this situation, usefulness of accelerated physical modelling using geotechnical centrifuge has been demonstrated to determine saturated hydraulic conductivity. Using hydraulic conductivity at higher centrifugal acceleration, hydraulic conductivity at 1g has been derived. Other than hydraulic conductivity, the unconfined strength of fly ash based mixes were compared with that of sand-bentonite mixes. This study specifies the importance of determining saturated hydraulic conductivity using geotechnical centrifuge for very low permeable soil in small interval of time and the results of centrifuge hydraulic conductivity shows good agreement with conventional falling head method.

# 6

# Retention Capacity of Bentonite

## General

This chapter mainly focused on the contaminant retention characteristics of B for its potential application as liner material in waste containment facility. Lead ($Pb^{2+}$) was taken as the model contaminant for the retention study by conducting the 24 hrs batch equilibrium test. For the present laboratory experimentation B was collected from Barmer district of Rajsthan state (one of the major source of B in India).

## 6.1 Appropriate Liquid to Solid Ratio for Sorption Studies of Bentonite

This study demonstrates the importance of selecting appropriate liquid to solid ratio (L/S) for batch adsorption study (BAS) of bentonite (B). The recommended L/S is 20 according to ASTM D 4646 (ASTM 2008a) procedure for BAS of soils and sediments. This L/S works well for most of the soils/ sediments. However, for expansive soil like B, L/S=20 was found to be inadequate due to the formation of thick gel like consistency preventing proper interaction of metal ion with solid surface. This resulted in considerable underestimation of sorption capacity of B. Effort was made to identify appropriate L/S for B for which there is no specific guideline available in the literature. Under controlled pH condition and lead ($Pb^{2+}$) as the model heavy metal ion, it was noted that the sorption capacity of B increases with L/S beyond 20 and with an increase in initial metal ion concentration. The highest percentage removal of $Pb^{2+}$ was observed at L/S=50 and lowest at L/S=100 for initial concentration greater than 300 mg/L. The minimum L/S possible for B is 20, below which

the interaction between the solution and soil solids becomes difficult due to formation of thick gel like consistency. The interaction of Be with $Pb^{2+}$ was further investigated from the results of Field emission scanning electron microscopy (FESEM) integrated with Energy Dispersive X-ray spectroscopy (EDX). Fourier transform infrared (FTIR) spectrometer was used to identify the variations in interaction between the $Pb^{2+}$ ions and functional group present on B for various L/S. It was concluded that for all practical purpose, L/S=50 is a suitable ratio for determining sorption capacity of expansive soil like B.

### 6.1.1 Background

Sorption is an economical and feasible method for the removal of trace metals from wastewater and water supplies (Fu and Wang, 2011; Lakherwal, 2014; Gopi Kiran et al., 2016; Arul Manikandan et al., 2016; Burakov et al., 2018). Bentonite (B), an expansive clay with high cation exchange capacity (CEC) is found to be an efficient adsorbent due to its high negatively charged specific surface area and affinity towards positively charged heavy metal ions (Lo et al., 1997; Babel and Kurniawan, 2003; Gupta and Bhattacharyya, 2012; Dutta and Mishra, 2016; Uddin, 2017). Bentonite is a proven buffer material in the disposal of radioactive nuclear waste and liner material in hazardous waste containment facilities, due to its low flow and high sorption capacity (Khan et al., 1995a,b; Kaya and Ören, 2005; Xu et al., 2006a,b). In most cases, B is mixed with sand or local soil for achieving the aforementioned characteristics along with adequate strength.

It is explicit that sorption capacity is an important characteristic for evaluating the contaminant retention of B and its mixes. Batch adsorption study (BAS) is an established first hand method for assessing the sorption capacity of soils and sediments according to ASTM D 4646 (ASTM 2008a). It can be noted that one of the prominent factors affecting batch sorption is liquid to solid ratio (L/S), which varies approximately from 4 to 1000 for soils and sediments according to the literature. This study is a result of inconsistent and unexpected sorption behavior observed during the conduct of batch test for B and its mix (with fly ash) by considering ASTM D 4646 (ASTM 2008a) recommended L/S of 20. It was noted that B with its high specific surface area exhibited lower sorption than B-fly ash mix. Further investigation revealed that at L/S of 20, B exhibited a gel like consistency due to its expansive nature there by inhibiting soil-contaminant interaction. This indicates that ASTM D 4646 (ASTM 2008a) recommended L/S of 20 may not be appropriate for characterizing sorption capacity of expansive soils like B. There are studies which clearly demonstrates the

importance of L/S for conducting batch test for the removal of heavy metal using soils and sediments (Du and Hayashi, 2006). Jain and Ali (2000) showed that sorption of Cadmium ($Cd^{2+}$) on riverine sediments increased with decreasing L/S (varying from 100 to 1000) due to increased sorption sites. Al-Hamdan and Reddy (2006) observed the decrease in equilibrium concentration with a decrease in L/S from, 200 to 4. Puls et al. (1991) have shown that the sorption of lead ($Pb^{2+}$) and $Cd^{2+}$ on kaolinite increased with an increase in L/S. Triantafyllou et al. (1999) reported that lower value of L/S resulted in a better sorption but lower removal per unit mass of B. Several studies reported in the past have used wide range of L/S varying from 10 to 5000 for B (Bereket et al., 1997; Naseem and Tahir, 2001; Xu et al., 2008).

It was noted that the previous studies do not evaluate the appropriateness of L/S adopted in BSS of B. This can be appraised better only if there is a comparative evaluation among the sorption characteristics of B and B based mixes. The objective of the present study is to investigate and recommend appropriate L/S for B that would adequately represent its sorption behavior. For this purpose, a detailed experimental study was conducted in order to determine the influence of L/S under controlled pH condition and varying initial metal ion concentration. Three L/S of 20, 50 and 100 were chosen for characterizing the sorption behavior of Barmer B and B-FA mix with $Pb^{2+}$ as the model contaminant. It was concluded that for all practical purpose, an optimal L/S of 50 is suitable for determining the sorption capacity of expansive soil like B.

### 6.1.2 Batch sorption experiment

Batch sorption experiment was performed by following the guidelines stated in ASTM D 4646 (ASTM, 2008a) for soils and sediments. Kinetic studies of the sorption of $Pb^{2+}$ in soils conducted by past researchers stated an equilibrium time of 2-3 h (Cho et al., 2005; Alinnor, 2007). Therefore, a separate kinetic study was not conducted and the time of 24 h recommended by ASTM D 4646 (ASTM, 2008a) was followed in this study. The required concentrations were obtained by dilution of the stock solution using ultrapure de-ionized (DI) water. The concentration of the solutions was measured by AAS (55 B, Spectra AA Varian, Australia). Initially, pH of the solution was adjusted to 5 by adding 0.1 M $HNO_3$ and 0.1 M NaOH to avoid precipitation of $Pb^{2+}$ in the aqueous solution and also to mimic pH values found in landfill leachate reported in the literature (Rowe, 1995; Lo, 1996; Li and Li, 2000).

Required amount of air-dried soil sample was mixed with desired concentration of $Pb^{2+}$ solution in a conical flask at L/S of 20, 50 and 100. The pH of B is 9.2 and would result in the precipitation when it comes in contact with $Pb^{2+}$ solution. To avoid this, half volume of DI water was added in a 250 ml conical flask and pH was measured (pH electrode, Systronics, India) and adjusted to 5 by adding buffer solution. It was shaken on the rotary shaker for 2 hrs. The pH was measured again and re-adjusted to 5, if required. After pH stabilization, remaining half volume of conical flask was filled with $Pb^{2+}$ solution of double the required concentration. The initial concentration of the prepared solution was measured using AAS. To avoid any change in pH during BAS, 0.1 ml of acetate buffer of pH 5 was added to ensure that $Pb^{2+}$ metal ions do not precipitate (Nakano et al., 2008). Finally, the conical flask containing the sorbent and the solution was placed on a rotatory shaker at 200 rpm. After 24 h of shaking, the solution was centrifuged at 3000 rpm for 10 minutes to separate solids and liquid. The sample was collected using a pipette and filtered through Whatman grade 42 filter paper. The equilibrium concentration of the solution was measured using AAS. The sorbed amount of $Pb^{2+}$ retained on the solid surface was determined by Eq. 6.1.

$$q_e = (C_i - C_e) \times \frac{V_l}{M_s} \tag{6.1}$$

Where, $q_e$ is the sorbed amount per unit mass of sorbent (mg/g) $V_l$ is the volume of solution used in batch test in mL, $M_s$ is the mass of solid (g) used in the test, $C_i$ is the initial concentration of the solution (mg/L) and $C_e$ is the equilibrium concentration (mg/L) of the solution after 24 h batch test. The percentage removal (PR) of $Pb^{2+}$ from the aqueous solution was determined using Eq. 6.2.

$$PR(\%) = \frac{C_i - C_e}{C_e} \times 100 \tag{6.2}$$

### 6.1.3 Sorption isotherms

The sorption behavior was quantified using sorption isotherms, which is the relationship between the amount of metal ions sorbed on the soil surface and the equilibrium concentration of metal ions remaining in the aqueous phase at equilibrium condition. The popular Langmuir and Freundlich isotherm equations (Langmuir, 1918; Freundlich, 2002) were fitted to BAS. The Langmuir isotherm is based on the sorbed monolayer metal ions on the

homogeneous active sites of the sorbent and it is represented by Eq. 6.3.

$$q_e = \frac{q_m b c_e}{1 + b c_e} \tag{6.3}$$

where, $q_m$ is the maximum capacity of metal monolayer sorbed in mg/g and $b$ is the constant that refers to the binding energy of adsorption in L/mg. Furthermore, the favorability of $Pb^{2+}$ sorption was checked using dimensionless parameter $R_L$ (known as separation factor) given by Eq. 6.4 (Yap et al., 2017)

$$R_L = \frac{1}{1 + b c_e} \tag{6.4}$$

where, $C_0$ is the initial metal concentration in mg/L. The value of $R_L$ indicates if the type of Langmuir isotherm is irreversible ($R_L = 0$), favorable ($0 < R_L < 1$) or unfavorable ($R_L > 1$). The Freundlich isotherm is considered to be appropriate for describing both multilayer sorption and sorption on heterogeneous surfaces and can be expressed by Eq.6.5.

$$q_e = K_f c_e^{\frac{1}{n}} \tag{6.5}$$

where, $K_f$ and $n$ are the constants representing relative sorption capacity of the sorbent and intensity of sorption, respectively.

### 6.1.4 Effect of initial concentration of $Pb^{2+}$

The initial concentration of $Pb^{2+}$ was varied from 50 mg/L to 1000 mg/L. The results of $Pb^{2+}$sorption on B and B-FFA30 mix for varying initial ion concentration corresponding to L/S = 20 is shown in Fig. 6.1(a). As expected, sorption capacity increases with increasing initial metal ion concentration, which is similar to those reported in the literature (Melichová and Hromada, 2013; Deka and Sekharan, 2017). For initial ion concentration upto 300 mg/L of $Pb^{2+}$, B and B-FFA30 show similar uptake (Fig. 6.1a). Beyond 300 mg/L of initial metal ion concentration, B-FFA30 shows higher sorption as compared to B. The difference in sorption increases with an increase in initial metal ion concentration. Such a trend is highly unexpected due to the highly reactive specific surface area (SSA) of B. Such an anomaly of sorption behavior of B at L/S= 20 was captured only due to the comparison of B and B-FFA30 mix. It is worthy to mention here that such comparisons are missing in the literature. The possible reason for the low adsorption capacity of B could be due to the

higher expansive behavior as compared to B-FFA30 mix. The expansiveness results in gel like consistency leading to improper interaction of ions with the solid surface. Addition of FFA to B reduces the expansiveness and results in improved interaction of solids with $Pb^{2+}$. To understand this further, effort was made to increase L/S for facilitating better interaction of B. Higher L/S means less solids as compared to liquid and hence the gel like consistency considerably reduces.

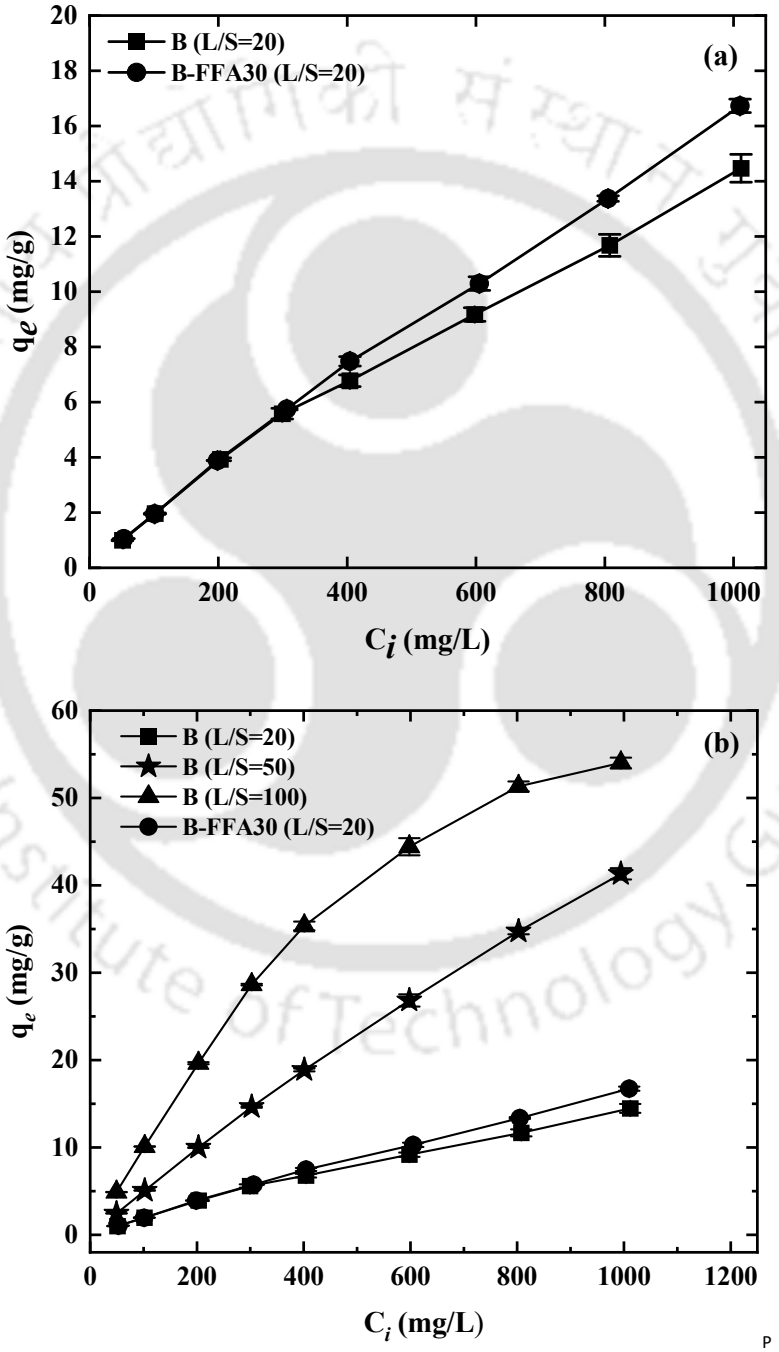


Figure 6.1: Effect of (a) initial concentration and (b) L/S on the sorption of $Pb^{2+}$ on B and B-FFA30

Fig. 6.1(b) shows the effect of L/S on sorption of $Pb^{2+}$ on B and B-FFA30 corresponding to varying initial concentration. There is a drastic increment in sorption capacity of $Pb^{2+}$ from 14 mg/g to 41 mg/g for an increment in L/S from 20 to 50 for B, thereby clarifying the role of gel consistency (L/S = 20) on soprtion. Comparatively lower increment of sorption capacity was observed (41mg/g to 54 mg/g) for L/S varying from 50 to 100. Similar increase in sorbed $Pb^{2+}$ with increase in L/S was reported by Du and Hayashi (2006) for the sorption of $Cd^{2+}$ on Ariake clay. In this study, the largest amount of sorbed $Pb^{2+}$ was observed at L/S of 100 (4 times more than L/S=20) and lowest at L/S of 20. Since the subject of interest is B, different L/S for the mixes was not attempted in this study. Another observation from Fig. 6.1(b) is that the variation of $Pb^{2+}$ sorption with initial concentration exhibited linear trend for L/S 20 and 50 and non-linear trend for L/S of 100. This indicates that sufficiently large sorption sites were available for $Pb^{2+}$ uptake for L/S 20 and 50 whereas the sorption sites progressively decrease with concentration for L/S=100 (less number of solids). For better appraisal of the above discussion, the consistency of B - $Pb^{2+}$ solution after completion of BAS is depicted in Fig. 6.2 for different L/S (20, 50 and 100). The figure clearly corroborates the gel like consistency for B in the case of L/S of 20 leading to diminished solid-contaminant interaction. For L/S 50 and 100, the solution is progressively clear and there is better possibility of $Pb^{2+}$ interaction with B.


Figure 6.2: Bentonite suspension after 24 hours batch test for different L/S of (a) 20 (b) 50 and (c) 100

### 6.1.5 Effect of L/S on percentage removal of $Pb^{2+}$ by B

Fig. 6.3(a) shows the percentage removal of $Pb^{2+}$ by B and B-FFA30 mix with initial concentration ranging from 50mg/L to 1000 mg/L for L/S of 20 as recommended by ASTM D 4646 (ASTM 2008a). The results indicate that the percentage removal of both sorbents are comparable (greater than 90%) up to an initial concentration of 300 mg/L. The effect of gel

like consistency on Be-contaminant interaction is more pronounced for initial concentration greater than 300 mg/L.

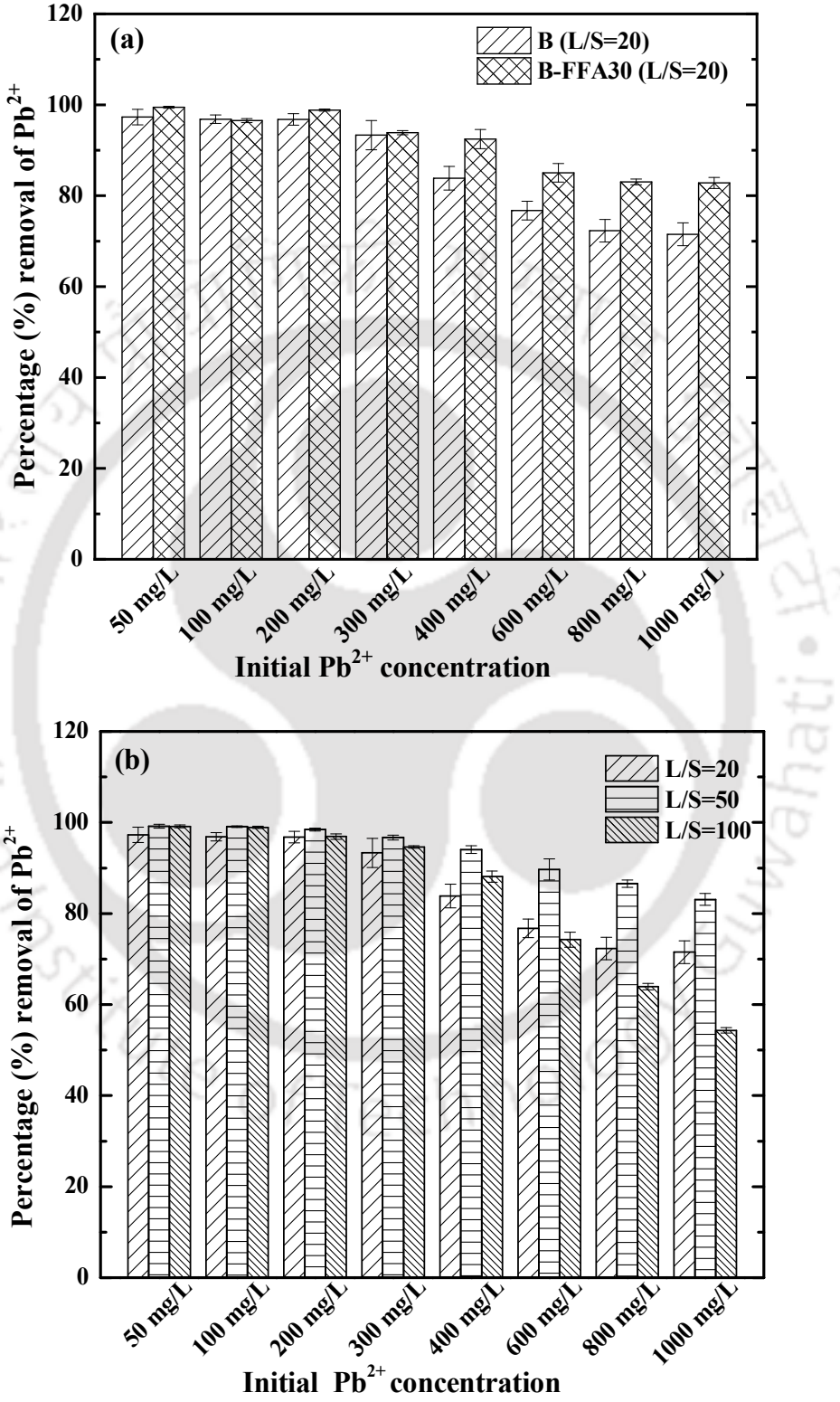


Figure 6.3: Comparison of percentage $Pb^{2+}$ removal for Be and Be-FFA30 corresponding to L/S=20 (b) Percentage $Pb^{2+}$ removal by B at different L/S

Hence, the percentage removal of $Pb^{2+}$ by B-FFA mix is greater than B for the initial metal ion concentrations above 300 mg/L. The percentage removal of $Pb^{2+}$ by B for different initial metal ion concentration and L/S ratios (20, 50, 100) is shown in Fig. 6.3(b). It is quite explicit that the effect of L/S is more prominent for initial concentration greater than 300 mg/L. The highest percentage removal of $Pb^{2+}$ was observed at L/S of 50. The lowest percentage removal of $Pb^{2+}$ was observed for L/S of 100. Therefore, for expansive soils like B, L/S of 50 is recommended for the removal of heavy metals, specifically when the concentration of the wastewater is relatively higher. The same L/S is further recommended for conducting BAS of B as it demonstrates the maximum removal efficiency of the expansive soil.

### 6.1.6 Investigation of B surface post $Pb^{2+}$ sorption

FESEM analysis was performed to understand the effect of L/S ratio on the sorption and the change in morphology of B particle corresponding to an initial concentration of 1000 mg/L. Fig. 6.4 presents the comparison of FESEM images of B before and after BSS for different L/S. It can be clearly observed from Fig. 6.4 that surface morphology of $Pb^{2+}$ sorbed B is different from only B. Pure B can be visualized with relatively loose porous structure as noted in Fig. 6.4 (a), whereas the pore space progressively reduces with increase in L/S. For L/S $>$ 50, pores are considerably reduced, which can be attributed to increase in sorption of $Pb^{2+}$ ions on the surface with increase in L/S. The morphology also indicates that all sorption sites on B are progressively saturated with $Pb^{2+}$ as L/S increases to 100. This observation is in line with the experimental result presented in Fig. 6.1(b) where the curve for L/S $=$ 100 approaches asymptote. Fig. 6.5 (a-d) presents the EDX spectra of B before and after BSS for an initial concentration of 1000 mg/L. The elemental composition (weight %) of common exchangeable cations ($Na^+$, $Ca^{2+}$, $K^+$, and $Mg^{2+}$) before and after BSS for an initial concentration of 1000 mg/L is shown in Fig. 6.6. From the EDX spectrum (Fig. 6.5a) and Fig. 6.6 it can be observed that the weight % of $Pb^{2+}$ in B is 0.1. The weight % of $Pb^{2+}$ increases from 1.7 to 7.6 with an increase in L/S ratio from 20 to 100, which corroborates the increase in adsorption capacity from 14 mg/g to 54 mg/g (for L/S varying from 20 to 100). Among all the exchangeable cations, $Na^+$ ion shows the maximum replacement with $Pb^{2+}$ ion. This is due to the higher CEC of $Na^+$ ions (33.91 meq/100g) in comparison to the other respective cations ($K^+$=0.61, $Ca^{2+}$=14.46 and $Mg^{2+}$=4.68 meq/100g) as listed in Table 3.3). As the weight % of $Pb^{2+}$ increased from 0.1 to 7.6, the weight % of $Na^+$ reduced

from 2 to 0.1 as shown in Fig. 6.6. Also, with an increase in L/S, there is further increase in the replacement of $Na^{+}$ ion, which led to the increased sorption of $Pb^{2+}$ ions on B. The B after BAS was further investigated using FTIR spectrometer to identify the interaction between the $Pb^{2+}$ ions and functional group present on the sorbent as depicted in Fig. 6.6 for an initial concentration of 1000 mg/L. FTIR spectra can be used for discerning the location of $Pb^{2+}$ ions. The structural modification of montmorillonite unit due to sorbed $Pb^{2+}$ ions influence the fundamental vibration of Si-O and OH groups at different L/S of 20, 50, and 100. FTIR patterns of B after BSS showed that a broad band of water (-OH) near wave number 3448, 3467 and 3467 $cm^{-1}$ (Goswami et al., 2017) at different L/S ratio of 20, 50, and 100 were shifted from 3450 $cm^{-1}$ for B (Zhirong et al., 2011). After the sorption of $Pb^{2+}$ ion on B, a change in Si environment can be observed in the shape of the Si-O stretching band near 1034 $cm^{-1}$. The strong band near 1034 $cm^{-1}$, assigned to complex Si-O stretching vibration in tetrahedral sheet, moved to 1032, 1033, and 1032 $cm^{-1}$ at different L/S ratio after $Pb^{2+}$ sorption on B.

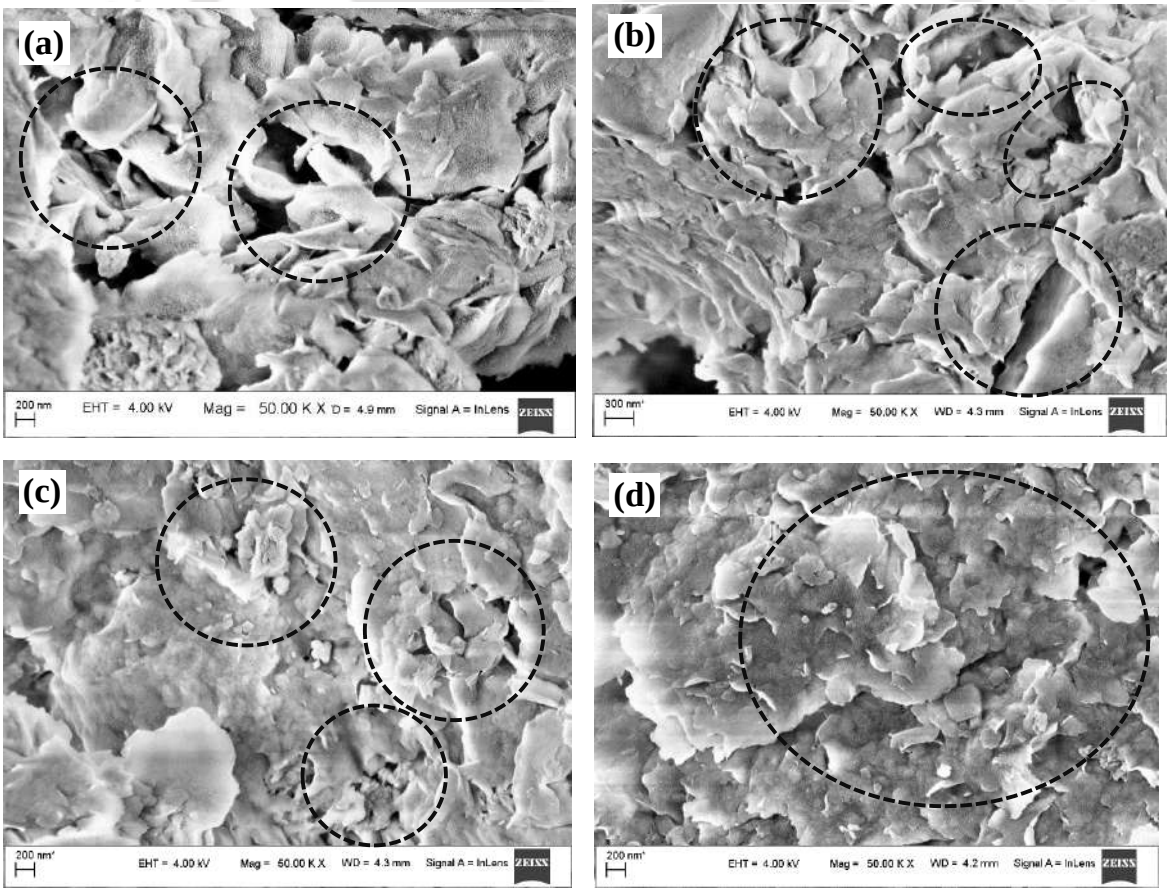


Figure 6.4: FESEM image of bentonite (a) before BAS and after BAS for (b) L/S=20 (c) L/S=50 (d) L/S=100 with an initial concentration 1000 mg/L

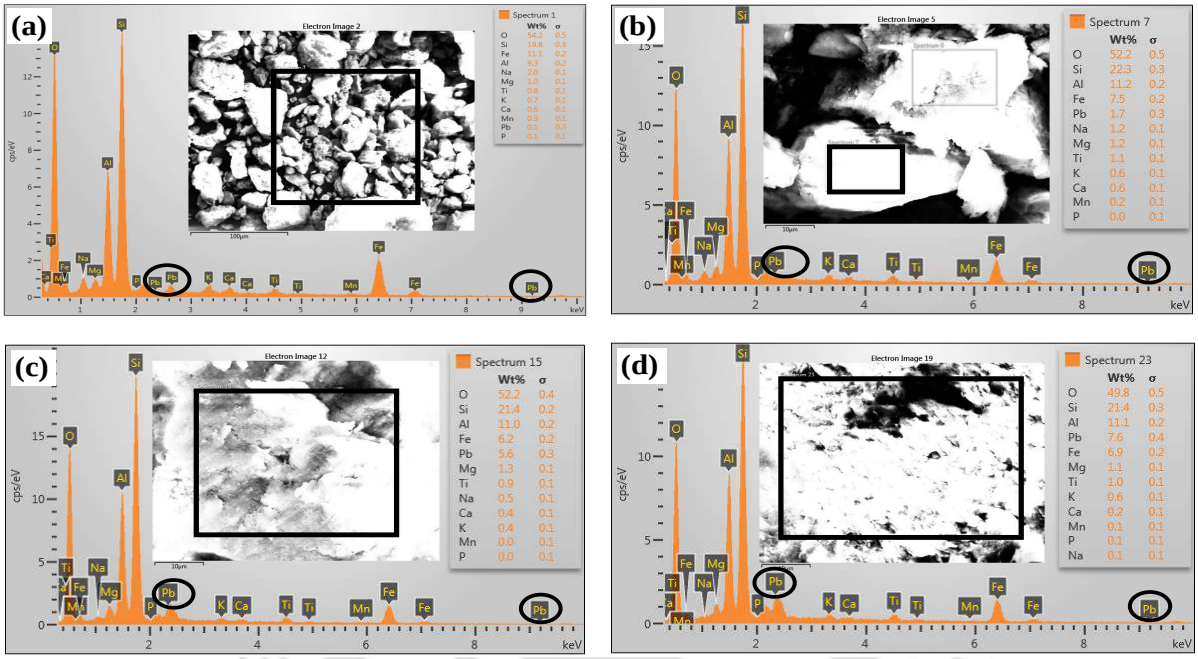


Figure 6.5: EDX spectrum of (a) bentonite (a) before BSS and after BSS for (b) L/S=20 (c) L/S=50 (d) L/S=100 (Inserted image shows B loaded with $Pb^{2+}$) for an initial concentration 1000 mg/L

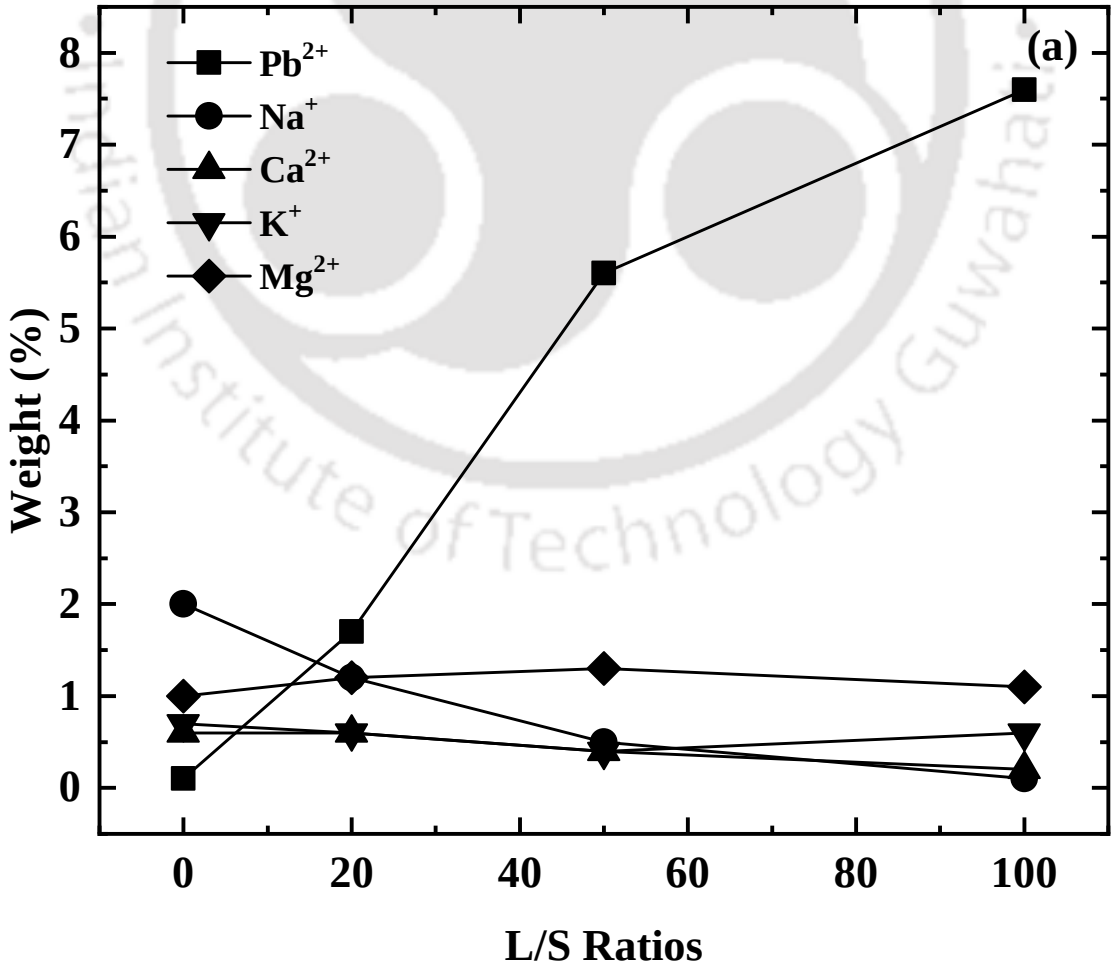

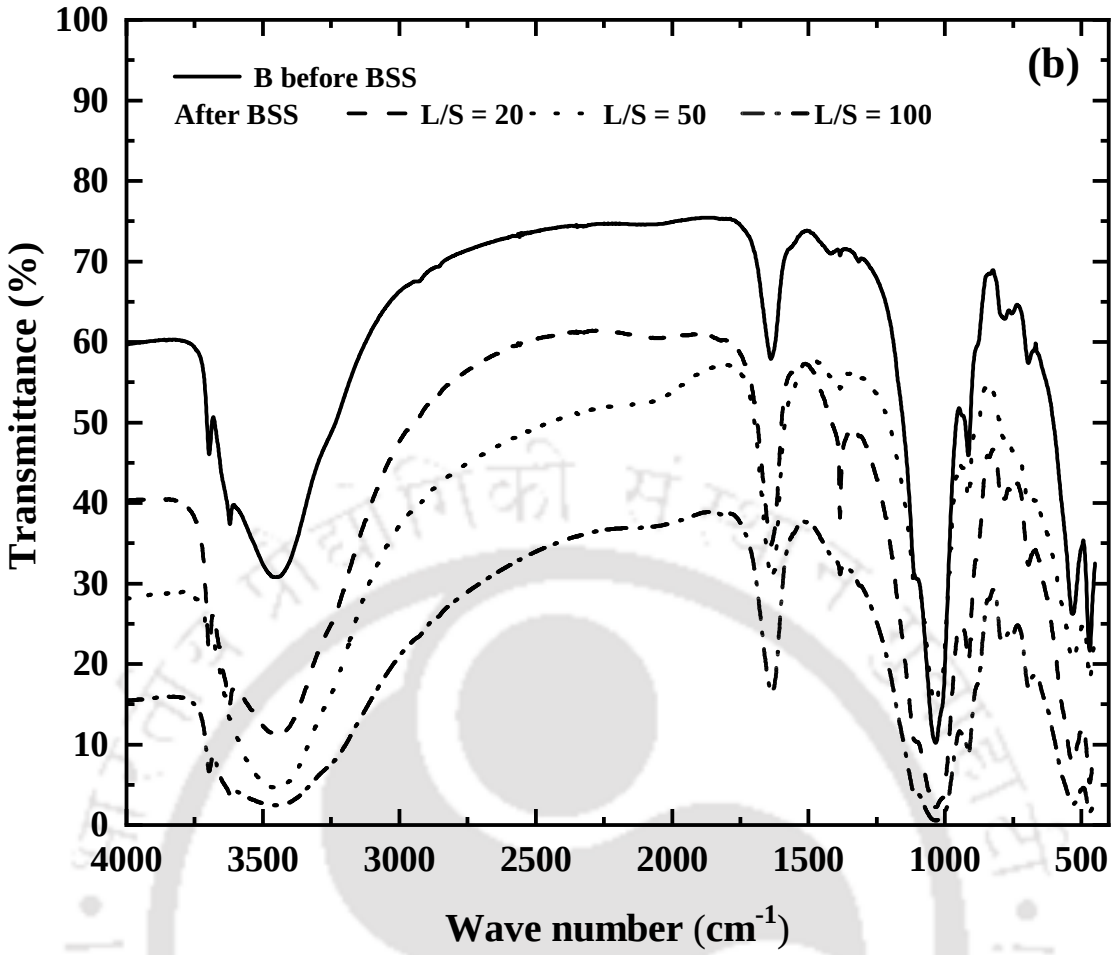


Figure 6.6: (a) Variation of exchangeable cations of B after $Pb^{2+}$ sorption and (b) FTIR spectrum of B before and after BSS for an initial concentration of 1000 mg/L and varying L/S

### 6.1.7 Sorption isotherm

The non-linear Freundlich and Langmuir isotherm models were fitted to the measured sorption data shown in Fig. 6.7(a), respectively. The fitting parameters of both the isotherms are presented in Table 6.1. It can be noted that Freundlich model can be a better model for representing the increasing trend of data with regression coefficient $R^2 \geq 0.95$. However, Langmuir model also could adequately represent the experimental data with $R^2 \geq 0.9$. Bennour (2013) reported that the adsorption of lead by B follows the Freundlich sorption isotherm. The values in Table 6.1 can be primary inputs for assessing the contaminant migration in a contaminant barrier using B. Based on the Freundlich and Langmuir isotherm model parameters, the retention capacity followed the order B (L/S = 100) > B (L/S = 50) > B-FFA30 (L/S = 20) > B (L/S = 20). The Langmuir sorption parameters were used to determine dimensionless separation factor $R_L$ and are presented in Fig. 6.7(b). It can

be observed that the values of $R_L$ is in the range of $0 < R_L < 1$ which indicates favorable sorption process. It can also be concluded that sorption is highly favorable at higher initial metal ion concentration and higher L/S ratio. Dimensionless factor $R_L$ also confirms the fact that L/S ratio is an important factor for determining sorption characteristics of B.

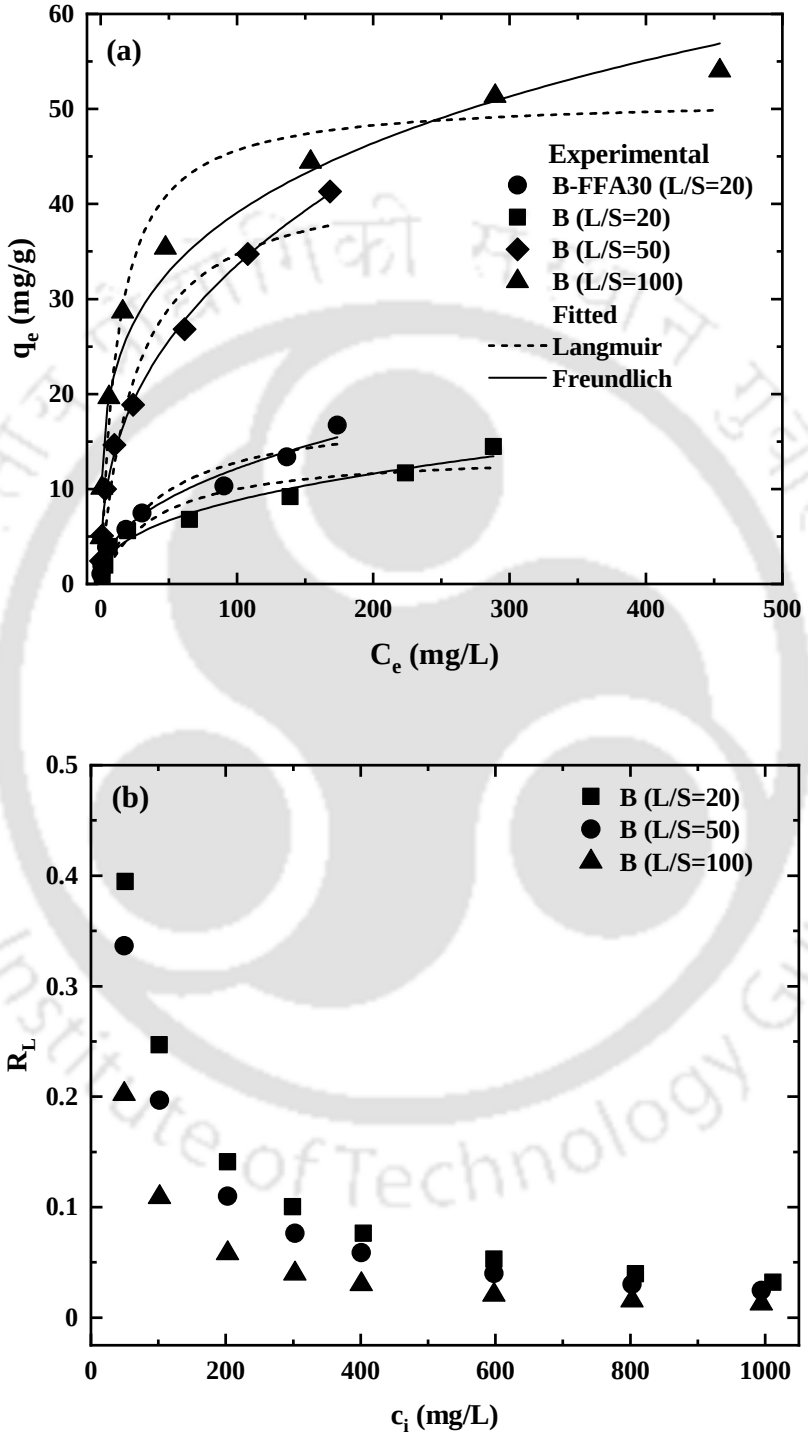


Figure 6.7: (a) Langmuir and Freundlich isotherm model fitted to BAS of B and B-FFA30 mix (b) Separation factor for $Pb^{2+}$ adsorption on B at different L/S

Table 6.1: Freundlich and Langmuir isotherm model fitted parameters for B and B-FFA30 mix

| Materials | Freundlich isotherm | | | Langmuir isotherm | | |
|---|---|---|---|---|---|---|
| | $K_f$ | $n$ | $R^2$ | $q_m$ (mg/g) | $b$ (L/mg) | $R^2$ |
| B-FFA30 (L/S=20) | 1.65 | 2.31 | 0.98 | 18.44 | 0.02 | 0.90 |
| B (L/S=20) | 1.40 | 2.50 | 0.96 | 13.90 | 0.03 | 0.87 |
| B (L/S=50) | 5.57 | 2.57 | 0.99 | 43.29 | 0.04 | 0.93 |
| B (L/S=100) | 12.45 | 4.03 | 0.97 | 51.20 | 0.08 | 0.95 |

## 6.2 Adsorption characteristics of Barmer bentonite for hazardous waste containment application

### 6.2.1 Background

As shown in Fig. 6.8, landfill liner system and slurry trenches are used to contain hazardous wastes (Du et al., 2015; Müller and Wöhlecke, 2017), which mainly constitute of bentonite as a mandatory construction material. The bentonite is known for its low hydraulic conductivity, expansive behavior in the presence of water, high specific surface area and contaminant retention properties.

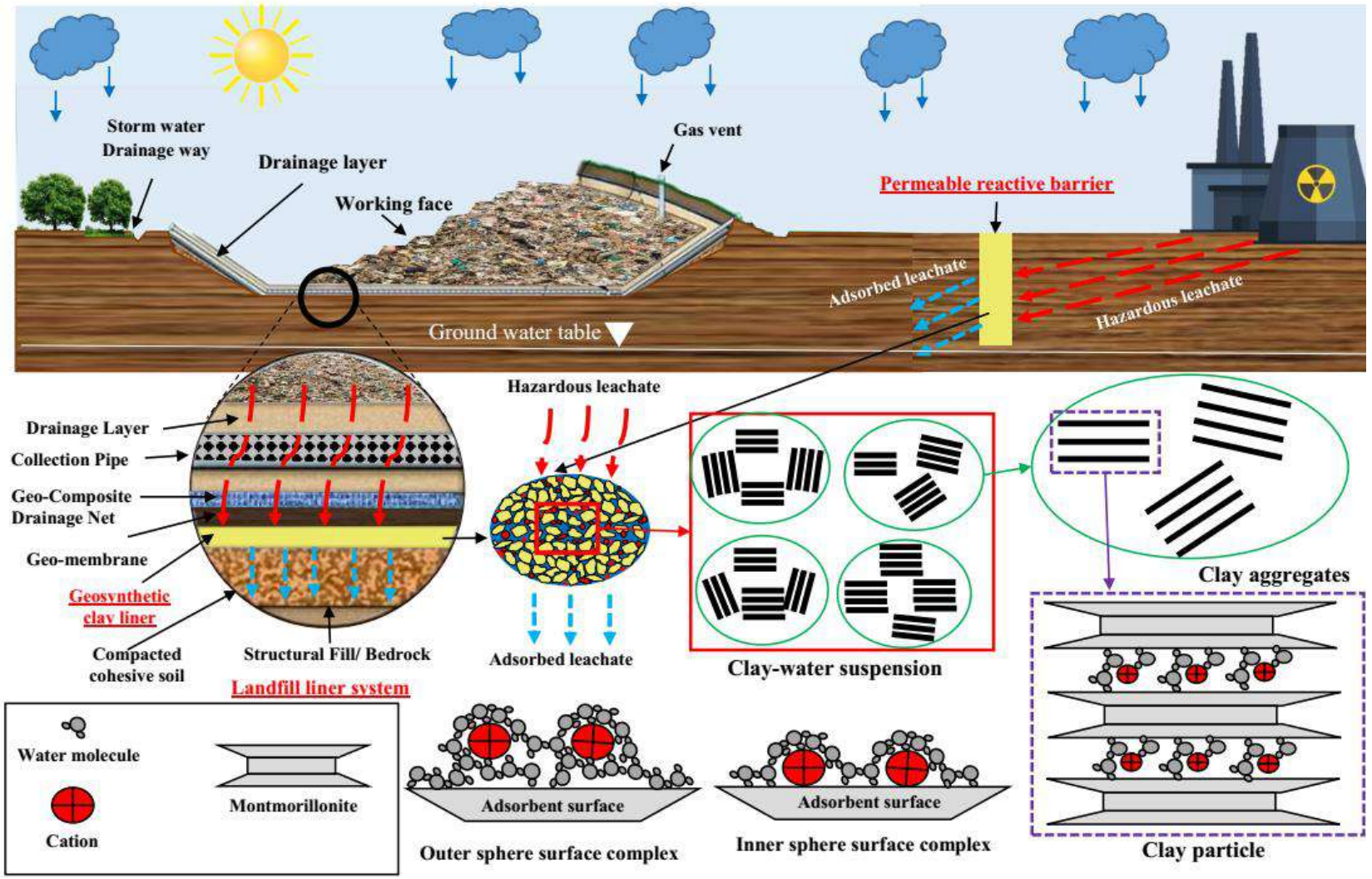


Figure 6.8: Utility of bentonite in liners and permeable reactive barrier for hazardous waste containment facility

These properties make it an ideal candidate construction material for waste containment liners and hydraulic barriers. The use of compacted clay (bentonite) liners has been found to reduce the migration of heavy metals through sub-soil (Sari et al., 2007; Xu et al., 2008; Mohammad et al., 2010). The shallow and deep nuclear waste disposal facilities across the world require bentonite as the compacted liner material for preventing the interaction of nuclear wastes with the surrounding environment. For the design and execution of hydraulic barriers and liners, hydraulic conductivity and contaminant sorption characteristics of bentonite are mandatory inputs.

Among the heavy metals, lead ($Pb^{2+}$) has been identified in literature as a causal agent for various health hazards (such as anemia, headache, diarrhea and poisoning leading to the kidney dysfunction, infertility, liver and brain damage), and this is particularly true for India (Das et al., 2016, 2018; Goswami et al., 2017; Kushwaha et al., 2018). Hence, $Pb^{2+}$ can be used as a model contaminant for establishing the contaminant sorption characteristics of soils. The adsorption capacity of bentonite makes it a candidate material for decontamination and treatment of harmful metal cations due to its negative charge (dos Reis et al., 2018). Usage of bentonite clay-water suspension for adsorbing detrimental metal ions in liner material and permeable reactive barrier was investigated and reported in the literature (Table 6.2). The process of retention of metal ions is mainly dominated by mechanisms such as outer-sphere complexation, inner-sphere complexation or precipitation at varying pH, which play an important role on the ultimate fate of metals contained in the landfills (Fig.6.8).

Adsorption capacity of bentonite for contaminants such as $Pb^{2+}$ depends on the source of extraction because the inherent mineralogy, local geological conditions directly influence specific surface area (SSA), cation exchange capacity (CEC), particle size distribution and zeta potential (Eren et al., 2009; Wang et al., 2009; Glatstein and Francisca, 2015; Lima et al., 2018). The geological influence is evident in the case of adsorption characteristics of $Pb^{2+}$ on clay from varied sources, as summarized in Table 6.2. The adsorption kinetics further vary with bentonite concentration, ionic strength of leachate, pH and temperature. Table 6.2 shows the effect of these parameters on $Pb^{2+}$ adsorption. However, there is a dearth of information on the adsorption characteristics of Indian origin bentonite for metals such as lead.

Table 6.2: State of the art on the use of different clays for lead adsorption

| Sl. No. | Bentonite type | Source | Maximum adsorption capacity (mg/g) | Corresponding equilibrium time (min) | Investigated parameters | | | | References |
|---|---|---|---|---|---|---|---|---|---|
| | | | | | pH | Temperature | Ionic strength | Adsorbent dose | |
| 1 | MX-80 bentonite | China | 68.58 | 125 | ✓ | ✓ | ✓ | ✓ | Xu et al., 2008 |
| 2 | Natural Bentonite | Saudi Arabia | 107 | 20 | x | ✓ | x | x | Hefne et al., 2008 |
| 3 | Jordanian bentonite | Jordan | 149.3 | NA | ✓ | ✓ | x | ✓ | Hamadneh et al., 2015 |
| 4 | Dijah-Monkin bentonite | DijahMonkin, Nigeria | 9.32 | 18 | x | ✓ | x | x | Alexander et al., 2018 |
| 5 | Turkish raw bentonite | Unye, Turkey | 16.70 | NA | ✓ | ✓ | x | x | Eren et al., 2009 |
| 6 | GMZ bentonite | Gaomiaozi County, China | 23.82 | 240 | ✓ | ✓ | ✓ | ✓ | Wang et al., 2009 |
| 7 | Montmorillonite-Illite composite clay | Gulbarga, Karnataka | 52 | 20 | ✓ | ✓ | x | x | Oubagaranadin and Murthy 2009 |
| 8 | Sodium polyphosphate modified kaolinite clay | Jordan | 40 | 9 | ✓ | ✓ | x | ✓ | Mohammad et al., 2010 |
| 9 | Palygorskite clay | Gansu, China | 68 | 480 | ✓ | x | x | ✓ | Chen and Wang, 2007 |
| 10 | Phosphate-modified kaolinite clay | Ubulu-Ukwu, Nigeria | 18 | 90 | x | ✓ | x | x | Unuabonah et al., 2007 |
| 11 | Tetraethylenepentamine modified chitosan | Aladdin, China | 144 | 15 | ✓ | x | ✓ | x | Fan et al., 2017 |
| 12 | Patagonia bentonite | Northern Patagonia, Argentina | 210 | 45 | ✓ | x | ✓ | x | Glatstein and Francisca, 2015 |
| 13 | Chitosan immobilized on bentonite | NA | 28.77 | 55 | x | x | x | ✓ | Futalan et al., 2011 |
| 14 | Activated bentonite | Kütahya region, Turkey | 50 | 40 | x | ✓ | x | x | Kul and Koyuncu, 2010 |
| 15 | H2SO4 activated bentonite | Unye, Turkey | 8.92 | NA | ✓ | ✓ | x | x | Eren et al., 2009 |
| 16 | Manganese oxide-coated bentonite | Unye, Turkey | 58.88 | NA | ✓ | ✓ | x | x | Eren et al., 2009 |
| 17 | 8-hydroxy quinoline-immobilized bentonite | Canakkale, Turkey | 142.94 | 60 | ✓ | ✓ | ✓ | x | Özcan et al., 2009 |
| 18 | Turkish kaolinite clay | Bandrma Region, Turkey | 31.75 | 35 | ✓ | ✓ | x | ✓ | Sari et al., 2007 |
| 19 | Iranian bentonite-clay composite | Iran | 95 | 240 | x | x | x | x | Salem and Sene, 2011 |
| 20 | Present study (Barmer bentonite) | India | 55 | 5 | ✓ | ✓ | ✓ | ✓ | |

In India, bentonite is primarily sourced from the mines of Barmer district (state of Rajasthan) and is identified as a prominent construction material for municipal, industrial, nuclear hazardous waste containment and permeable reactive barriers (Rao and Ravi, 2013, 2015). India is at the forefront of industrial growth to sustain the second largest population in the world and thus producing higher amounts of hazardous wastes than ever before. Any steps to employ Barmer bentonite (B) for hazardous waste containment in landfill liner need prior knowledge of the adsorption kinetics and allied behavior for the contaminant in question. Previous studies on B have mostly focused on hydro-thermo-mechanical properties such as hydraulic conductivity, water retention, volume change, consolidation characteristics and strength (Bharat and Das, 2017; Gapak et al., 2017; Bharat and Gapak, 2018; Gapak and Tadikonda, 2018). The adsorption characteristics of B and the effect of different factors affecting contaminant interaction have not been studied in detail.

The objective of this study is to explore the adsorption characteristics of B for its application in hazardous and nuclear waste containment facilities by considering $Pb^{2+}$ as the model contaminant. For this purpose, B was characterized for its chemical structure, chemical composition, physical and geotechnical properties. Further, kinetics and equilibrium adsorption characteristics of B were performed at different solute to solution ratios. Thereafter, batch tests were performed to quantify the adsorption of $Pb^{2+}$ by B at varying experimental conditions, viz. pH, ionic strength, temperature and multiple contaminants. The obtained experimental data were quantified using different adsorption isotherm models and thermodynamic parameters. Additionally, the obtained results were interpreted with respect to the chemical characteristics and microstructural imaging.

### 6.2.2 Theoretical calculations

#### Adsorption kinetics

Kinetic models can help to understand the mechanism of metal adsorption by adsorbent with time. For the adsorption of heavy metal, the commonly used kinetic models are (a) pseudo-first-order kinetic model (Eq. 6.6) and (b) a pseudo-second-order kinetic model (Eq. 6.7) (Ho and McKay, 1999; Chen and Wang, 2007) based on solid-phase sorption

$$\ln(q_e - q_t) = \ln(q_e) - k_1 t \tag{6.6}$$

$$\frac{t}{q_t} = \frac{1}{2k_2 q_e^2} + \frac{1}{q_e} t \tag{6.7}$$

where $q_t$ (mg.g$^{-1}$) is the amount of $Pb^{2+}$ adsorbed on B at time t (min), $q_e$ (mg.g$^{-1}$) is the equilibrium adsorption capacity, $k_1$ (min$^{-1}$) is the pseudo-first-order adsorption rate constant, $k_2$ (g.mg$^{-1}$.min$^{-1}$) is the pseudo-second-order rate constant.

**Adsorption isotherms**

The Langmuir and Freundlich adsorption isotherm models were adopted in this study to understand the equilibrium sorption behavior of $Pb^{2+}$ as affected by various experimental conditions. Sorption isotherm is the relationship between the ions sorbed on the adsorbent and the consequent equilibrium concentration in the aqueous phase. The linear form of the Langmuir isotherm equation was used in the current study as follows:

$$\frac{C_e}{q_e} = \frac{1}{bq_{max}} + \frac{C_e}{q_{max}} \tag{6.8}$$

where $C_e$ represents the equilibrium metal ion concentration remaining in the solution (mg.L$^{-1}$); $q_e$ is the adsorbed amount of metal ions per unit weight of adsorbent solid after attaining equilibrium (mg.g$^{-1}$); b (L.mg$^{-1}$) and $q_{max}$ (mg.g$^{-1}$) are the constants, which represents adsorption energy and maximum adsorption capacity, respectively. The Freundlich isotherm accommodates multi-layers of adsorption sites on the solid as against a single layer for the Langmuir model. It is mostly suitable for assessing the adsorption data at low and intermediate concentrations on heterogeneous surfaces. The linearized form of the model is as below:

$$\ln(q_e) = \ln(K_f) + n\ln(C_e) \tag{6.9}$$

Where $q_e$ is the sorbed concentration (mg.g$^{-1}$), $C_e$ is the equilibrium solution concentration (mg/L), $K_f$ is the Freundlich coefficient (mg$^{1-N}$L$^n$kg$^{-1}$) and n is the exponent, which determines the degree of sorption linearity.

The Elovich isotherm model is associated with the kinetic principle which is based on the assumption that adsorption site on adsorbent surfaces increases exponentially with the adsorption of metal ions, which indicates a multilayer adsorption. The linear form of Elovich isotherm equation for this study is presented below:

$$\ln(\frac{q_e}{c_e}) = \ln(K_e q_m) - \ln(\frac{q_e}{q_m}) \tag{6.10}$$

Where $q_m$ is the maximum Elovich adsorption capacity, $K_e$ is the constant, which can be evaluated using the slope and intercept obtained from the plot $\ln(\frac{q_e}{c_e})$ and $q_e$.

**Thermodynamic parameters**

Thermodynamic parameters viz. change in free energy ($\Delta G^o$), enthalpy ($\Delta H^o$) and entropy ($\Delta S$) were evaluated by considering the equilibrium adsorption data obtained at different temperatures. It was noted from the literature that the earlier methods (Xu et al., 2008; Wang et al., 2009; Tran et al., 2017) for evaluating thermodynamic parameters related to adsorption was found to be inadequate as highlighted by Liu (2009) and Ghosal and Gupta (2017). In this study, the thermodynamic equilibrium constant, $K_e^o$(dimensionless) for the adsorption reaction was determined from Eq. 6.11 (Lima et al., 2019). The free energy change ($\Delta G^o$) for the adsorption of $Pb^{2+}$ on bentonite was calculated from Eq. 6.12.

$$K_e^o = \frac{1000.b.molecularweightofadsorbate.[Adsorbate]^o}{\gamma} \tag{6.11}$$

$$\Delta G^o = -RT\ln(K_e^o) \tag{6.12}$$

Where $R$ is the universal gas constant (8.314 J/mol K), $T$ is the temperature (in K) $[Adsorbate]^o$ is the standard adsorbate concentration equal to 1 mol.$L^{-1}$, $\gamma$ is the activity coefficient, which is a dimensionless quantity for the adsorption reaction. It is taken as unity for very dilute adsorbate solution, b is the Langmuir isotherm equilibrium constant. The Gibbs free energy ($\Delta G^o$) can also be expressed by the following equation:

$$\Delta G^o = \Delta H^o - T\Delta S^o \tag{6.13}$$

By combining Eqs. 6.11 to 6.13, Eq. 6.14 can be obtained.

$$\ln(K_e^o) = \frac{\Delta S^o}{R} - \frac{1}{T}.\frac{DeltaH}{R} \tag{6.14}$$

### 6.2.3 Adsorption kinetics of Barmer bentonite

Figure 6.9 presents the adsorption capacity of B and the percentage removal of $Pb^{2+}$ at different interaction times varying from 1 minute to 240 minutes. It can be noted that the adsorption reaction is rapid and reaches the equilibrium adsorption capacity within 5 min for B. For a low initial concentration of 200 mg.$L^{-1}$, the percentage removal is close

to 100% for all three doses of B. As the initial concentration of $Pb^{2+}$ increases, there is not much change in the time required to reach equilibrium adsorption capacity. Hence, it can be summarized that there is no effect of adsorbent dose and initial concentration of $Pb^{2+}$ on the kinetics of adsorption reaction for B. However, the percentage removal was found to decrease as the initial concentration of $Pb^{2+}$ increases and the dose of B decreases. The difference is pronounced for the initial concentration of 1000 mg. $L^{-1}$, which could be attributed to the higher competition of ions for the available adsorption sites, which progressively reduces as the dose decreases.

Figures 6.10a and 6.10b present the linear plots to determine the first-order and second-order adsorption rate constants, respectively. The rate constant parameters are summarized in Table 6.3, from where it can be observed that the kinetics of adsorption of B with $Pb^{2+}$ follows second-order equation as compared to the first-order equation, which is indicated by a high coefficient of regression ($R^2$) close to 1. The inadequacy of first-order kinetics reaction for clays like bentonite was also reported in the literature (Hamidpour et al., 2011; Hamadneh et al., 2015). The suitability for the second-order kinetic equation for B is indicative of the possible chemisorption occurring on B sorption sites (Hefne et al., 2008; Hamidpour et al., 2011).

### 6.2.4 Effect of adsorbent and adsorbate concentration

The adsorption capacity and percentage removal of $Pb^{2+}$ by B as a function of adsorbent concentration are shown in Fig. 6.11a. It can be observed that the percentage removal increased with an increase in adsorbent dosage, while the adsorption capacity gradually decreased. The adsorption capacity or, in other words, adsorption efficiency, was found to be high at a lower adsorbent dose as the majority of the clay surface area was readily available for the $Pb^{2+}$ ions (Gupta and Bhattacharyya, 2012). This finding is mostly true for those soils, which react with water and exhibit swelling. As the adsorbent dose increases, the solution becomes more turbid and gel-like consistency, as shown in Fig. 6.11b. For low adsorbent dose, the solution is relatively clear and swelling is less. At higher adsorbent dose, the thick gel-like consistency inhibits the proper interaction of metal ion with solid surface. Hence, the uptake on solids decreases, which is different from non-expansive soils and sediments. Furthermore, as stated by Xu et al. (2008), the competition among the functional groups on a solid surface is inevitable at higher adsorbent dose, thereby decreasing the adsorption ability.

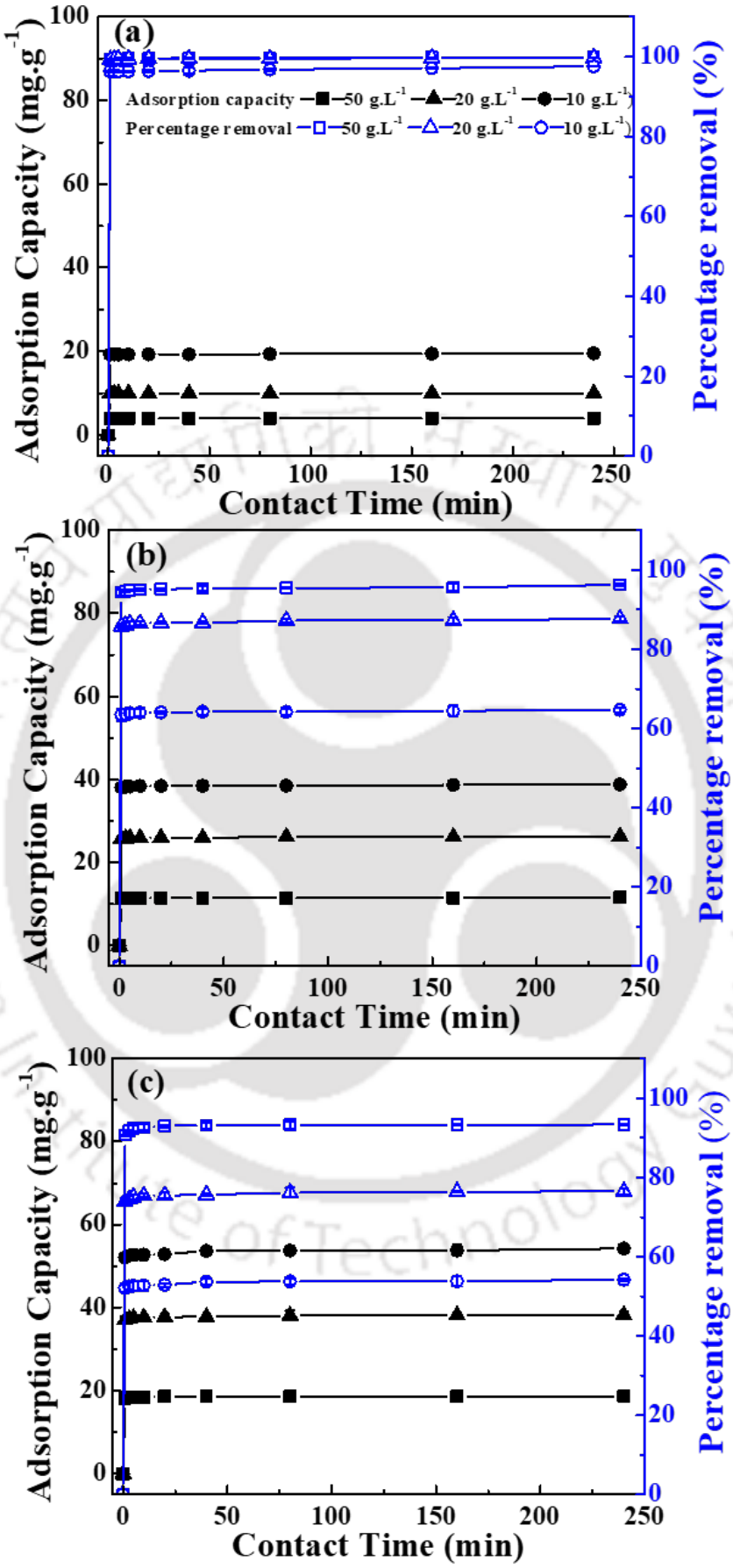


Figure 6.9: Adsorption capacity as a function of contact time at (a) 200 (b) 600 and (c) 1000 mg $L^{-1}$

Table 6.3: Comparison between the Adsorption Rate Constants, $q_e$, associated with Pseudo-first-order and second-order equation

| Initial $Pb^{2+}$ conc. ($mg.L^{-1}$) | Adsorbent concentration ($g.^{-1}$) | Pseudo-first-order rate equation | | | Pseudo-second-order rate equation | |
|---|---|---|---|---|---|---|
| | | $K_1$ ($min^{-1}$) | $q_e$(exp) ($mg.g^{-1}$) | $R^2$ | $K_2$ ($g.mg^{-1}.min^{-1}$) | $R^2$ |
| 200 | 50 | 0.0167 | 3.994 | 0.960 | 2.852 | 1 |
| | 20 | 0.0124 | 9.971 | 0.876 | 1.143 | 1 |
| | 10 | 0.0063 | 19.519 | 0.988 | 0.122 | 0.9999 |
| 600 | 50 | 0.0049 | 11.554 | 0.688 | 0.202 | 0.9999 |
| | 20 | 0.0087 | 26.31 | 0.782 | 0.1 | 0.9999 |
| | 10 | 0.0085 | 38.811 | 0.802 | 0.078 | 0.9999 |
| 1000 | 50 | 0.0154 | 18.676 | 0.591 | 0.321 | 1 |
| | 20 | 0.0238 | 38.23 | 0.973 | 0.07 | 1 |
| | 10 | 0.0102 | 54.213 | 0.729 | 0.03 | 0.9999 |

However, with the increase in adsorbent dosage, the percentage removal increases (regardless of lower adsorption efficiency) due to readily available sites for binding $Pb^{2+}$. From Eq. 6.2, it may be noted that the determination of percentage removal is based on the initial and equilibrium concentration of the solution. Even with diminished adsorption capacity (lead uptake on the solid surface), there are still enough binding sites, and hence the equilibrium concentration left in the solution is considerably less. This observation is similar to the findings reported earlier in the literature (Chen and Wang, 2007; Sari et al., 2007; Xu et al., 2008).

In terms of adsorbate dosage, the knowledge of the requisite amount of bentonite mass per liter required for complete adsorption is essential. It was observed in Fig. 6.11a that for a particular adsorbent dosage, percentage removal was highest for lower adsorbate concentration (i.e., 200 $mg.L^{-1}$) followed by 600 and 1000 $mg.L^{-1}$. For 200 $mg.L^{-1}$ of adsorbate concentration, nearly 100% removal was achieved at 10 g $L^{-1}$ of adsorbent dosage. However, only 93-95% removal was possible even at 50 $g.L^{-1}$ of adsorbent dosage for the higher adsorbate concentration. Even though there is a drastic change in percentage removal between 200 and 600 $mg.L^{-1}$, there is only a minimal variation as the initial concentration increases from 600 to 1000 $mg.L^{-1}$. The sorbed concentration of $Pb^{2+}$ on the B surface was found to be less for lower initial concentration due to the low concentration gradient between the solution and the solid surface (Akpomie and Dawodu, 2015).

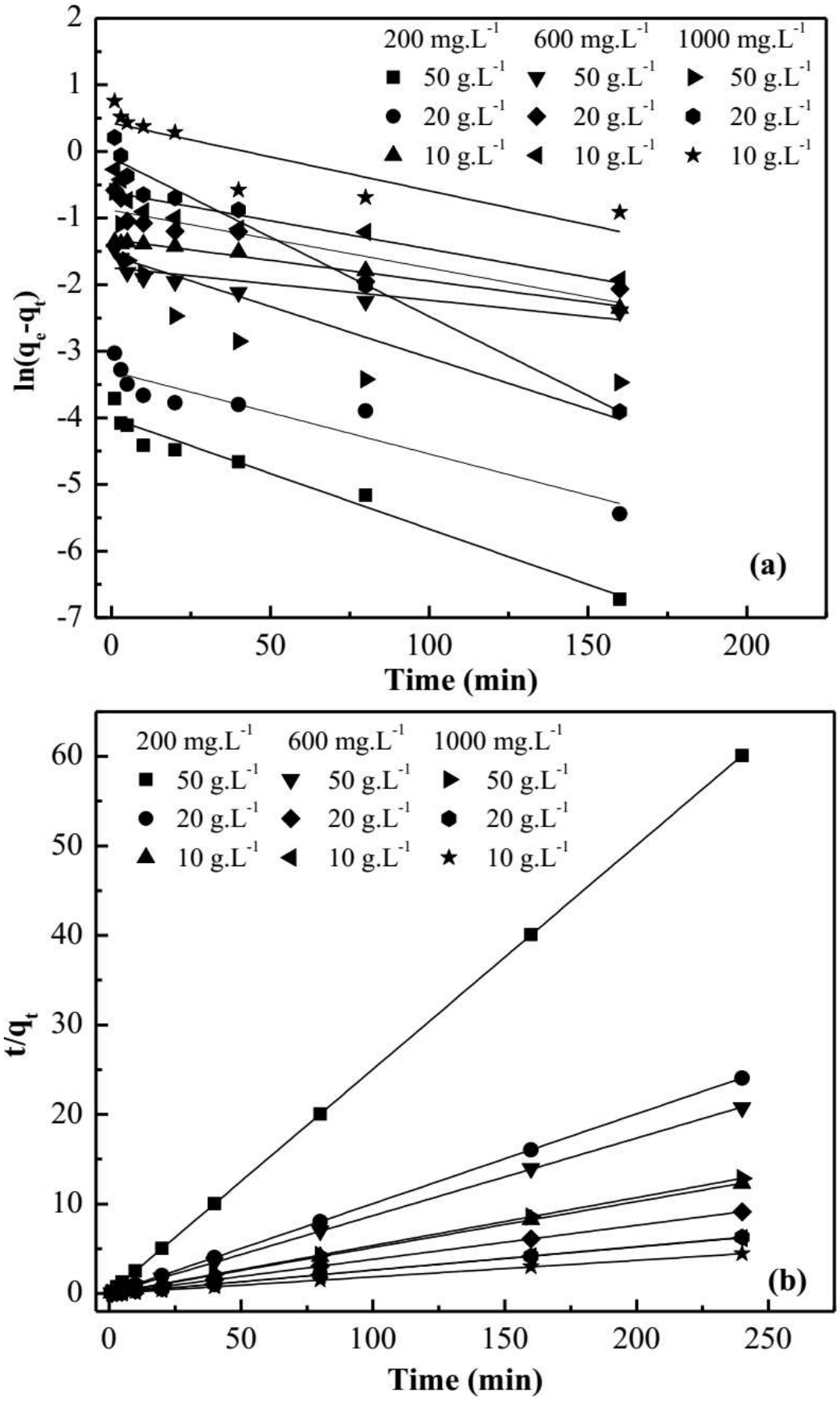


Figure 6.10: Kinetics model for Barmer bentonite (a) Pseudo-first-order kinetics (b) pseudo-second-order kinetics

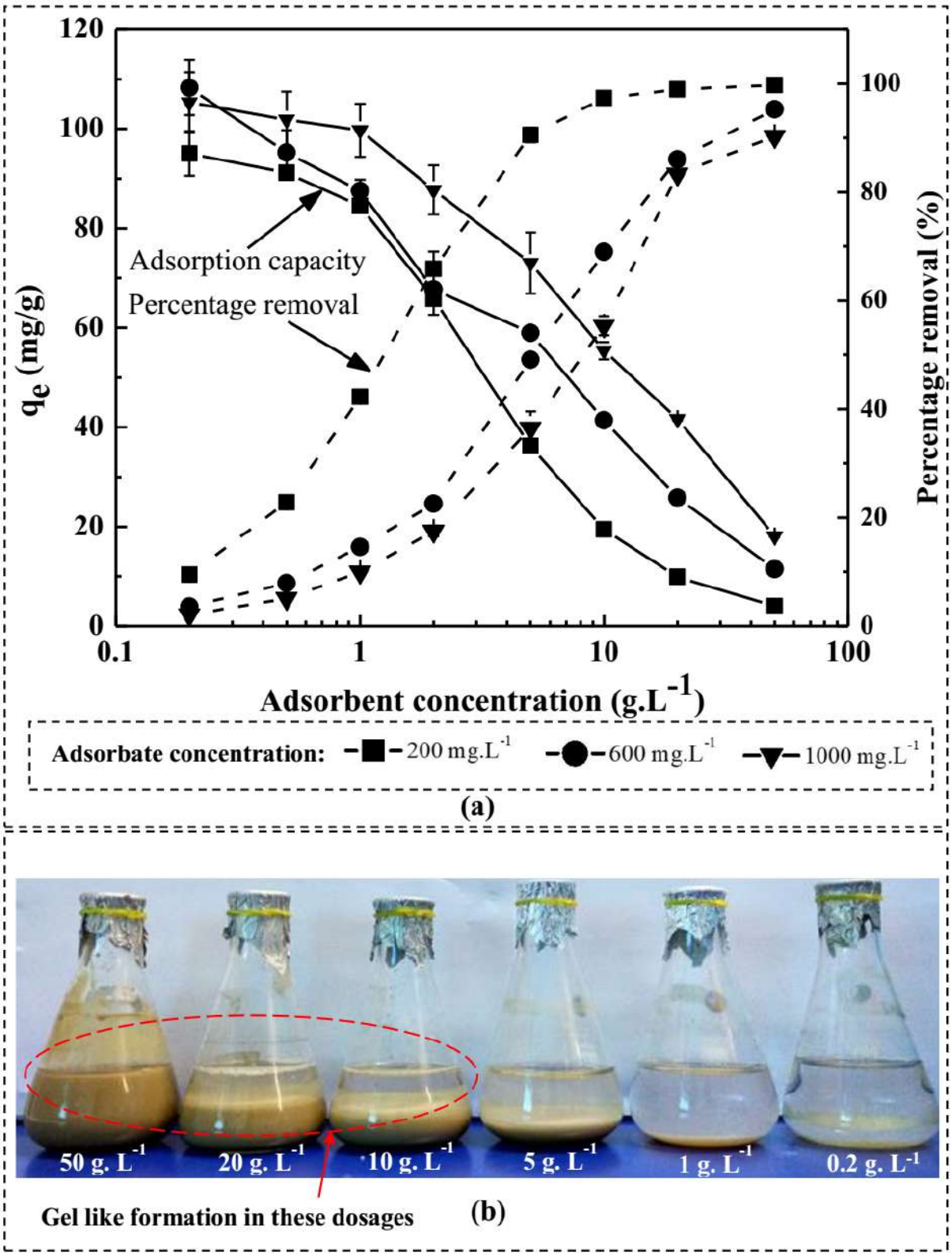


Figure 6.11: (a) Adsorption capacity of $Pb^{2+}$ at different bentonite dosage (b) Pictorial images of bentonite suspension after 24-hr batch test at different bentonite dosage

### 6.2.5 Effect of ionic strength on adsorption capacity of Barmer bentonite

The influence of ionic strength on $Pb^{2+}$ adsorption capacity and percentage removal at varying concentration (0.01M  0.75M) was investigated by considering four different salts (Fig. 6.12 ). The effect of four salts, namely LiCl (expected from e-waste leachate), NaCl, KCl and $CaCl^2$ (expected from municipal waste) on $Pb^{2+}$ sorption was explored. Fig. 6.12a shows the suppressive impact of competing salt ions on $Pb^{2+}$ adsorption capacity and percentage removal (Xu et al., 2008). The adsorption capacity and percentage removal exponentially decreased with an increase in molar concentration of competing salt ions. At lower salt concentration ($< 0.3$M), $CaCl^2$ salt distinctly suppresses the adsorption capacity and percentage removal to the highest magnitude when compared with other salts. On the contrary, at a higher concentration of the salt solution, there is a minimal variation of adsorption capacity regardless of salt solution. The EDX analysis (not presented for brevity) of sorbed B also confirms the increase in salt ions and a decrease in $Pb^{2+}$ weight percentage. For the same lower concentration of the salt solution ($< 0.1$ M), the agglomeration of B after sorption was observed to be highest (from FESEM images not presented here) for $CaCl^2$ and lowest for NaCl, which affects the uptake of $Pb^{2+}$ as shown in Fig. 6.12.

It is well established in the literature that the fabric of fine-grained bentonite clay at micro-scale influences macroscopic emergent properties such as Atterberg limits, compression index, hydraulic conductivity and mechanical strength (Cuevas et al., 2012). The expected particle arrangement of bentonite clay at varying ion concentrations has been discussed in the literature (Luckham and Rossi, 1999; Palomino and Santamarina, 2005; Shen et al., 2017; Zhang et al., 2019b). The clay particles remain at a dispersed state when there is no salt solution interaction. With the increase in ion concentration, clay particles are expected to arrange from edge-to-edge orientation to edge-to-face orientation and finally face-to-face orientation (Fig. 6.12b). These microscopic morphology changes with varying ionic strength were captured using FESEM images (micrographs) on adsorbed clay particles for KCl salt solution (Fig. 6.13). An examination of Fig. 6.13 reveals that at a dispersed orientation, the clay faces are available for adsorption due to high diffused double layer (DDL) thickness.

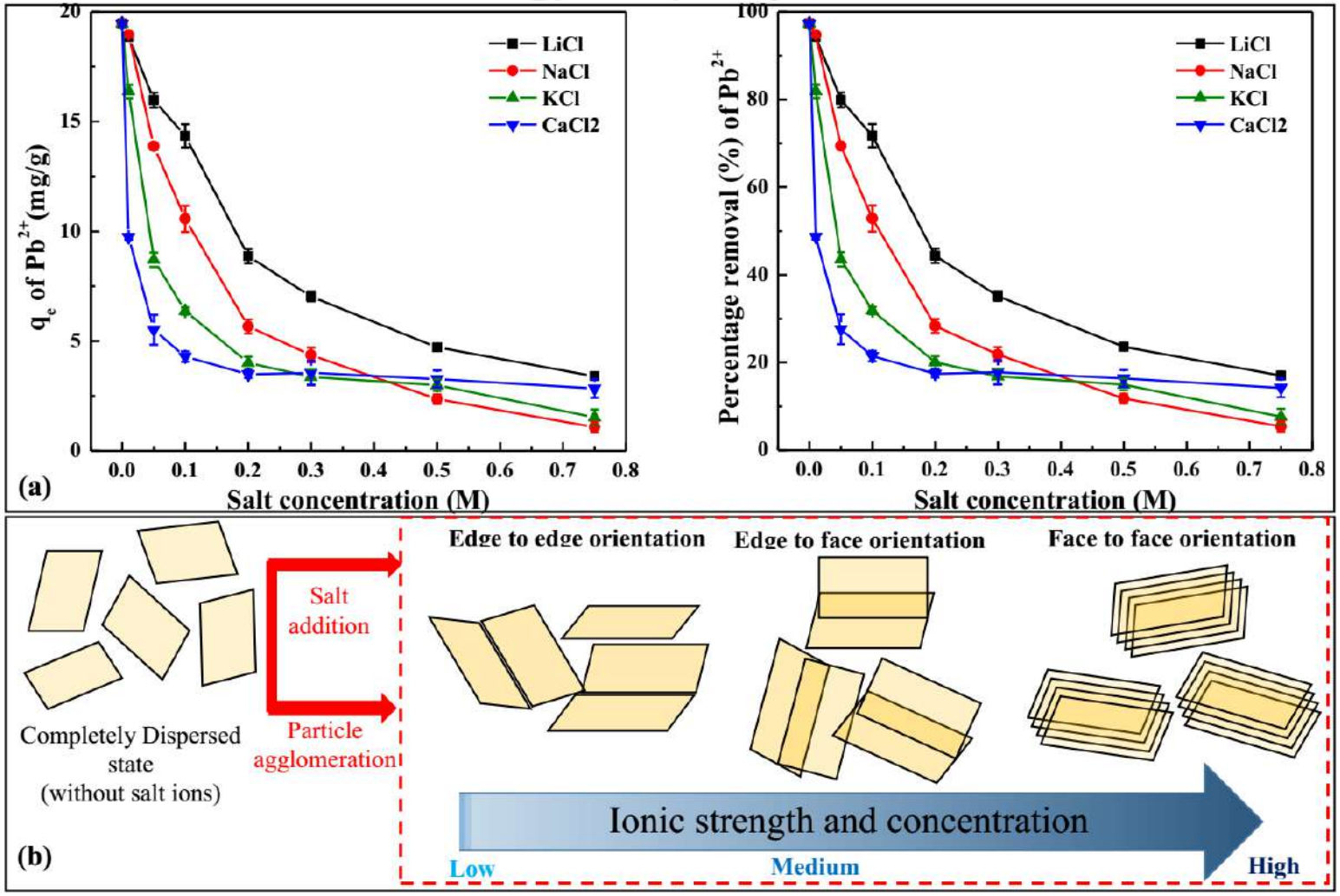


Figure 6.12: Effect of ionic strength on the (a) adsorption capacity and percentage removal of $Pb^{2+}$ at (Ci= 200 mg. $L^{-1}$, pH= 5, adsorbent concentration=10 g.$L^{-1}$, T = 300 K), (b) Fabric map for bentonite particles at varying ionic strength (modified after Zhang et al. 2019)

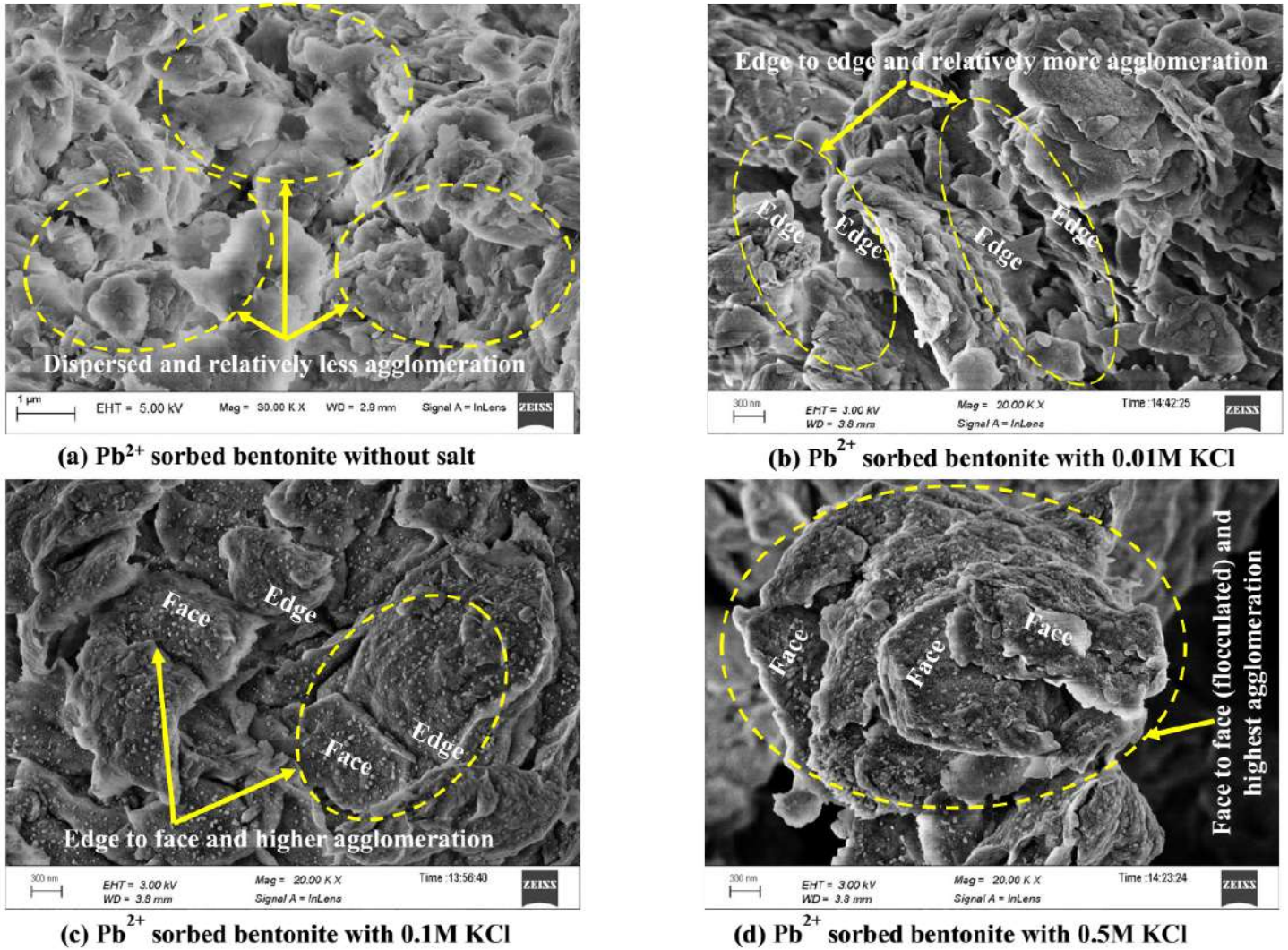


(a) $Pb^{2+}$ sorbed bentonite without salt

(b) $Pb^{2+}$ sorbed bentonite with 0.01M KCl

(c) $Pb^{2+}$ sorbed bentonite with 0.1M KCl

(d) $Pb^{2+}$ sorbed bentonite with 0.5M KCl

Figure 6.13: Orientation of clay fabric at different concentration of salt solution (KCl) prepared at 200 mg. $L^{-1}$ of adsorbate dosage

In contrast, an increase in ionic strength reduces the DDL thickness between clay particles, promoting less available surface area (Glatstein and Francisca, 2015). Along the same lines, aggregation and flocculation of bentonite particles reduce the exposed adsorption area and diminishes adsorption capacity (Musso et al., 2014).

The $CaCl^2$ salt distinctly suppresses the adsorption capacity to the highest magnitude as compared with other salts as it is divalent ($Ca^{2+}$) in nature, which can easily repel the $Pb^{2+}$ ions. This phenomenon was recently reported by Fan et al. (2017), wherein divalent ions ($Ca^{2+}$ and $Mg^{2+}$) were found to exhibit a higher suppressive impact on $Pb^{2+}$ adsorption compared to $Na^+$ and $K^+$. While there is no variation for the divalent salt beyond 0.2M of salt concentration, the monovalent salts show a further decrease in adsorption capacity at higher concentrations. The observation could be attributed to the repelling effect between monovalent salt ions with the already present exchangeable cations ($Na^+$, $Ca^{2+}$, $Mg^{2+}$ and $K^+$). This was quite apparent for NaCl and KCl exhibiting lowest $Pb^{2+}$ adsorption capacity at the highest concentration. This is due to already present $Na^+$ and $K^+$ (refer Table 3.2) ions in the parent bentonite material. In terms of monovalent salts, the ionic radius of cation further governs the adsorption capacity with $Li^+$ (182 pm), showing the least repulsive action as compared to $Na^+$ (227 pm) and $K^+$ (280 pm).

The suppressing effect of salt concentration was further investigated by conducting XRD tests on adsorbed clay samples at the different salt concentrations for NaCl salt solution (Fig. 6.14). It can be observed from the XRD spectra that at higher concentrations (specifically after 0.3M), peaks of NaCl became more consistent, which shows the competitive effect of $Na^+$ ions on $Pb^{2+}$ adsorption. Similar peaks were observed for both $K^+$ and $Li^+$ (data not reported). Furthermore, with an increase in concentration, it was noticed that the montmorillonite peaks decreased in the XRD spectra, which may be indicative of diminishing adsorption capacity.

### 6.2.6 Effect of initial pH on adsorption capacity of Barmer bentonite

The adsorption of metals onto the bentonite surface is influenced by the pH of the solution because positively charged hydrogen ions themselves compete with adsorbate ions. The removal efficacy of $Pb^{2+}$ as a function of pH variation (2-9) is shown in Fig. 6.15 (a-c). The pH effect was investigated at three different adsorbent doses and adsorbate solute concentrations. Both adsorption capacity and percentage removal increased up to a certain pH (mostly in the acidic state) and after that became constant at pH of 6 (Wang et al.,

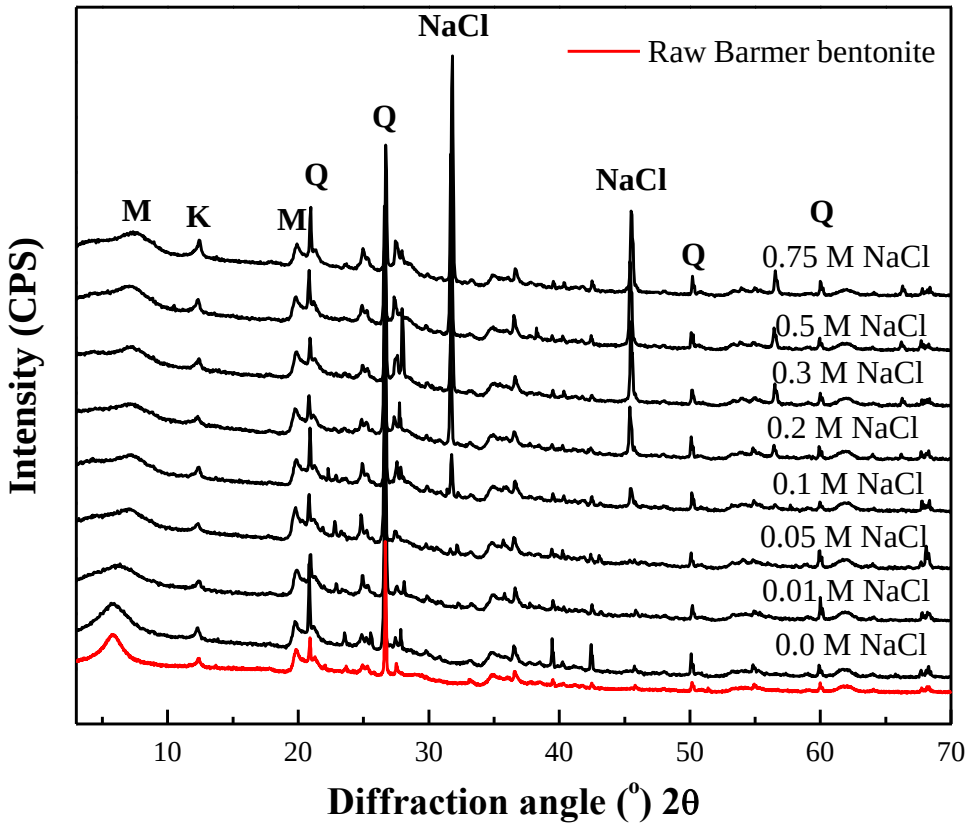


Figure 6.14: XRD spectra of raw Barmer bentonite and $Pb^{2+}$ adsorbed bentonite in presence of salt solution of varying concentration for Ci = 200 mg. $L^{-1}$

2009). Regardless of pH, adsorption capacity increased with a decrease in adsorbent dose (10 > 20 > 50 in g.$L^{-1}$) due to the explanation stated above. Adsorption capacity drastically increased at basic pH with adsorbate concentration (200, 600 and 1000 mg. $L^{-1}$), as shown in Fig. 6.15 (a-c). Under highly acidic conditions (pH 1), there was not a marked effect of adsorbent dose on the adsorption capacity. Wang et al. (2009) investigated the effect of varying pH at adsorption of $Pb^{2+}$ by GMZ bentonite. It was reported that in the range of pH 6.5-10, the removal of $Pb^{2+}$ maintained maximum level after initially increasing from pH (1- 6.5). The results from this study for BB also matched well with the findings reported by Wang et al. (2009).

The decrease in $Pb^{2+}$ adsorption at lower pH values can be attributed to the competition for exchange sites (i.e., negatively charged metal-binding sites) between $H^+$ and $Pb^{2+}$ cations (Eren et al., 2009; Fan et al., 2017). This was further substantiated from the zeta potential plot of the parent bentonite material (Fig. 6.15d), wherein it was observed that surface charge decreased at lower pH values. Further analysis through EDX spectra of adsorbed bentonite samples (Fig. 6.16) for 200 mg. $L^{-1}$ and adsorbent concentration = 10 g.$L^{-1}$) also showed a decrease in $Pb^{2+}$ weight percentage with a gradual reduction in pH

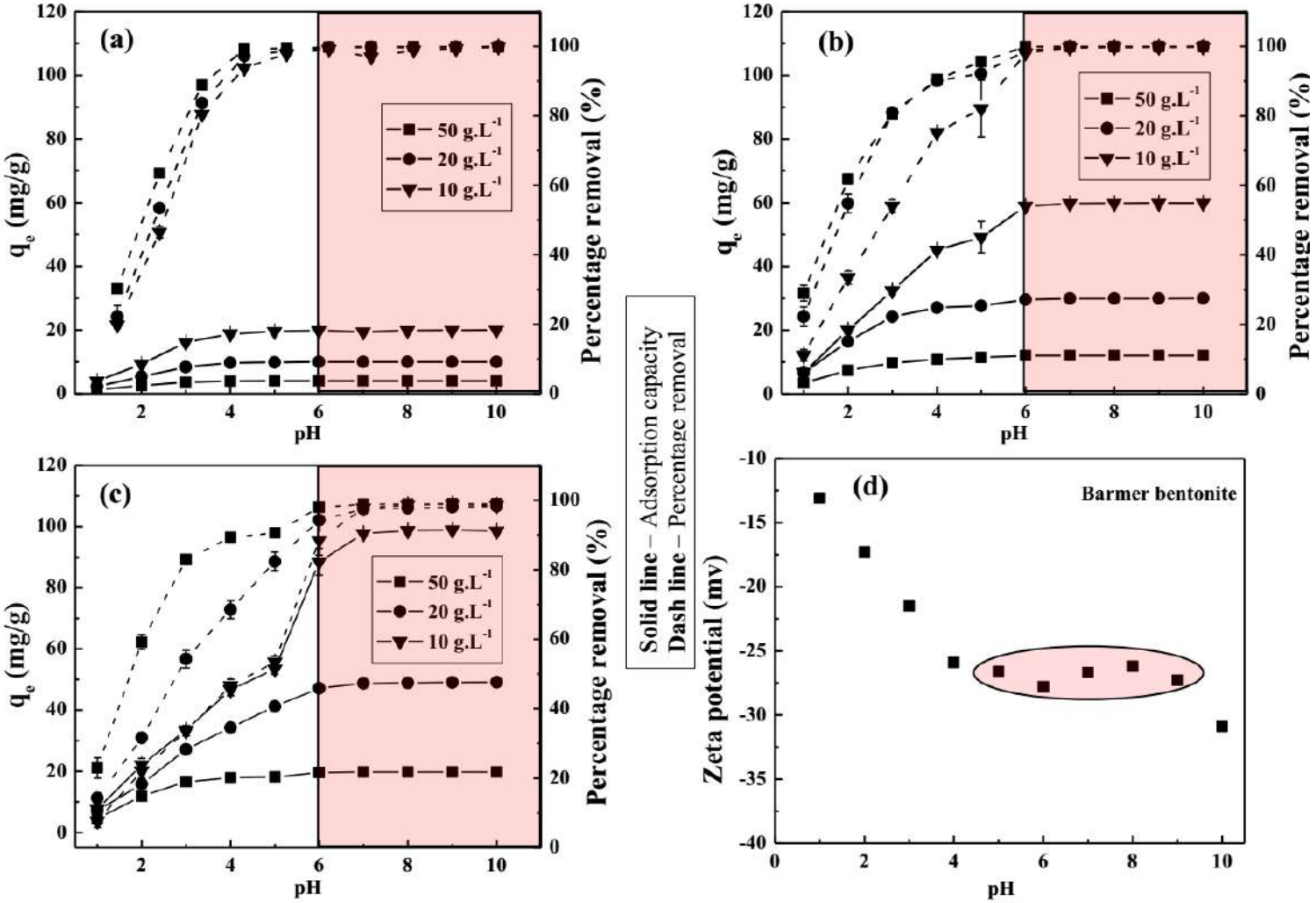


Figure 6.15: Effect of pH on adsorption capacity and percentage removal at (a) 200, (b) 600 and (c) 1000 mg. $L^{-1}$; and (d) Zeta potential response at different pH for Barmer bentonite

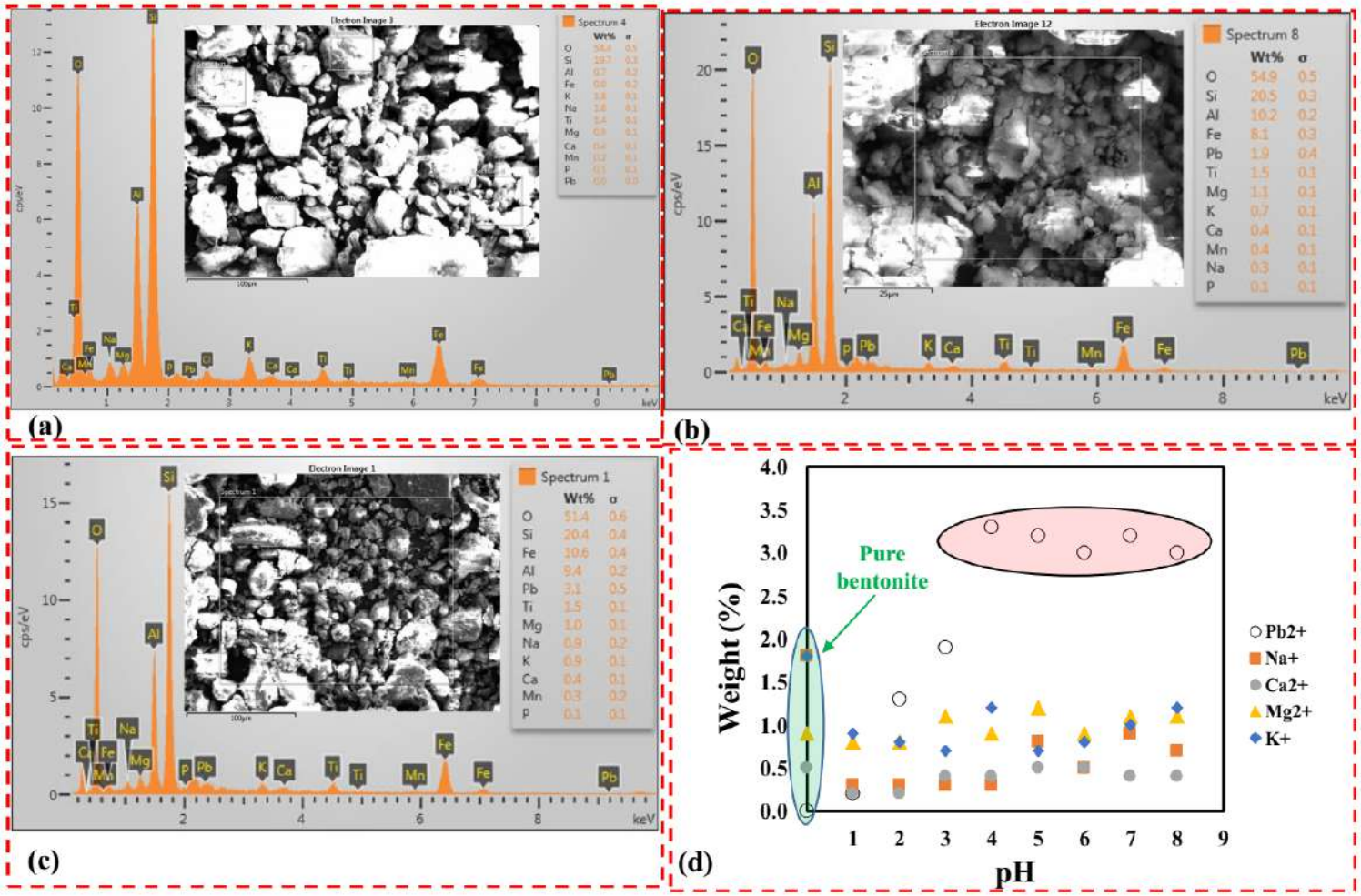


Figure 6.16: EDX spectra of (a) Pure bentonite, $Pb^{2+}$ adsorbed bentonite at (b) pH=3, (c) pH=6 and (d) variation of exchangeable cations and $Pb^{2+}$ ions obtained from EDX of adsorbed bentonite samples at different pH (1-8) for 200 mg. $L^{-1}$ and adsorbent concentration=10 g.$L^{-1}$

values (4 to 1). Regardless of adsorbent dose and adsorbate concentration, adsorption capacity reached its potential (95-100 percentage removal) close to pH 6 and thereafter became constant. Adsorption capacity becomes constant at higher pH conditions due to available binding sites of Barmer bentonite, reaching its potential for $Pb^{2+}$ sorption (zeta potential becomes constant after pH = 5). This was also characterized by a constant $Pb^{2+}$ weight percentage based on EDX results of adsorbed samples (refer highlighted portion) shown in Fig. 6.16.

### 6.2.7 Effect of temperature and thermodynamic parameters

Figures 6.17 a depict the variation of the adsorption capacity and percentage removal with initial concentration. The three most widely used isotherm models Freundlich, Langmuir and Elovich were fitted to the experimental data, as shown in Figs. 6.17 b-d for three different temperatures and the isotherm parameters are summarized in Table 6.4. It was observed that all the three isotherm models represent the data well with a regression coefficient of Langmuir, Freundlich and Elovich isotherm models equal to 0.99, 0.97 and 0.99, respectively. With an increase in temperature, the adsorption of $Pb^{2+}$ increased marginally, which is similar to the trend reported earlier for MX-80 bentonite (Xu et al., 2008) and kaolinite clay (Sari et al., 2007). It is worth mentioning that contrasting trends of $Pb^{2+}$ adsorption with temperature exists in the literature for GMZ bentonite (Wang et al., 2009), Turkish bentonite (Kul and Koyuncu, 2010) and phosphate modified kaolin clay (Unuabonah et al., 2007). The adsorption isotherm for T= 298 K is marginally higher, whereas the isotherm at T=328 K is the lowest. This contrasting trend of increase in adsorption with temperature can be hypothesized due to a decrease in the boundary layer thickness with the temperature around the adsorbent (Eren et al., 2009), resulting in a decrease of mass transfer resistance of adsorbate. However, experimental evidence of this hypothesis was not provided in the literature above.

The plots of the thermal equilibrium constant $\ln(K_e^o)$ versus 1/T for all the three temperatures are shown in Fig. 6.18. The values of $\Delta H^o$, $\Delta S^o$ and $\Delta G^o$ of $Pb^{2+}$ adsorption were calculated by fitting Eq. 6.14 to the experimental data and tabulated in Table 6.5. $\Delta H^o$ value was negative, which indicate that the adsorption of $Pb^{2+}$ on bentonite was an exothermic process. The $\Delta S^o$ value was found to be 31.39 J/mol K, indicating that randomness of $Pb^{2+}$ in aqueous solution at solid to liquid interface increases during the process of adsorption. (Hefne et al., 2008). The $\Delta G^o$ values are negative regardless of the temperature

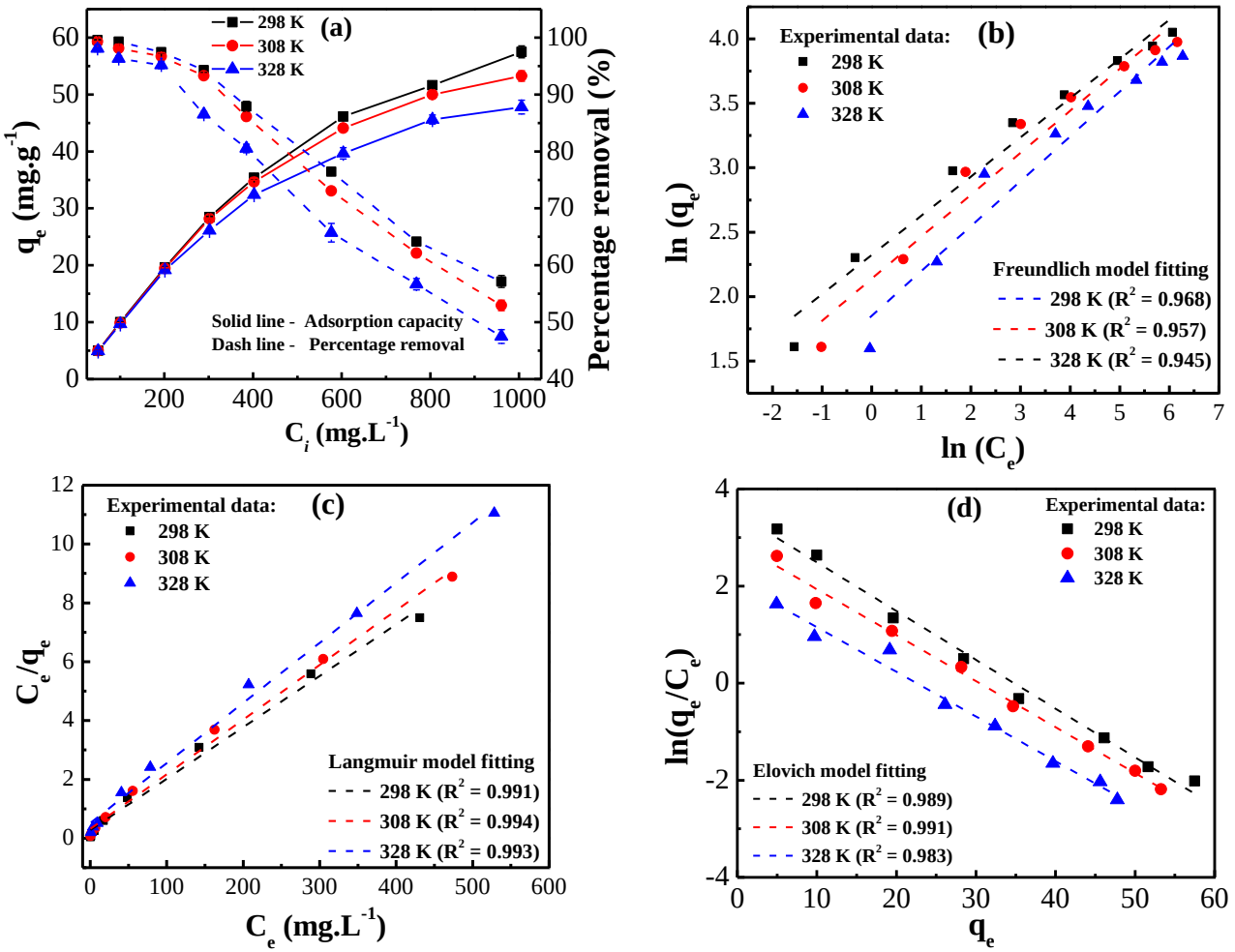


Figure 6.17: Effect of temperature on $Pb^{2+}$ (a) adsorption characteristics and percentage removal, adsorption isotherm model (b) Freundlich (c) Langmuir, and (d) Elovich one of $Pb^{2+}$ on Barmer bentonite

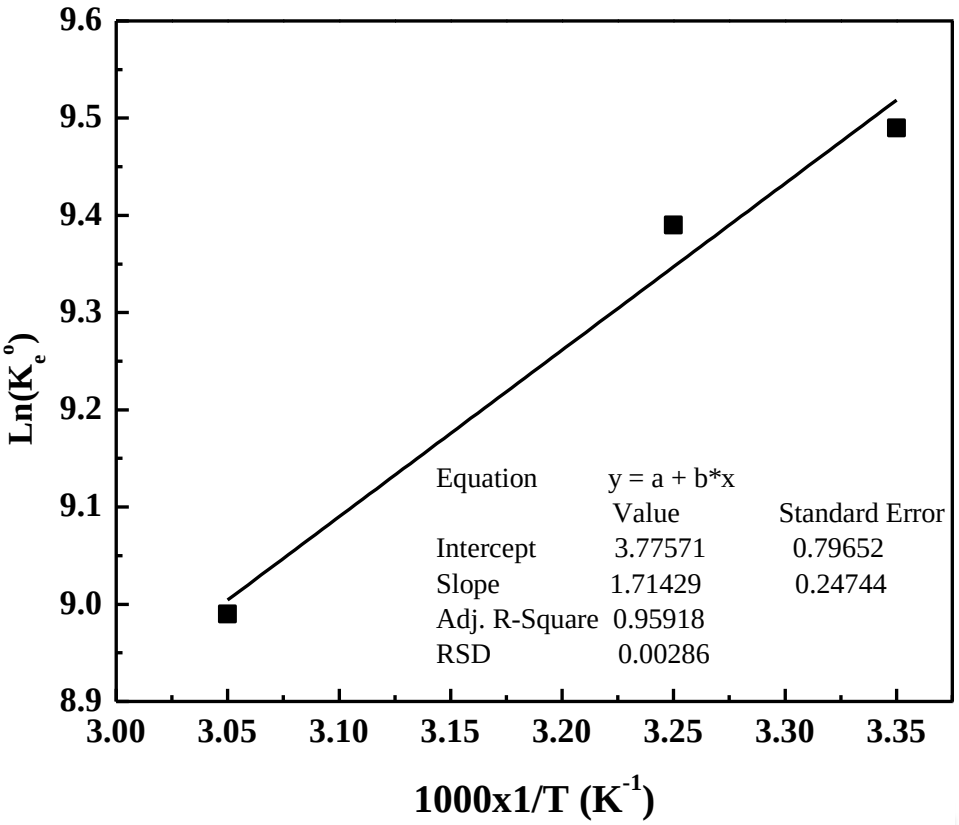


Figure 6.18: Plot of $\ln(K_e^\circ)$ versus 1/T for $Pb^{2+}$ sorption on Barmer bentonite

Table 6.4: Freundlich, Langmuir and Elovich isotherm model parameters for Barmer bentonite at different temperatures

| Temperature ($K$) | Freundlich isotherm | | | Langmuir isotherm | | | Elovich isotherm | | |
|---|---|---|---|---|---|---|---|---|---|
| | $K_f$ ($mg^{1-N}\ Ln\ kg{-}1$) | $n$ | $R^2$ | $q_m$ (mg.g-1) | $b$ ($L.mg^{-1}$) | $R^2$ | $q_m$ ($mg.g^{-1}$) | $K_e$ ($L.mg^{-1}$) | $R^2$ |
| 298 | 10.21 | 0.304 | 0.968 | 57.208 | 0.064 | 0.991 | 9.96 | 3.054 | 0.989 |
| 308 | 8.486 | 0.326 | 0.957 | 53.85 | 0.058 | 0.994 | 10.54 | 1.693 | 0.991 |
| 328 | 6.36 | 0.348 | 0.945 | 48.972 | 0.039 | 0.993 | 10.87 | 0.731 | 0.983 |

and become more negative gradually with an increase in temperature. $\Delta G^o$ being negative is indicative of the spontaneity of the adsorption processes (Wang et al., 2009), which was also supported by the results presented in Fig. 6.9. Based on the negative values of $\Delta H^o$ and $\Delta G^o$, it can be inferred that the reaction was more favorable at higher temperatures, which is similar to the results reported in earlier studies (Khan et al., 1995a; Pathak and Choppin, 2006).

Table 6.5: Thermodynamic parameters obtained for lead adsorption on Barmer bentonite

| Temperature (K) | $K_e°$ | $\ln(K_e°)$ | $\Delta G^o$ (kJ/mol) | $\Delta S^o$ (J/mol K) | $\Delta H^o$ (kJ/mol) |
|---|---|---|---|---|---|
| 298 | 13261 | 9.49 | - 23.52 | | |
| 308 | 12018 | 9.39 | - 24.01 | 31.39 | -14.25 |
| 328 | 8081 | 8.99 | - 25.54 | | |

## 6.3 Impact of Buffering Agent on Lead Adsorption of Bentonite: An Appraisal

This section deals with the impact of sodium acetate (Na-Ac) buffer used for pH adjustment on adsorption capacity and percentage removal determination of $Pb^{2+}$ on bentonite (B) through batch adsorption study (BAS), which was not quantified in the previous literature. The BAS was conducted at three different liquid to solid ratio (L/S) 20, 50, and 100. The pH of the solution was adjusted using (a) nitric acid and (b) Na-Ac buffer (for working pH=5). It was noted that the sediment volume of bentonite suspension in water at pH=5 adjusted with Na-Ac buffer was less than that using nitric acid. The lesser sediment volume was mainly due to the agglomeration of bentonite particles in the presence of Na-Ac buffer. The experimental findings corroborate that the use of Na-Ac buffer for BAS results in notable reduction of adsorption capacity and percentage removal of lead ($Pb^{2+}$) from the solution. The highest percentage removal of $Pb^{2+}$ ions was observed at L/S =20 on B, where pH of the solution was adjusted with nitric acid. The lowest percentage removal was noted at L/S =100 in which pH was maintained using Na-AC buffer. The influence of Na-Ac buffer was also evaluated by conducting the BAS for $Pb^{2+}$ removal on B in a competitive environment of Na+ using sodium chloride (NaCl) and Na-Ac buffer. The interaction of $Pb^{2+}$ with bentonite in two different environments was confirmed by the mineralogical, morphological, and spectral analysis of the lead ($Pb^{2+}$) post adsorption. Based on this study, nitric acid can be a better alternative instead of acetate buffer for adsorption study of metal ions on B for controlled pH environment. If buffer is used for the adjustment of pH in BAS, its effect on the adsorption capacity and percentage removal should be taken into account for its practical application in the field of water decontamination, waste containment system, and chemical reactive barrier.

### 6.3.1 Background

Bentonite (B) is a natural clay with diverse applications due to its unique surface properties such as negative surface charge, high specific surface area, and high cation exchange capacity (Lo et al., 1997; Babel and Kurniawan, 2003; Gupta and Bhattacharyya, 2012; Du et al., 2016; Uddin, 2017; Kollannur and Arnepalli, 2019. Its unique properties make it an excellent adsorbent for removing heavy metals from the wastewater (Bourliva et al., 2013; Yin et al., 2018). The accumulation of heavy metals in water and wastewater is a serious concern due to its non-biodegradability and toxicity. Lead ($Pb^{2+}$) is one of the common hazardous heavy metals found in landfill leachate and wastewater that can cause severe health issues (Naiya et al., 2009; Gilbert et al., 2011). The permissible level of $Pb^{2+}$ in wastewater is 0.05 $mg.L^{-1}$ as per Environment Protection Agency (EPA 1990) and 0.1 $mg.L^{-1}$ according to Bureau of Indian Standards (BIS) (IS: 10500, 1992). Due to its predominance and toxicity, $Pb^{2+}$ is considered as the model contaminant in this study. Bentonite is used to remove various contaminants from the wastewater before discharge to preserve water bodies and its aquatic life (Kapoor and Viraraghavan, 1998; Li and Li, 2000; Liu and Zhou, 2010; Goswami et al., 2017; Kakaei et al., 2020). Bentonite is a proven buffer material in the disposal of hazardous, radioactive nuclear waste and liner material in waste containment facilities due to its low flow characteristics and high contaminant retention capacity (Khan et al., 1995a,b; Kaya and Ören, 2005; Xu et al., 2006a).

Adsorption is an economical, popular and feasible method for removing toxic metals from wastewater and water supplies (Fu and Wang, 2011; Lakherwal, 2014; Burakov et al., 2018; Ray et al., 2022). It is obvious that adsorption capacity is an essential characteristic for assessing the contaminant retention of B for its potential application in waste containment and nuclear waste repository. Batch adsorption study (BAS) is a conventional method for evaluating geomaterials adsorption capacity (ASTM D4646 (2008a)). One of the prominent factors affecting the BAS is the pH of the solution, which generally varies from 2 to 12 reported in the literature (Naseem and Tahir, 2001; Sari et al., 2007; Xu et al., 2008; Wang et al., 2009). The solution pH plays a vital role in determining adsorption capacity and percentage removal of heavy metals.

Several past studies used a buffer to maintain constant pH during BAS to observe the effect of pH on the adsorption capacity of bentonite for the removal of metal ions (Sari et al., 2007; Özcan et al., 2009; Tahir and Naseem, 2007; Kakaei et al., 2020). Adsorption

of chromium on the bentonite was examined for the solutions with varying pH of 1.6 5.6 (Tahir and Naseem, 2007). Sari et al. (2007) studied the removal of Pb(II) and Cr(III) using Celtek clay and observed the removal of metal in the pH range (2-12). The above researchers maintained the pH of the solution using different buffer solutions (Sodium phosphate, ammonium acetate, sodium borate, and ammonium chloride). These studies have not considered the effect of the buffer used for pH adjustment on the adsorption capacity of B (Liu and Zhou, 2010; Chai et al., 2017; Tohdee et al., 2018; Zahafa et al., 2018; Zou et al., 2019; Musso et al., 2019; Chang et al., 2020; Niu et al., 2020). These studies have not considered the effect of the buffer used for pH adjustment on the adsorption capacity of B. Also, the past studies have not highlighted the difference in adsorption of $Pb^{2+}$ on B under controlled pH conditions (pH adjusted using acetate buffer and $HNO_3$). . İNEL et al. (1998) restricted the use of buffer for the pH adjustment in the adsorption process to avoid the complex formation and strong adsorption of a buffering agent on the surface of the clay. Buffer was not used to equilibrating the solution pH during adsorption due to unknown effects of buffer compounds on adsorption (Donat et al., 2005).

The characteristic pH of the landfill leachate reported (Rowe, 1995; Lo, 1996; Li and Li, 2000) is 5. Also, it was observed that above pH 5.5, lead starts to precipitate (Nakano et al., 2008). Therefore, for the present study, pH=5 was selected to assess the actual adsorption capacity of the metal ions ($Pb^{2+}$ chosen as the model contaminant) on B. Sodium acetate (Na-Ac) buffer is a versatile buffer to adjust the solution pH in the range of 3.6 to 5.6 and also used by previous researchers (Yilmaz and Yapar, 2004; Tahir and Naseem, 2007; Kakaei et al., 2020). The objective of this study is to quantify the impact of acetate buffer on the metal adsorption capacity of a swelling soil like bentonite. For this purpose, BAS was conducted at three different L/S (20, 50, and 100) to observe the effect of acetate buffer on adsorption. $Pb^{2+}$ adsorption was also performed in a competitive environment of $Na^+$ using NaCl and Na-Ac buffer for concentration ranging from 0.01 to 0.75 M. It was concluded that acetate buffer is not a viable method for controlling the pH of the solution for evaluating the adsorption capacity of bentonite. If it is used for the pH adjustment, its effect should be compensated for the adsorption capacity and percentage removal of metal ions using B. For determining the adsorption capacity of B, this study recommends using acid for the adjustment of pH while conducting BAS of bentonite.

### 6.3.2 Effect of Na-Ac buffer and nitric acid on adsorption capacity of $Pb^{2+}$ by B

Fig.6.19 shows the adsorption capacity of B with varying initial ion concentration conducted at controlled pH=5 conditions using nitric acid and Na-Ac buffer at three different liquid to solid ratio (20, 50, and 100). As expected, adsorption capacity increases with an increase in initial adsorbate concentration of $Pb^{2+}$, which is in line with results reported in the past studies (Melichová and Hromada, 2013; Deka and Sekharan, 2017).

Results show that L/S ratio has a significant effect on the adsorption capacity of bentonite. It was found that the adsorption capacity of B increases with an increase in L/S ratio. The lower adsorption capacity of $Pb^{2+}$ at L/S = 20 is mainly due to improper interaction of metal ions with B particles because of gel like formation of B solution reported in the present study in section 6.1. Fig.6.19 shows the effect of Na-Ac buffer on the adsorption capacity of bentonite at three different L/S ratios 20, 50, and 100. Results indicate that the use of Na-Ac buffer in BAS suppresses the adsorption capacity of $Pb^{2+}$ on B by 25 to 30 %. Notably, such an impact of Na-Ac buffer on the adsorption capacity of B was not focused in the literature.

Figs. 6.20a and 6.20b show the pictorial image of B suspension in water at pH=5 adjusted using nitric acid and Na-Ac buffer, respectively, for three different liquid to solid ratios 20, 50, and 100. It can be noted from the figure that the sediment volume of bentonite solution at L/S (20, 50, and 100) is higher for the pH equilibrated with nitric acid as compared to Na-Ac buffer. In acidic conditions, bentonite particles are arranged edge to face as depicted by schematic representation in Fig.6.20a (Permien and Lagaly, 1995; Wilkinson et al., 2018). In case of the Na-Ac buffer, agglomeration of B intra particles takes place, which is depicted by the schematic representation in Fig. 6.20b, resulting in the lower sediment volume of bentonite suspension in solution. The figure also illustrates the aggregation of B particles at a lower L/S ratio, which prevents the proper interaction of metal ions with the B and causes the lower adsorption capacity at a lower L/S ratio (as shown in Fig. 6.19).

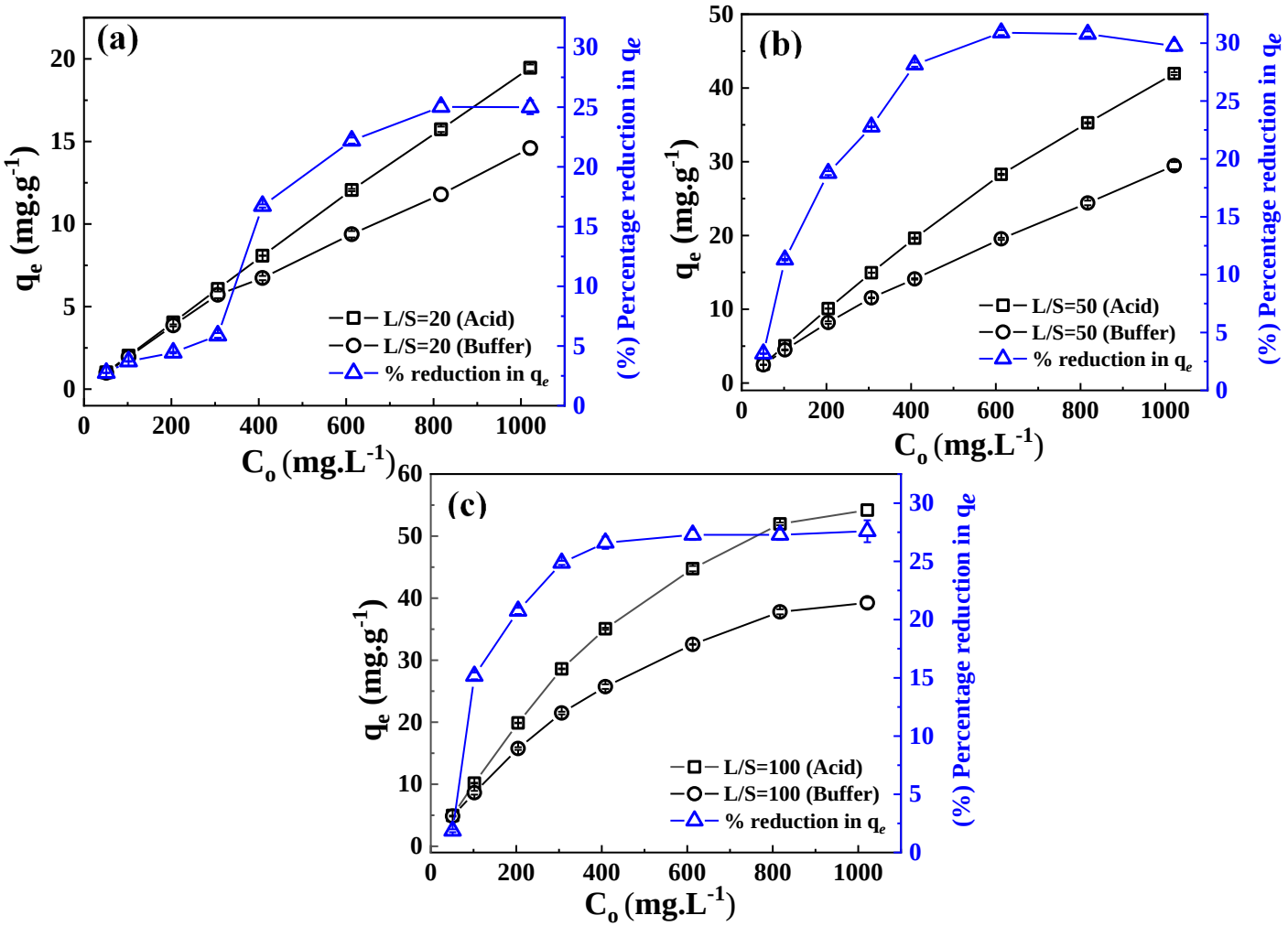


Figure 6.19: Effect of Na-Ac buffer on adsorption capacity with varying initial concentration at different liquid to solid ratio (a) 20 (b) 50 and (c) 100

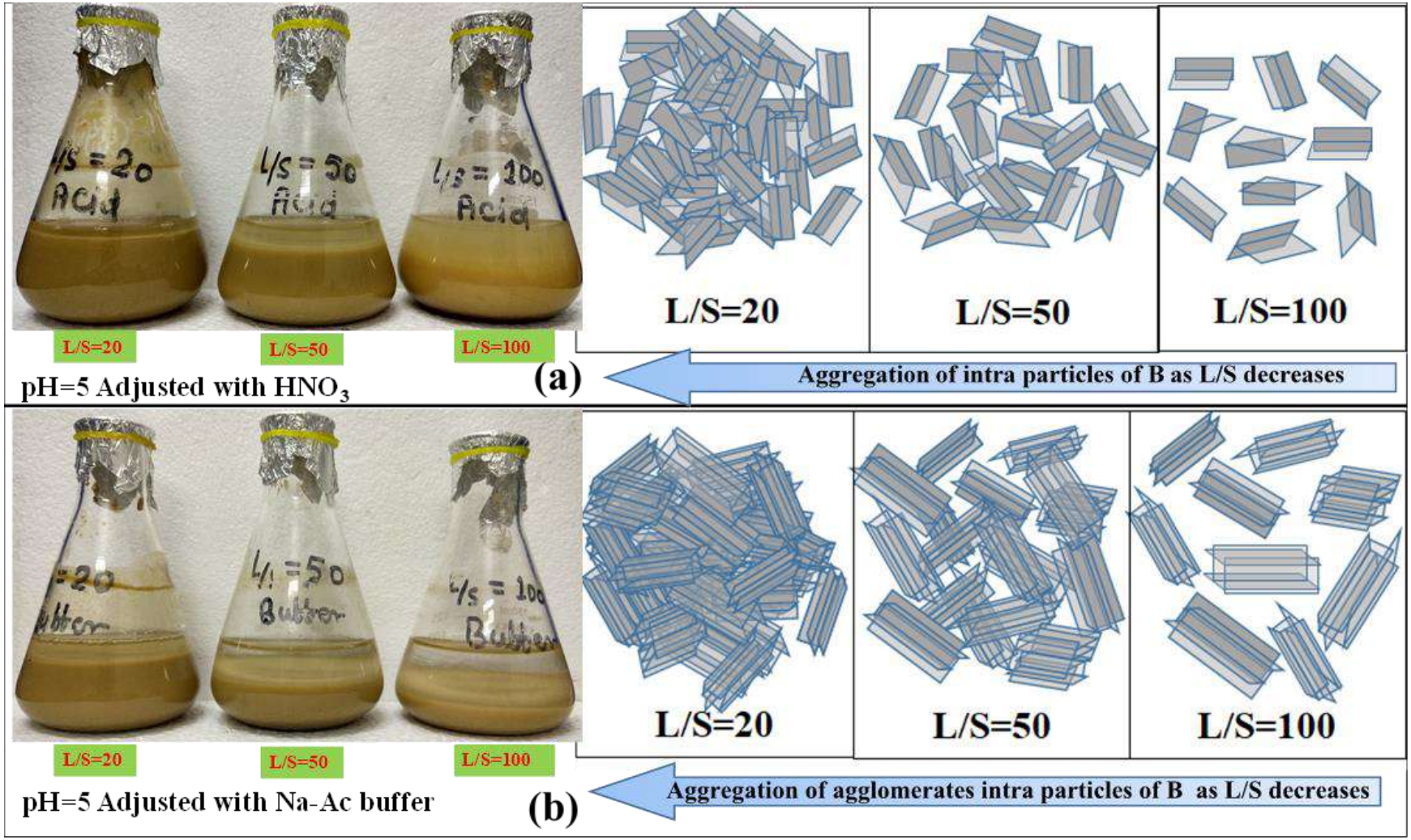


Figure 6.20: Physical state of the solution at pH=5 adjusted with $HNO_3$ and Na-Ac buffer at L/S ratio 20, 50, and 100

### 6.3.3 Effect of Na-Ac Buffer and Nitric Acid on Percentage removal of $Pb^{2+}$ by B

Figure 6.21 illustrates the percentage removal of metal ions $Pb^{2+}$ by B at different L/S (20, 50, and 100) for the initial concentration of $Pb^{2+}$ in the range of 50 to 1000 $mg.L^{-1}$. The results show that the higher percentage removal of metal ions at lower L/S ratio and lower initial concentration. This is consistent with the results reported by past researchers (Naseem and Tahir, 2001; Hamadneh et al., 2015). The highest percentage removal of metal ions is for the L/S = 20 while the lowest for the L/S = 100. The higher percentage removal of metal ions is due to the availability of the large number of the B particles for the metal ion adsorption at lower L/S=20. The results also indicate that the percentage removal of $Pb^{2+}$ by the B is lower for the BAS conducted in the presence of Na-Ac buffer. Fig. (6.21a) shows that there is no significant difference in the percentage removal of $Pb^{2+}$ up to the initial concentration of 300 $mg.L^{-1}$. But a significant difference in the percentage removal is observed beyond 300 $mg.L^{-1}$ for the L/S = 20, which is mainly due to the competition between the $Na^{+}$ present in acetate buffer and $Pb^{2+}$ ions in the higher concentration range. For L/S 50 and 100, a remarkable difference in the percentage removal of $Pb^{2+}$ is noted except for the initial concentration of 50 $mg.L^{-1}$. It is mainly because of a relatively lower number of adsorbent particles at higher L/S. Fig. 6.21 concludes that the percentage removal of sorbate ions in the presence of Na-Ac buffer is lower than that using nitric acid.

### 6.3.4 Effect of Na-Ac Buffer on Adsorption Isotherm

The linear form of Freundlich and Langmuir isotherm models were fitted to the obtained sorption data illustrated in Fig. 6.22. The fitting parameters of the isotherms are presented in Table 6.6. The Langmuir model fits better than the Freundlich model to the experimental data obtained from BAS conducted using acid for pH adjustment with a regression coefficient $R^2 \geq 0.98$. While Freundlich model can be a better model for representing the increasing trend of data with a regression coefficient $R^2 \geq 0.96$. Both the models fitted well to the experimental data with a regression coefficient $R^2 \geq 0.90$. The values of fitted parameters can be used as primary inputs for evaluating the contaminant migration in contaminant barrier using B. Freundlich isotherm model fitted well to the adsorption of $Pb^{2+}$ on B reported by Bennour (2013) while İNEL et al. (1998) observed that adsorption of lead by

B follows the Langmuir isotherm model. It can be noted from the fitted isotherms parameters presented in Table 6.6 that there is a significant difference in the model parameters for pH adjusted using acid and buffer. The maximum adsorption capacity of B, obtained from the Langmuir isotherm model, was 25-30 % higher for pH adjusted with acid as compared to the buffer. The Langmuir adsorption isotherm parameters were used to evaluate the dimensionless separation factor $R_L$ and presented in Table 6.6. It can be noted that the values of $R_L$ are in the range of $0 < R_L < 1$, which elucidates a favourable adsorption process. The values of $R_L$ obtained for the BAS conducted using acid for all the three L/S (20, 50, 100) is less than those obtained using a buffer. This indicates that adsorption of $Pb^{2+}$ is more favourable for the solution pH adjusted using acid.

### 6.3.5 Comparative study of $Pb^{2+}$ adsorption on B in presence of NaCl and Na-Ac buffer

The results presented above show that acetate buffer suppresses the adsorption capacity and the percentage removal of $Pb^{2+}$ on B. For demonstrating the effect of acetate buffer on metal ion adsorption of B for, it was compared with the adsorption of $Pb^{2+}$ in the presence of NaCl and Na-Ac buffer for the same concentration. An adsorption study was conducted with an initial metal ion concentration of 200 $mg.L^{-1}$ at L/S=100. Fig. 6.23a and Fig. 6.23b show the adsorption capacity and percentage removal of $Pb^{2+}$ in multiple contaminant system of NaCl and Na-Ac buffer for concentration ranging from 0.01 to 0.75 M. The results indicate that the Na-Ac buffer having a more suppressive effect for the removal of metal ions. The effect is more prominent for an initial concentration of 0.01M of Na-Ac buffer. Beyond, 0.01M concentration of NaCl and Na-Ac buffer, a marginal variation in the adsorption capacity and percentage removal was noted. Fig. 6.23c presents the relationship between the percentage removal and electrical conductivity (EC) of the solution. A non-linear trend was found between percentage removal and EC with regression coefficient $R^2 = 0.92$, which can be used to predict the percentage removal of $Pb^{2+}$. From these experimental results, it can be concluded that $Pb^{2+}$ removal in the presence of Na-Ac buffer (used a organic salt, sodum acetate) is lower than in the presence of NaCl salt for the same molar concentrations. This proves that organic salt (Na-Ac) having more supessive effect than normal salt (NaCl), for the metal ion ($Pb^{2+}$) removal on B.

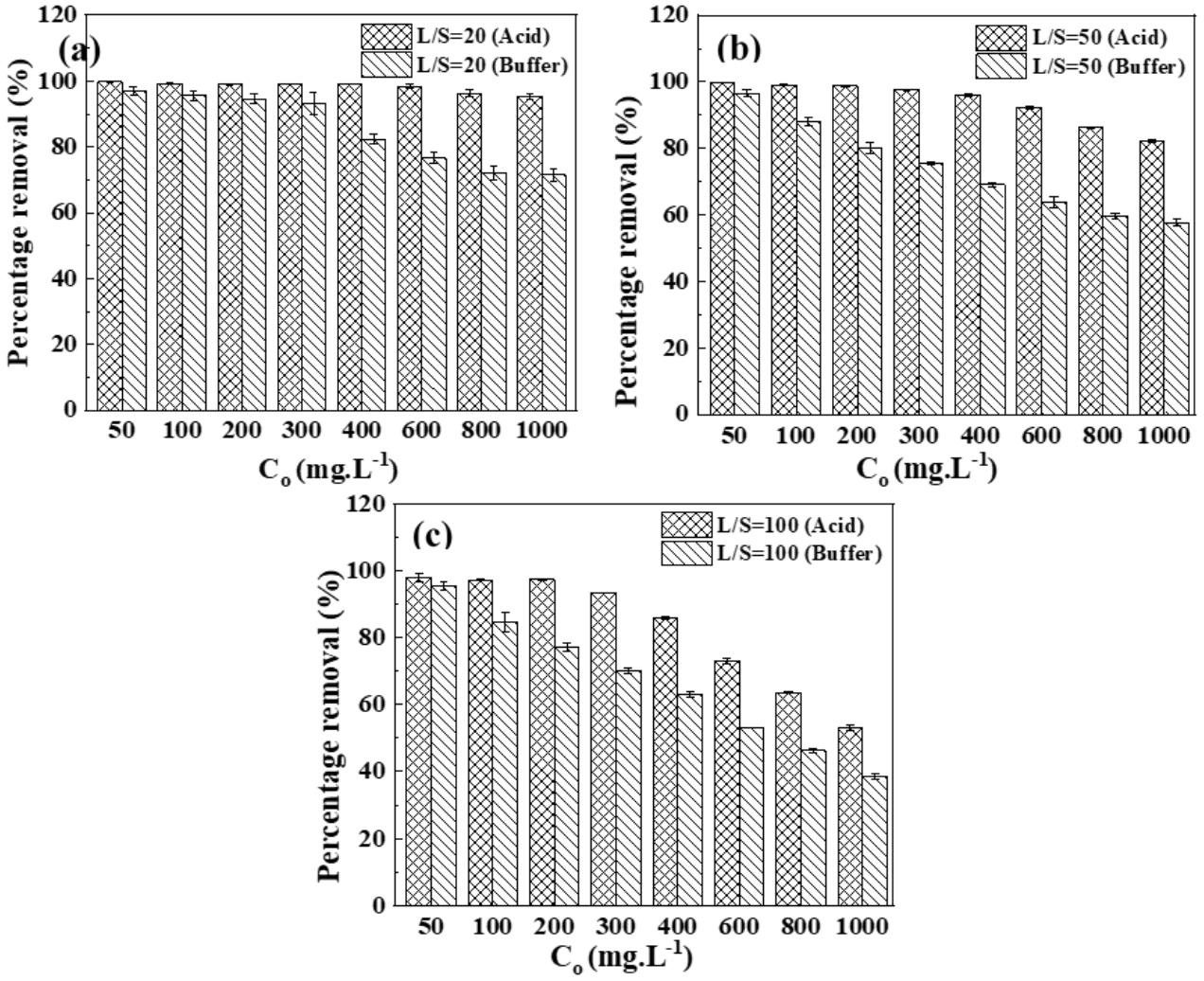


Figure 6.21: Effect of Na-Ac buffer on percentage removal with varying initial concentration at different liquid to solid ratio (a) 20 (b) 50 and (c) 100

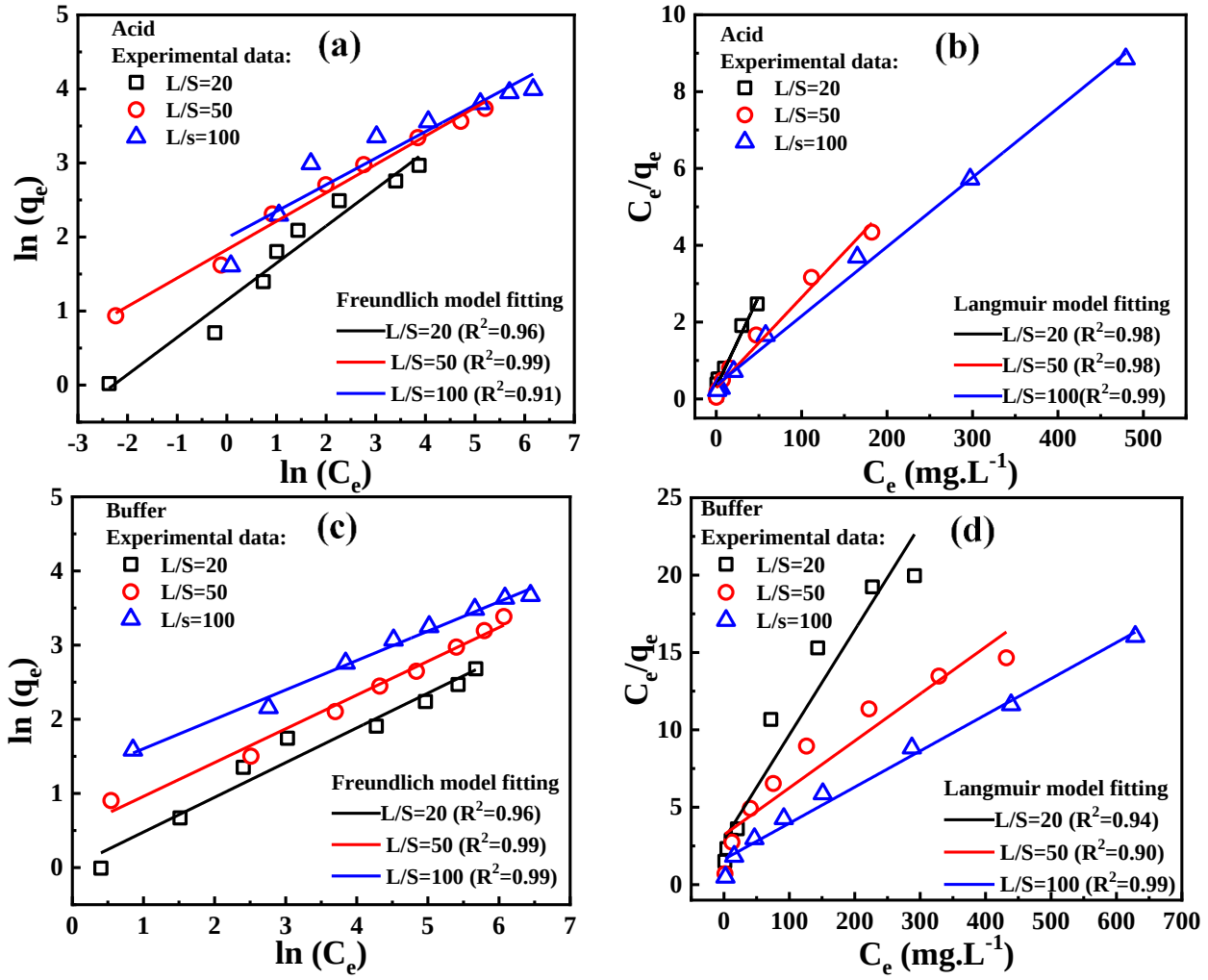


Figure 6.22: Langmuir and Freundlich isotherm model fitted to BAS of $Pb^{2+}$ on B conducted with acid and buffer for pH adjustment

Table 6.6: Freundlich, Langmuir isotherm model fitted parameters and dimensionless separation factor $R_L$ for B

| Parameters | | | pH adjusted with acid | | | pH adjusted with buffer | | |
|---|---|---|---|---|---|---|---|---|
| | | | L/S=20 | L/S=50 | L/S=100 | L/S=20 | L/S=50 | L/S=100 |
| Freundlich isotherm | $K_f$ | | 3.14 | 6.23 | 7.30 | 1.01 | 1.65 | 3.34 |
| | $n$ | | 0.50 | 0.38 | 0.36 | 0.47 | 0.46 | 0.40 |
| | $R^2$ | | 0.96 | 0.99 | 0.91 | 0.96 | 0.99 | 0.99 |
| Langmuir isotherm | $q_m$ (mg/g) | | 21.15 | 42.43 | 55.43 | 14.76 | 32.94 | 42.83 |
| | $b$ (L/mg) | | 0.15 | 0.08 | 0.05 | 0.02 | 0.01 | 0.01 |
| | $R^2$ | | 0.98 | 0.98 | 0.99 | 0.94 | 0.90 | 0.99 |
| Dimensionless separation factor RL for $C_\circ$ (mg.L$^{-1}$) | $C_\circ$ (mg.L$^{-1}$) | 51.06 | 0.115 | 0.197 | 0.281 | 0.457 | 0.685 | 0.578 |
| | | 102.12 | 0.061 | 0.109 | 0.164 | 0.296 | 0.521 | 0.406 |
| | | 204.24 | 0.032 | 0.058 | 0.089 | 0.174 | 0.352 | 0.255 |
| | | 306.36 | 0.021 | 0.039 | 0.061 | 0.123 | 0.266 | 0.186 |
| | | 408.48 | 0.016 | 0.030 | 0.047 | 0.095 | 0.214 | 0.146 |
| | | 612.72 | 0.011 | 0.020 | 0.032 | 0.065 | 0.154 | 0.102 |
| | | 816.96 | 0.008 | 0.015 | 0.024 | 0.050 | 0.120 | 0.079 |
| | | 1021.2 | 0.006 | 0.012 | 0.019 | 0.040 | 0.098 | 0.064 |

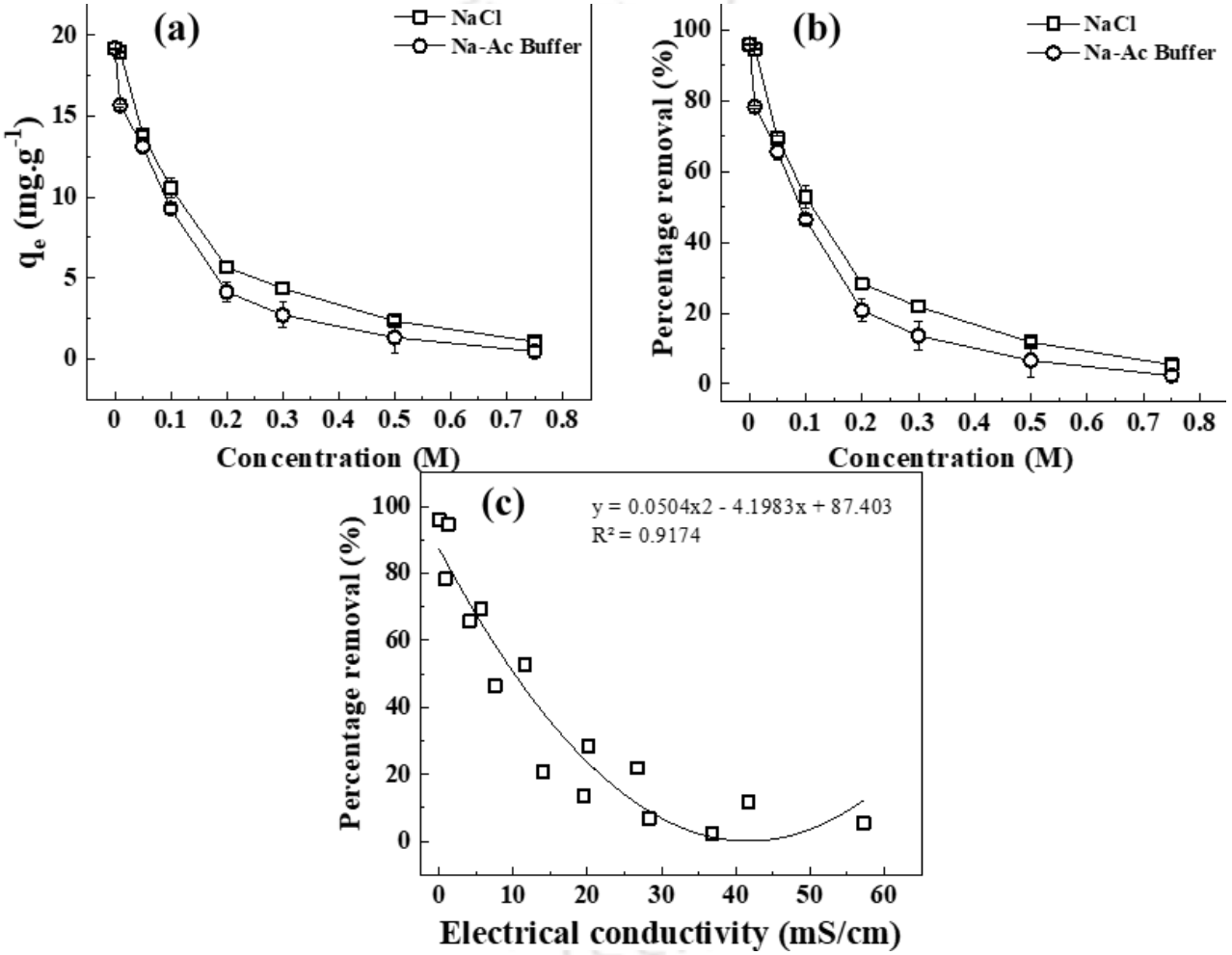


Figure 6.23: Effect of NaCl and Na-Ac buffer of its various concentration on (a) Adsorption capacity (b) percentage removal of $Pb^{2+}$ on B and (c) correlation between percentage removal and electrical conductivity of the solution for $Pb^{2+}$ removal ($C_\circ$ = 200 mg.L$^{-1}$, pH=5)

### 6.3.6 Mineralogical and spectral analysis of $Pb^{2+}$ loaded B after adsorption

The XRD analysis of raw B and $Pb^{2+}$ loaded B was conducted for an initial concentration of 200 $mg.L^{-1}$ in a competitive environment of NaCl and Na-Ac buffer of concentration ranging from 0.0 to 0.75M after the BAS. Fig. 6.24a presents the XRD pattern of $Pb^{2+}$ sorbed B with (ranging from 0.01 to 0.75M) and without NaCl and compared with XRD pattern of raw B highlighted in red color. It can be observed from (Fig. 6.24a) XRD spectra that at a higher concentration of NaCl (beyond 0.1M), peaks of NaCl (Bao et al., 2017) were noted (highlighted in the shaded region), which shows the competitive effect of $Na^{+}$ ions on $Pb^{2+}$ adsorption. Similarly, Fig. (6.24b) shows the peaks of Na-Ac for the concentration of Na-Ac buffer beyond 0.1M, which reiterates the competitive effect of $Na^{+}$ ions on $Pb^{2+}$ adsorption. Furthermore, with a gradual increase in NaCl and Na-Ac buffer concentration, it was observed that the peaks of montmorillonite decreased in the spectra of XRD, which may be the cause for diminishing adsorption capacity of $Pb^{2+}$ on B surfaces (Svensson and Hansen, 2013). It was reported that collase of monmorillonite structure or the formation amorphous layer decrease the $Pb^{2+}$ capability in exchange process with exchangeable cations present in the interlayer space of the clay (Kara et al., 2003; Al-Jlil and Alsewailem, 2009). Also ions adsorption depend on the interlayer space of the clay units because of $Pb^{2+}$ ions exchange present in the solution with ions present in the interlayer of the B. From XRD spectra shown in Fig. 6.24 indicates that reduction in interlayer of B takes place, since the main peaks of montmorillonite mineral presenr in the B slightly shift to higher value of 2 theta angle. Another ways the reduction in lead adsorption in presence of NaCl and Na-Ac also can be explained in terms of suface charge of the clay particle. It is reported that suface charge is less negatively in higher concentration of the salts solution (Niriella and Carnahan, 2006; Baik and Lee, 2010). Which is one of the reason in decrease in $Pb^{2+}$ adsorption on B suface with gradual increase in salt concetration in the solution. The above results clearly indicate that $Na^{+}$ ions present in acetate buffer and sodium chloride are capable of suppressing the $Pb^{2+}$ adsorption on B.

Figure 6.25 shows the FTIR spectra of $Pb^{2+}$ sorbed bentonite for varying concentrations of salt (NaCl and Na-Ac buffer) and in the absence of salt. The initial concentration of $Pb^{2+}$ is considered as $C_o$=200 $mg.L^{-1}$. The $Pb^{2+}$ sorbed B shows the transmittance band

near wavenumber of 3620 $cm^{-1}$ due to the stretching vibrations of structural OH groups of B. A broad band in the region of wavenumber 3413 - 3482 $cm^{-1}$ is associated with $H_2O$-stretching vibrations, mainly due to the presence of adsorbed water in B. The band at 696 $cm^{-1}$ is due to the deformation and banding modes of the Si-O bond. The bands at 534 and 469 $cm^{-1}$ are due to the Si-O-Si and Al-O-Si bending vibrations, respectively (Kong et al., 2019). The band associated with Al-Al-OH is observed at 913 $cm^{-1}$(Zhirong et al., 2011). The strong transmittance band at 1033 $cm^{-1}$ is mainly due to the vibrations bending of Si-O bonds (Xu et al., 2008). The band at 1637 $cm^{-1}$ is due to the overtone of the bending vibration of water (Saja et al., 2020). In the presence of Na-Ac buffer, the FTIR spectra of $Pb^{2+}$ sorbed B are presented in Fig. 6.25a. It can be noted from the figure that for the concentration of Na-Ac buffer beyond 0.01M, an additional peak is visible between the wavenumber 1300 to 1600 $cm^{-1}$, which is mainly due to the stretching vibration of carboxyl salts (Iacovita et al., 2015) present in the Na-Ac buffer. The presence of a peak in the FTIR spectrum due to carboxyl salt confirms the significant reduction in the adsorption capacity of $Pb^{2+}$, which is in line with the results presented in Figs. 5.23a and 5.23b. The spectra also show a gradual increase in the peak intensity between the wavenumber 1300 to 1600 $cm^{-1}$ (highlighted in Fig 6.25a) for the increase in the concentration of Na-Ac buffer from 0.05M to 0.75M. A similar observation in the FTIR spectra of $Pb^{2+}$ sorbed B in presence of NaCl was found. An additional peak at the wavenumber 1384 $cm^{-1}$ and between wavenumber 2500 to 3000 $cm^{-1}$ (highlighted in Fig. 6.25b) was mainly due to the presence of NaCl in B. The alteration in transmittance band was also observed in $Pb^{2+}$ sorbed B for varying concentrations of NaCl. The band shift in this study is similar to the bentonite treated with NaCl. The alteration in transmittance band was noted with varying concentrations of NaCl and Na-Ac buffer as presented in Figure 6.25. The intensity of the additional peak and shift in transmittance band is more prominent in case of Na-AC buffer as compared to NaCl. This supports the more suppressive effect of Na-Ac buffer on adsorption capacity as compared to NaCl salt.

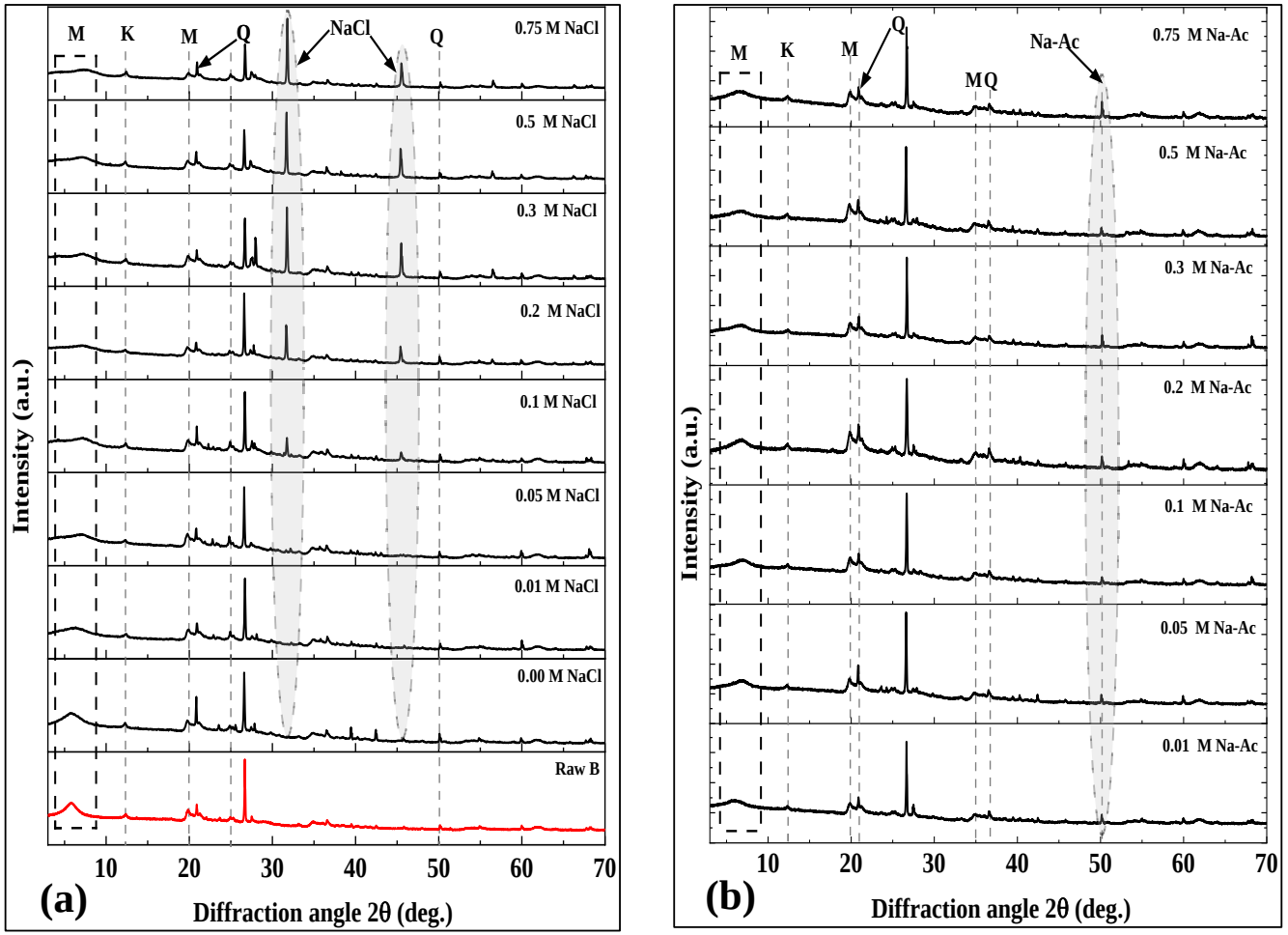


Figure 6.24: XRD of post adsorption of $Pb^{2+}$ on B at various concentration of (a) NaCl (Gupt et al. 2020) and (b) Na-AC buffer ($C_o$= 200 ppm, pH=5) M- Montmorillonite, K- Kaolinite, Q- Quartz, NaCl- Sodium Chloride, Na-Ac- Sodium Acetate

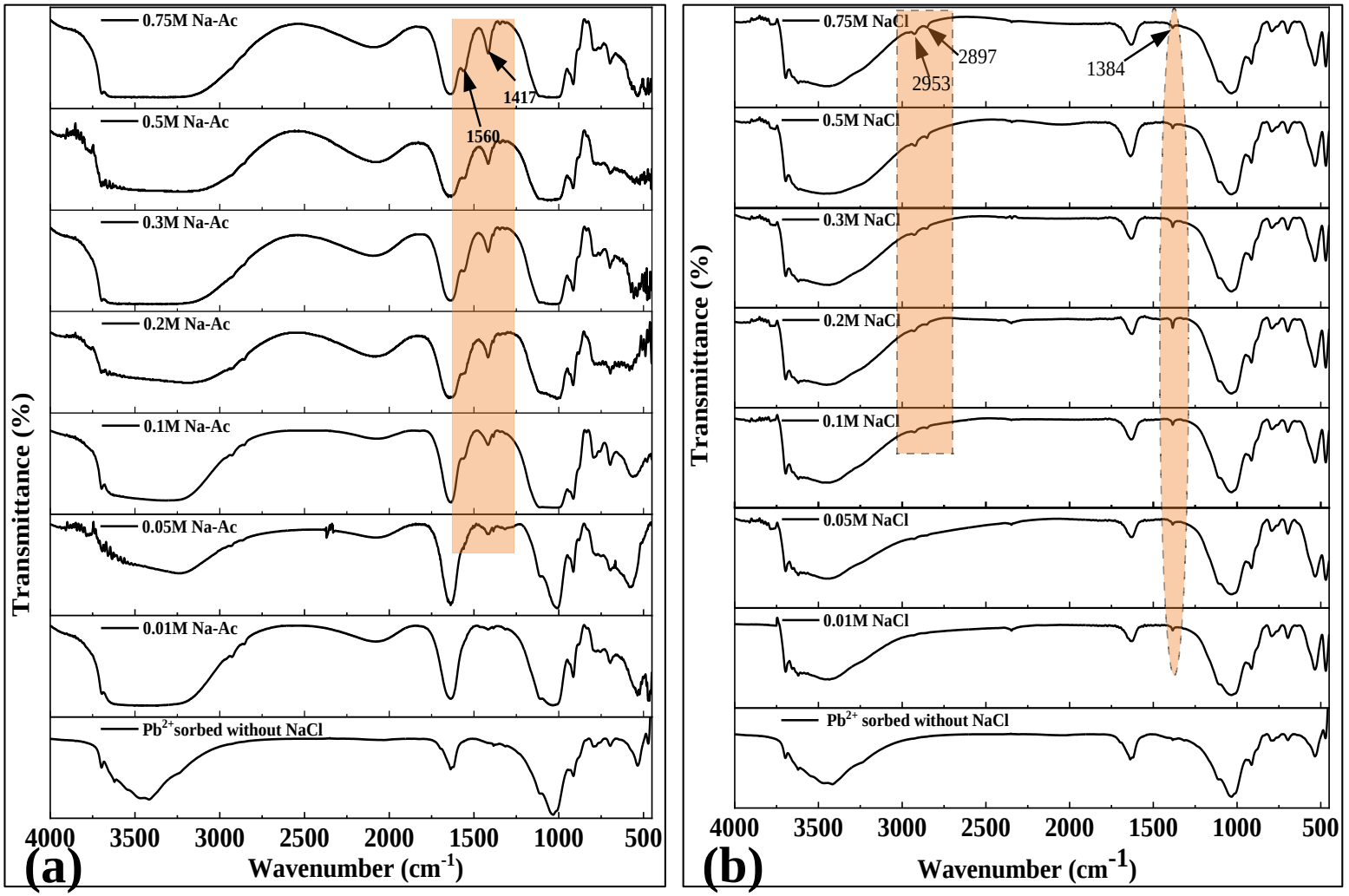


Figure 6.25: FTIR spectra of $Pb^{2+}$ adsorbed B in presence of (a) Na-Ac and (b) NaCl buffer for its various concentration ($C_\circ$ = 200 mg.$L^{-1}$, pH=5)

### 6.3.7 Microstructural analysis of $Pb^{2+}$ sorbed B

FESEM analysis was performed for $Pb^{2+}$ sorbed B (both for single and multiple contaminant system) to understand the influence of NaCl and Na-Ac buffer on the change in adsorption associated with the morphological changes in B particles. FESEM analysis was performed for an initial concentration of 200 $mg.L^{-1}$ in a controlled pH=5 environment. Fig. 6.26 shows photomicrographs of B particles, $Pb^{2+}$ sorbed bentonite, and $Pb^{2+}$ sorbed B in the presence of NaCl and Na-Ac buffer for the concentration of 0.01, 0.05, and 0.1M. The morphological results indicate that only $Pb^{2+}$ sorbed B particle is in a completely dispersed state, while $Pb^{2+}$ sorbed with NaCl and Na-Ac buffer shows an agglomerate state. From the FESEM photomicrograph, it was observed that agglomeration of the bentonite particles is relatively more in Na-Ac buffer as compared to NaCl salt. Relatively higher agglomeration of the B particles in Na-Ac buffer is in line with the results presented in Figs. 6.23a and 6.23b. It can also be observed from Fig. 6.26 that the increase in the salt concentration agglomeration is more and the highest for the 0.75 M (not presented for the brevity) in both cases of Na-Ac and NaCl salt . As adsorption of $Pb^{2+}$ marginally deoends on surface area of clays (Al-Jlil and Alsewailem, 2009). Thus, a reduction in $Pb^{2+}$ adsorption may also be the cause due to decrease in surface area of the B clay, which results due to the agglomeration of bentonite particles in presence of salts confirmed from FESEM images. Therefore, the gradual increase in the salt concentration results in a decrease in the adsorption capacity and percentage removal of $Pb^{2+}$ ions, as depicted in Figs. 6.23a and 6.23b.

Fig. 6.27 presents the EDX spectra of only $Pb^{2+}$ loaded B and $Pb^{2+}$ sorbed in different concentrations of NaCl and Na-Ac buffer after BAS for an initial concentration of 200 $mg.L^{-1}$. EDX spectra analysis was performed for $Pb^{2+}$ sorbed bentonite for all concentrations of NaCl, and Na-Ac buffer ranging from 0.01M to 0.75 M. For the sake of brevity, only the concentration of 0.01, 0.2, and 0.75 M is shown in the given Fig. 6.27. EDX spectra confirm the sorption of $Pb^{2+}$ on the surfaces of B highlighted with dotted red colour circles on the spectral images. The composition of elements (% weight) of common exchangeable cations and their variation due to the presence of NaCl and Na-Ac buffer before and after BAS for an initial concentration of 200 $mg.L^{-1}$ is shown in Fig. 6.28. The results of EDX spectra depicts that the percentage of $Pb^{2+}$ is negligible in B before adsorption . The weight percent of $Pb^{2+}$ increases to 2 while the weight percentage of $Na^{+}$ decreases to 0.2 from 2, after the sorption of $Pb^{2+}$ in the absence of any salt. Fig. 6.28a

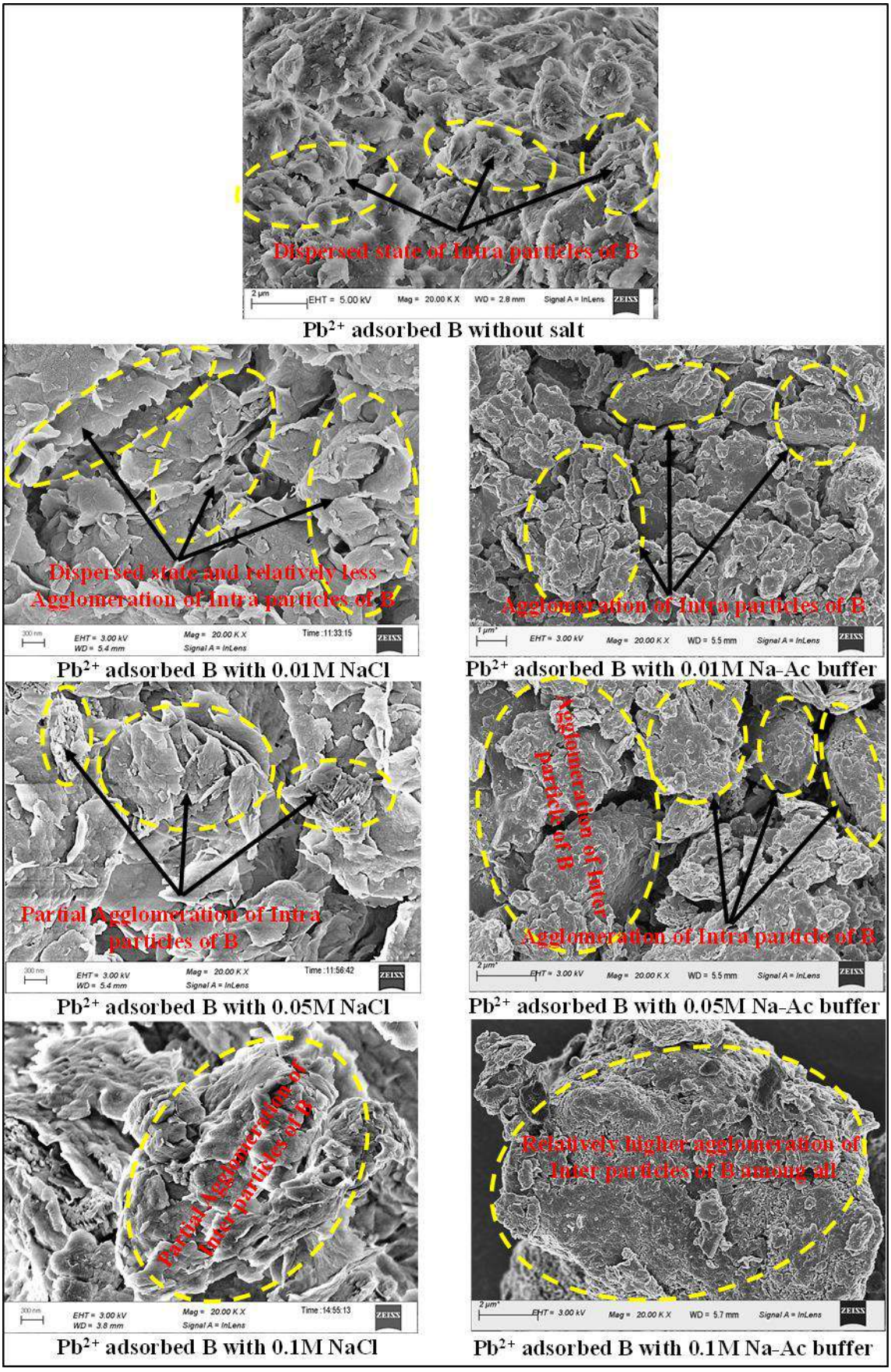


Figure 6.26: FESEM Photo micrograph of $Pb^{2+}$ sorbed bentonite with various concentration of NaCl and Na-Ac buffer ($C_\circ$ = 200 mg.$L^{-1}$, pH=5)

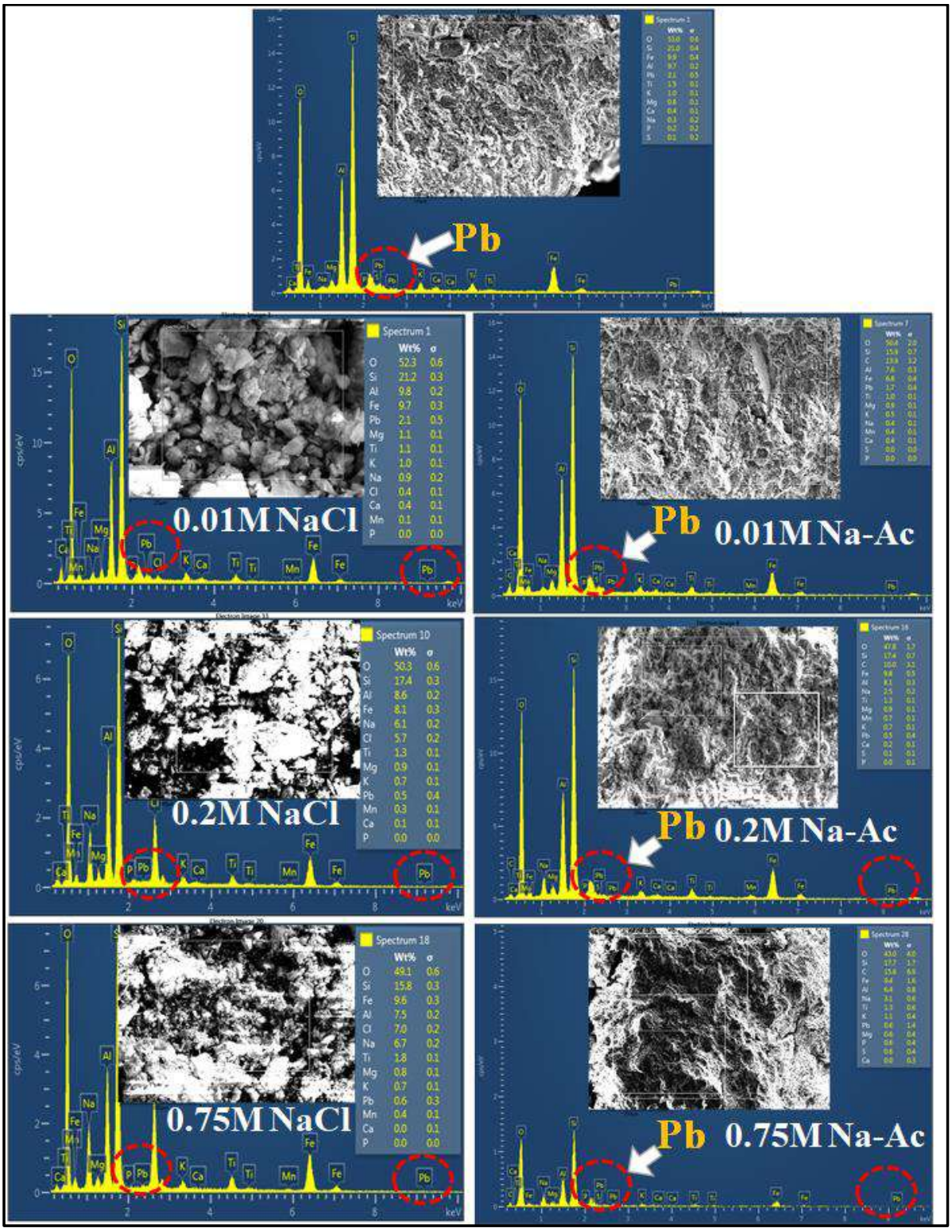


Figure 6.27: EDX spectra of $Pb^{2+}$ sorbed for different concentration of NaCl and Na-Ac buffer ($C_\circ = 200$ mg.L$^{-1}$, pH=5)

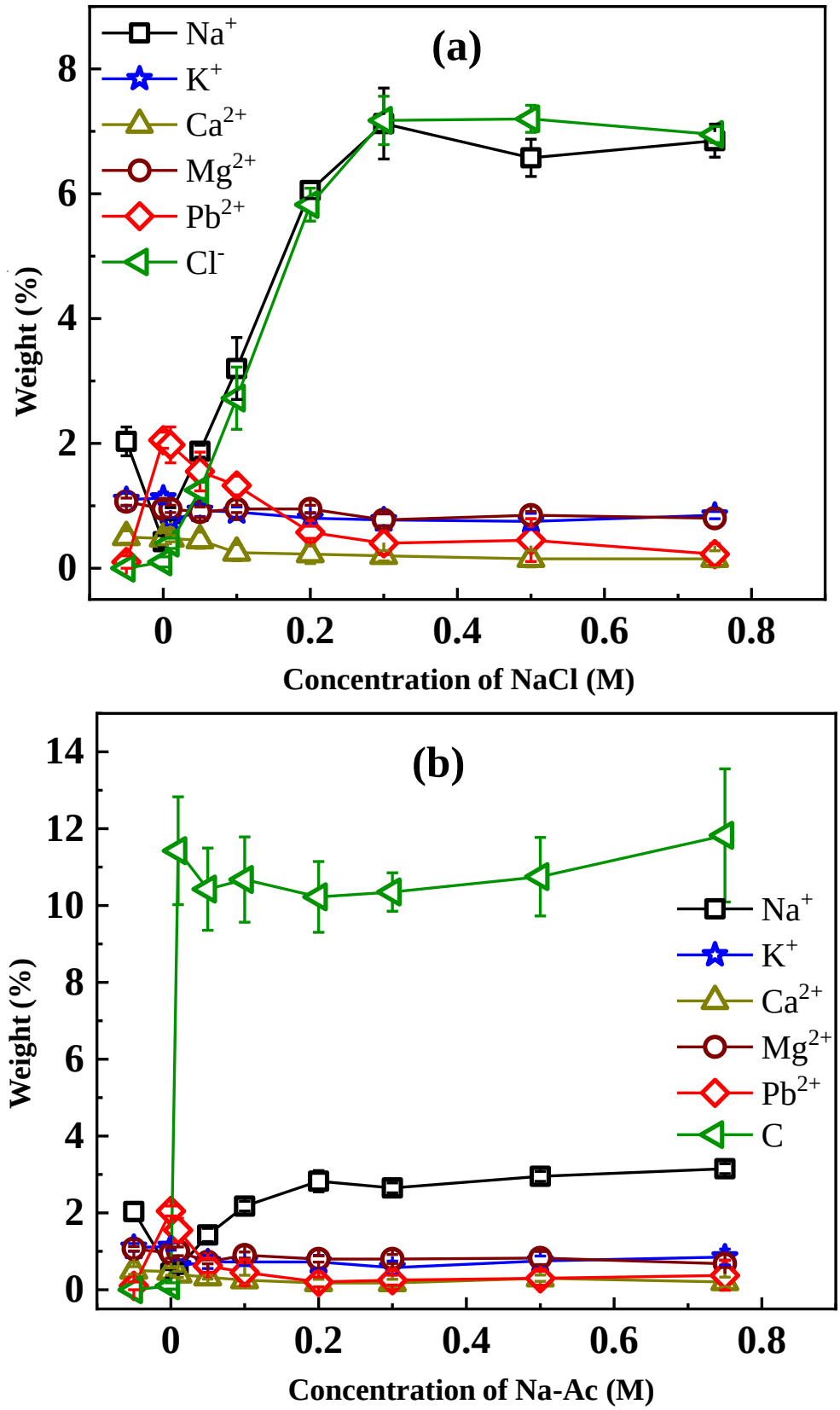


Figure 6.28: Variation of exchangeable cation of B for $Pb^{2+}$ adsorption in presence of (a) NaCl and (b) Na-Ac buffer

presents the variation of weight percentage of $Pb^{2+}$ and exchangeable cations for the sorption in presence of NaCl for the concentration ranging from 0.01M to 0.75M. From the figure, it can be noted that the weight percentage of $Pb^{2+}$ decreases from 2 to 0.2 as a concentration of NaCl increases to 0.75 M. The weight percentage of $Na^{+}$ and $Cl^{-}$ increases to 6.5, which supports the results found in the XRD analysis (ref. Fig. 6.24a). It can be concluded from EDX spectra that the weight percentage of $Na^{+}$ is higher in $Pb^{2+}$ sorbed B (post adsorption) as compared to the natural B. This indicates that the presence of NaCl and Na-Ac results in the competition of $Na^{+}$ ions with $Pb^{2+}$. Therefore, the combined influence of interlayer space, agglomeration, and competition of ions result in reduced $Pb^{2+}$ adsorption on B as the concentration of the salt solution increases. Similar results are presented in Fig. 6.28b for the variation of exchangeable cations and $Pb^{2+}$ for the adsorption conducted in the presence of Na-Ac buffer. The difference was found at a lower concentration below 0.05M, and it was observed that Na-Ac buffer suppresses $Pb^{2+}$ more as compared to NaCl for the same concentration. These EDX results are in line with the results presented in Fig. 6.23 and Fig. 6.26, where higher agglomeration was noted for the Na-Ac buffer at the same concentration.

## 6.4 Summary

This study deals with the investigation of appropriate liquid to solid ratio (L/S) to be used for determining soil-contaminant interaction of expansive soil like bentonite (B) by batch adsorption study (BAS). It was found from this study that the L/S = 20 recommended by ASTM D 4646 (2008a) procedure for soils and sediments would be inadequate for B. This observation was based on the comparison of maximum adsorption capacity of B and 70 % B-30 % fly ash mix (B-FFA30) where in the latter had higher sorption capacity than the former. This was mainly due to the gel like consistency of B-contaminant solution at L/S = 20 resulting in improper interaction. The study categorically indicates the importance of L/S for BSS of expansive soil like B. Based on the results, present study recommends L/S = 50 for the removal of heavy metal from the aqueous solution using B and for performing BSS of B. This is different from the recommended value of L/S = 20 as suggested by ASTM D 4646 (2008a) for non-expansive soils and sediments.

The adsorption behavior of Barmer bentonite for $Pb^{2+}$ under varying experimental conditions. The maximum sorption capacity of the adsorbent for $Pb^{2+}$ was found to be 55 mg.

$g^{-1}$ at pH 5 and 27±2°C. An increase in adsorbent dosage resulted in higher $Pb^{2+}$ percentage removal, while adsorption capacity decreased. The observation was mostly attributed to the reactivity or expansive behavior of bentonite, leading to a gel-like consistency different from non-expansive soils. Ionic strength played a fundamental role in suppressing the adsorption of $Pb^{2+}$ wherein the salt concentration, valency and ionic radius played a critical role. The results from sorption isotherm and kinetic modeling indicated the possibility of chemisorption of $Pb^{2+}$ on B. It can be concluded that Barmer bentonite is at par with bentonites from different countries reported in the literature for effectively removing $Pb^{2+}$ (model contaminant). This ensures a better reactivity of the contaminants with the adsorbent resulting in higher adsorption capacity at low dosages.

Buffer solutions are used for adjusting the pH during batch adsorption study (BAS) of geomaterials. This study investigated the impact of buffer on the adsorption of $Pb^{2+}$ on bentonite at three different liquid to solid ratio (20, 50, and100) in a controlled pH=5 environment adjusted using nitric acid and Na-Ac buffer. A significant suppression in the adsorption capacity of $Pb^{2+}$ was observed for all the three L/S in the presence of Na-Ac buffer. The highest percentage removal for all the initial metal ion concentrations was found for the L/S=20 in the presence of nitric acid. The lowest percentage removal for the $Pb^{2+}$ was noted at L/S=100 in the presence of acetate buffer. The use of a buffer to control pH underestimated the adsorption capacity by 25 to 30% for all liquid to solid ratios. The results from this study can be used to recommend the appropriate use of buffer for characterizing adsorption capacity of swelling soils like B. The present study suggests the use of nitric acid for the adjustment of pH for the actual evaluation of the adsorption capacity of B in a controlled pH environment.

# 7

# Contaminant Retention of B-FA and B-S Mixes

## General

This chapter mainly emphasized the contaminant retention characteristics of B-FA and B-S mixes for its potential application as liner material in waste containment. $Pb^{2+}$ ions was taken as the model contaminant for the retention study by conducting the 24 hrs batch equilibrium test. For this study four Indian fly ashes collected from the different parts of the country for its variability. Out of four FA, three belongs from class F and one of them belongs to class C FA according to ASTM- C618 (ASTM, 2003) guide lines. Batch retention test was conducted under two different pH conditions i) controlled pH and ii) uncontrolled pH. The adsorption characteristics of B, B-FA and B-S mixes was correlated with the index properties of parent materials and its mixes. Also the retention capacity of the B-FA was evaluated with the interaction time of B-FA mixes upto the interaction time of four years to see any variability on the adsorption capacity of the material. It is very essential to observe the effect of interaction of B-FA mixes on its retention properties for its application in long run as liner material. The study investigates the contaminant retention capacity of the B-FA mixes is more the contamiant retention capacity of the B-S mixes. Specifically, under uncontrolled pH conditions through precepitation mechanism due the high value of the fly ash. Finally, it can be concluded that use of B-FA mixes having the advantage over the use of B-S mixes by minimise the waste and the saving construction cost of waste containment. Therefore, B-FA mixes is a better substitue to replace the B-S mixes for the waste containment.

## 7.1 Contaminant rention of the B-FA and B-S mixes under controlled pH environment

### 7.1.1 Background

The exponential increase in hazardous and municipal solid waste (MSW) due to urbanization and increased population has necessitated the construction of engineered landfills (Busch et al., 2010; Naveen et al., 2017; Kumar et al., 2019). Multi-layered engineered landfill consists of the liner layer on which the hazardous wastes are dumped (Fig. 7.1) (Slack et al., 2007). The cover layer is employed over the waste only after the landfill reaches its full capacity. During this stage, the waste layer is exposed to multiple cycles of rainfall wherein the rainwater reacts with the hazardous waste and progresses downwards as leachate (Öman and Hynning, 1993). Low permeable soil layer, having hydraulic conductivity less than $10^{-9}$ m/s is generally employed in liners to restrict or delay the leachate migration to the groundwater table (Shaikh et al., 2019). The bentonite clay (B) was employed due to its rheological properties (fine-grained with high surface area and negative charge), resulting in low permeability and high metal io adsorption (Xu et al., 2008; Mohammad et al., 2010). However, bentonite liner is susceptible to shrinkage cracks upon drying, has low compressive strength and expensive material to import where it is not found locally (Sivapullaiah and Baig, 2011). Thus, there is a need for finding an alternative liner material for amending the negative consequences of using only bentonite and minimize its use, which is a costly mined material.

The current demand for electricity from thermal power plants (Fig. 7.1) in developing countries like India (70% in comparison to other sources) has grown in the past few decades (Singh et al., 2015; Goswami et al., 2020). Burning of coal in thermal power plants results in the production of waste fly ash (FA), which is dumped on land or transported to ash ponds (Asokan et al., 2004; Sandeep et al., 2016; Sarode et al., 2010). Indian FA majorly contains varying amounts of $SiO_2$ (20.60%), $Al_2O_3$ (5.35%), $Fe_2O_3$ (10.40%), CaO (1.12%) and MgO (0.5%) (Ahmaruzzaman, 2010; Shivpuri et al., 2011; Sivapullaiah and Baig, 2011, 2010). It was reported that only 60% of FA produced in India was utilized in sectors such as the cement industry, geotechnical and transportation infrastructures and agriculture (Yao et al., 2015). Ash deposits adjacent to the thermal power plants are piling up rapidly and

the problem of its disposal is reaching an alarming state with limited disposal space. FA is pozzolanic (can increase soil strength), cohesionless (resists shrinkage), and has relatively high cation exchange capacity (CEC) as compared to sand (Palmer et al., 2000; Sivapullaiah et al., 2000). In current practice, coarse-grained and inert sand (S) has been mixed with bentonite to mitigate the negative effects of using bentonite alone in the liner (Sivapullaiah et al., 2000; Mukherjee and Mishra, 2019). Sand is getting costlier, has negative effects of river dredging and its global resources are dwindling as reported in current literature (de Leeuw et al., 2010; Meng et al., 2018). Judging from the inherent properties of FA and the need for bulk usage of the accumulating waste, it is viable to explore the utilization of bentonite-fly ash (B-FA) mixes as an alternate liner material.

Notable research has been done on bentonite-fly ash composite as liner material in the past decade (Nhan et al., 1996; Hettiaratchi et al., 1999; Phani Kumar and Sharma, 2004; Younus and Sreedeep, 2012a). However, all of these studies focus majorly on the hydromechanical assessment of the composite for liner applications. Hettiaratchi et al. (1999) investigated the compressive strength, tensile strength, flexibility, cracking potential of different fly ashbentonite composites and found the majority of them suitable for liner materials. The inclusion of FA in bentonite decreased the plasticity, swelling potential, optimum moisture content (OMC), while increased the maximum dry density (MDD), which further makes it suitable for liner material (Phani Kumar and Sharma, 2004; Singh et al., 2015). The hydraulic conductivity value also ranges as per landfill liner material in multiple studies (Sivapullaiah and Lakshmikantha, 2004; Younus and Sreedeep, 2012a). However, majority of these studies focused on the heavy metal retention capacities of fly ash-bentonite composites as future scope to have a holistic understanding as a liner material. Deka and Sekharan (2017) conducted batch adsorption tests on Indian fly ash bentonite samples based on 1:1 ratio of the two material and the model contaminant was chosen as lead ($Pb^{2+}$). $Pb^{2+}$ is a common contaminant in MSW and sources out from batteries, and electronic goods with a reported concentration in landfill at 400 mg/L (Aucott, 2006). $Pb^{2+}$ poses various health hazards (anemia, headache, diarrhea and poisoning) leading to the kidney and brain dysfunction, which is particularly true for Indian subcontinent (Das et al., 2016, 2018; Kushwaha et al., 2018; Goswami et al., 2018). In this context, $Pb^{2+}$ adsorption of different fly ash-bentonite mixes, its reaction kinetics, and the comparison with sand bentonite mixes warrant further evaluation.

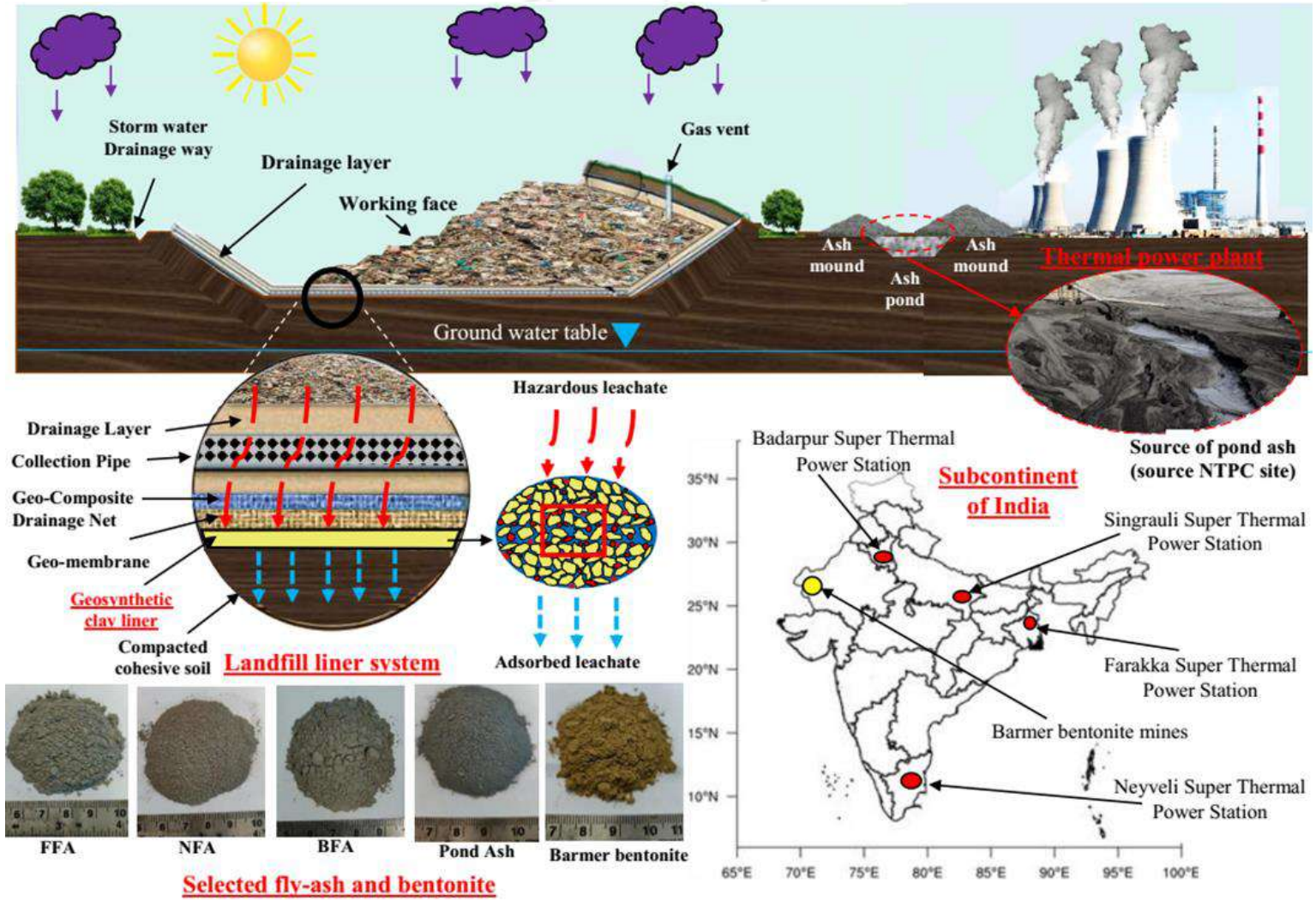


Figure 7.1: Overview and origin of fly-ash bentonite composites sourced from different parts of India

The objective of this study is to explore the adsorption characteristics of four B-FA composite mixes sourced from various locations in India, considering $Pb^{2+}$ as a model contaminant. The effect of fly ash type, fly ash amendment rate and adsorbate concentration was explored (ASTM C 618 (2003)) in the current study and juxtaposed with B-S mixes. Batch tests were conducted at varying $Pb^{2+}$ concentrations from 50 to 1050 mg/L. This was systematically performed by initially assessing the basic geotechnical properties followed by interpretation with respect to the chemical characteristics and microstructural imaging. The obtained experimental data on adsorption kinetics and adsorbate concentration were quantified using different adsorption isotherm. Based on the maximum adsorption capacity ($q_m$) obtained from isotherm models, an attempt was also made to explore a correlation between $q_m$ of the tested materials with the easily measurable Atterberg limits. This provides geo-environmental practitioners, a simple and practical approach of estimating the range of adsorption expected for fly ash-bentonite composites.

### 7.1.2 Test plan and experimental investigations

Batch adsorption study was performed according to ASTM D 4646 (2008a) guidelines for soil and sediments. For performing the batch sorption study of FAs, B-FA, and B-S mixes, liquid to solid (L/S) ratio of 20 was considered (ASTM D 4646 (2008a)). For bentonite (B), L/S was 50 due to the formation of a thick gel-like consistency at L/S equal to 20, which prevents proper interaction of $Pb^{2+}$ with the bentonite particles (Du and Hayashi, 2006). Batch sorption study was performed under controlled pH of 5 for comparing the adsorption potential of different materials.

This was done to avoid the precipitation of $Pb^{2+}$ in the solution which could take place in the range 8—11.5. Half volume of deionized water was taken in a volumetric flask, and the required amount of air-dried adsorbent was added and left overnight. The pH of the solution was adjusted to 5 by adding 0.1M $HNO_3$ and 0.1 M NaOH and shaking it for 2 h on a rotatory shaker. Any increase in the pH of the solution was again adjusted to pH = 5 followed by shaking, and this process was repeated till pH gets stabilized to 5. After that, the remaining half volume was filled with $Pb^{2+}$ solution of double the concertation to get the desired concentration of the solution. The precipitation of $Pb^{2+}$ associated with higher pH was prevented by adopting the above procedure. Any further change in the pH of the solution and associated precipitation was minimized by adding 0.1 ml of acetate buffer of pH = 5. The conical flask containing the solution of sorbent and $Pb^{2+}$ was kept

on the rotatory shaker at 200 rpm. After 24 h of shaking, the solution was transferred into the centrifuge tube and centrifuged at 4000 rpm for 10 min to separate the solid and liquid phase of the solution. The separated liquid phase sample was collected using the pipette and filtered through the Whatman grade 42 filter paper with the help of a vacuum filtration unit. The concentration in the filtrate was measured using the atomic absorption spectrophotometer (AAS) to check the equilibrium concentration of the solution.

### 7.1.3 Adsorption kinetics and adsorption capacity at varying adsorbate concentrations

Fig. 7.2 shows the adsorption capacity and percentage removal kinetics of $Pb^{2+}$ for the B-FA and B-S mixes at 1000 mg/L adsorbate concentration. The concentration of $Pb^{2+}$ observed in the leachate from different sources was reported to be varying in the range of 50 mg/L to 1000 mg/L (Jang and Townsend, 2003; Dutta and Mishra, 2016). Parent bentonite having extremely high CEC (53.7 meq/100 g) and SSA (450 $m^2/g$) reaches equilibrium adsorption capacity almost instantaneously within 5 min. In general, parent FA (except NFA-class C) requires 120—230 min to attain equilibrium adsorption capacity (Alinnor, 2007; Mohan and Gandhimathi, 2009). However, NFA exhibited comparatively faster equilibrium adsorption within 7 min. The quick adsorption of NFA was attributed to the higher CEC (9 times higher than other FAs) and inherently high alkaline nature (pH = 11.5) (Wang et al., 2009). It was also noted that controlling the pH of the solution for NFA was difficult and showed the tendency to increase. This would also have contributed to the high adsorption exhibited by NFA.

For B-FA and B-S mixes, the adsorption process was found to be relatively faster than parent FAs and reaches equilibrium adsorption capacity within 65 min. The trend indicates that the presence of bentonite particles regardless of percentage amendment dominates and attenuates the adsorption process. In terms of magnitude, NFA mixes showed higher adsorption capacity as NFA itself is a good adsorbent. As the hydraulic conductivity of typical B-FA mixes is extremely low within the range of ($10^{-8}$-$10^{-12}$) m/s (Sivapullaiah and Lakshmikantha, 2004; Younus and Sreedeep, 2012a), the contact time is sufficient to adsorb $Pb^{2+}$ ions in field conditions. A higher amendment of FA in bentonite resulted in greater $Pb^{2+}$ percentage removal. Moreover, the B-FA mixes showed higher percentage removal (i.e., 70.95%) as compared to B-S mixes (65.78%). The highest percentage removal was

also observed for B—NFA mixes in comparison to the other three B-FA mixes.

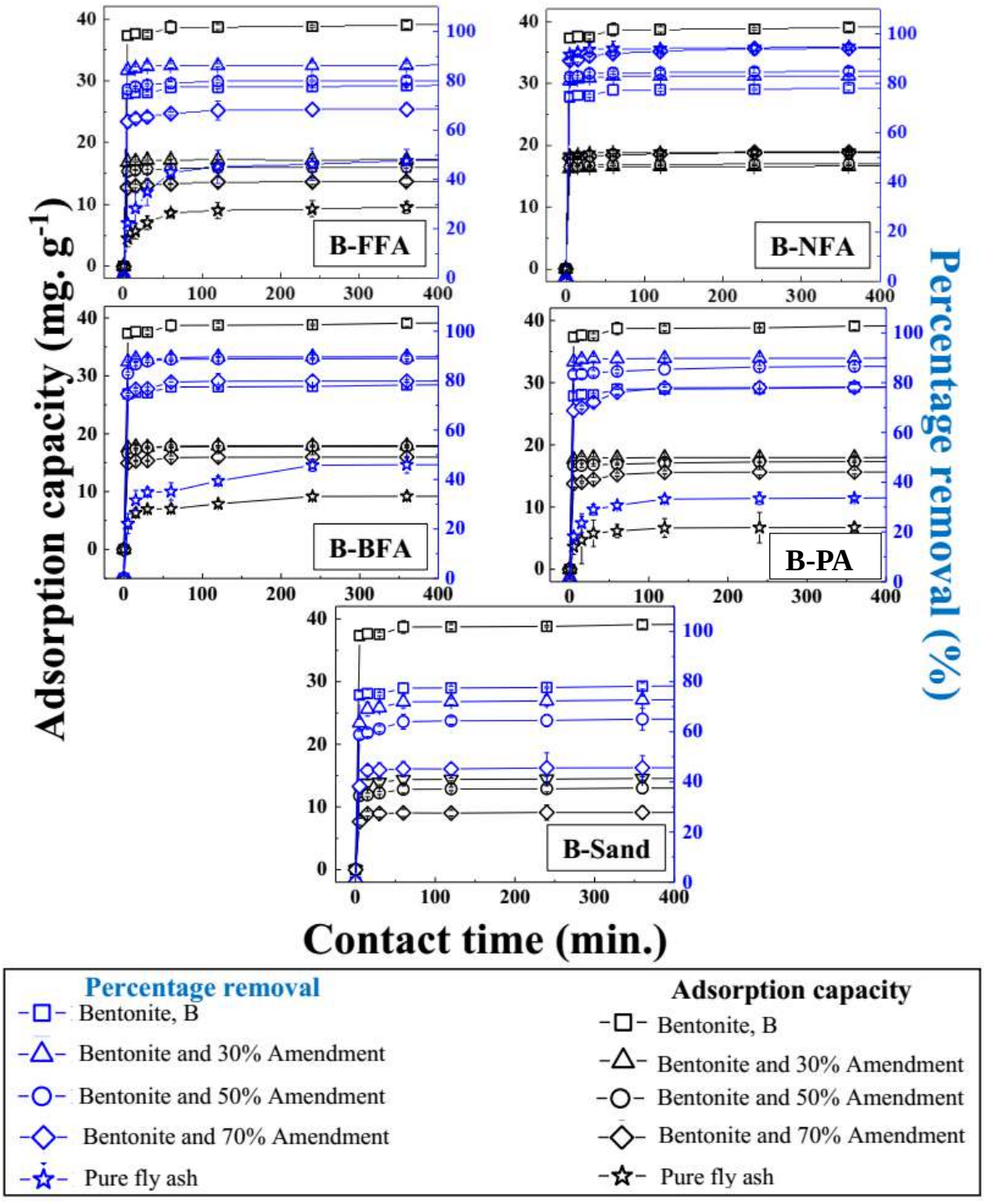


Figure 7.2: Adsorption capacity vs contact time response of bentonite-fly ash mix and bentonite-sand mix

Figure 7.3 presents the adsorption capacity of all parent soils and mixtures with different concentrations of adsorbate (50—1025 mg.$L^{-1}$). The adsorption capacity naturally increases with higher adsorbate concentration for all parent materials, as reported in the

literature (Melichová and Hromada, 2013; Deka and Sekharan, 2017).

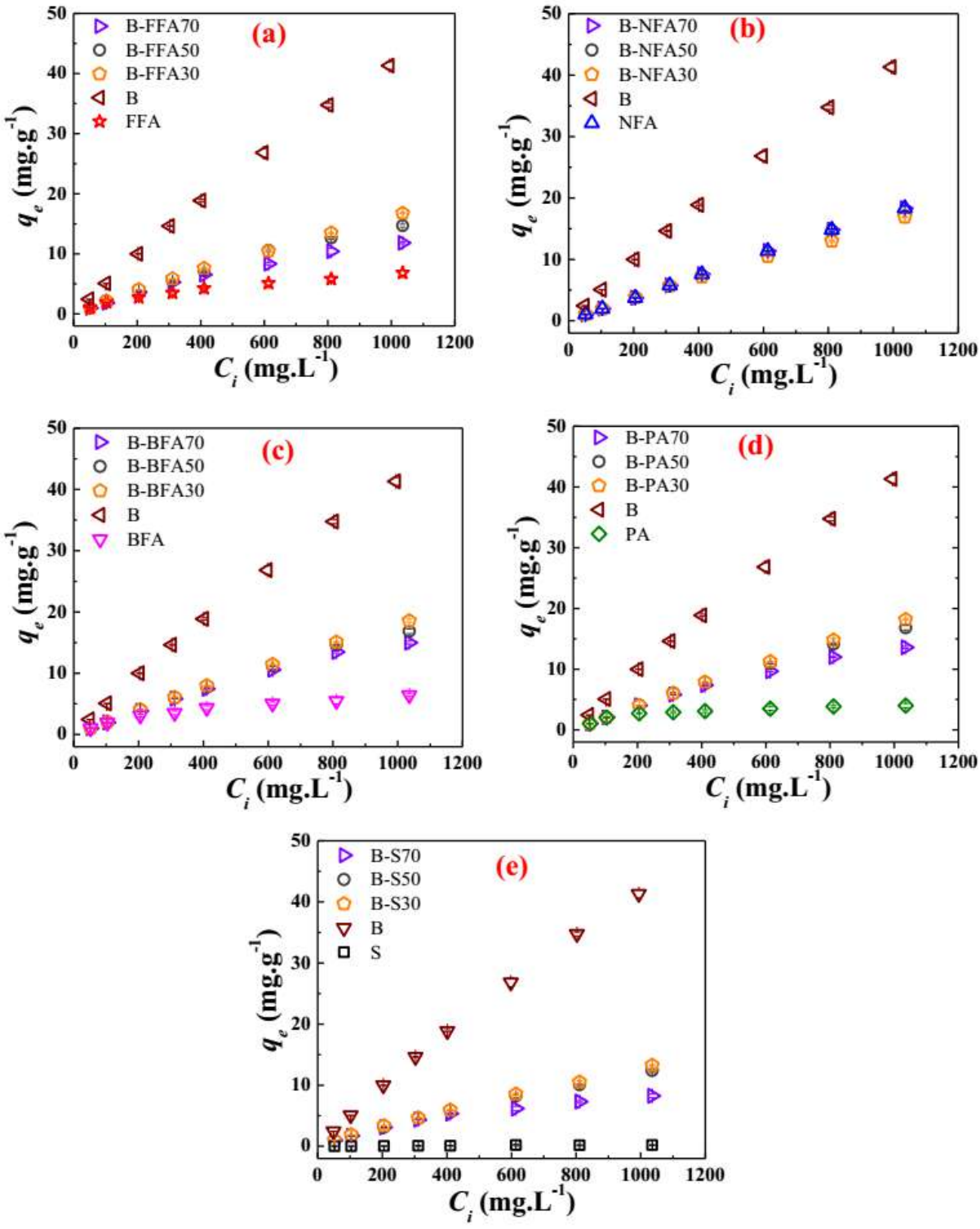


Figure 7.3: Adsorption capacities of B-FAs and B-S mixes

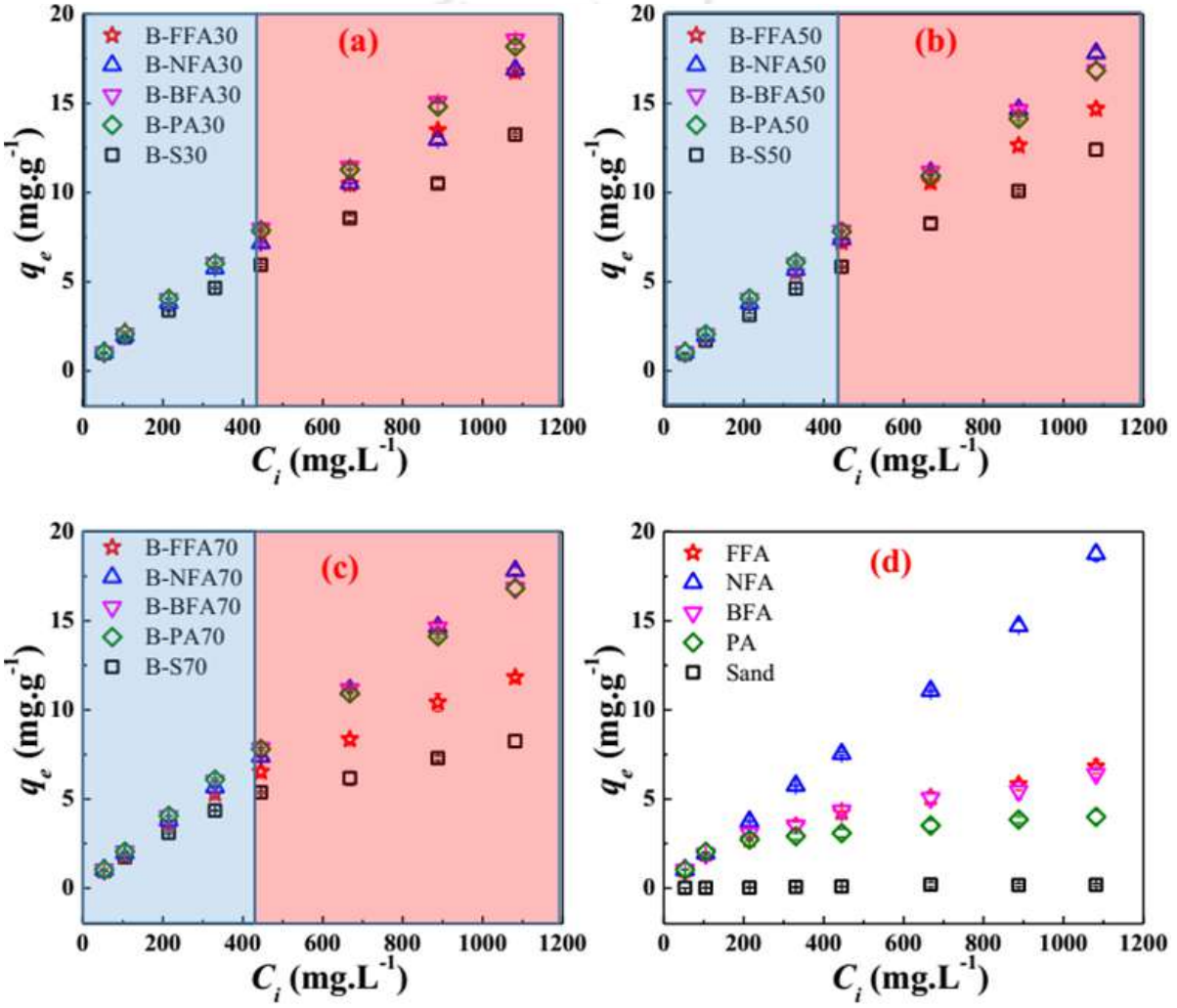


Figure 7.4: Comparison of adsorption capacities in (a-c) mixes (B-FAs and B-S) at a particular amendment proportion and (d) parent amendments

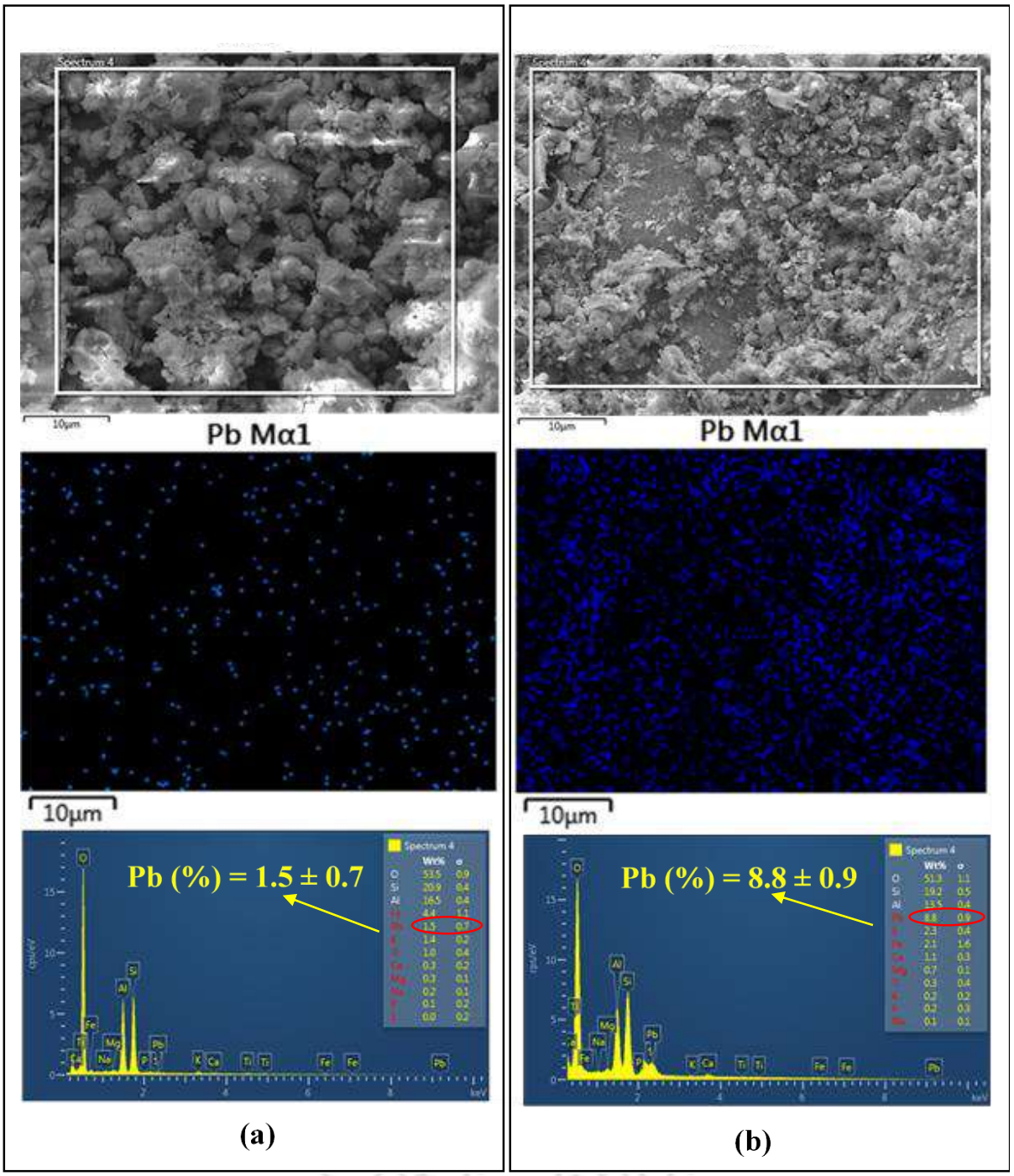


Figure 7.5: Microstructure of tested materials, Pb concentration mapping and EDX spectra of (a) BFA and (b) NFA

The magnitude was highest for pure bentonite and negligible for sand at all adsorbate concentrations. There was no appreciable effect of amendment rates on the adsorption capacity for different adsorbate concentration. The effect of amendment type was noticeable when the comparison was made at the same amendment rate (Fig. 7.4 a-c). All amendments (both B-FA and B-Sand) result in almost similar adsorption capacity at lower

adsorbate concentrations (marked in blue). This may be due to the availability of sufficient adsorption sites of the mixes at lower concentrations. As the concentration of $Pb^{2+}$ ions increase (marked in red), the adsorption sites of B-S mixes are saturated, while B-FA mixes facilitate for more adsorption. Thus, the usage of B-FA mixes is more efficient for metal adsorption at higher $Pb^{2+}$ concentrations commonly expected for landfill leachates (Wadanambi et al., 2008). Fig. 7.4 d shows that pure NFA is more effective in adsorbing $Pb^{2+}$ ions as compared to other parent amendment materials. This higher adsorption capacity of NFA was further validated by conducting Energy Dispersive X-Ray Analysis (EDX) tests on two parent FAs (NFA and BFA) at 1025 mg. $L^{-1}$ adsorbate concentration. The NFA adsorbs almost six-times more $Pb^{2+}$ as compared to BFA based on EDX mapping data ( Fig. 7.5), which further indicates the efficacy of NFA as an adsorbent material. This is further evident from the percentage of $Pb^{2+}$ shown in the EDX results.

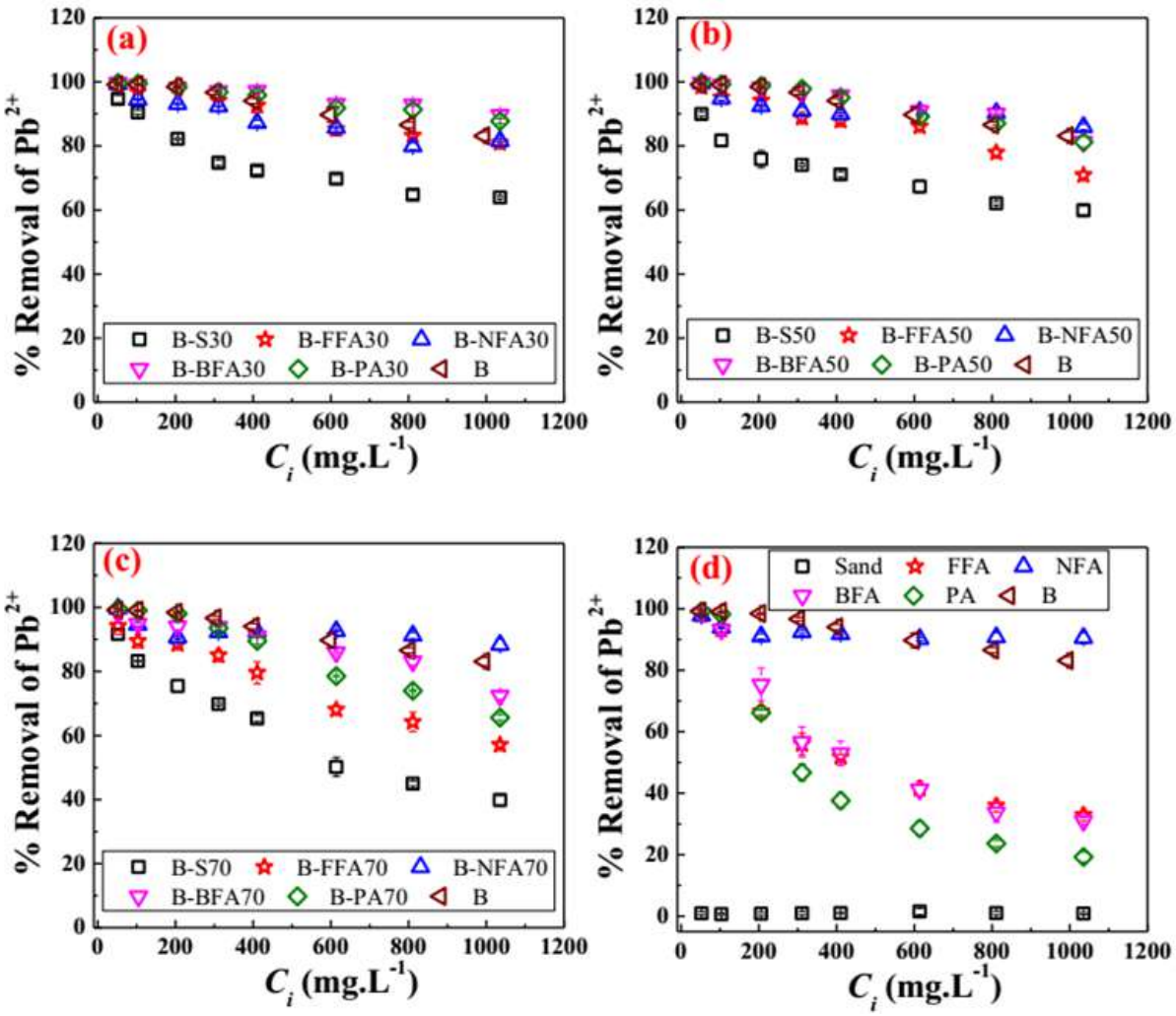


Figure 7.6: Comparison of percentage removal of B-FAs and B-S mixes for a particular amendment proportion (a) 30% (b) 50% (c) 70% and (d) parent materials

The percentage removal of $Pb^{2+}$ decreases with an increase in the adsorbate concentration for all mixes, as shown in Fig. 7.6 (a-c). This can be attributed to available adsorption sites of the mixes for $Pb^{2+}$ to be adsorbed at lower adsorbate concentration. As the concentration increases, the sites for adsorption diminishes and this is particularly evident for mixes with high amendments. In the case of 30% and 50% FFA amendment rates and adsorbate concentration of 1025 mg. $L^{-1}$, the percentage removal was 80% and 72%, respectively. This percentage removal was further reduced to 57% for 70% FFA amendment rate. The percentage removal of NFA was comparable to pure bentonite for all the adsorbate concentration range, as shown in Fig. 7.6 d.

### 7.1.4 Adsorption isotherms and relating adsorption capacity with Atterberg limits

Figure 7.7 shows the fitted Langmuir and Freundlich isotherm or the measured data for all mixes and parent materials. The obtained modelling parameters for both isotherms are tabulated in Table 7.1. It was observed from the regression coefficient that both Freundlich and Langmuir isotherm model fitted well with the measured data with reasonable accuracy ($R^2 > 0.95$). However, for parent FAs, Freundlich isotherm fitted better ($R^2 > 0.94$) as compared to the Langmuir isotherm model ($R^2 > 0.78$). The obtained maximum adsorption capacity (qm) from the isotherm was used to correlate the Atterberg limits for B, B-FA and B-S mixes. Fig. 7.8 presents the interrelationship of equilibrium adsorption rate with liquid limit and plasticity index. The LL and PI of all mixes and bentonite are reported in the chaper 3 (ref. Table 3.5). Apart from the current study, data points of B and B-FA mixes are also plotted to explore whether any relationship exists between adsorption potential of fine-grained soils and its Atterberg limits (LL, Plasticity index (PI)). Based on the measured and literature datapoints considering only divalent metal contamiants ($Pb^{2+}$, $Zn^{2+}$, $Cu^{2+}$), an increase in Atterberg limits directly implies a high equilibrium adsorption rate. This can be explained because an increase in SSA (due to inherent mineralogy) directly increases the water holding capacity, i.e., the liquid limit increases (Muhunthan, 1991; Dolinar et al., 2007). A recent study by Spagnoli and Shimobe (2019) co-related the inter-relationship between these two parameters based on 60 datasets from literature and formulated an empirical relationship with relative accuracy ($R^2 = 0.7$). Similarly, it is fathomable that an increase in available SSA can facilitate more sites for adsorption.

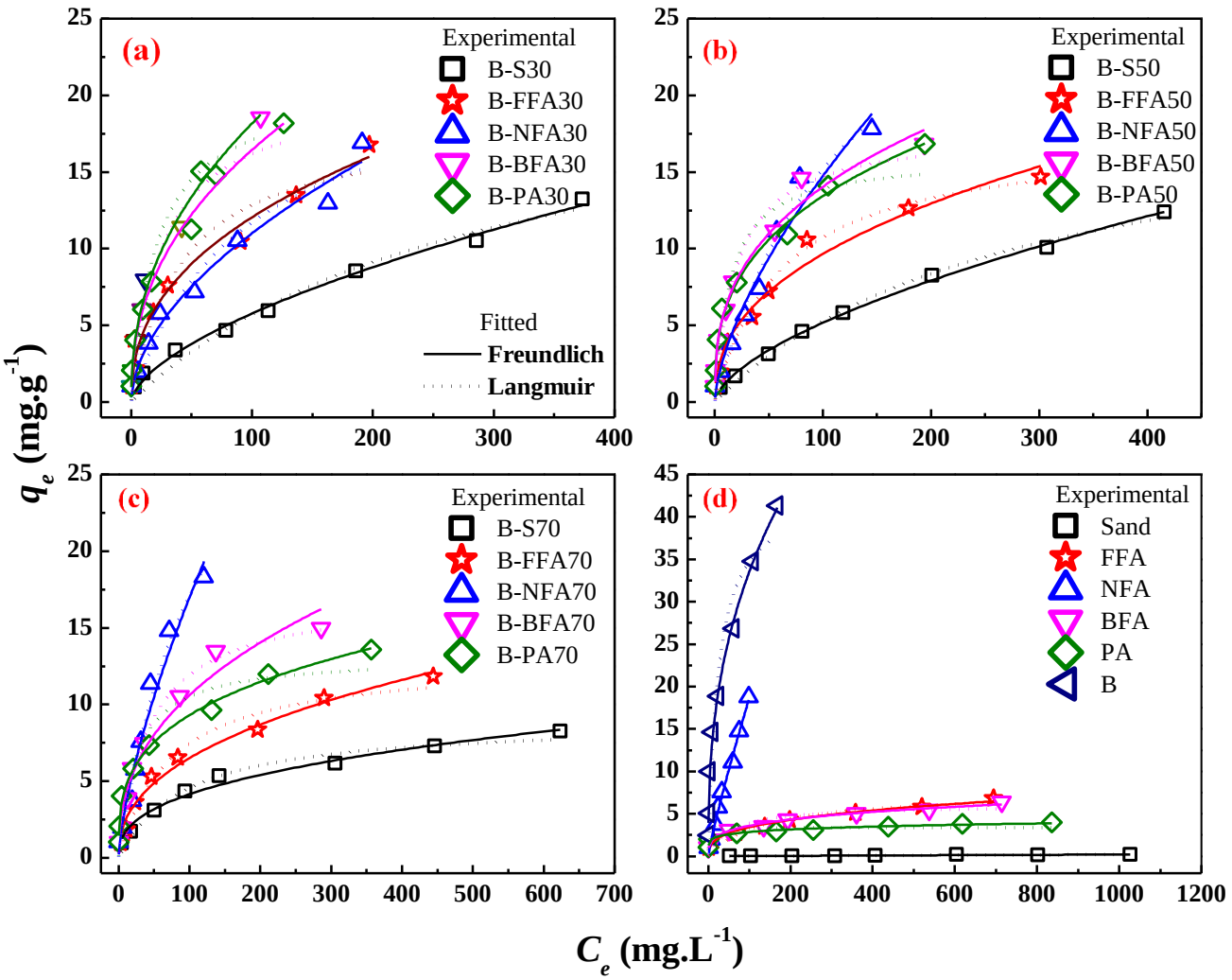


Figure 7.7: Freundlich and Langmuir isotherm model fitted to FAs, sand, B-FAs mixes and B-S mixes

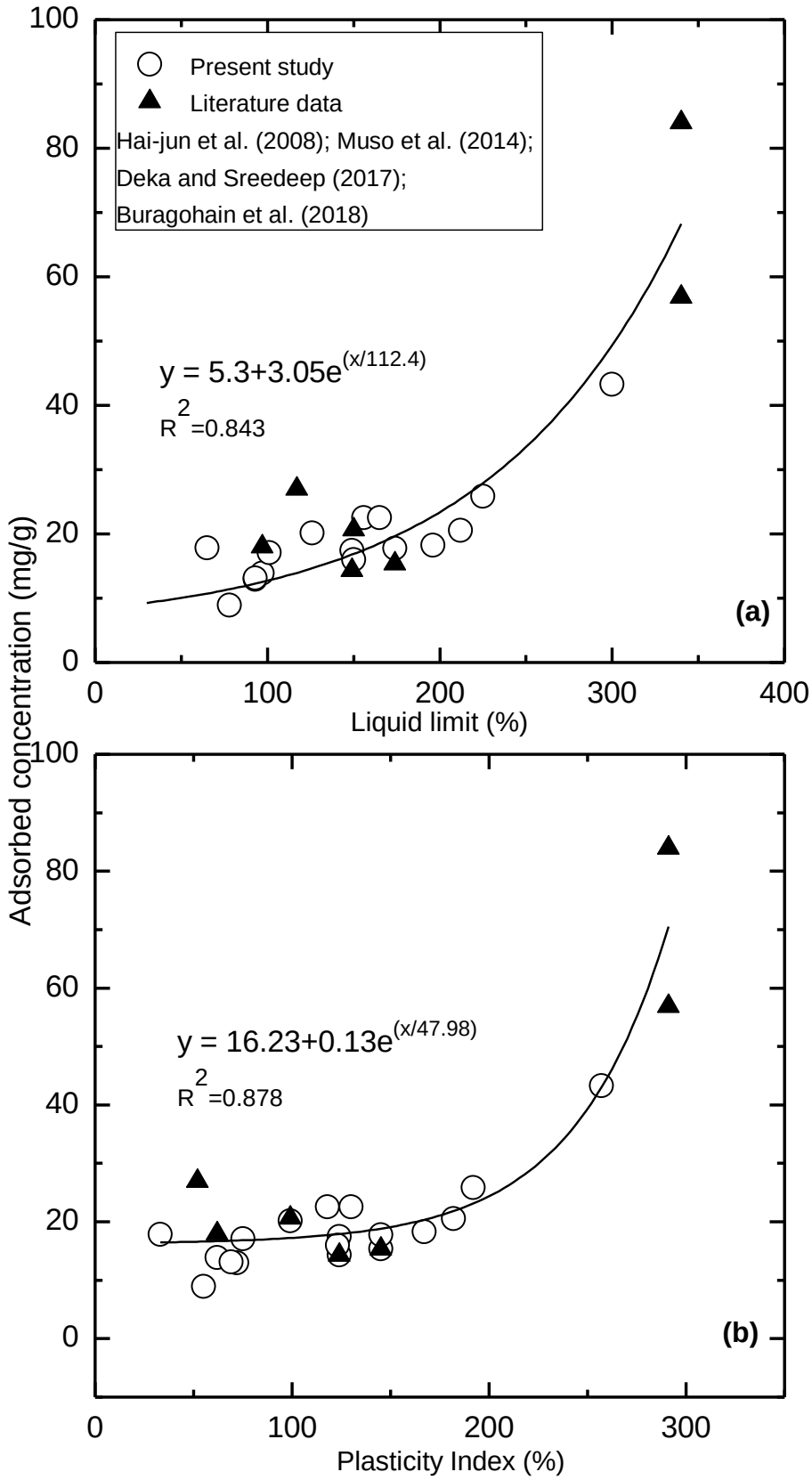


Figure 7.8: Interrelationship of equilibrium adsorbed concentration with (a) Liquid limit and (b) Plasticity Index

Table 7.1: Freundlich and Langmuir isotherm model fitted parameters for B, FAs, S, B-FAs mixes and B-S mixes under controlled pH environment

| Materials | Freundlich isotherm | | | Langmuir isotherm | | |
|---|---|---|---|---|---|---|
| | $K_f$ | n | $R^2$ | $q_m$ ($mg.g^{-1}$) | b (L/mg) | $R^2$ |
| B | 5.57 | 2.57 | 0.99 | 43.29 | 0.04 | 0.93 |
| FFA | 0.75 | 3.04 | 0.97 | 7.54 | 0.01 | 0.83 |
| B-FFA30 | 1.76 | 2.39 | 0.97 | 18.25 | 0.02 | 0.90 |
| B-FFA50 | 1.38 | 2.37 | 0.97 | 17.43 | 0.02 | 0.98 |
| B-FFA70 | 0.95 | 2.40 | 0.98 | 12.95 | 0.01 | 0.97 |
| NFA | 0.33 | 1.14 | 0.99 | 104.61 | 0.002 | 0.99 |
| B-NFA30 | 0.88 | 1.83 | 0.97 | 22.54 | 0.01 | 0.95 |
| B-NFA50 | 0.74 | 1.53 | 0.96 | 33.87 | 0.01 | 0.98 |
| B-NFA70 | 0.70 | 1.44 | 0.96 | 37.84 | 0.01 | 0.98 |
| BFA | 1.04 | 3.71 | 0.98 | 6.04 | 0.02 | 0.80 |
| B-BFA30 | 2.38 | 2.27 | 0.99 | 20.83 | 0.05 | 0.96 |
| B-BFA50 | 2.74 | 2.82 | 0.98 | 17.74 | 0.05 | 0.96 |
| B-BFA70 | 1.65 | 2.48 | 0.96 | 17.10 | 0.02 | 0.99 |
| PA | 1.47 | 6.95 | 0.94 | 3.36 | 0.87 | 0.78 |
| B-PA30 | 2.30 | 2.34 | 0.99 | 20.53 | 0.04 | 0.94 |
| B-PA50 | 2.77 | 2.92 | 0.99 | 15.98 | 0.07 | 0.91 |
| B-PA70 | 2.32 | 3.31 | 0.99 | 13.11 | 0.04 | 0.90 |
| S | 4.3E-4 | 1.13 | 0.87 | 0.72 | 3.7E-4 | 0.88 |
| B-S30 | 0.35 | 1.65 | 0.99 | 22.55 | 0.003 | 0.97 |
| B-S50 | 0.31 | 1.63 | 1.00 | 20.15 | 0.003 | 0.99 |
| B-S70 | 0.71 | 2.61 | 0.98 | 8.90 | 0.011 | 0.97 |

In geotechnics, the LL indicates the water content at which there is a gradual transition of soil from plastic to liquid consistency (Yong et al., 2012) and can be measured easily in both field and laboratory. Two relationships (Eqs. 7.1 and 7.2) are put forward to predict the equilibrium adsorption rate $q_m$ with Atterberg limits (LL and PI) with $R^2$ value ranging from 0.84 to 0.88.

$$q_m = 5.3 + 3.1e^{\frac{LL}{112.4}} \tag{7.1}$$

$$q_m = 16.2 + 0.1e^{\frac{PI}{48}} \tag{7.2}$$

## 7.2 Contaminant retention capacity for B-FA and B-S mixes under uncontrolled pH environment

### 7.2.1 Background

Clay and clay-based composites are used as hydraulic and chemical barrier in hazardous waste containment landfill liners (Daniel et al., 1984; Rowe, 2012; Younus and Sreedeep, 2012a; Chen et al., 2019a; Li et al., 2021). They have two major functions, viz. minimize migration of leachate towards the ground water and retain the harmful metals constituted in the leachate by the clay-based composites (Lange et al., 2007; Chalermyanont et al., 2009; Mazzieri et al., 2013; Budihardjo et al., 2021). Assessment of leachate migration through the liner layer is characterized by the hydraulic conductivity of the liner material (Giroud et al., 1997; Zhan et al., 2014; Chen et al., 2018; Bradshaw et al., 2016). As per United States Environment Protection Agency (USEPA) guidelines (EPA/ 530-SW-86-007-F, 1987; USEPA, 1989), for any material to qualify for use in a liner layer, the saturated hydraulic conductivity would be lower than $10^{-9}$ m/s. On the other hand, there is no well-defined guidelines related to the contaminant retention capacity of the liner material. Nevertheless, the contaminant retention for liner material is generally characterized by the adsorption capacity of the adsorbent, percentage removal of the contaminant considered and the isotherm model parameters (Hong et al., 2016; Deka and Sekharan, 2017). These adsorption isotherm model parameters of the adsorbent are generally obtained by conducting batch test considering a single contaminant or a mixture of contaminants (Deka and Sekharan, 2017).

General procedure of adsorption studies in batch experiments necessitates the initial pH to be controlled (Li and Li, 2001; Huang et al., 2011; Hong et al., 2016; Liu et al., 2016; Kumar et al., 2019). In majority of these studies, the pH of adsorbent is controlled at 5 to simulate the pH of leachate in field conditions (Rowe, 1995; Lo, 1996; Li and Li, 2000). The adsorption capacity of adsorbent obtained from batch studies at this initial controlled pH would give us the minimum or representative contaminant removal, predominantly based on adsorption phenomenon. However, contaminant retention is governed by both adsorption and precipitation, typically at higher pH (Liu et al., 2016; Deka and Sekharan, 2017). At uncontrolled pH, typically higher than 5.5, precipitation of heavy metal ($Pb^{2+}$) would

be dominant followed by adsorption of the adsorbate as the pH of the solution decreases. The pH of the adsorbent in field will be different based on its minerology. Typically, for reactive material such as clay and clay-based composites the range would be at 8-12 (Li and Li, 2000; Liu et al., 2016; Tahervand and Jalali, 2017). Thus, to account for maximum adsorption capacity (due to both adsorption and precipitation), it would be ideal to conduct adsorption tests at an initial uncontrolled pH of the adsorbent.

The pH of these fly ash based geomaterials is relatively high ranging from 8-11 (Kaufhold et al., 2008; Rao and Acharya, 2014; Bhatt et al., 2019). In field applications, coarse grained sand (S) is mixed with bentonite clay to mitigate the negative effects of using bentonite alone (i.e., low shear strength and high-volume change) in liner layer (Sivapullaiah et al., 2000; Mukherjee and Mishra, 2019). Use of sand does not change the pH of the bentonite, that typically ranges between 6-10, i.e., which is also highly susceptible to precipitation phenomenon. Therefore, characterizing the adsorption capacity of bentonite-based liner or GCLs would not be ideal by solely conducting the adsorption tests at controlled pH. Judging from the inherent properties of FA and need for bulk usage of the accumulating waste, it is viable to explore the utilization of bentonite-fly ash (B-FA) mixes as an alternate liner material. To do so for bentonite-fly ash (B-FAs) composites with a very high inherent pH (6-11), it is essential to obtain adsorption parameters (adsorption capacity, percentage removal, kinetic parameters) based on uncontrolled pH condition. This change in adsorption capacity due to precipitation would of course affect the required liner thickness and thus affect construction cost and economy.

The objective of this study is to explore the adsorption characteristics of four B-FA composites considering $Pb^{2+}$ as model contaminant at both controlled and uncontrolled pH condition. The effect of fly ash type, fly ash amendment rate and adsorbate concentration were also explored in the current study and juxtaposed with both pH conditions. Batch tests were conducted at varying $Pb^{2+}$ concentrations from 50 to 2000 $mgL^{-1}$. This was systematically performed by initially assessing the basic geotechnical properties followed by interpretation with respect to the chemical characteristics and micro-structural imaging. The obtained experimental data on retention experiments were fitted using different adsorption isotherm models.

### 7.2.2 Test plan and experimental investigations

The batch sorption study of FAs, B-FA, and bentonite-sand (B-S) mixes were conducted by considering liquid to solid (L/S) ratio as per ASTM guidelines (ASTM D 4646 2008a). While for the sorption study of B L/S ratio 50 was taken as per the recommendation givent in the previous section 6.1 in the present study. For controlled condition, batch sorption study was performed at pH of 5, while for uncontrolled conditions the pH of the FAs, B-FA and B-S were observed in the range of 8 to 11.5. In the case of experiments with controlled pH, half volume of deionized water was initially taken in the conical flask and necessary amount of the air-dried adsorbent was mixed to it and left overnight. Thereafter, pH of the solution was adjusted to the target pH of 5 by gradually adding 0.1M $HNO_3$ and 0.1 M NaOH to the solution and mixed uniformly for 2h using a rotatory shaker. Any increase in the pH of the solution made was further adjusted to pH of 5 by repeating the mentioned process till pH gets stabilized at 5. After this stage, the remaining half volume was gradually filled with $Pb^{2+}$ solution (double the concertation) to obtain the desired concentration of the solution. To avoid any further change in the pH of the solution during the batch adsorption study, 0.1 ml of acetate buffer of pH of 5 was added into the solution to minimize any precipitation of $Pb^{2+}$. For uncontrolled pH condition, initially only pH of the adsorbate solution of desired volume was taken in conical flask and then pH was adjusted to 5 using 0.1M $HNO_3$ and 0.1 M NaOH. There after required amount of dried mass of adsorbent was added into the adsorbate solution. After that, conical flask containing the solution of sorbent and $Pb^{2+}$ was mixed using the rotatory shaker at 200 rpm. After 24 hours of mixing, solution was transferred into the centrifuge tube and centrifuged at 4000 rpm for 10 minutes to separate the phases of the resultant solution. The separated liquid phase was collected using the pipette and filtered through the Whatman grade 42 filter paper using the vacuum filtration assembly. The pH of the filtrate was adjusted below two using nitric acid and was stored at 4 $^{o}$C for further analysis of metal concentration present in the filtrate. The concentration in the filtrate was measured using the atomic absorption spectrophotometer to check the equilibrium concentration of the solution.

### 7.2.3 Contaminant retention capacity of fly ash and bentonite

Fig. 7.9 demonstrates the $Pb^{2+}$ retention capacity ($q_e$) and equilibrium solution pH of the four-fly ash and bentonite with different contaminant concentration ($C_i$). The qe increases

with an increase in $C_i$ linearly at lower $C_i$ and reaches an equilibrium condition at higher $C_i$. This $q_e$ at equilibrium for the range of $C_i$ was not reached for NFA (for both controlled and uncontrolled conditions) as well as for FFA and B at uncontrolled condition. The $q_e$ at equilibrium of the samples under controlled condition were in the sequence of B (50 $mg.g^{-1}$), NFA (34 $mg.g^{-1}$), FFA (11.5 $mg.g^{-1}$), BFA (10 $mg.g^{-1}$) and PA (6.8 $mg.g^{-1}$). The qe at equilibrium of the samples under uncontrolled condition were also in the sequence of B (71 $mg.g^{-1}$), NFA (40.2 $mg.g^{-1}$), FFA (21.8 $mg.g^{-1}$), BFA (13.3 $mg.g^{-1}$) and PA (11.4 $mg.g^{-1}$). Regardless of samples taken, the $q_e$ at equilibrium for uncontrolled condition increased within the range of 40 % to 98%. This increase in $q_e$ at equilibrium at uncontrolled condition can be attributed to two possible reasons. These reasons are due to an increase in competition of $H^+$ ions with $Pb^{2+}$ ions to the surface sites as well as a corresponding decrease in metal ion precipitation as hydroxides at higher pH conditions (in our case at the uncontrolled condition). These observations were also reported by Liu et al. (2016) wherein they studied the heavy metal retention properties of kaolin and bentonite for a wide range of adsorbate concentration and varying pH conditions. In their study, the $q_e$ at equilibrium for bentonite increased by (approx. 200 %) for uncontrolled pH as compared to controlled pH conditions. The precipitation as hydroxides can be visualized based on the highlighted section of equilibrium solution pH ranging from pH greater than 5.5. $Pb^{2+}$ precipitation occurs above pH greater than 5.5 (Holan and Volesky, 1994; Tseveendorj et al., 2017). It is evident from Fig. 7.9 that precipitation will dominate in metal retention as well as with adsorption in lower $C_i$ for B, FFA and NFA. Precipitation will however not play a major role in retention characteristics of BFA and PA due to inherently lower pH value (8-8.5) as compared to the other FAs (10.5-11.5). Comparing the equilibrium solution pH for B and FFA, it can be inferred that precipitation occurs even at lower $Pb^{2+}$ concentration of 50 $mg.L^{-1}$ (indicated by drop of equilibrium solution pH) along with adsorption.

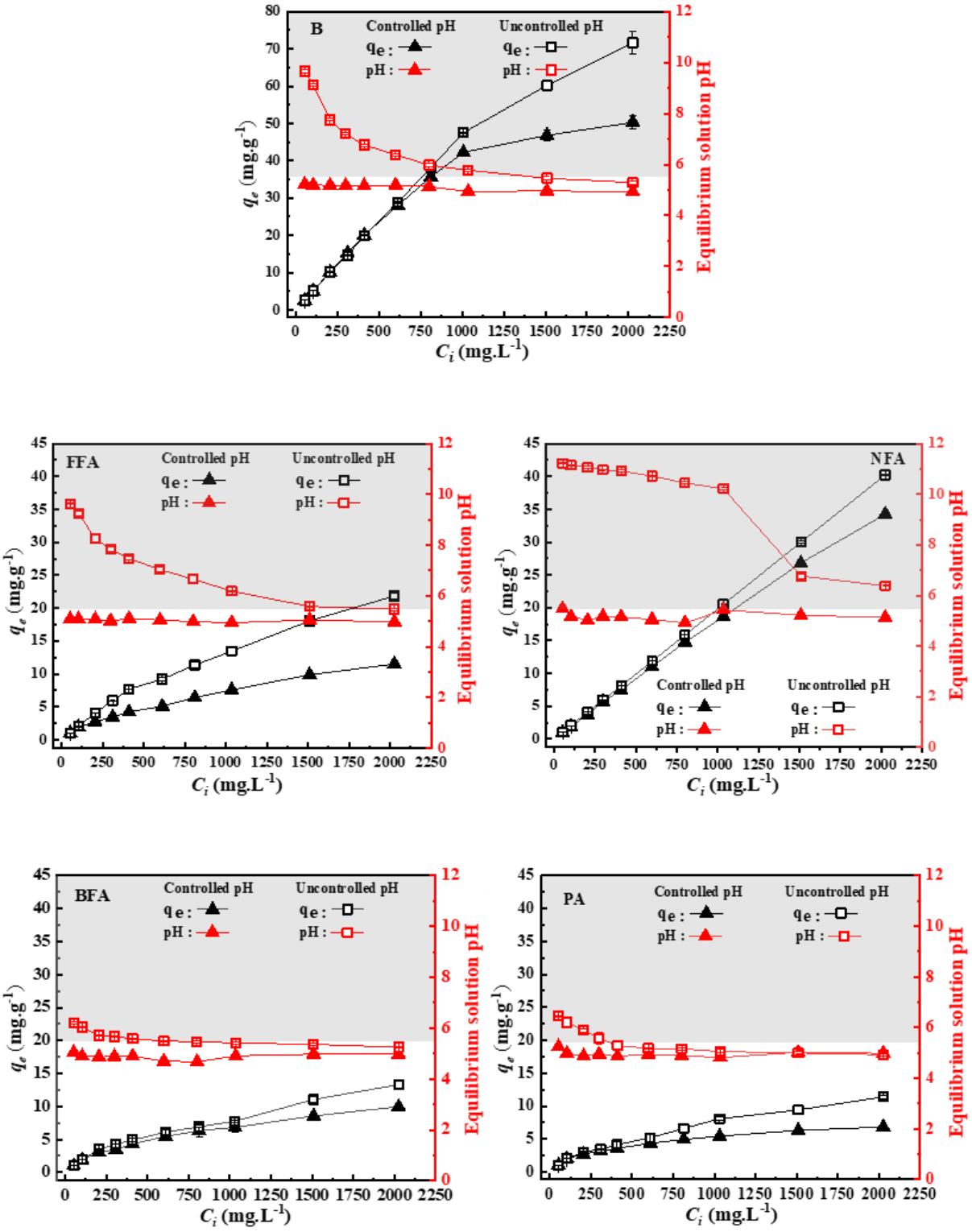


Figure 7.9: Retention capacity and equilibrium solution pH of parent materials under controlled pH and uncontrolled pH conditions

Contrastingly for NFA, the equilibrium solution pH decreases significantly after around 1000 mg.L$^{-1}$ which implied that precipitation dominates only at higher $Pb^{2+}$ concentration. Even at 2000 mg.L$^{-1}$ the equilibrium solution pH is at 6.4, indicating that $Pb^{2+}$ can

be precipitated at even higher $C_i$. The $Pb^{2+}$ retention results of the parent materials indicate that at high pH condition, the adsorbate will be retained due to adsorption as well as precipitation. Further evidence based on analytical approaches related to the statement is provided in the next sub-section. The results in the current section indicate that the current approach of determining the metal retention capacity of clay liner layer based on batch test at low pH is likely conservative and uneconomical. As the liner thickness is designed based on the retardation factors obtained from the adsorption isotherm (Garg et al., 2020), the higher equilibrium $q_e$ for realistic in-situ uncontrolled condition would likely result in low liner thickness.

### 7.2.4 Analytical characteristics of fly-ash and bentonite

The micrographs of bentonite and fly ash at initial state and after $Pb^{2+}$ sorbed state (both at controlled and uncontrolled condition) are presented in Fig. 7.10. The parent materials and their sorbed state are shown to investigate whether any precipitation crystals were formed on the surface of the adsorbents at 10 KX 20 KX magnification. In case of bentonite, the precipitation was not visually observed, either due to the magnification or the inherent pH of the bentonite itself. Liu et al. (2016) provides evidence that an enhanced metal retention adsorption takes place on the bentonite surface due to subsequent mobilization of $H^+$ ions at higher pH and absence of further ion precipitation. Based on visual inspection, FFA and NFA exhibited highest amount of $Pb^{2+}$ precipitate like crystals on the fly ash cenospheres for the uncontrolled condition. FFA and NFA exhibits more precipitation at their sorbed state as they inherently have a high pH (10.5-11.5). The other two fly ash had relatively lower pH values (8-8.5) and exhibit moderate precipitated crystals (refer Fig. 7.10) as compared to NFA and FFA. The mineralogical change in the parent materials were investigated by comparing the XRD spectra (Fig. 7.12) at virgin and sorbed conditions (both controlled and uncontrolled). In case of bentonite, significant suppression of montmorillonite mineral peak was observed at uncontrolled condition as compared to its virgin state as well as at controlled condition. The main peak of montmorillonite at d001 shift in the right ward as compared to the XRD peak of parent B. This confirms the reduction of basal spacing of interlayer due to the sorption of $Pb^{2+}$. Past researchers also reported similar reductions in d001 inter layer spacing of montmorillonite upon adsorption of $Pb^{2+}$, $Cu^{2+}$ and $Zn^{2+}$ (Auboiroux et al., 1996; Godelitsas et al., 2003; Eren and Afsin, 2008; Zhirong et al., 2011).

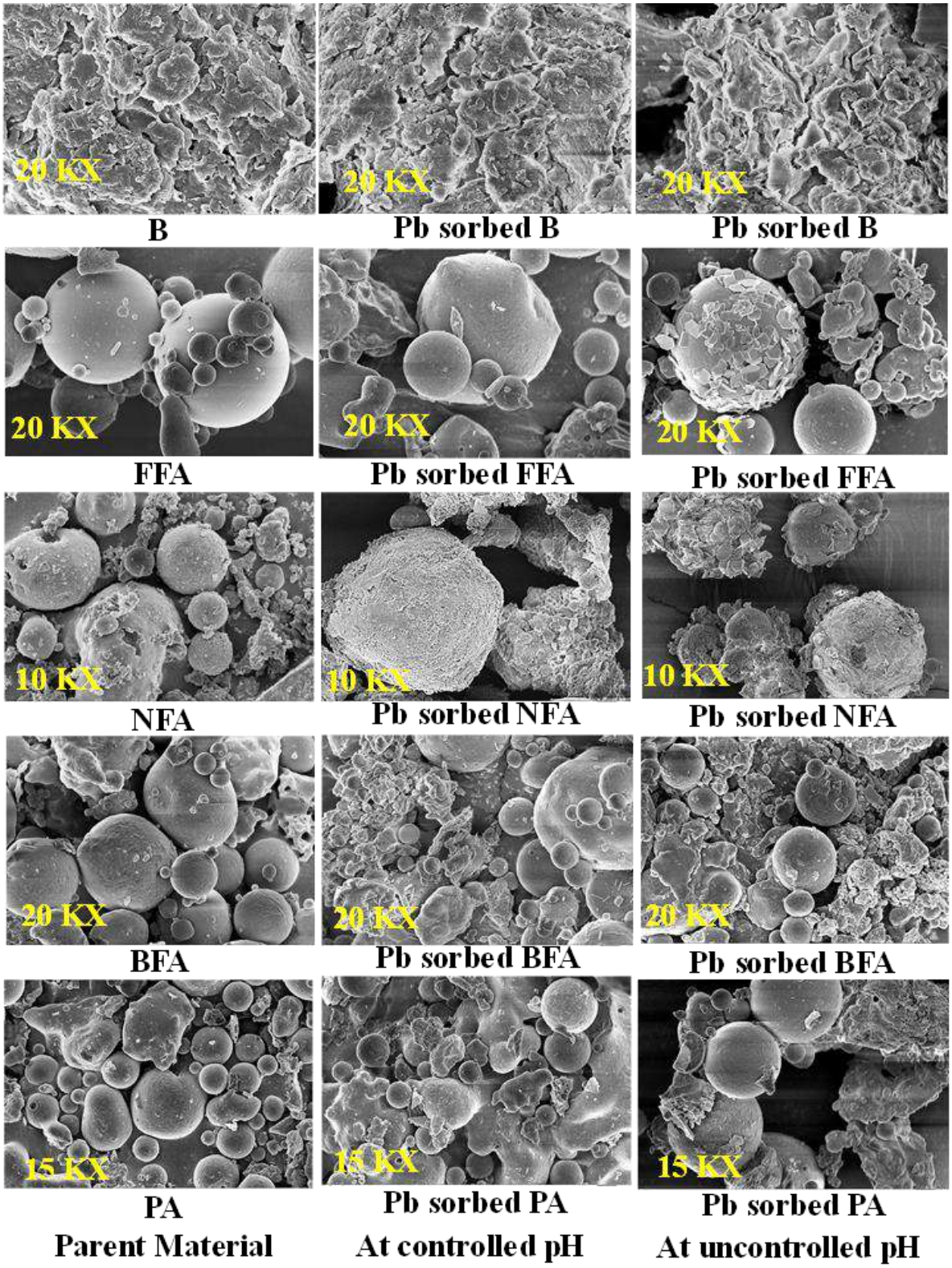


Figure 7.10: FESEM image of $Pb^{2+}$ sorbed parent material under controlled pH and uncontrolled pH conditions (Ci=2000 $mg.L^{-1)}$

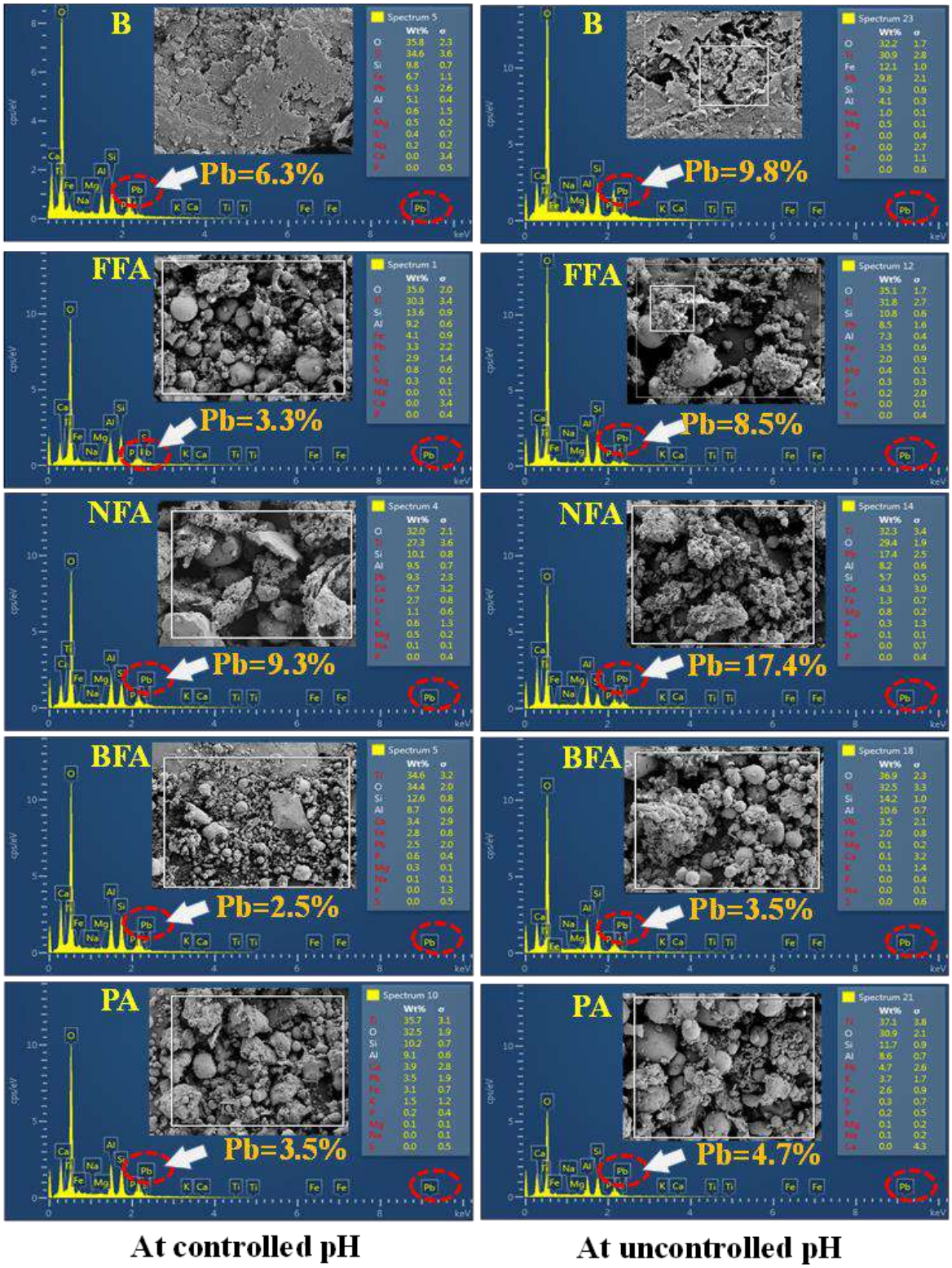


Figure 7.11: EDX spectra of $Pb^{2+}$ sorbed parent material under controlled pH and uncontrolled pH conditions ($C_i$ =2000 mg.$L^{-1}$)

In case of fly ash at uncontrolled condition, particularly for FFA and NFA, the Mullite and Quartz peaks are suppressed almost completely with respect to its virgin state, while for

BFA and PA these minerals are suppressed partially (Jin et al., 2010; Yahya et al., 2017; Chen et al., 2019b). The quantitative increase in $Pb^{2+}$ retention of the parent materials at both controlled and uncontrolled conditions were further confirmed using EDX spectra (Fig. 7.11).

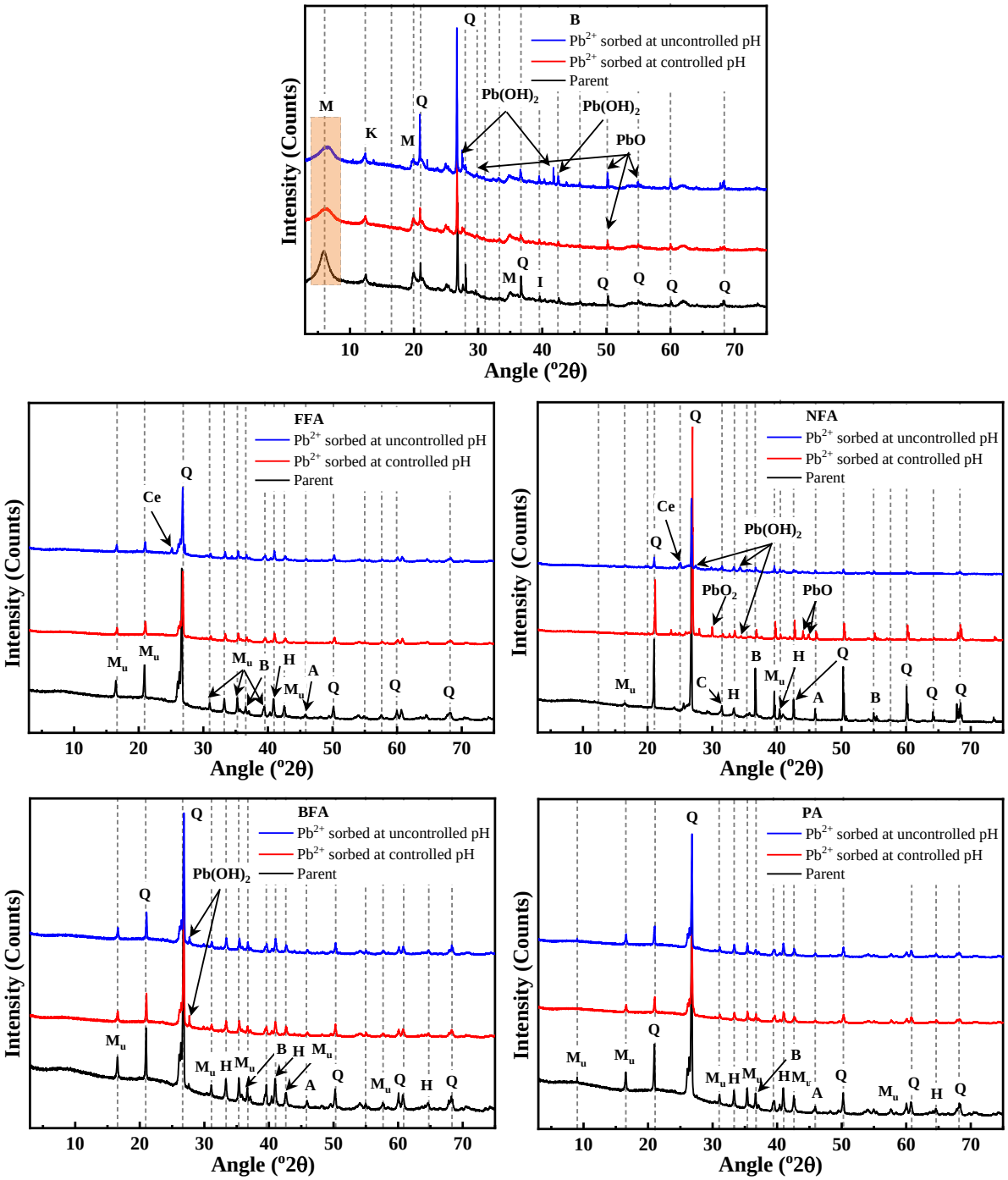


A – Agragonite, B - Anhydrite, C – Calcium oxide, Ce – Cerusite , H- Hematite, I – Illite, K – Kaolinite, M – Montmorillonite, $M_u$ – Mullite, Q – Quartz

Figure 7.12: XRD spectra of parent material and with $Pb^{2+}$ sorbed under controlled pH and uncontrolled pH conditions (Ci=2000 $mg.L^{-1}$)

In case of bentonite, $Pb^{2+}$ precipitation increased by 55 % whereas for NFA and FFA, even higher $Pb^{2+}$ precipitation was observed at 87% and 157 %, respectively. Of course, caution should be taken on these values as they are point measurement on the parent material. Nonetheless, it gives a quantitative representation of $Pb^{2+}$ precipitation on the bentonite and fly ash at controlled and uncontrolled condition. The $Pb^{2+}$ precipitation at uncontrolled condition for BFA and PA increased by 39 % and 34 %, respectively. Based on the $Pb^{2+}$ precipitation values observed for FFA, BFA and PA from the EDX spectra, it could be inferred that the magnitude of precipitation at uncontrolled condition for a particular Class of FA is majorly dependent on the inherent pH of the material itself.

### 7.2.5 Retention kinetics, capacity, percentage removal and isotherms of mixes

Fig. 7.13 shows the retention kinetics in terms of retention capacity with contact time of $Pb^{2+}$ for the bentonite, B-FA, and B-S mixes at 1000 $mgL^{-1}$ adsorbate concentration. The adsorbate concentration of 1000 $mgL^{-1}$ was selected based on reported values of $Pb^{2+}$ in the leachate from various sources (Jang and Townsend, 2003; Ray et al., 2022). In case of bentonite, equilibrium adsorption capacity was achieved within 5 minutes and can be attributed to extremely high CEC (53.7 meq/100g) and SSA (450 $m^2/g$). In terms of magnitude, B-NFA mixes showed higher adsorption capacity among the B-FA mixes studied. This is expected as NFA itself is a good adsorbent (refer previous section). When compared between uncontrolled and controlled conditions, the contact time at equilibrium for uncontrolled condition ranged between 5 to 30 mins, whereas, for controlled it was between 15 to 120 mins. In field condition, the results imply that B-FA mixes at both uncontrolled and controlled conditions would be readily able to adsorb $Pb^{2+}$ to its potential. This can be inferred based on reported the hydraulic conductivity values ($10^{-10}$-$10^{-12}$ m/s) of B-FA mixes (Sivapullaiah and Lakshmikantha, 2004), which would facilitate sufficient contact time for retention to occur.

Fig. 7.14 presents the $Pb^{2+}$ retention capacity ($q_e$) of the bentonite-fly ash (B-FA) and bentonite-sand (B-S) mixes with different contaminant concentration ($C_i$). The qe naturally increases with higher $C_i$ for all mixes as also observed for parent materials (refer section 3.1). All mixes (B-FA and B-S) result in almost similar adsorption capacity at lower $C_i$ (marked in highlighted section). This $C_i$ was found to vary with amendment rates for each

mix. This is likely due to the availability of sufficient adsorption sites of the mixes for the $Pb^{2+}$ ions at lower $C_i$. Progressively, as the concentration of $Pb^{2+}$ ions increase (non-highlighted section), the adsorption sites of B-S mixes are limited (Du and Hayashi, 2006).

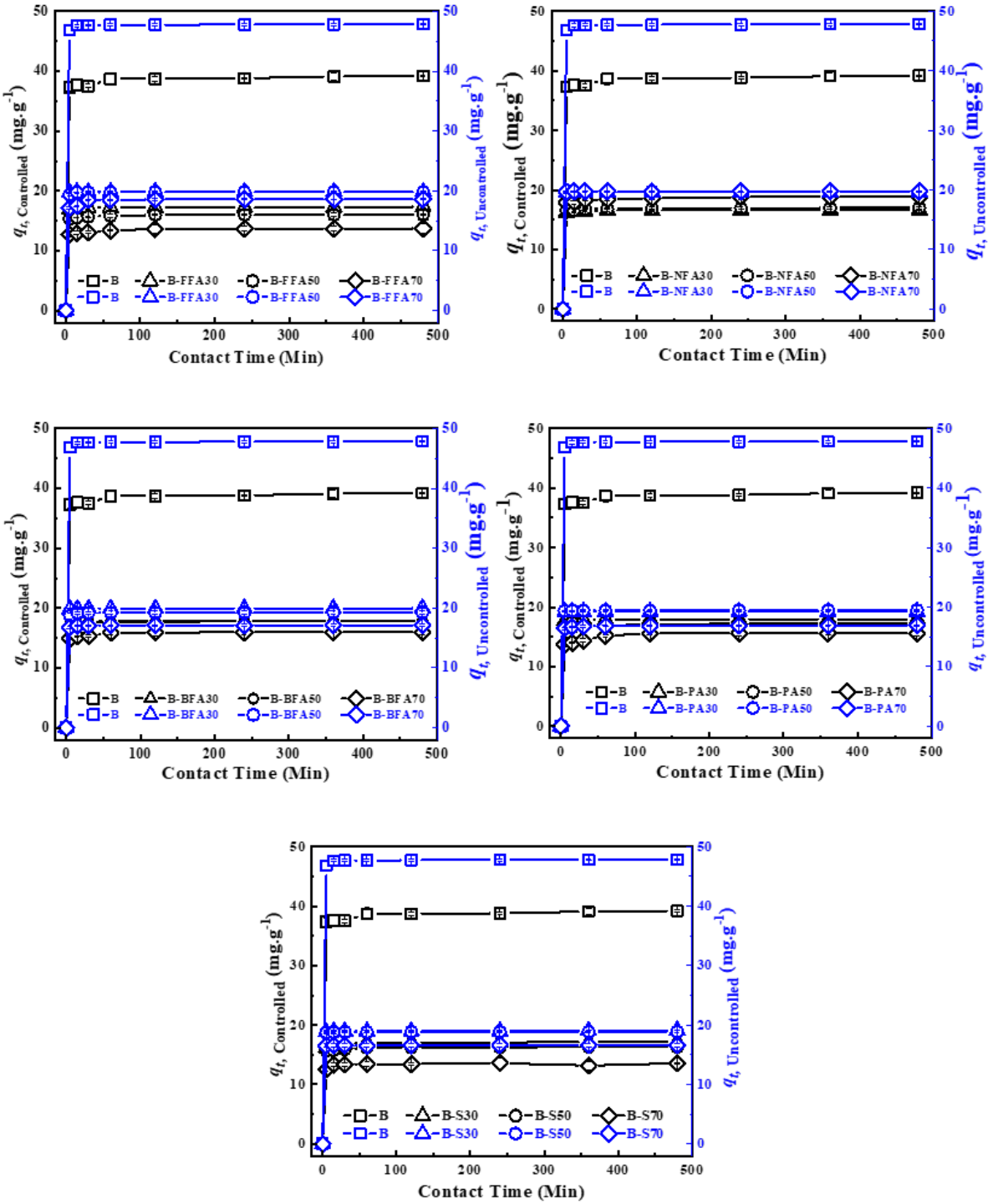


Figure 7.13: Retention capacity vs contact time response of B-FA and B-S mixes under controlled and uncontrolled pH conditions

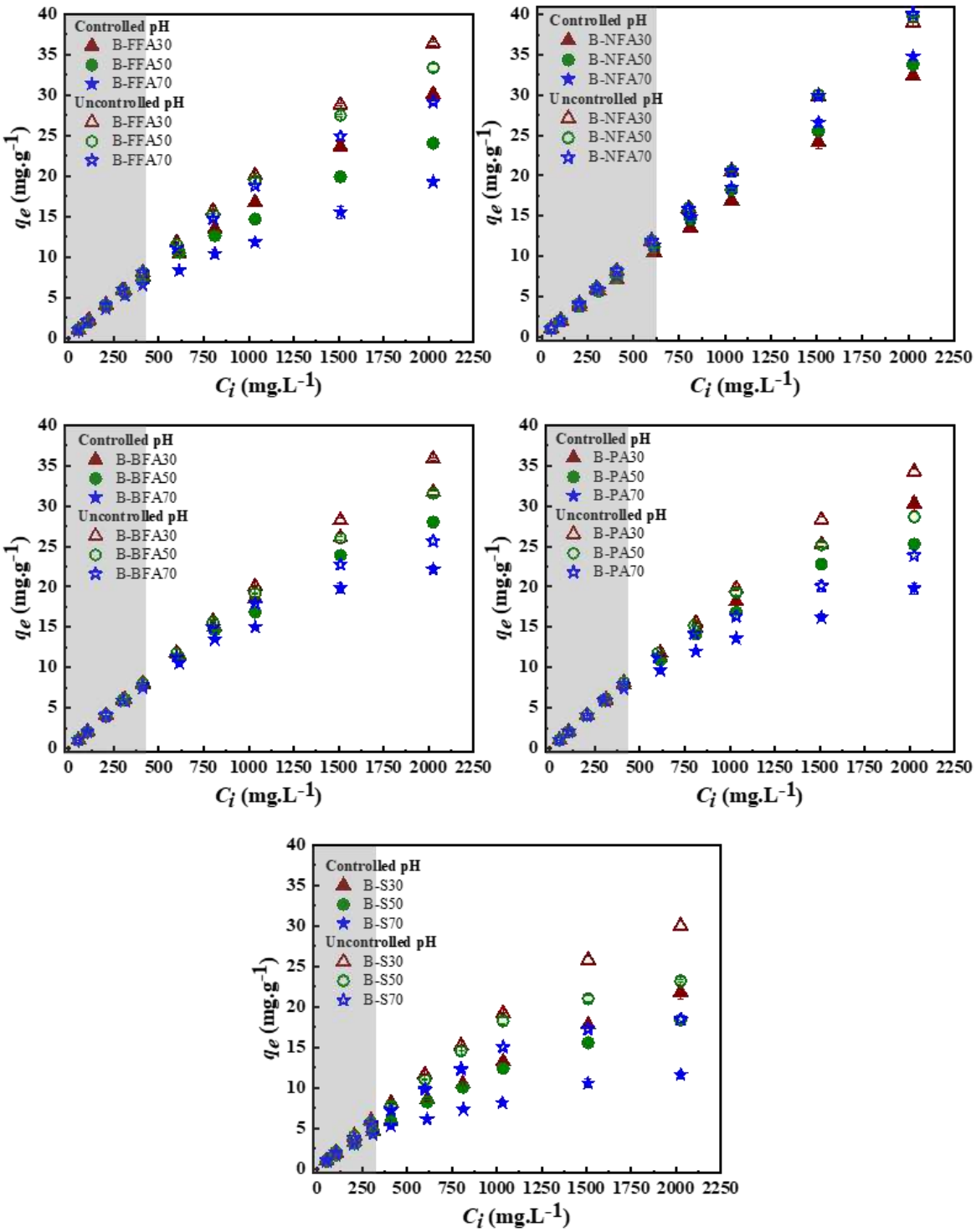


Figure 7.14: Retention capacity vs initial $Pb^{2+}$ adsorbate concentration of B-FAs and B-S mixes under controlled pH and uncontrolled pH conditions

On the other hand, for B-FA mixes there is possibly more sites that still facilitate for more adsorption or even precipitation at uncontrolled condition (as observed in previous section for the parent materials). Thus, the usage of B-FA mixes can be deemed to be more efficient for metal retention at higher $Pb^{2+}$ concentrations as expected for landfill

leachates (Wadanambi et al., 2008). Regardless of the amendment rate and type of FA, the uncontrolled condition exhibited higher qe at greater $C_i$ (the non-highlighted section) as compared to their counterparts at controlled condition. Thus, we can conclude that at higher pH, both parent materials and the B-FA mixes would ideally exhibit higher $q_e$. With respect to B-S mixes, the qe of B-FA mixes were observed to be higher at greater $C_i$ (the non-highlighted section) regardless of the amendment rate. For instance, at $C_i$ at 2000 $mg.L^{-1}$ and amendment rate of 50 % to bentonite, the B-FA mixes exhibited higher qe than B-S mixes by at least 24 %. This implied that usage of B-FA mixes is much ideal than that of B-S mixes considering criteria of retention (this study), hydraulic conductivity (Younus and Sreedeep, 2012a)) and compressive strength (Younus and Sreedeep, 2012a)).

Fig. 7.15 presents the percentage removal capacity of $Pb^{2+}$ (PR) of the bentonite-fly ash (B-FA) and bentonite-sand (B-S) mixes with different contaminant concentration ($C_i$). PR of $Pb^{2+}$ decrease with increase in adsorbate concentration for all mixes in controlled conditions and majority of mixes in uncontrolled condition. This can be attributed to abundant adsorption sites of the mixes for $Pb^{2+}$ to be adsorbed at lower $C_i$. As the $C_i$ increases, the site for adsorption diminishes and this is evident for mixes having high amendment rates (50 % and 70 %). The only exception to these results were observed for B-NFA70 mix at uncontrolled conditions, wherein 100 % removal of $Pb^{2+}$ was observed for all range of $C_i$. This is expected as pure NFA is more effective in adsorbing $Pb^{2+}$ ions as compared to other parent amendment materials. This higher adsorption capacity of NFA can further be validated by EDX spectra (refer Fig.7.11). Thus, it is evident that B-NFA70 mix would have metal removal capacity even beyond the $C_i$ of 2000 $mg.L^{-1}$.

The change in equilibrium solution pH of the bentonite-fly ash (B-FA) and bentonite-sand (B-S) mixes with different contaminant concentration ($C_i$) is shown in Fig. 7.16. Regardless of the mixes and percentage admixtures (30, 50 or 70), the equilibrium solution pH of the uncontrolled condition reduced with an increase in $C_i$. This indicates that apart from adsorption there is a gradual precipitation occurring up to a certain $C_i$, after which the pH gets stabilized near around 5.5 for certain mixes. The equilibrium solution pH for the controlled condition was shown in the thin shaded region near pH of 5 ± 0.2. pH for the Apart from B-NFA mixes, all mixes exhibit this trend of tapering down of equilibrium solution pH up to a certain $C_i$ and remain constant thereafter. Among the class F based B-FA mixes, equilibrium solution pH of B-FFA was observed to be highest, regardless of

percentage admixture. Class C based B-FA mixes showed a distinct trend from the other mixes. The reduction of equilibrium solution pH was relatively less as compared to other mixes.

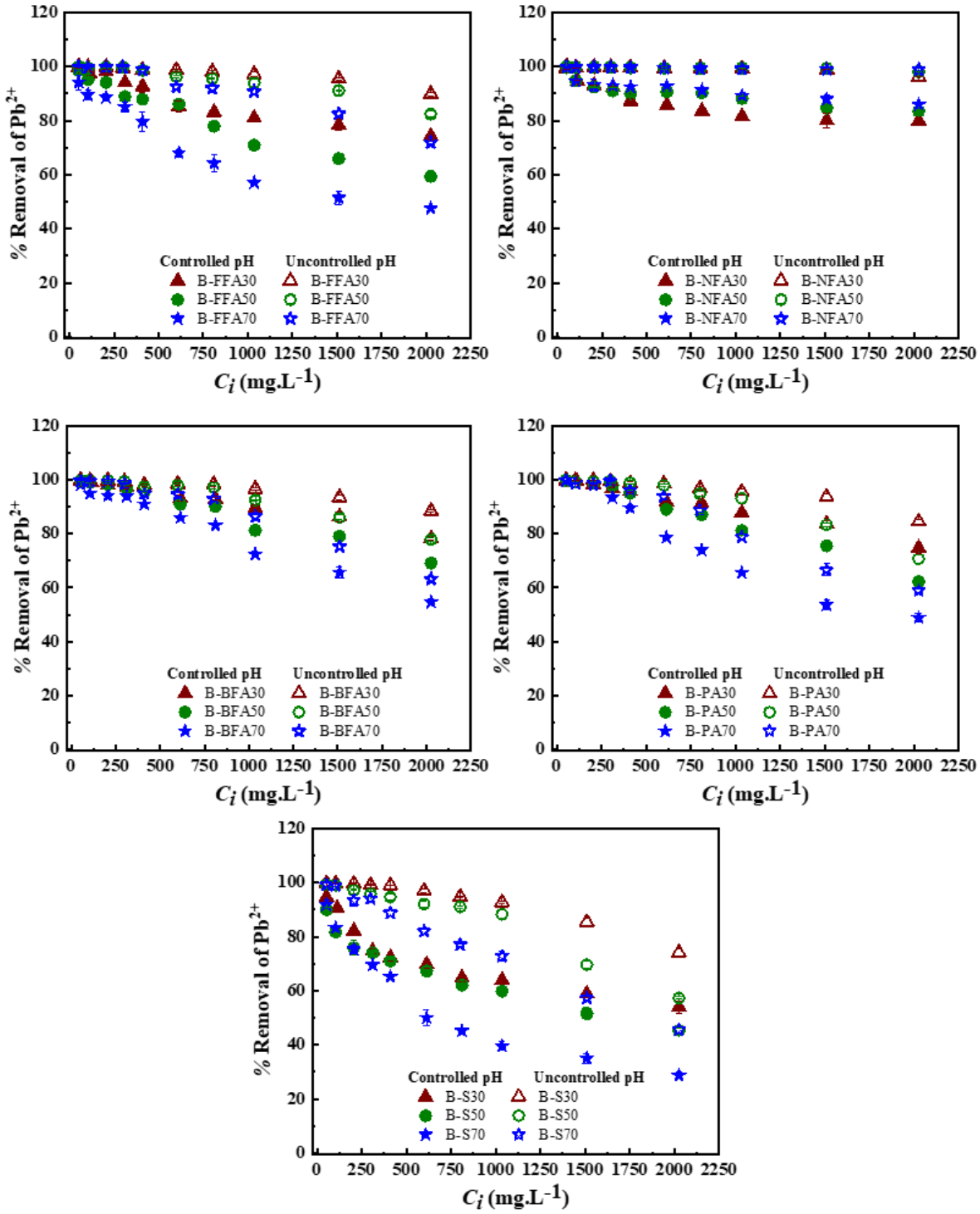


Figure 7.15: Percentage removal of $Pb^{2+}$ vs initial $Pb^{2+}$ adsorbate concentration for B-FAs and B-S mixes under controlled pH and uncontrolled pH conditions

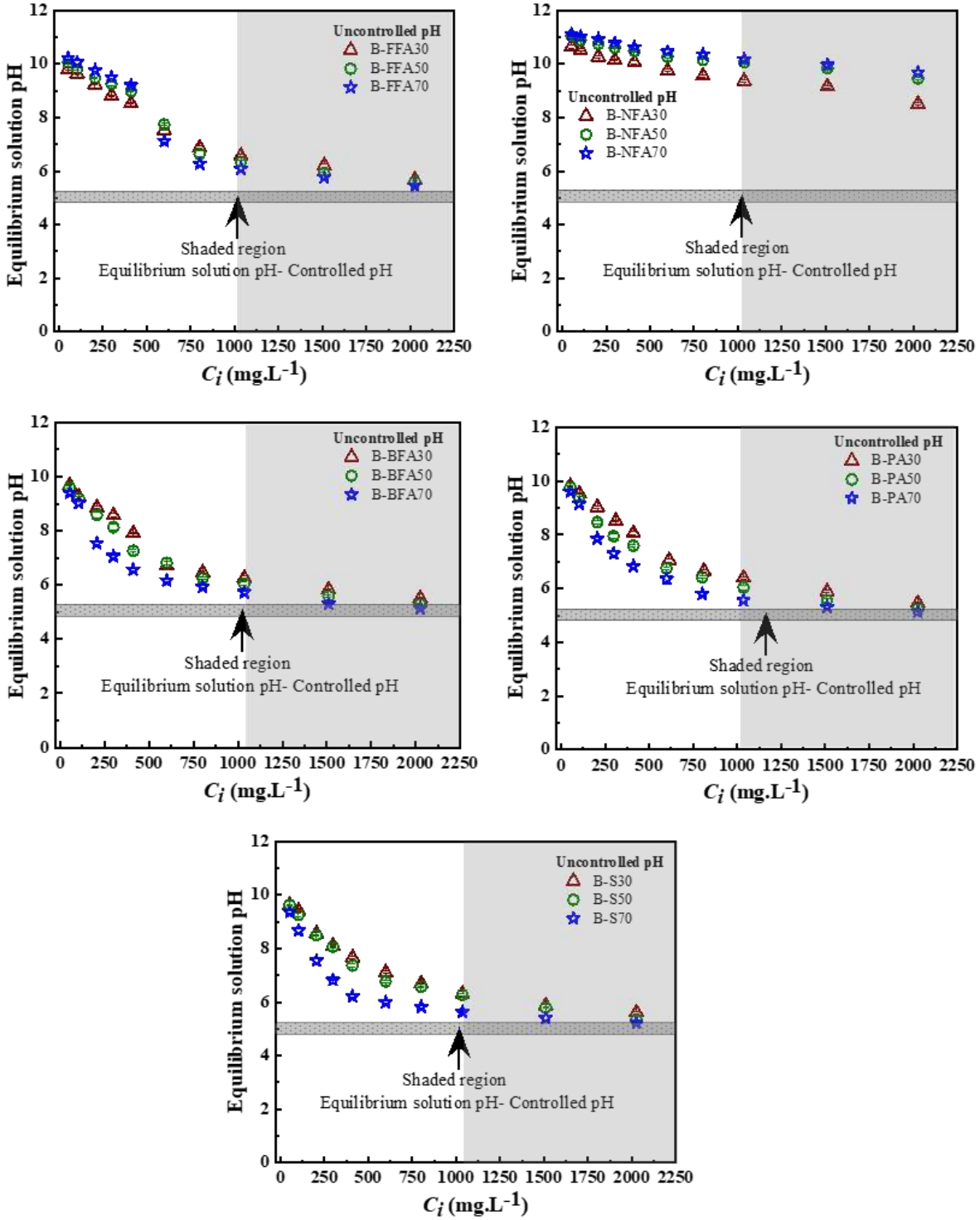


Figure 7.16: Equilibrium solution pH vs initial $Pb^{2+}$ adsorbate concentration for B-FA and B-S mixes under controlled and uncontrolled pH conditions

In fact, even at $Pb^{2+}$ concentration of 2000 mg.L$^{-1}$, B-NFA mixes retained equilibrium solution pH of 9 to 10, indicating that the adsorbent still has potential to retain at higher concentration of $Pb^{2+}$ through precipitation mechanism. Thus, for realistic conditions in landfill leachate, the B-FA mixes from Class F fly ash would be ideal choice for contaminant

retention. For $Pb^{2+}$ concentration of less than 1000 mg.$L^{-1}$, B-S and B-FA mixes (constituting BFA and PA) do not exhibit visible difference in equilibrium solution pH. However, at higher $Pb^{2+}$ concentration beyond 1000 mg.$L^{-1}$ (refer shaded section), it is clear that they will not be effective as an adsorbent media. Thus, for battery disposal units and industries wherein $Pb^{2+}$ would be a major constituent of effluent, B-FA mixes can be ideal if only the parent fly ash has pH higher than 10.5 (refer FFA and NFA based mixes).

Fig. 7.17 presents the retention isotherms of all the parent materials and mixes in terms of $q_e$ with the $C_e$. The $C_e$ of the uncontrolled condition was seen to be lower than that of the controlled condition for all studied samples. This would indicate that more $Pb^{2+}$ was retained at a higher pH, primarily due to additional precipitation, apart from the adsorption (discussed in previous sections). In case of Class F fly ash, the $C_e$ obtained can be directly correlated with the material pH, i.e., higher the pH lower is the $C_e$. In case of Class F based B-FA mixes, higher the bentonite amendment rate, lower was the $C_e$. This is expected as the $q_e$ of bentonite was relatively higher than that of other Class F FA. On the contrary for Class C FA based B-FA mixes, higher the B amendment rate, lower was the $C_e$. This can be explained by the higher adsorption capacity of NFA in comparison to bentonite at the liquid to solid ratio of 20. Based on results presented in section 6.1 , the $q_e$ of B is lower approximately by 66 % than that of NFA at the liquid to solid ratio of 20. The results encourage the use of Class C FA as a replacement material for sand in hydraulic barrier construction for landfill liner as it satisfies the criterion of USEPA for hydraulic conductivity (EPA/ 530-SW-86-007-F, 1987; USEPA, 1989) as well as being efficient at retarding contaminant leachate (this study).

### 7.2.6 Effect of pH condition on retention properties and Langmuir model parameters of mixes

The retention characteristics of all mixes based on controlled and uncontrolled condition were compared with an adsorbate concentration of $Pb^{2+}$ ranging from 600 mg.$L^{-1}$ to 2000 mg.$L^{-1}$. This range is selected as it is the typical $Pb^{2+}$ concentration observed in landfill leachate (Palma-Fleming et al., 2000) and those expected for battery industrial disposal facility (Arbabi et al., 2015; Kinuthia et al., 2020). Fig. 7.18a compares the variability of $q_e$ determination and it was observed that considerable deviation occurred among the values with respect to 1:1 line. A linear fit was developed based on least square regression

approach with $R^2$ value of 0.97. This simple equation can provide estimates of $q_e$ in uncontrolled condition based on the data of $q_e$ in controlled condition for the selected range of $C_i$. This indicates that there is almost 20 % increase in $q_e$ in uncontrolled condition as compared to the controlled condition for the selected range of $C_i$. However, caution should be practiced in using this empirical equation for other clay composites as well as at lower adsorbate concentration. Moreover, at lower initial $Pb^{2+}$ concentration ranging up to 400 $mg.L^{-1}$, the variation between the two pH conditions were less than 5 %. Similar observations can also be drawn for percentage removal for both pH conditions (Fig. 7.18b). The two equations provided in this section, can help designers to evaluate any change in contaminant transport for existing geo-environmental infrastructures (liners or even fly ash dumps) wherein fly ash and clay is employed (Nguyen et al., 2019; Xu et al., 2008).

The best-fit parameters based on Langmuir and Freundlich isotherm for the mixes considering both pH conditions are plotted in Fig. 7.19. These parameters are obtained from the fitting of experimental data provided in Fig. 7.17 and summarized in Table 7.2. All the values of Freundlichs exponent n were less than unity, indicating concave (favorable) and nonlinear adsorption. Almost all the data points were below the 1:1 line towards the controlled pH condition axis. This indicates that n values under uncontrolled conditions were lower implying that the reactions would readily occur as compared to those under controlled conditions. $K_F$ parameter is indicative of the energy of adsorption on a homogeneous surface and is independent of surface coverage. This portioning coefficient from Freundlich isotherm was higher in case of uncontrolled pH condition than that of controlled condition. The $K_L$ value which indicates the energy of adsorption was found to be higher at uncontrolled conditions as compared to the controlled conditions. The $K_L$ value indicates the extent of interaction between $Pb^{2+}$ ions and the surface of the B-FA and B-S mixes. A larger value of $K_L$ indicates that there is a strong interaction between adsorbate ($Pb^{2+}$ ions) and adsorbent (mixes) while smaller value implies a weak interaction. Based on this, it can be inferred that B-S mixes have weaker interaction as compared to B-FA mixes. $Q_m$ is the maximum amount of $Pb^{2+}$ per unit mass of adsorbent to form a complete monolayer on the surface of the adsorbent. This was observed to be of similar magnitude for all the mixes regardless of pH condition.

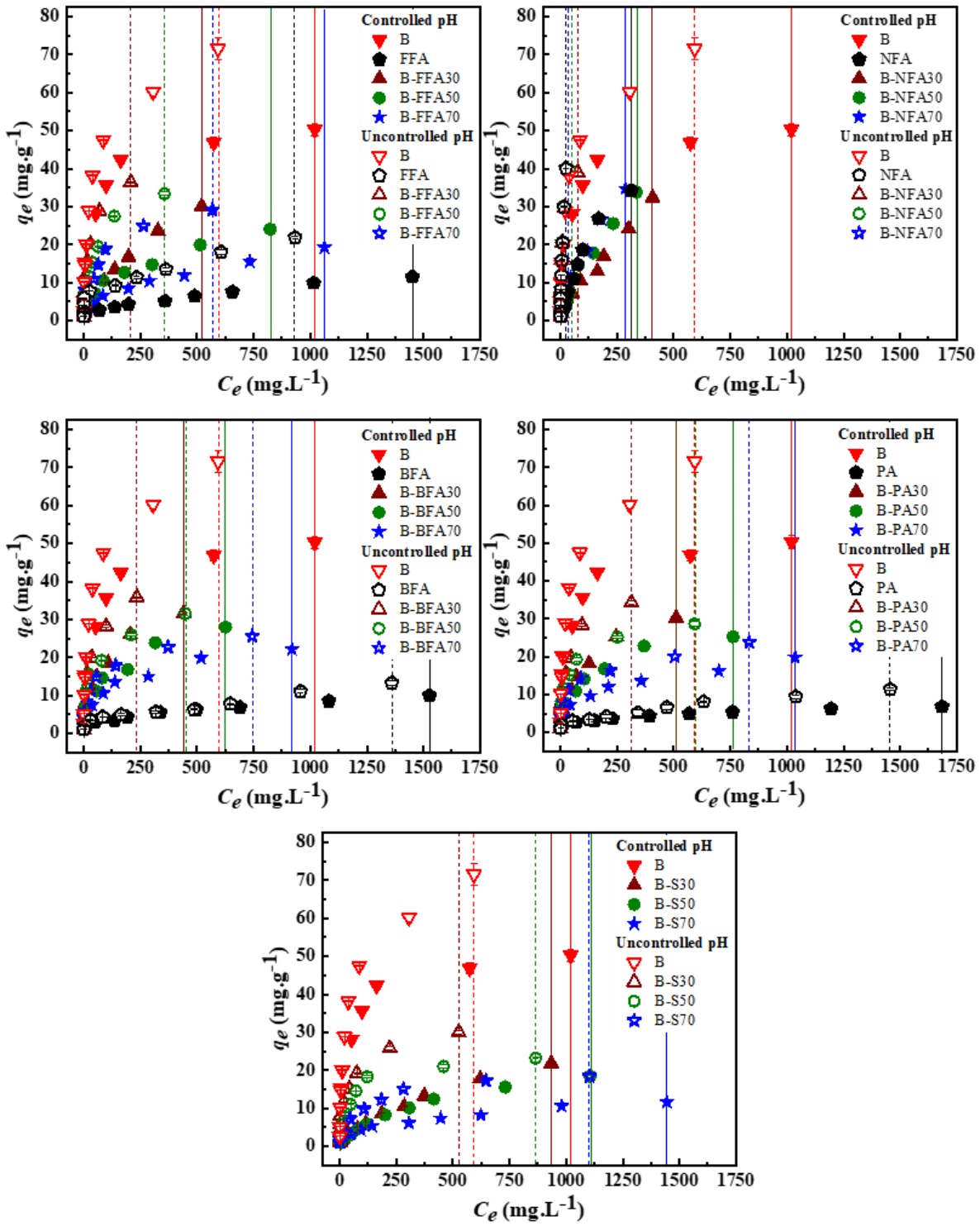


Figure 7.17: Retention isotherm of B-FAs and B-S mixes under controlled pH and uncontrolled pH conditions

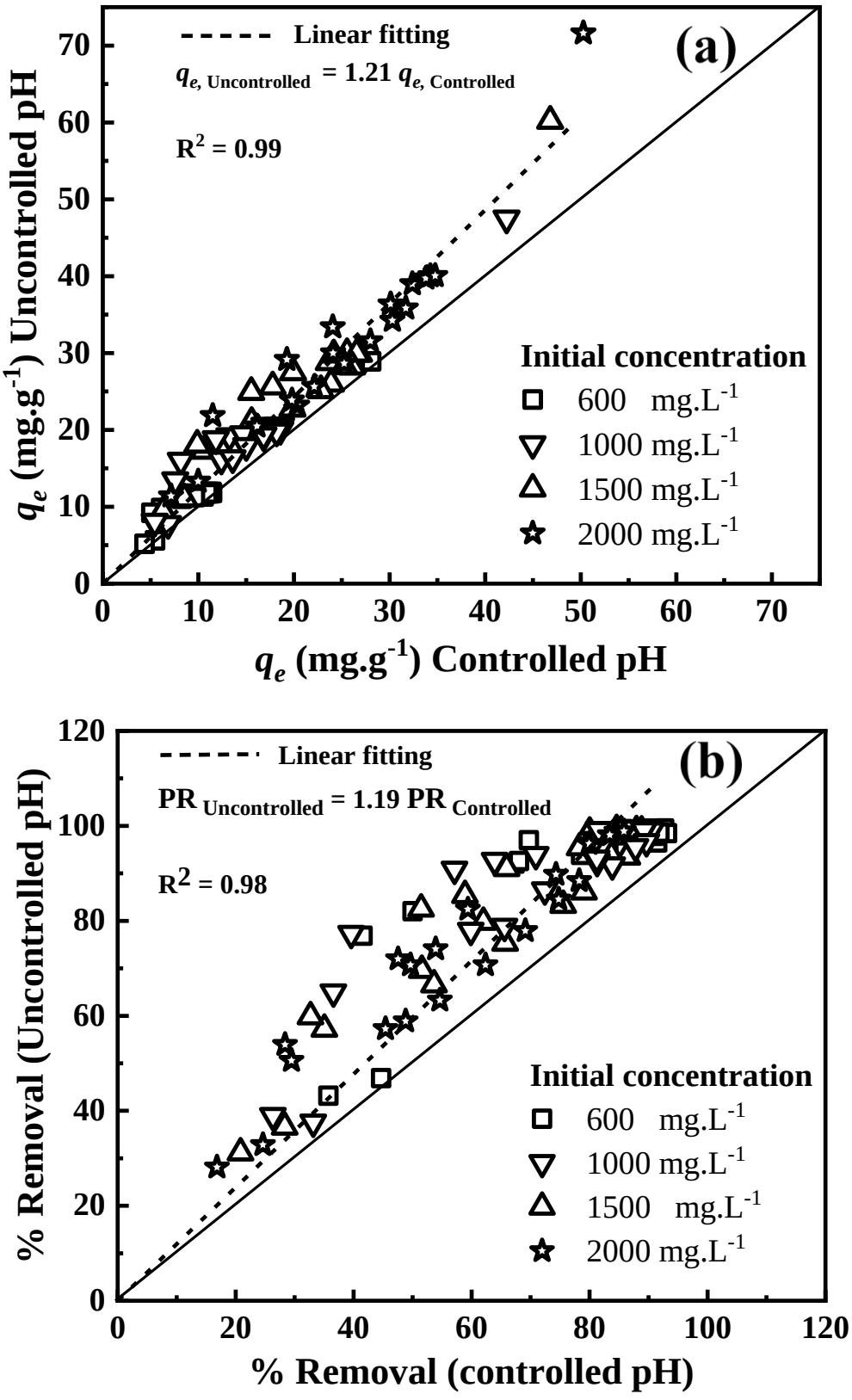


Figure 7.18: Comparison of retention characteristics of B, FAs, B-FAs and B-S mixes between controlled and uncontrolled pH conditions (a) retention capacity and (b) percentage removal

Table 7.2: Freundlich and Langmuir isotherm model fitted parameters for B, FAs, S, B-FAs mixes and B-S mixes under controlled and uncontrolled pH conditions

| Materials | Freundlich isotherm | | | | | | Langmuir isotherm | | | | | |
|---|---|---|---|---|---|---|---|---|---|---|---|---|
| | Controlled pH | | | Uncontrolled pH | | | Controlled pH | | | Uncontrolled pH | | |
| | $K_f$ | n | $R^2$ | $K_f$ | n | $R^2$ | qm | $K_L$ | $R^2$ | $q_m$ | $K_L$ | $R^2$ |
| B | 10.95 | 0.23 | 0.95 | 11.50 | 0.29 | 0.98 | 44.95 | 0.084 | 0.94 | 69.41 | 0.034 | 0.96 |
| FFA | 0.33 | 0.49 | 0.98 | 2.99 | 0.27 | 0.93 | 15.62 | 0.002 | 0.93 | 25.99 | 0.004 | 0.78 |
| B-FFA30 | 1.09 | 0.53 | 0.99 | 5.53 | 0.36 | 0.98 | 44.82 | 0.004 | 0.95 | 38.78 | 0.046 | 0.97 |
| B-FFA50 | 1.33 | 0.43 | 0.99 | 4.47 | 0.35 | 0.98 | 26.11 | 0.007 | 0.96 | 36.78 | 0.022 | 0.94 |
| B-FFA70 | 0.80 | 0.45 | 0.99 | 4.47 | 0.30 | 0.98 | 21.46 | 0.004 | 0.94 | 31.86 | 0.015 | 0.90 |
| NFA | 0.75 | 0.68 | 0.98 | 4.90 | 0.66 | 0.99 | 64.82 | 0.004 | 1.00 | 78.97 | 0.041 | 0.98 |
| B-NFA30 | 0.43 | 0.71 | 0.99 | 11.10 | 0.31 | 0.94 | 75.94 | 0.002 | 0.98 | 43.86 | 0.057 | 0.99 |
| B-NFA50 | 0.74 | 0.66 | 0.99 | 8.14 | 0.45 | 0.98 | 57.24 | 0.004 | 0.99 | 49.16 | 0.120 | 0.94 |
| B-NFA70 | 0.81 | 0.67 | 0.99 | 5.88 | 0.59 | 0.99 | 61.41 | 0.004 | 0.99 | 63.53 | 0.061 | 0.98 |
| BFA | 0.66 | 0.37 | 0.98 | 0.63 | 0.41 | 0.95 | 10.83 | 0.003 | 0.90 | 15.36 | 0.003 | 0.85 |
| B-BFA30 | 2.71 | 0.41 | 0.99 | 5.42 | 0.35 | 0.99 | 35.92 | 0.013 | 0.97 | 36.08 | 0.050 | 0.97 |
| B-BFA50 | 2.62 | 0.37 | 0.99 | 4.95 | 0.31 | 0.98 | 28.95 | 0.013 | 0.94 | 30.02 | 0.042 | 0.94 |
| B-BFA70 | 1.99 | 0.36 | 0.98 | 6.65 | 0.21 | 0.89 | 22.48 | 0.003 | 0.97 | 25.49 | 0.025 | 0.95 |
| PA | 0.96 | 0.26 | 0.96 | 0.44 | 0.44 | 0.96 | 7.06 | 0.005 | 0.80 | 14.48 | 0.002 | 0.91 |
| B-PA30 | 2.58 | 0.40 | 0.99 | 5.57 | 0.33 | 0.98 | 34.32 | 0.011 | 0.97 | 35.14 | 0.041 | 0.93 |
| B-PA50 | 2.62 | 0.33 | 0.99 | 4.95 | 0.27 | 0.98 | 26.56 | 0.013 | 0.93 | 26.33 | 0.062 | 0.93 |
| B-PA70 | 1.99 | 0.31 | 0.99 | 6.65 | 0.27 | 0.98 | 18.43 | 0.012 | 0.90 | 21.55 | 0.031 | 0.90 |
| S | NA | NA | NA | NA | NA | NA | NA | NA | NA | NA | NA | NA |
| B-S30 | 0.37 | 0.60 | 0.99 | 4.95 | 0.30 | 0.99 | 34.81 | 0.002 | 0.99 | 29.27 | 0.036 | 0.93 |
| B-S50 | 0.49 | 0.52 | 0.99 | 3.47 | 0.29 | 0.93 | 24.26 | 0.003 | 0.99 | 23.81 | 0.023 | 0.99 |
| B-S70 | 0.67 | 0.39 | 0.99 | 2.35 | 0.31 | 0.97 | 12.27 | 0.005 | 0.94 | 18.93 | 0.013 | 0.96 |

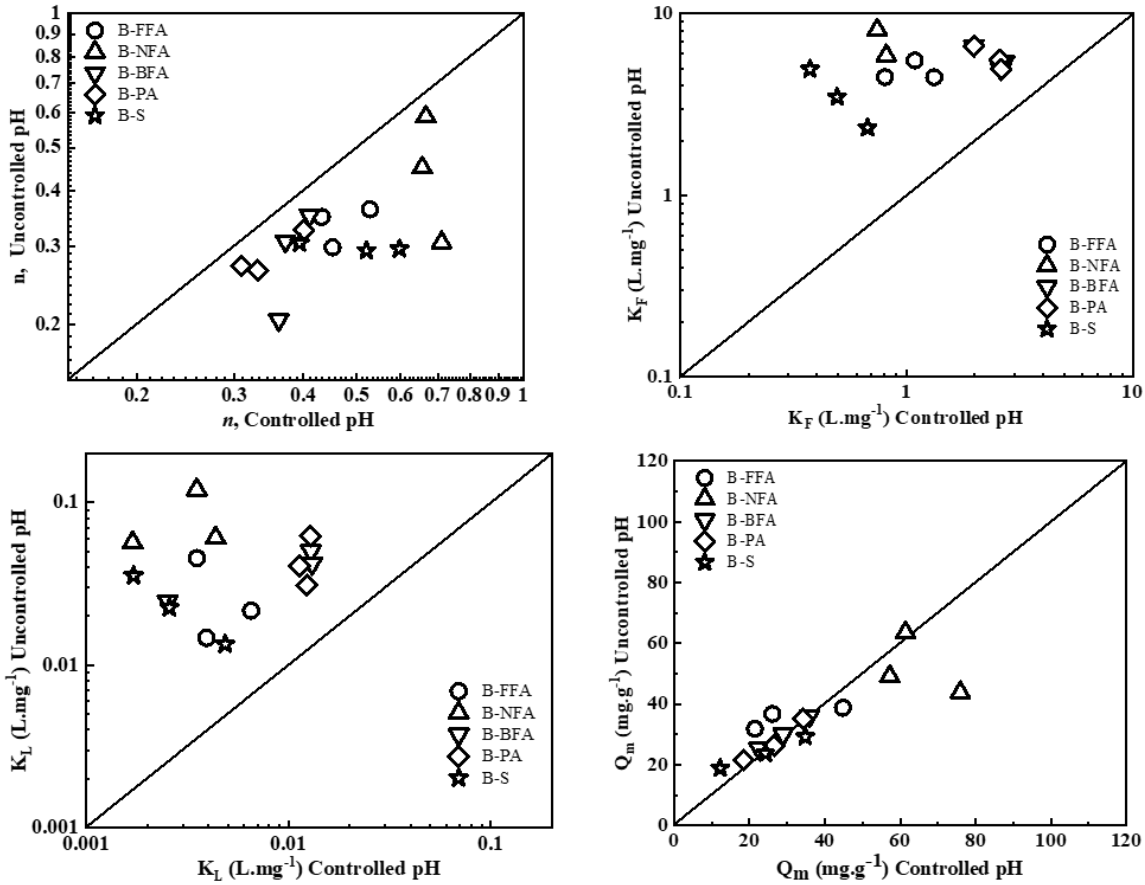


Figure 7.19: Comparison of Freundlich and Langmuir model fitting parameters under controlled pH and uncontrolled pH conditions

## 7.3 Variation in contaminant retention capacity of geomaterials associated with long term interaction of geomaterials

Similar to hydraulic conductivity, efforts were made to study the variation in contaminant retention capacity associated with long term interaction of geomaterials. The study was conducted under controlled pH. Figs. 7.20 and 7.21 depicts the adsorption capacity and percentage removal, respectively for different mixes corresponding to 1000 mg.L$^{-1}$ of $Pb^{2+}$. It can be noted that there is not much significant variation of contaminant retention characteristics with interaction time upto 48 months.

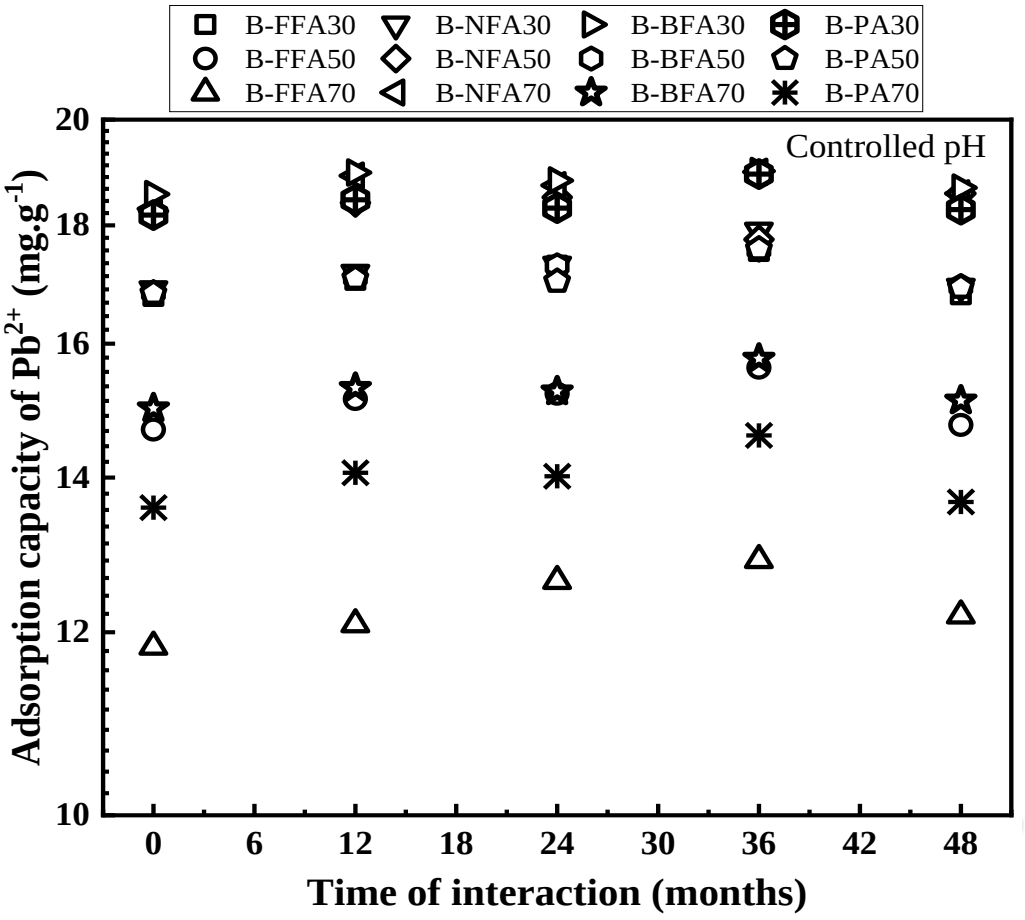


Figure 7.20: Effect of interaction of time on adsorption capacity of $Pb^{2+}$ of mixes under controlled pH

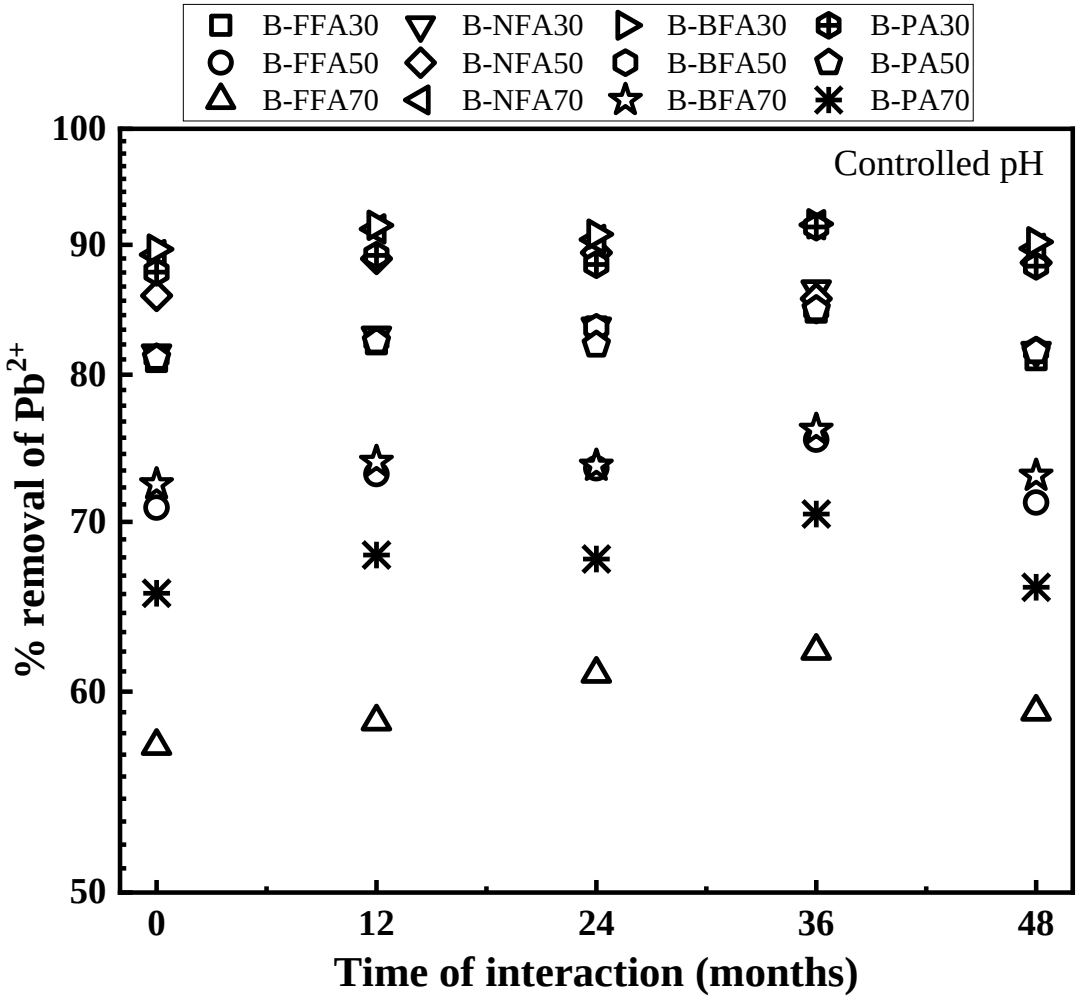


Figure 7.21: Effect of interaction of time on percentage removal of $Pb^{2+}$ of mixes under controlled pH

## 7.4 Summary

The feasibility of Indian bentonite-fly ash (B-FA) mixes in comparison with conventionally used bentonite-sand (B-S) mix was demonstrated for landfill liner applications by studying the adsorption kinetics and capacity. Results showed that both B-FA and B-S mixes reached equilibrium adsorption capacity within 65 min. In terms of magnitude, B-NFA mixes showed the highest. $Pb^{2+}$ adsorption capacity among the tested mixes, which can be attributed to the high CEC and pH of parent fly ash. The obtained maximum adsorption capacity ($q_m$) from the isotherm was correlated to Atterberg limits (Liquid limit and Plasticity index) by two empirical relationships. The study further advocates the usage of waste fly ash with bentonite as an effective adsorption medium for large scale application in landfill liners. This limits the usage of expensive and ecologically sensitive sand in liner materials

while maintaining the integrity of landfill liner adsorption requirements.

The potential use of four fly ash, i.e., two Class F fly ash (FFA and BFA), one Class C fly ash (NFA) and another Class F conforming pond ash (PA), as landfill liner amendment material in bentonite-fly ash (B-FA) mixes was investigated for its metal retention characteristics. $Pb^{2+}$ was selected as the model contaminant and batch equilibrium retention tests were conducted on the B-FA mixes having percentage amendment ratio (by weight) of 30, 50 and 70. The sorbents also included parent materials, i.e., bentonite and the four-fly ash (FFA, BFA, NFA and PA); and also conventionally used bentonite-sand mixes having percentage amendment ratio (by weight) of 30, 50 and 70. The batch equilibrium tests were conducted in two distinct conditions; viz. 1) The pH of the solution was maintained at 5 throughout as per conventional testing approach for landfill leachate; 2) The pH of the solution was not controlled throughout the study and the initial pH corresponded to that of 5. The batch tests included retention kinetics, retention capacity and isotherms of the adsorbent material tested. At uncontrolled pH conditions, retention capacity of all parent materials and mixes and their percentage removal ability were higher than controlled pH condition, predominantly due to precipitation of heavy metal as well as adsorption of the adsorbate on to the adsorbent. For $Pb^{2+}$ concentration of less than 1000 $mg.L^{-1}$, B-S and B-FA mixes (constituting BFA and PA), the adsorption capacity would be comparable under uncontrolled pH condition. However, beyond 1000 $mg.L^{-1}$, it is clear that they will not be effective as an adsorbent media under uncontrolled pH condition. Beyond 1000 $mg.L^{-1}$, B-FA mixes (FFA and NFA based mixes) will be ideal adsorbent if only the parent fly ash has pH higher than 10.5.

# 8

# Mechanical Performance and Micro-structure of B-FA and B-S Mixes

## General

Low permeability ($10^{-9}$ m/s) and adequate unconfined compressive strength (UCS = 200 kPa) forms the basis of using compacted bentonite (B) clay in landfill liner. However, B induces cracks or swells upon excessive drying and wetting events, respectively. To overcome failure of liner layer, B is amended with cohesionless sand (S), despite S being costly and ecologically unsustainable. In the recent past, fly ash (FA) a by-product from thermal power plants, has been explored as a suitable additive material in landfill liner, in line with the adoption of cleaner usage of waste material in construction. The objective of this study was to investigate the mechanical performance of both B-FA and B-S mixes along with the related changes in microstructure and physio-chemistry. 180 sets of UCS tests were conducted on 4 B-FA mixes (including class C and F) and B-S mixes at different compaction state and additive rate. Unlike B-S mixes, all B-FA mixes showed an increase in UCS with respect to B regardless of compaction state and additive rate. Detailed microstructure and physio-chemical characterization for B-FAs revealed the relative abundance in the formation of calcium alumino silicate hydrate, calcium aluminosilicate hydrate, and ettringite minerals after curing as compared to B-S mixes. In fact, Class C FA exhibited the largest UCS even at high moisture content, which can be attributed to higher formation of minerals

upon curing. All B-FA mixes showed UCS greater than the minimum limit for liner application regardless of the compaction state. All B-S mixes did not adhere to the minimum UCS criterion at higher moisture content. FA additive at 50% showcased the highest increase in strength improvement factor (10 out of 12 cases), while for B-S mixes, this factor decreased with an increase in additive rate. Based on the measured data, two new linear relationships of UCS with pH and electrical conductivity (both indicative of reaction) of the mixes were observed. The relationship with respect to pH was more pronounced at higher moisture content as pH indicates the existence of CaO minerals.)

## 8.1 Background

Hazardous and municipal solid waste disposal necessitates the construction of engineered landfills (Lee et al., 2017; Kumar et al., 2019). A typically engineered landfill consists of three primary layers, i.e., the liner layer system, the waste layer, and the cover layer (Narani et al., 2020). The overlying cover layer and bottom liner layer function to restrict water from reaching the waste layer and leachate reaching the groundwater table, respectively (Pandey and Shukla, 2019; Patra et al., 2020; Sathe et al., 2020). Engineered liner layer consists of compacted fine-grained soil, satisfying the criteria of minimal permeability ($10^{-7}$ cm/s) and adequate strength (unconfined compressive strength, UCS = 200 kPa) as per USEPA (1989). Typically, bentonite (B), a mined clay, was used to construct this liner layer adhering to both the permeability and UCS criterion (Al-Badran et al., 2017). B, due to its rheological properties (fine-grained with high surface area and negative charge) is also an excellent adsorption medium (Mukherjee and Mishra, 2020). However, bentonite liner is susceptible to shrinkage cracks upon drying, barely suffices the compressive strength criteria, and a rather costly material to import wherein it is not mined locally (Sivapullaiah and Baig, 2011). To overcome this, the conventional practice has been to add coarse-grained sand (S) with B to alleviate the detrimental effects of using B alone in the liner layer (Sivapullaiah et al., 2000; Mukherjee and Mishra, 2019). S is exhaustive in nature, costly, and its mining has negative effects on river dredging (de Leeuw et al., 2010; Meng et al., 2018).

In the past decades, the demand for electricity from coal-based thermal power plants in developing countries such as India (70% in comparison to other energy resources) has grown (Singh et al., 2015). Burning of coal in these thermal plants results in mass produc-

tion of cohesionless waste material called fly ash (FA) which is dumped nearby or transported to ash ponds (Asokan et al., 2004). In India, FA is majorly constituted of a varying percentage of minerals such as $SiO_2$ ($21-61\%$), $Al_2O_3$ ($6-36\%$), $Fe_2O_3$($9-40\%$), CaO ($1-11\%$), and MgO ($0-6\%$) (Ahmaruzzaman, 2010). In India, only 60% of FA waste was utilized in cement industry, transportation avenues, and some agricultural usage. Storage deposits adjacent to the plants have already surpassed permissible storage capacity (Yao et al., 2015). FA being pozzolanic in nature (high compressive strength), cohesion-less (resists cracks) and having relatively high cation exchange capacity (CEC) can be a suitable additive material in landfill liner (Palmer et al., 2000; Sivapullaiah and Lakshmikantha, 2004). Judging from the inherent and rheological properties of FA, it is practical to explore the utilization of bentonite-fly ash (B-FA) mixes as a liner material, in line with the concept of cleaner usage of waste material in construction.

B-FA as liner material has been explored in the past decade for its hydraulic conductivity, adsorption capacity, and mechanical strength (Nhan et al., 1996; Younus and Sreedeep, 2012a). B-FA as liner material also meets the minimum permissible hydraulic conductivity as found in multiple studies (Sivapullaiah and Lakshmikantha, 2004; Younus and Sreedeep, 2012a). FA inclusion in bentonite decreased the Atterberg Limits, optimum moisture content (OMC) while increased the maximum dry density (MDD), which further makes it suitable as a liner material (Sun et al., 2019; Singh et al., 2015). However, these studies do not compare in detail the strength efficacy of B-FA mixes against conventionally used B-S mixes. Also, the compressive strength of contrasting FA (i.e., class C and class F) mixed with B was not comparatively investigated. The effect of pH and electrical conductivity (EC) of B-FA mixes on compressive strength has also not been investigated in the literature. This is relevant as these easily measurable electrochemical properties are directly dependent on the unique mineralogical content of the B-FA mixes. For instance, pH is a direct indication of the CaO content of a FA (Antoni et al., 2016) and can even vary within its individual class. Furthermore, a detailed study on its microstructure and the consequent effect of strength characteristics of B-FA mixes is lacking in literature.

The objective of this study is to investigate and compare the mechanical performance of compacted B-FA mixes with that of conventional B-S mixes for landfill liner application. UCS tests on B-FA mix considering 4 FAs (includes both class C and F) from India were done at three different compaction state and additive rate. The UCS was compared with B-S mix

and 4 parent material at the three different compaction state and additive rate. In total, 180 UCS tests including replicates were conducted, and their microstructure was monitored before and after the curing period. Electrochemical properties such as pH and EC of the parent materials and its mixes before sample preparation were measured to explore any correlation with UCS. Detailed spectroscopic tests were further conducted to interpret the effect of individual FA on the consequent UCS of the material.

## 8.2 Sample preparation and test setup

### 8.2.1 Unconfined compression test

UCS tests were conducted on both parent materials (except cohesionless sand), B-FA mixes, and B-S mixes at three different compaction states along the individual compaction curve. These compaction states correspond to three moisture contents (OMC, OMC -5% and OMC +5%) and at MDD. It is worthwhile to mention that 5% moisture variation might have a dramatic impact on the hydration process of lime-based materials as reported in the literature (Castro-Fresno et al., 2011; Mohammadinia et al., 2019). The rationale of choosing 5% moisture variation in this study was to evaluate the effects of variable compaction state expected in the field (Bordoloi et al., 2018). Any associated change due to lime content of any of the composite materials will be reflected in the compressive strength of the material. The influence of variation in fly ash percentage in the mixes (at 30%, 50%, and 70% by dry weight of bentonite) on UCS was also investigated. The percentage additive selected was based on previous literature (Younus and Sreedeep, 2012a). Tests were repeated thrice for each compaction state to check any variability in observed UCS. Moisture in all samples was cross-checked by oven-drying after the sample was tested in UCS setup. In total, 45 tests for parent material and 135 tests for mixes were carried out. The amount of FA or sand to be added were initially weighed and dry mixed uniformly with oven-dried bentonite soil. Following this mixing process, the requisite amount of water (according to test program) was added to the mixture. Thereafter, UCS samples (of size 38 mm × 76 mm) were prepared by static compaction in a specially prepared cast-iron mold, which facilitates uniform compaction along both ends. The compaction effort for each sample was adjusted in such a way that the same impact energy per unit volume was applied to achieve (OMC and MDD) based on obtained results from compaction curve (ref. Table 3.5). After compacting, the samples were extruded with a hydraulic jack, sealed in an airtight plastic bag, and cured

for 14 days in a desiccator maintained at 100% relative humidity and 27řC. These UCS samples were cured to simulate the early curing conditions post-construction, wherein soils are expected to have strength gain for calcium-based additives (Zhang et al., 2018). An automatic loading machine with proving rings having capacities of 2 kN and resolutions of 0.0018 kN, respectively, were used for the UCS tests. All UCS tests were conducted at a constant strain rate of 1.25 mm/min, as suggested by ASTM-D5102 (ASTM, 2009). Failure criterion was decided based on the gradual drop-down of stress or if there is no increment in stress for a strain rate more than 10% of the sample dimension. To investigate any change in surface morphology along the shear failure plane, samples were immediately taken out after UCS tests and captured using FESEM.

### 8.2.2 Consolidated undrained triaxial test

Consolidated Undrained (CU) tests were conducted to determine the shear strength parameters of selected bentonite-fly ash samples using triaxial apparatus as per ASTM D4767 (ASTM, 2000). Soil specimens conforming to aspect ratio 2:1 (height 76 mm and diameter 38 mm) was statically compacted to an initial compaction state of MDD and OMC. Skemptons pore water pressure parameter (B) of 0.92 was achieved to ensure near saturation. Time elapsed to achieve the back pressure saturation of mix was around 2-3 weeks to conduct the triaxial experiment of the selected B-FA mixes. The saturated samples were isotropically consolidated at an effective confining pressure of 75, 150, and 225 kPa by raising the confining pressure. Thereafter, the soil sample was sheared at a strain rate of 0.08%/min. Shearing was terminated at 20% of axial strain. Only B-NFA and B-BFA mixes at 70% additive rate were tested for triaxial to represent the difference in shear strength parameters for the two contrasting classes of fly ash. 70% additive rate was chosen as it requires the least time for saturation while also being representative of the shear strength properties of the two tested fly ash.

## 8.3 Results and discussion

### 8.3.1 Stress-strain response of parent material and mixes

Figure 8.1a illustrates the stress-strain response of the parent material and mixes during the UCS tests at compaction state (OMC, MDD). The compressive stress increases as the samples are strained and typically fail after attaining peak UCS (the maximum compressive

stress during shearing). As seen in the figure, B clay does not fail abruptly, rather maintains peak stress beyond 4% of straining. This can be attributed to the true cohesion induced by Montmorillonite mineral in B clay (Skempton, 1953; Sridharan et al., 1971). The B clay sample fails under gradual bulging, and there is no development of a clear-cut shear plane (Fig. 8.1b).

The stress-strain response of all parent FA was same; wherein there is an abrupt failure after reaching peak stress. The initial increase of strength upon straining is due to resistance provided by the inter-particle frictional force, which is mobilized along a clear-cut shear plane (Fig. 8.1b). Thereafter, upon reaching the peak UCS, the inter-particle frictional forces cease, and FA being cohesionless in nature, there is a dramatic decrease in the compressive stress upon further shearing. Except NFA, all parent FA had lower peak strength than B clay. NFA shows relatively higher peak stress than other FA and bentonite due to the presence of calcium oxide mineral (refer XRD Fig. 3.2), which induces pozzolanic activity upon curing (Antiohos and Tsimas, 2004). Detailed changes in pozzolanic activity for each B-FA type are discussed in later sections. For the B-FA mixes (except B-BFA at 70% additive), peak UCS was observed to be higher than B regardless of the FA additive. This is contrary to B-S mixes wherein the peak UCS was lower than that of pure B regardless of additive rate, and the failure mode was also in bulging (Fig. 8.1b). In the case of B-FA mixes, an increment in percentage additive gradually increases the peak UCS. Except NFA which is Class C fly ash, all the other B-FA mixes show a gradual transition of post-peak ductility with an increase in percentage additive. At 30% FA addition, all samples maintain peak stress beyond (4-6) % of strains. As the additive rate increases to 50%, the samples maintain peak stress beyond 5% of straining up to (10-12) %, after which there is a drop-down of post-peak stress. However, at an additive rate of 70%, all B-FA samples exhibit somewhat a plastic failure wherein there is a rapid drop down of stress post-peak. The gradual change in ductility can be discussed based on how B clay particles and FA particles arrange themselves in a compacted state.

Figure 8.2 presents a pictorial and schematic illustration of surface morphology of compacted B-FFA samples (before UCS tests) at a different additive percentage. The individual flaky and fine particles (less than 2$\mu$m) of B uniformly engulf fly ash at a lower additive rate, thus providing enough sites where true cohesion bonds can be formed. This engulfment appears to gradually decrease when FA percentage increases to 70. As the contact

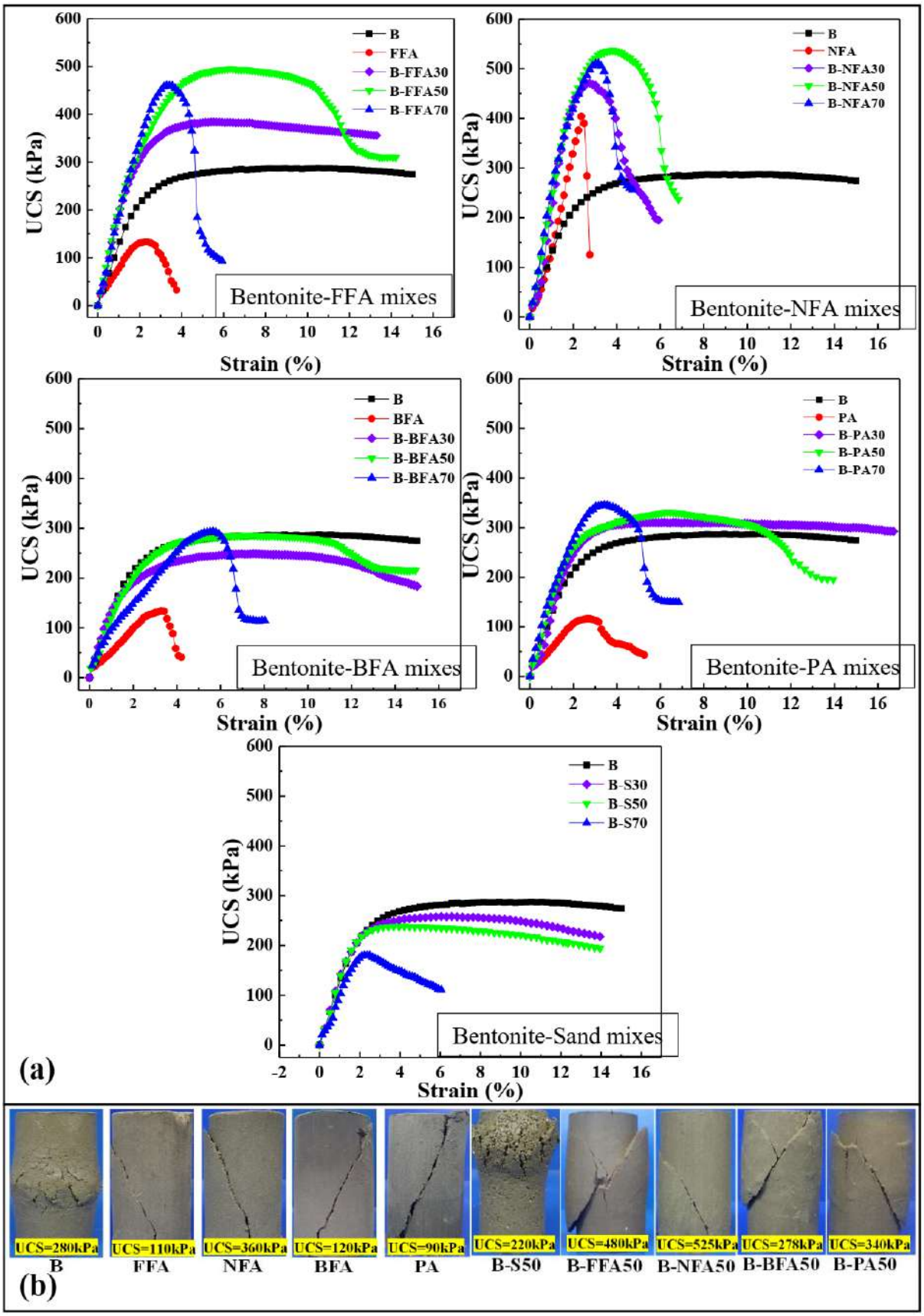


Figure 8.1: Stress-strain curve of parent materials and bentonite mixes

between individual flaky clay particle decreases, the true cohesion component in the compacted samples reduced. B-NFA mixes showcase contrasting trends in terms of post-peak ductility and exhibits higher peak UCS than any other B-FA and B-S mixes, regardless of the additive rate. B-NFA exhibits inherent pozzolanic activity among FA particles and would induce a higher inter-frictional resistance owing to larger particle size (refer Table 3.2).

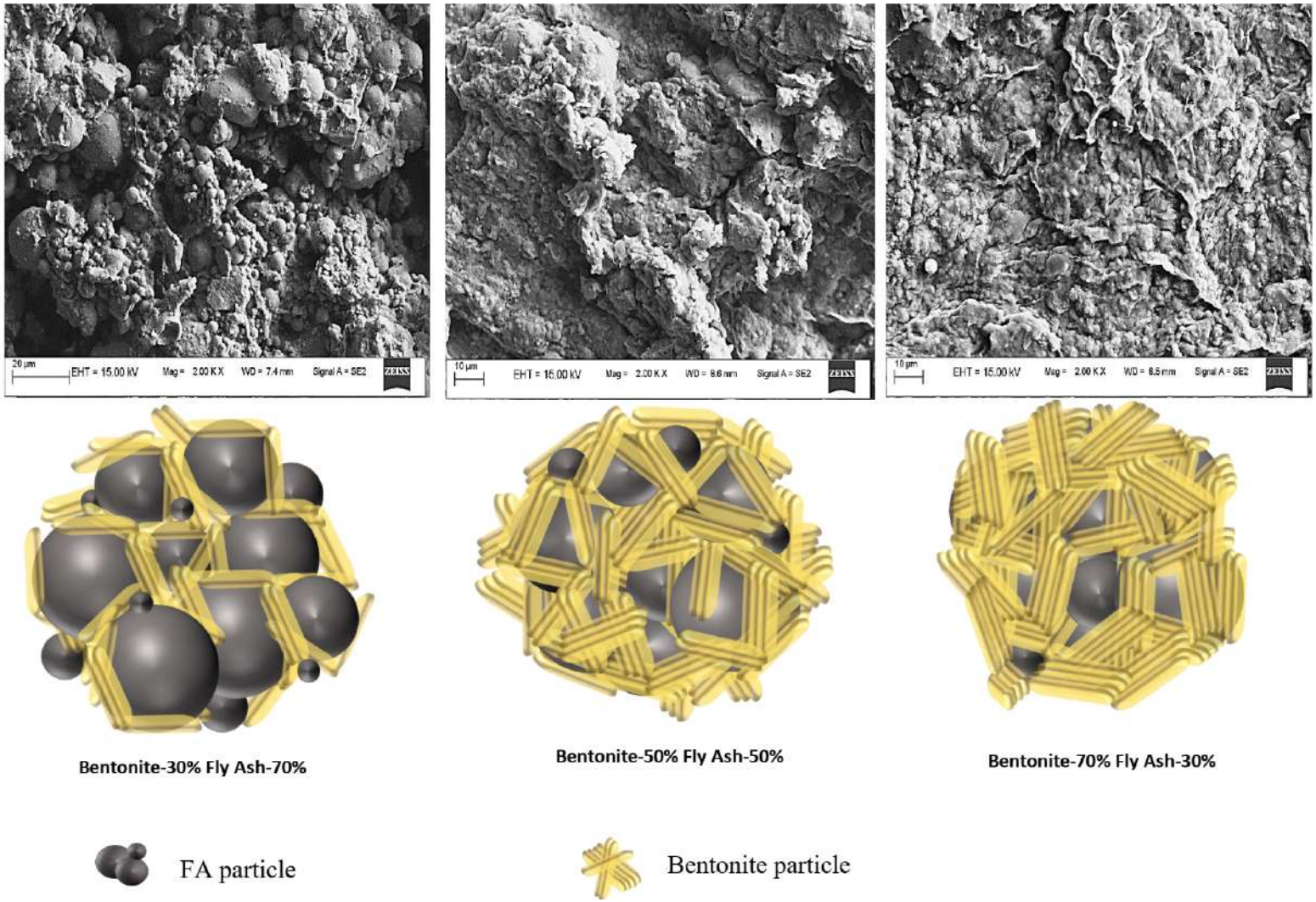


Figure 8.2: Pictorial and schematic illustration of surface morphology at different amendment percentage

The larger particle size of individual NFA particles also inhibits contact between flaky B particles, thus resulting in a rapid decrease of strength upon straining post-peak UCS. It is interesting to note that in all B-FA mixes, a well-defined shear plane was developed regardless of additive rate (Fig. 8.1b).

### 8.3.2 Effect of compaction state and additive rate on UCS

Figure 8.3 illustrates the peak UCS variation for all parent material, B-S mix, and B-FA mixes at three different initial compaction states, as discussed in the earlier section. The red line indicates the minimum peak UCS (i.e., 200 kPa) required to satisfy as landfill liner material (USEPA, 1989). Among the parent materials, only B and NFA meet the strength criteria at all compaction state. As the compaction changes from (OMC-5%) to (OMC+5%), the UCS gradually decreases. This is expected as the apparent cohesion component decreases with an increase in soil moisture content (Bordoloi et al., 2019). The magnitude of decrease in apparent cohesion (due to lower air-water menisci within the soil matrix) influences the UCS of the soil (Bordoloi et al., 2018). For instance, peak UCS of B-S mixtures fail drastically at OMC+5% and is well below the permissible limit. In field scenario, this compaction state (i.e., wet of OMC) will be more pronounced in liner layer when leachate reaches it. On the contrary to B-S mixes, all B-FA mixes showed higher UCS than the permissible limit regardless of the compaction state. In fact, B-NFA showcased the highest UCS among all the B-FA mixes at all compaction states and percentage additive. B-NFA exhibits higher UCS at OMC+5% than at OMC due to the formation of Calcium Aluminosilicate Hydrate (C-A-S-H) and ettringite minerals upon interaction with water (Kanchanason and Plank, 2018). These minerals are formed due to curing of pozzolanic material and have been captured in FE-SEM images of samples post failure in Fig.8.4. These formations were also exhibited by B-FFA mixes, which showed the second-highest strength regardless of compaction state and percentage additive. B-PA mixes only showed C-A-S-H mineralogy and not ettringite mineral on its surface. The same was observed for B-BFA (not reported in current study). Ettringite minerals are needle-shaped formations reported by Shizong et al. (1995), and the same was detected in FESEM imaging analysis. Which are the results of pozzolanic reaction of fly ash with bentonite in B-FA mixes. The presence of ettringite minerals was further detected in the XRD analysis (ref. Fig. 8.7). The ettringite mineral formation was predominantly observed for NFA mixes as the high pH of 11.5 facilitated its formation (Puppala et al., 2005).

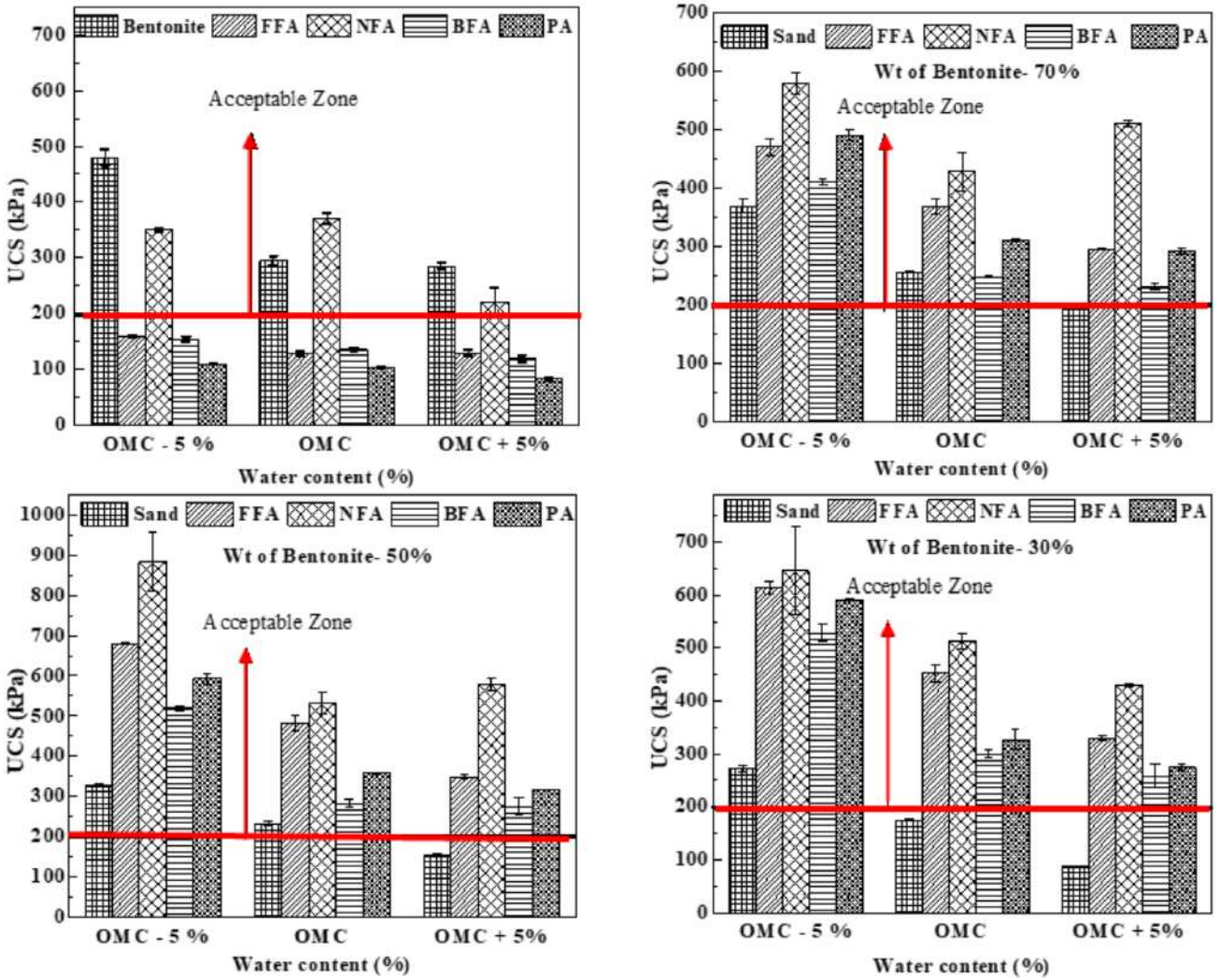


Figure 8.3: Effect of compaction state on UCS of parent materials and mixes

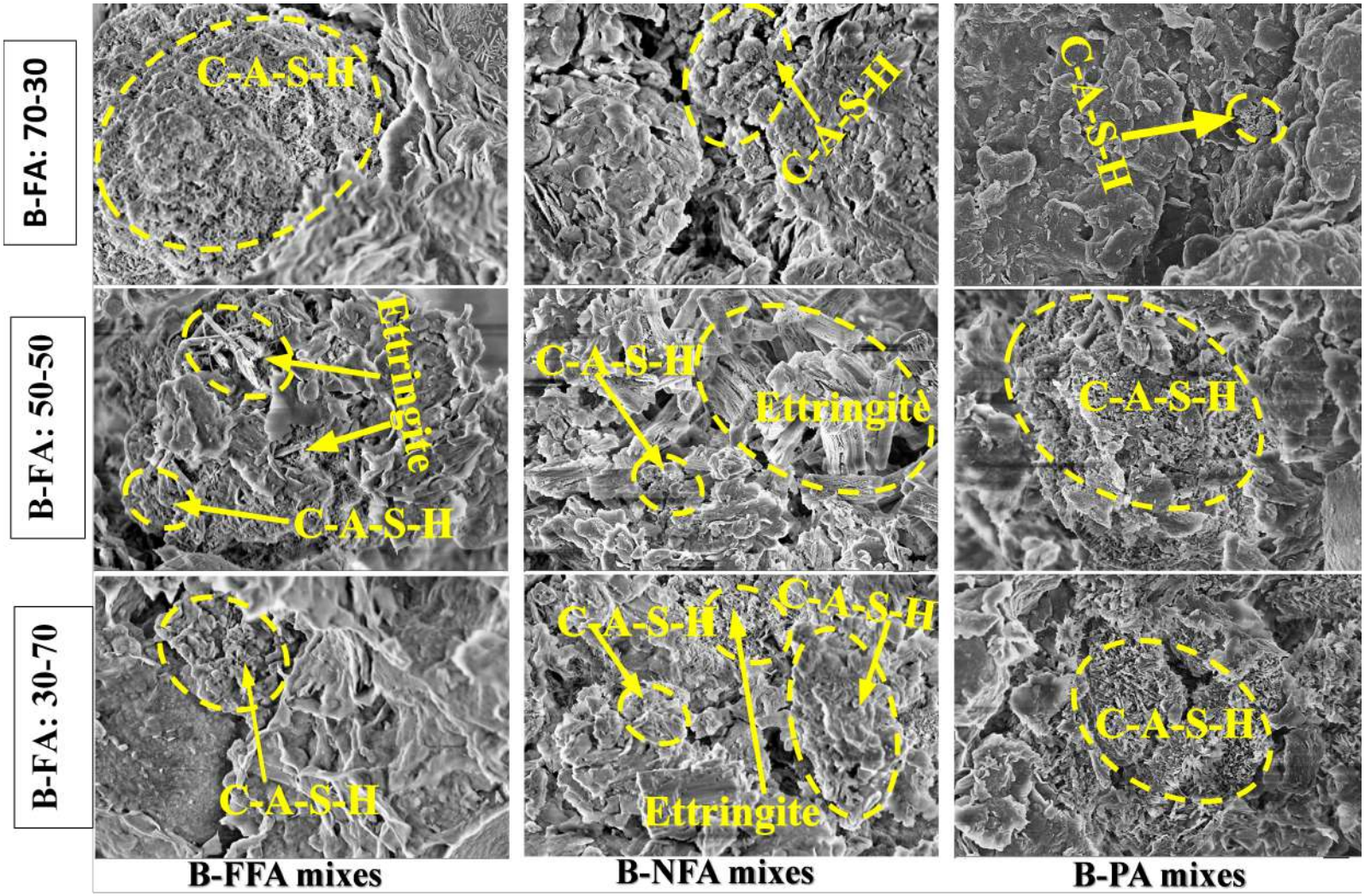


Figure 8.4: FESEM micrograph of B-FAs mixes after 14 days of curing post UCS test showing formation of CSH and Ettringite minerals (All magnification at 20KX)

The CASH mineral formation can be gel-like and porous, which is reported to increase the compressive strength of soils (Dash and Hussain, 2012). The stoichiometry of CASH minerals is discussed in terms of the Ca/(Al+Si) ratio. EDX analysis (Fig. 8.6) of B-NFA mixes was conducted to present the Ca/(Al+Si) ratio as these mixes showcased the highest lime content among all tested bentonite-fly ash mixes. The Ca/(Al+Si) ratio obtained from EDX analysis ranged between 0.20 to 0.53 for the studied composites. This ratio is lower than those CASH minerals formed in pure pozzolanic cement (Pardal et al., 2009).

The improvement in strength and ductility of all mixtures can be ascertained from the strength improvement factor (SIF) and mobilized peak strain factor (MPSF) (Eq.8.1 and Eq.8.2). Any value greater than 1 indicates an improvement in strength and ductility of the material with respect to bentonite.

$$SIF = \frac{Peak\ UCS\ \ for\ B-FA\ mix}{Peak\ UCS\ \ for\ B\ clay} \tag{8.1}$$

$$MPSF = \frac{Strain\ rate\ at\ peak\ UCS\ \ for\ B-FA\ mix}{Strain\ rate\ at\ peak\ UCS\ \ for\ B\ clay} \tag{8.2}$$

Fig. 8.5 presents the SIF and MPSF values of all B-FA mixes at all three compaction states. It was observed that all B-FA mixes except B-BFA could enhance or at least retain (refer yellow section) the strength with respect to bentonite (i.e., SIF 1). Even for B-BFA mixes, SIF varied in the range of 0.8 to 1.6 based on compaction state while adhering to the minimum permissible UCS criterion (refer Fig.8.3). In fact, for B-NFA mixes, even at high moisture content (OMC+5%), the SIF ranged from 1.6 to 2.2, indicating the efficacy of class C fly ash. FA additive at 50% showcased the highest increase in SIF (10 out of 12 cases) while for B-S mixes, SIF decreased with increase in additive rate. The ductility of the material however, decreased for all mixes with respect to bentonite regardless of the percentage additive and compaction state. Both S and NFA based mixes show the lowest MPSF. Quantitatively, the drop in post-peak ductility with respect to pure bentonite was seen to be highest for class C fly ash mixes ranging from 50% to 70%. On the other hand, for class F fly ash, the drop in post-peak ductility ranged between 10% and 45%. The results of the triaxial tests conducted for B-NFA and B-BFA at 70% additive rate are tabulated in Table 8.1, wherein B-NFA exhibited a higher effective cohesion by 120% than that of B-BFA. This can be attributed to relatively higher formation of cementitious gel formation in case of B-NFA mixes that will increase the true cohesion of the sample (Skempton, 1953; Sridharan et al., 1971).

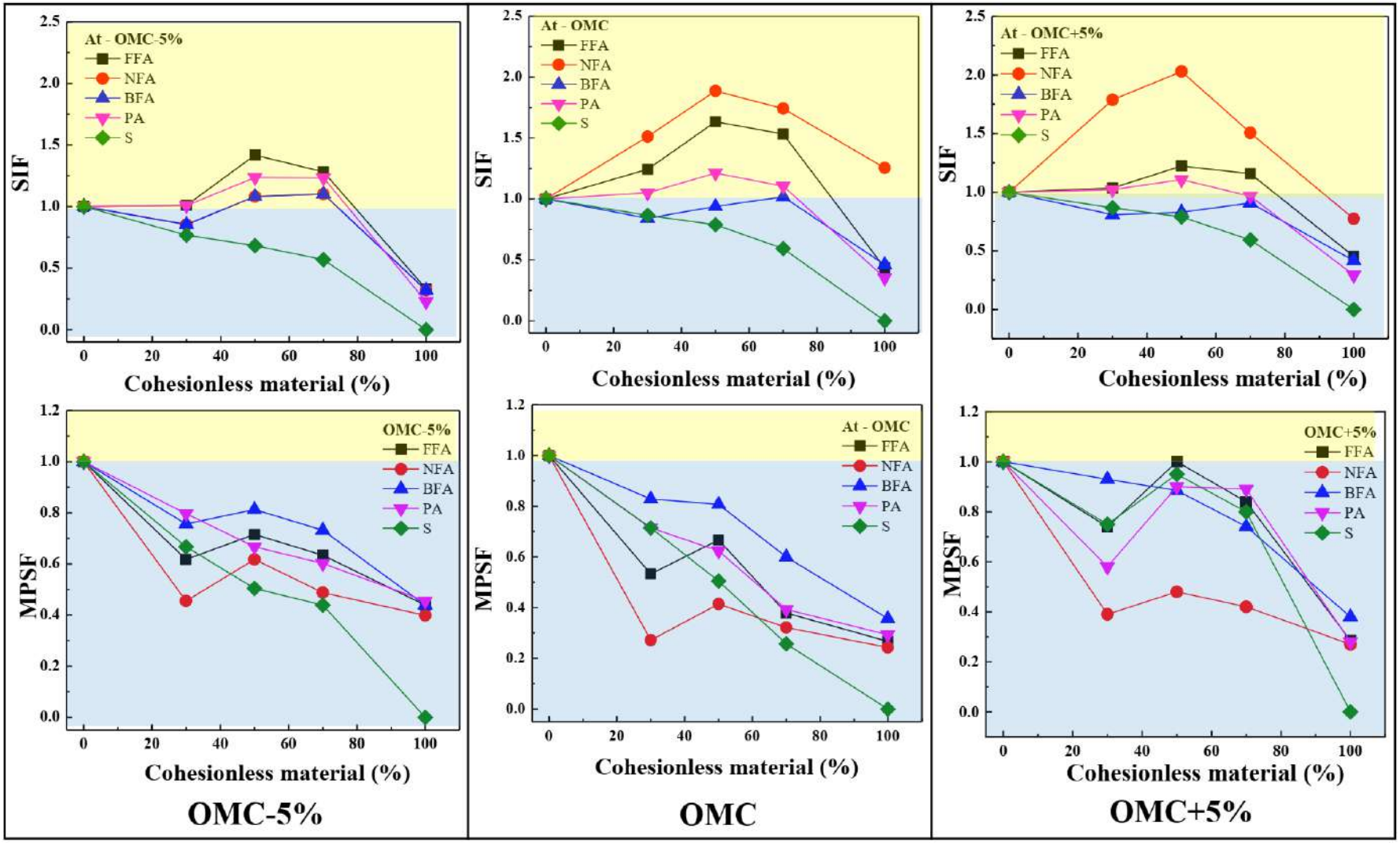


Figure 8.5: SIF and MPSF of the parent material and mixes with respect to bentonite

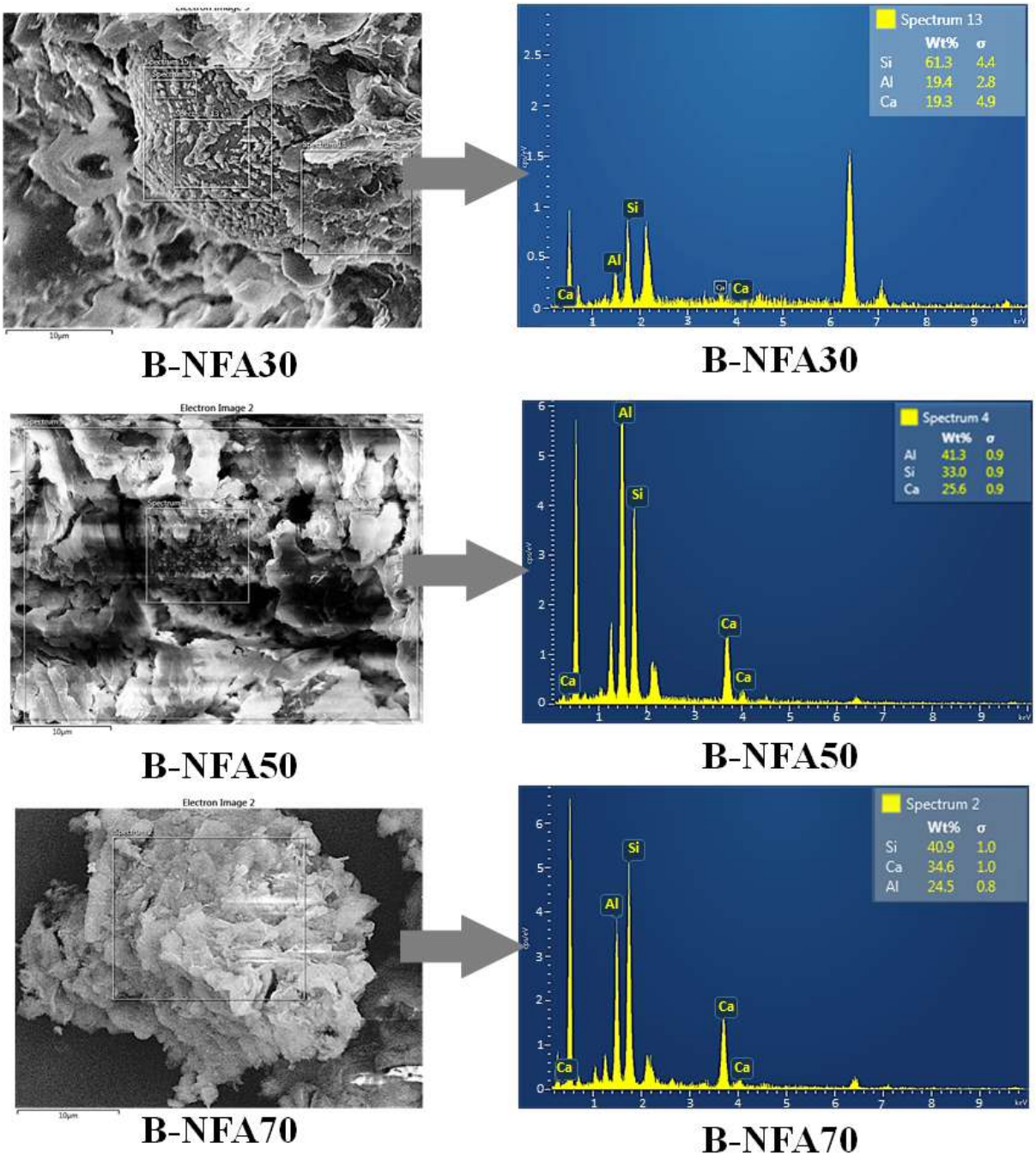


Figure 8.6: EDX analysis of B-NFA mixes showing the relative percentage of Si, Ca, and Al

Nevertheless, the value of effective cohesion for B-NFA and B-BFA was higher by up to 411% than that of bentonite-sand mix at 80% additive rate (Mukherjee and Mishra, 2020). The effective angle of internal friction was observed to be higher in the B-BFA mix by 8% than that of B-NFA mix. This might be due to the particle surface roughness, which was not quantified in the current study. It is interesting to note that the effective angle of internal friction was higher by at least 16% than that of bentonite-sand mix at 80% additive rate (Mukherjee and Mishra, 2020). Hence, even at confining stresses corresponding to field

conditions, both classes of FA showcased superior shear strength characteristics than that of conventional sand-bentonite mixes.

### 8.3.3 Spectroscopy analysis and relation of UCS with electro-chemical properties

Figure 8.7 presents the XRD spectra of the B-FA mixes at 50% additive rate for air-dried mixed samples (marked as control) and after the completion of UCS tests. XRD spectra are commonly used to identify the formation of calcium aluminosilicate hydrates in porous material (Garbev et al., 2008; Li et al., 2019). It can be seen from the spectra that there are peaks of C-A-S-H and ettringite, indicating that these minerals are formed during curing, which contributes to the higher UCS observed in B-NFA and B-FFA mixes. Ettringite minerals were not formed in case of B-BFA mixes. In addition, B-BFA does not exhibit any CSH or CASH mineralization, which can be a plausible explanation as to the relatively low UCS in comparison to the other B-FA mixes. The magnitude of pozzolanic reaction of a material can also be confirmed by the shift of FTIR peaks, both in terms of peak intensity and change in peak wave number (Geng et al., 2017). Fig. 8.8 presents the FTIR spectra of all B-FA mixes for an additive rate of 50% after sample preparation (marked as control) and after completion of UCS tests. The transmittance band in the range 1100 $cm^{-1}$ to 900 $cm^{-1}$ is associated with the asymmetric stretching vibration of Si-O-T (T: tetrahedral Si or Al) (Abdalqader et al., 2016). The presence of band near 795 $cm^{-1}$ is related to the symmetric and asymmetric vibration of Al-OH band in $Al(OH)_6$ octahedral structure of fly ash. A reduction in the peak intensity near the 795 $cm^{-1}$ is an indication on the formation of CASH gel. Also, a shift near the wavenumber of 470 $cm^{-1}$ confirms the involvement of Si-O-Si for the formation of new bond, which results in CASH formation in B-FA mixes. Further, the Widening of the transmittance band near the wavenumber 3640 $cm^{-1}$ indicated the formation of CASH minerals (Kapeluszna et al., 2017). It can be clearly seen that the highest change in peak intensity in the functional groups occurred for NFA followed by FFA. In both FA mixes, -OH peak intensity decreases significantly and shifts in wavenumber, indicating that pozzolanic reactions have readily occurred, giving forth minerals such as CASH and ettringite. B-BFA mix showed the lowest shift in the FTIR peaks, which indicates that pozzolanic reaction might not have readily occurred, resulting in relatively low strength. A similar increase in FTIR peaks corresponding to the formation of CASH and ettringite minerals were observed in previous studies (Walkley et al., 2016).

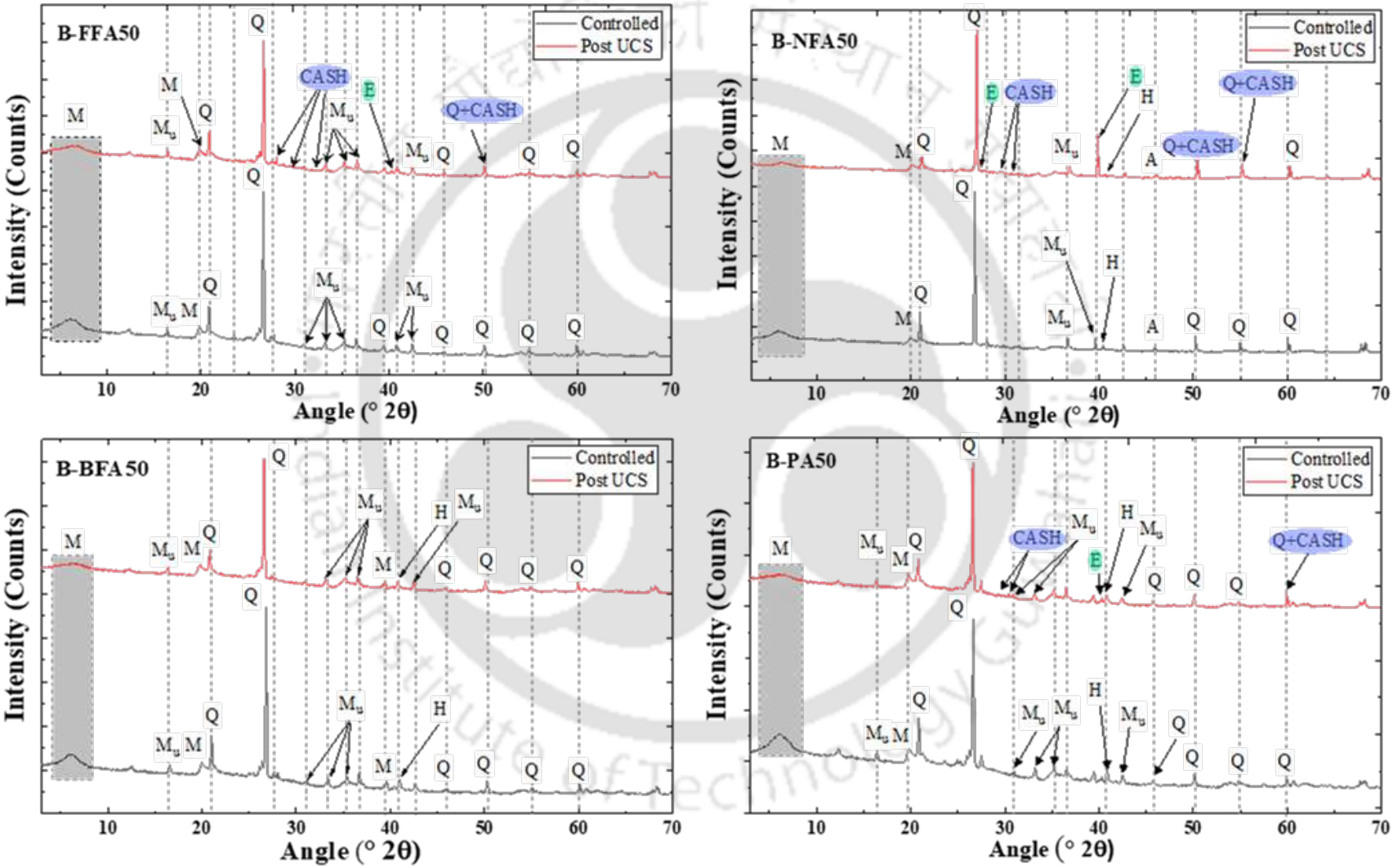


Figure 8.7: X-ray diffraction pattern of B-FAs50 mixes without interaction and post UCS test (after 14 days curing)

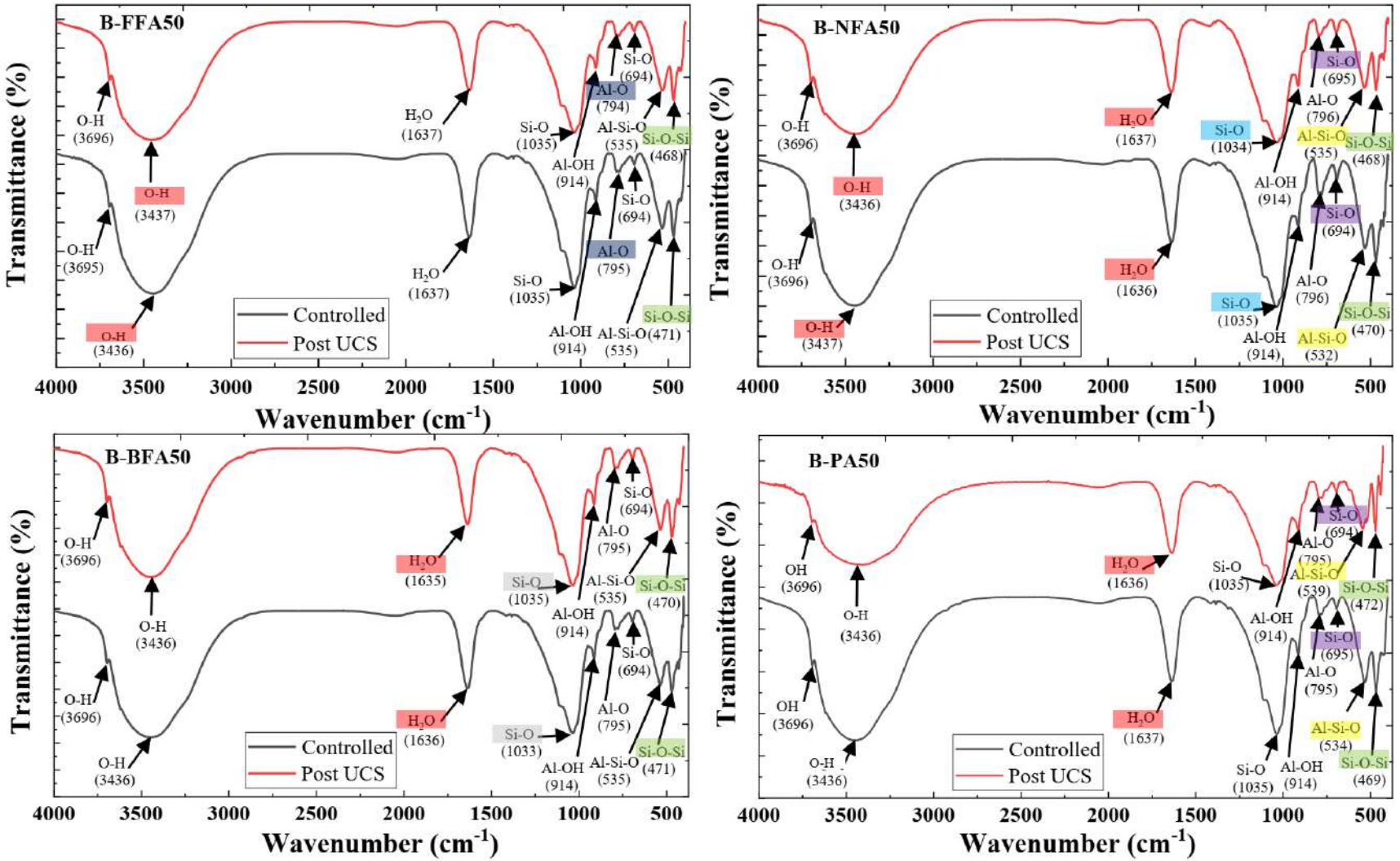


Figure 8.8: FTIR analysis of B-FA mixes without interaction and after 14 days curing post UCS test

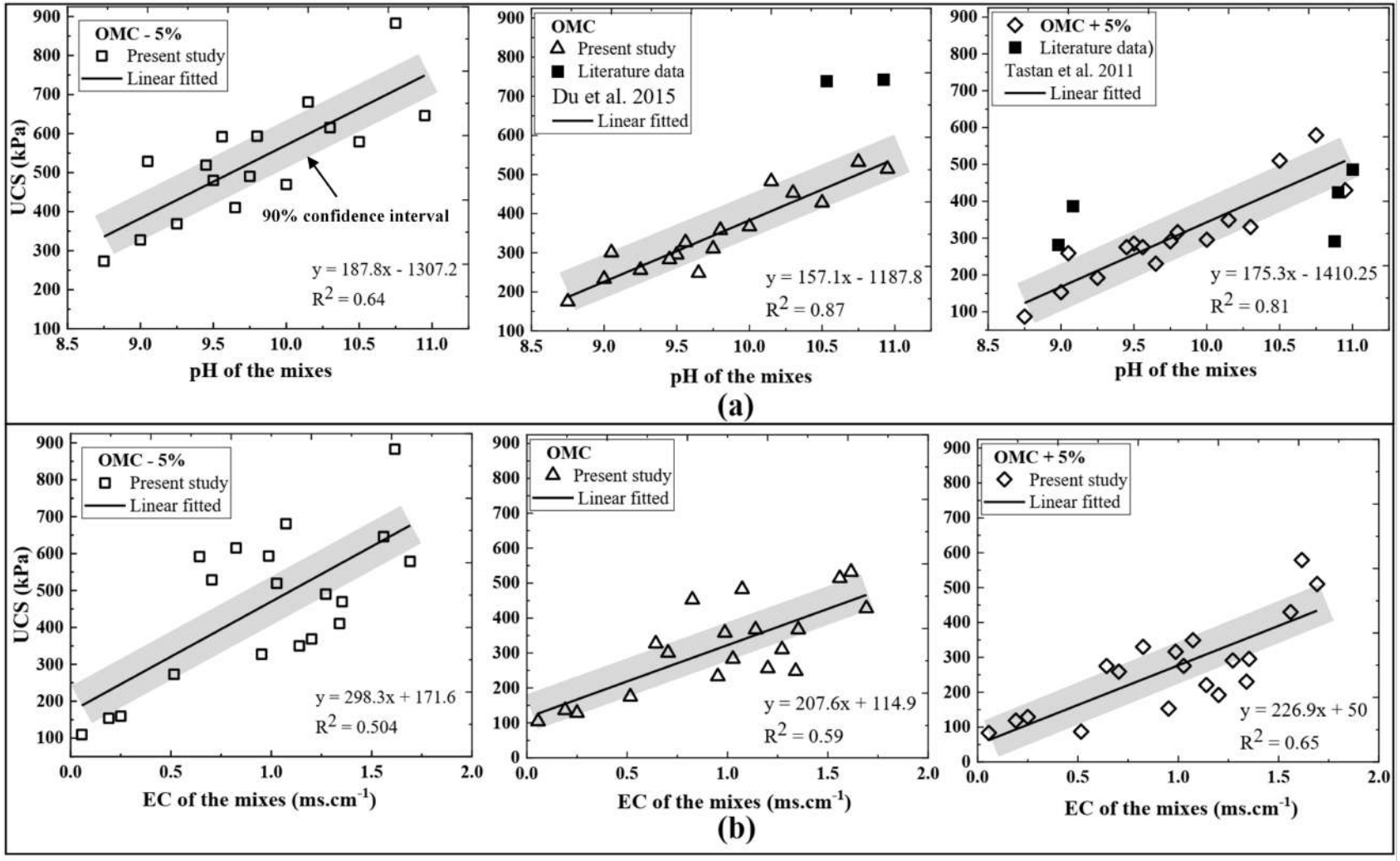


Figure 8.9: Correlation of UCS with (a) pH and (b) electrical conductivity of the mixes

Table 8.1: Shear strength parameters obtained from Triaxial test (consolidated undrained) for B-FA mix

| Mix | Effective angle of internal friction | Effective cohesion (kPa) |
|---|---|---|
| B-BFA70 | 31° | 42 |
| B-NFA70 | 29° | 92 |

Fig. 8.9a shows the variation of UCS at different initial pH for the B-FA and B-S mixes, at three different compaction states. Based on data from the present study, it was observed that UCS increases almost linearly with an increment in pH at all compaction states. Based on the linear fit line of the measured data, it can be inferred that an increase in pH by a magnitude of 2.25 resulted in an increase of UCS by 400 (±20) kPa, regardless of the compaction state. An increase in pH indicates available -OH ions in the material. Pozzolanic reactions readily take place when Si and Al of Montmorillonite mineral dissolve and combine with the available $Ca^{2+}$ giving rise to cementitious gel composed of calcium silicate hydrates and calcium aluminate hydrates (Yong and Ouhadi, 2007). FTIR spectra of all cured B-FA mixes in Fig. 8.8 provide evidence of this reaction as there was a noticeable decrease in the intensity of -OH peak, which is indicative of the involvement of OH in the formation of CSH and CASH gel. This was accompanied by a shift in wavenumber for Si-O, Al-Si-O, and Si-O-Si. This phenomenon is more pronounced for B-NFA and B-FFA, which show higher UCS values. Additionally, an increase in pH also results in change of orientation of the clay particle from edge-to-edge to face-to-face, as seen in the case of kaolinite clay (Ghobadi et al., 2014). The face-to-face orientation favour the increase in shear resistance of the soil. The linear correlation was also compared with existing literature data (Tastan et al., 2011; Du et al., 2016), and the empirical linear co-relation matched relatively well. Fig. 8.9b shows the variation of UCS at different initial EC for all three compaction states. UCS showed a moderate positive relation with initial EC. The linear fit with $R^2$ value ranging from (0.55-0.65) show that EC can be a secondary indicator for the shear strength of a pozzolanic soil mixture. Greater EC values indicate high number of ions dissociated to the free water of the B-FA mixes and this can cause positive pore pressure in base materials (Saarenketo and Scullion, 1996). Thus, the empirical correlation of EC with UCS should be used with caution.

## 8.4 Summary

This study investigates the mechanical performance of compacted bentonite-fly ash (B-FA), and bentonite-sand (B-S) mixes through a series of 180 unconfined compressive strength (UCS) tests. The effect of FA class type, percentage additive and compaction state on the UCS of B-FA mixes was studied in conjuncture with B-S mixes. Additionally, the microstructure and physio-chemical response of mixes before and after failure were studied. Two unique relationships of UCS with electro-chemical properties, i.e., pH and EC were observed. All B-FA mixes showed an increase in UCS with respect to bentonite and is attributed to the presence of CaO mineral inducing pozzolanic activity. For B-S mixes, UCS was lower than that of bentonite regardless of compaction state and additive rate. Although B-NFA mixes exhibited the highest UCS (increases by at least 1.5 times with respect to B) among all tested mixes, the failure patterns were relatively plastic in nature based on MPSF values. The high strength was attributed to the formation of Calcium Silicate Hydrates and ettringite minerals as evident from the micro-structure, FTIR and XRD spectra. For all class F fly ash, failure was a gradual transition from ductile to plastic with a higher additive rate. For B and B-S mixes, failure occurred by bulging, and no intrinsic mineralization was seen due to curing. Based on the consolidated undrained triaxial tests, B-NFA exhibited a higher effective cohesion by 120% than that of B-BFA. On the other hand, the effective angle of internal friction was observed to be higher in the B-BFA mix by 110% than that of B-NFA mix. All B-FA mixes showed higher UCS than the permissible limit set by USEPA guidelines regardless of the compaction state. The B-S mixes failed to adhere to the minimum UCS criterion of 200 kPa at (OMC+5%) compaction state regardless of the percentage additive.

# 9

# Conclusion and Future Scope

## 9.1 Major conclusions from this study

* Balloon method was found to be effective for the determination of soil shrinkage characteristics curve (SSCC) of highly expansive soil and bentonite-fly ash mixes.

* A new predictive model was developed for the determination of SSSC of highly plastic soils based on easily measurable soil parameters.

* Class F FA at the amendment rate of 70% with B fulfills the hydraulic conductivity criteria under constant volume and free swelling conditions.

* Geotechnical centrifuge can effectively be used to evaluate the hydraulic conductivity of expansive soil like B.

* Bentonite-fly ash interaction for long term (from zero to 48 months) had significant effect on class C fly ash. Class F fly ash exhibited hydraulic conductivity close to the acceptable value under free swelling condition.

* Dilution ratio (liquid to solid =L:S) has a significant effect on the sorption behavior of B. It was observed that with an increase in L:S ratio, adsorption of lead on B increase significantly.

* Adsorption of $Pb^{2+}$ on B is very rapid and reached equilibrium within 5 minutes.

* The impact of buffering agent on adsorption capacity of $Pb^{2+}$ on B was evaluated and well correlated with microstructural analysis.

* The $Pb^{2+}$ sorption result indicated that fly ash-bentonite mix performed better than sand-bentonite mix under controlled and uncontrolled pH conditions.

* Long term interaction (up to 48 months) of mixes did not result in appreciable changes in the contaminant retention characteristics.

* The calcium content of class C fly ash was found to have a significant effect on the sorption of $Pb^{2+}$.

* Two new linear relationships of UCS with pH and electrical conductivity (both indicative of reaction) of the mixes (B-FAs and B-S mixes) were proposed.

## 9.2 Major contributions of this study

* Development of the predictive model for soil shrinkage characteristic curve of high plastic soils.

* Determined the hydraulic conductivity variation in compacted bentonite-fly ash mixes under constant volume and free swelling conditions.

* Effect of bentonite fly ash interaction with time on hydraulic conductivity under constant volume and free swelling conditions were explored.

* Hydraulic conductivity of bentonite under constant volume and free swelling conditions at 1g and Ng (using a small geotechnical centrifuge) was investigated.

* Proposed appropriate L:S ratio (=50) for the sorption studies of bentonite against the existing L:S ratio (=20) recommended by ASTM for the soils and sediments.

* Explored the adsorption characteristics of Barmer bentonite for hazardous waste containment application.

* Demonstrated the impact of buffering agent on lead adsorption of bentonite.

* Studied the feasibility of Indian fly ash-bentonite as an alternative adsorbent composite to sand-bentonite mixes in landfill liner.

* Effect of bentonite fly ash interaction with time on the adsorption capacity was evaluated for the B-FA mix.

* Explored the mechanical performance and microstructure of bentonite-fly ash and bentonite-sand mixes for landfill liner application

## 9.3 Limitations and future scope

* Column study should be performed to determine the actual retention capacity, which replicates the field condition of these mixes for the design of landfill liner.

* Interaction of the bentonite fly ash mixes in the presence of landfill leachate and radioactive ions needs to be investigated to see the actual performance of these materials under real field conditions.

* Compatibility of these fly ashes need to be assessed with the bentonite of different plasticity to satisfy the hydraulic conductivity criteria of the landfills liner under constant volume and free swelling conditions.

* Contaminant retention of B-FA mixes used in the present study needs to be investigated in the presence of the landfills leachate.

# Bibliography


Abdalqader, A. F., Jin, F., and Al-Tabbaa, A. (2016). Development of greener alkali-activated cement: utilisation of sodium carbonate for activating slag and fly ash mixtures. *Journal of Cleaner Production*, 113:66–75.

Abeele, W. (1986). The influence of bentonite on the permeability of sandy silts. *Nuclear and chemical waste management*, 6(1):81–88.

Abou Najm, M. R. (2009). *Soil-water interaction: Lessons across scales*. PhD thesis, Purdue University.

Agus, S. S., Arifin, Y. F., Tripathy, S., and Schanz, T. (2013). Swelling pressure–suction relationship of heavily compacted bentonite–sand mixtures. *Acta Geotechnica*, 8(2):155–165.

Ahmaruzzaman, M. (2010). A review on the utilization of fly ash. *Progress in energy and combustion science*, 36(3):327–363.

Ahn, H.-S. and Jo, H. Y. (2009). Influence of exchangeable cations on hydraulic conductivity of compacted bentonite. *Applied Clay Science*, 44(1-2):144–150.

Akpomie, K. G. and Dawodu, F. A. (2015). Potential of a low-cost bentonite for heavy metal abstraction from binary component system. *Beni-suef university journal of basic and applied sciences*, 4(1):1–13.

Al-Badran, Y., Baille, W., Tripathy, S., and Schanz, T. (2017). Swelling behavior of bentonite-based backfilling materials in nuclear waste repository conditions. *Journal of Hazardous, Toxic, and Radioactive Waste*, 21(1):D4015006.

Al-Hamdan, A. Z. and Reddy, K. R. (2006). Adsorption of heavy metals in glacial till soil. *Geotechnical & Geological Engineering*, 24(6):1679–1693.

Al-Jlil, S. A. and Alsewailem, F. D. (2009). Lead uptake by natural clay. *Journal of Applied Sciences*, 9(22):4026–4031.

Al-Yaqout, A. and Townsend, F. (2001). Strategy for landfill design in arid regions. *Practice Periodical of Hazardous, Toxic, and Radioactive Waste Management*, 5(1):2–13.

Alam, J., Khan, M., Alam, M., and Ahmad, A. (2012). Seepage characteristics and geotechnical properties of fly ash mixed with bentonite. *International Journal of Scientific Engineering Research*, 3(8):1–11.

Alexander, J. A., Ahmad Zaini, M. A., Surajudeen, A., Aliyu, E.-N. U., and Omeiza, A. U. (2018). Insight into kinetics and thermodynamics properties of multicomponent lead (ii), cadmium (ii) and manganese (ii) adsorption onto dijah-monkin bentonite clay. *Particulate Science and Technology*, 36(5):569–577.

Ali, M. A., Bouazza, A., Singh, R. M., Gates, W. P., and Rowe, R. K. (2016). Thermal conductivity of geosynthetic clay liners. *Canadian Geotechnical Journal*, 53(9):1510–1521.

Alinnor, I. (2007). Adsorption of heavy metal ions from aqueous solution by fly ash. *Fuel*, 86(5-6):853–857.

Amadi, A. A. (2011). Hydraulic conductivity tests for evaluating compatibility of lateritic soilfly ash mixtures with municipal waste leachate. *Geotechnical and Geological Engineering*, 29(3):259–265.

Amenuvor, A. C., Li, G., Wu, J., Hou, Y., and Chen, W. (2020). An image-based method for quick measurement of the soil shrinkage characteristics curve of soil slurry. *Geoderma*, 363:114165.

Antiohos, S. and Tsimas, S. (2004). Activation of fly ash cementitious systems in the presence of quicklime: Part i. compressive strength and pozzolanic reaction rate. *Cement and concrete research*, 34(5):769–779.

Antoni, Wijaya, S. W., Hardjito, D., et al. (2016). Factors affecting the setting time of fly ash-based geopolymer. In *Materials Science Forum*, volume 841, pages 90–97. Trans Tech Publ.

Arbabi, M., Hemati, S., and Amiri, M. (2015). Removal of lead ions from industrial wastewater: A review of removal methods. *International Journal of Epidemiologic Research*, 2(2):105–109.

Arifin, Y. F. and Sambelum (2019). Bentonite enhanced soil as an alternative landfill liner in rikut jawu, south barito. In *IOP Conference Series: Earth and Environmental Science*, volume 239, page 012003. IOP Publishing.

Arul Manikandan, N., Alemu, A. K., Goswami, L., Pakshirajan, K., and Pugazhenthi, G. (2016). Waste litchi peels for cr (vi) removal from synthetic wastewater in batch and continuous systems: sorbent characterization, regeneration and reuse study. *Journal of Environmental Engineering*, 142(9):C4016001.

Arulanandan, K., Thompson, P., Kutter, B., Meegoda, N., Muraleetharan, K., and Yogachandran, C. (1988). Centrifuge modeling of transport processes for pollutants in soils. *Journal of Geotechnical Engineering*, 114(2):185–205.

Asokan, P., Saxena, M., Aparna, A., and Asoletar, S. R. (2004). Characteristics variation of coal combustion residues in an indian ash pond. *Waste Management & Research*, 22(4):265–275.

ASTM. Standard test method for specific gravity of soils. *ASTM D854-92. West Conshohocken, PA: ASTM International*.

ASTM (2000). Standard test methods for consolidated undrained triaxial compression test for cohesive soils. *ASTM D4767. ASTM, West Conshohocken, PA*.

ASTM (2003). Standard specification for coal fly ash and raw or calcined natural pozzolan for use in concrete. *ASTM C618-03. ASTM, West Conshohocken, PA*.

ASTM (2007a). Standard test method for particle-size analysis of soils. *ASTM D422-63. ASTM, West Conshohocken, PA*.

ASTM (2007b). Test method for shrinkage factors of soils by the mercury method. american society 440 for testing and materials. *ASTM D427. ASTM, West Conshohocken, PA*.

ASTM (2008a). Standard test method for 24-h batch-type measurement of contaminant sorption by soils and sediments. *ASTM D4646. ASTM, West Conshohocken, PA*.

ASTM (2008b). tandard test method for shrinkage factors of cohesive soils by the water submersion method. *ASTM 4943. ASTM, West Conshohocken, PA*.

ASTM (2009). Standard test methods for unconfined compressive strength of compacted soil-lime mixtures. *ASTM D5102-09. ASTM, West Conshohocken, PA*.

ASTM (2010). Standard test methods for liquid limit, plastic limit, and plasticity index of soils. *ASTM D4318-10.ASTM, West Conshohocken, PA*.

ASTM (2012). Standard test method for laboratory compaction characteristics of soil using standard effort. *ASTM D698-12. ASTM, West Conshohocken, PA*.

ASTM (2015). Standard test method for measurement of hydraulic conductivity of porous material using a rigid-wall, compaction-mold permeameter. *ASTM D5856-15 ASTM, West Conshohocken, PA*.

ASTM (2016). Standard test methods for measurement of hydraulic conductivity of saturated porous materials using a flexible wall permeameter. *ASTM D5084-16a. ASTM, West Conshohocken, PA*.

Auboiroux, M., Baillif, P., Touray, J., and Bergaya, F. (1996). Fixation of zn2+ and pb2+ by a ca-montmorillonite in brines and dilute solutions: preliminary results. *Applied Clay Science*, 11(2-4):117–126.

Aucott, M. (2006). *The fate of heavy metals in landfills: A Review*. New Jersey Department of Environmental Protection New Jersey.

Ayala, J., Blanco, F., Garcìa, P., Rodriguez, P., and Sancho, J. (1998). Asturian fly ash as a heavy metals removal material. *Fuel*, 77(11):1147–1154.

Babel, S. and Kurniawan, T. A. (2003). Low-cost adsorbents for heavy metals uptake from contaminated water: a review. *Journal of hazardous materials*, 97(1-3):219–243.

Baik, M. H. and Lee, S. Y. (2010). Colloidal stability of bentonite clay considering surface charge properties as a function of ph and ionic strength. *Journal of Industrial and Engineering Chemistry*, 16(5):837–841.

Bao, N., Miao, X., Hu, X., Zhang, Q., Jie, X., and Zheng, X. (2017). Novel synthesis of plasmonic ag/agcl@ tio2 continues fibers with enhanced broadband photocatalytic performance. *Catalysts*, 7(4):117.

Barman, D. and Mishra, A. (2022). Influence of salt and initial conditions on the shrinkage limit of bentonite. *International Journal of Geotechnical Engineering*, 16(1):64–73.

Barreto, P. N. M. (2019). A new method to correct void ratio for expansive soil. *PhD diss., University of British Columbia*.

Baumgartl, T. and Köck, B. (2004). Modeling volume change and mechanical properties with hydraulic models. *Soil Science Society of America Journal*, 68(1):57–65.

Bennour, H. (2013). Adsorption of lead, nickel, and cobalt ions onto libyan bentonite clay. *Int. J. Chem. Stud*, 1(3):118.

Bensallam, S., Bahi, L., Ejjaaouani, H., and Shakhirev, V. (2012). Shrinkage curve: Experimental study and modelling. *International Journal of Engineering*, 25(3):203–210.

Benson, C. and Yesiller, N. (2016). Variability of saturated hydraulic conductivity measurements made using a flexible-wall permeameter. *Geotechnical Testing Journal*, 39(3):476–491.

Benson, C. H., Daniel, D. E., and Boutwell, G. P. (1999). Field performance of compacted clay liners. *Journal of Geotechnical and Geoenvironmental Engineering*, 125(5):390–403.

Benson, C. H. and Trast, J. M. (1995). Hydraulic conductivity of thirteen compacted clays. *Clays and clay minerals*, 43(6):669–681.

Benson, C. H., Zhai, H., and Wang, X. (1994). Estimating hydraulic conductivity of compacted clay liners. *Journal of geotechnical engineering*, 120(2):366–387.

Bereket, G., Arog, A. Z., and Özel, M. Z. (1997). Removal of pb (ii), cd (ii), cu (ii), and zn (ii) from aqueous solutions by adsorption on bentonite. *Journal of Colloïd and interface science*, 187(2):338–343.

Berndt, R. and Coughlan, K. (1977). The nature of changes in bulk density with water content in a cracking clay. *Soil Research*, 15(1):27–37.

Bharat, T. V. and Das, D. S. (2017). Physicochemical approach for analyzing equilibrium volume of clay sediments in salt solutions. *Applied Clay Science*, 136:164–175.

Bharat, T. V. and Gapak, Y. (2018). Hydration kinetics of bentonite buffer material: Influence of vapor pressure, bentonite plasticity, and compaction density. *Applied Clay Science*, 157:41–50.

Bharat, T. V., Yadav, H., Mahaur, J. P., and Kushwaha, S. (2020). Effect of aging time on consistency limits of bentonites. *Geotechnical and Geological Engineering*, 38(4):3737–3749.

Bhatt, A., Priyadarshini, S., Mohanakrishnan, A. A., Abri, A., Sattler, M., and Techapaphawit, S. (2019). Physical, chemical, and geotechnical properties of coal fly ash: A global review. *Case Studies in Construction Materials*, 11:e00263.

Binal, A. (2016). The effects of high alkaline fly ash on strength behaviour of a cohesive soil. *Advances in Materials Science and Engineering*, 2016.

Blatz, J., Graham, J., and Chandler, N. (2002). Influence of suction on the strength and stiffness of compacted sand bentonite. *Canadian Geotechnical Journal*, 39(5):1005–1015.

Boivin, P., Schäffer, B., Temgoua, E., Gratier, M., and Steinman, G. (2006). Assessment of soil compaction using soil shrinkage modelling: Experimental data and perspectives. *Soil*

*and Tillage Research*, 88(1-2):65–79.

Bordoloi, S., Gopal, P., Boddu, R., Wang, Q., Cheng, Y.-F., Garg, A., and Sreedeep, S. (2019). Soil-biochar-water interactions: role of biochar from eichhornia crassipes in influencing crack propagation and suction in unsaturated soils. *Journal of Cleaner Production*, 210:847–859.

Bordoloi, S., Kashyap, V., Garg, A., Sreedeep, S., Wei, L., and Andriyas, S. (2018). Measurement of mechanical characteristics of fiber from a novel invasive weed: A comprehensive comparison with fibers from agricultural crops. *Measurement*, 113:62–70.

Bourliva, A., Michailidis, K., Sikalidis, C., Filippidis, A., and Betsiou, M. (2013). Lead removal from aqueous solutions by natural greek bentonites. *Clay Minerals*, 48(5):771–787.

Bowders Jr, J. J. and Daniel, D. E. (1987). Hydraulic conductivity of compacted clay to dilute organic chemicals. *Journal of Geotechnical Engineering*, 113(12):1432–1448.

Bradshaw, S. L., Benson, C. H., and Rauen, T. L. (2016). Hydraulic conductivity of geosynthetic clay liners to recirculated municipal solid waste leachates. *Journal of Geotechnical and Geoenvironmental Engineering*, 142(2):04015074.

Braudeau, E., Costantini, J., Bellier, G., and Colleuille, H. (1999). New device and method for soil shrinkage curve measurement and characterization. *Soil Science Society of America Journal*, 63(3):525–535.

Budihardjo, M., Gita, D., Sutrisno, E., Ramadan, B., Wardhana, I., and Yumaroh, S. (2021). Metals (fe, zn, mn) retention capacity of modified bentonite clay liner. In *IOP Conference Series: Earth and Environmental Science*, volume 623, page 012020. IOP Publishing.

Burakov, A. E., Galunin, E. V., Burakova, I. V., Kucherova, A. E., Agarwal, S., Tkachev, A. G., and Gupta, V. K. (2018). Adsorption of heavy metals on conventional and nanostructured materials for wastewater treatment purposes: A review. *Ecotoxicology and environmental safety*, 148:702–712.

Busch, J., Ahrens, L., Sturm, R., and Ebinghaus, R. (2010). Polyfluoroalkyl compounds in landfill leachates. *Environmental pollution*, 158(5):1467–1471.

Castro-Fresno, D., Movilla-Quesada, D., Vega-Zamanillo, Á., and Calzada-Pérez, M. A. (2011). Lime stabilization of bentonite sludge from tunnel boring. *Applied Clay Science*, 51(3):250–257.

Cerato, A. B. and Lutenegger, A. J. (2002). Determination of surface area of fine-grained soils by the ethylene glycol monoethyl ether (egme) method. *Geotechnical Testing Journal*, 25(3):315–321.

Chai, W., Huang, Y., Su, S., Han, G., Liu, J., and Cao, Y. (2017). Adsorption behavior of zn (ii) onto natural minerals in wastewater. a comparative study of bentonite and kaolinite. *Physicochemical Problems of Mineral Processing*, 53.

Chalermyanont, T., Arrykul, S., and Charoenthaisong, N. (2009). Potential use of lateritic and marine clay soils as landfill liners to retain heavy metals. *Waste Management*, 29(1):117–127.

Chang, Y. S., Au, P. I., Mubarak, N. M., Khalid, M., Jagadish, P., Walvekar, R., and Abdullah, E. C. (2020). Adsorption of cu (ii) and ni (ii) ions from wastewater onto bentonite and bentonite/go composite. *Environmental Science and Pollution Research*, 27(26):33270–33296.

Chapman, H. (1965). Cation-exchange capacity. *Methods of soil analysis: Part 2 Chemical and microbiological properties*, 9:891–901.

Chapuis, R. P. (2004). Permeability tests in rigid-wall permeameters: determining the degree of saturation, its evolution, and its influence of test results. *Geotechnical Testing Journal*, 27(3):304–313.

Chapuis, R. P. (2012). Predicting the saturated hydraulic conductivity of soils: a review. *Bulletin of engineering geology and the environment*, 71(3):401–434.

Chapuis, R. P., Gatien, T., and Marron, J.-C. (2019). How to improve the quality of laboratory permeability tests in rigid-wall permeameters: a review. *Geotechnical Testing Journal*, 43(4):1037–1056.

Chen, H. and Wang, A. (2007). Kinetic and isothermal studies of lead ion adsorption onto palygorskite clay. *Journal of Colloid and Interface Science*, 307(2):309–316.

Chen, J., Salihoglu, H., Benson, C. H., Likos, W. J., and Edil, T. B. (2019a). Hydraulic conductivity of bentonite–polymer composite geosynthetic clay liners permeated with coal combustion product leachates. *Journal of Geotechnical and Geoenvironmental Engineering*, 145(9):04019038.

Chen, J. N., Benson, C. H., and Edil, T. B. (2018). Hydraulic conductivity of geosynthetic clay liners with sodium bentonite to coal combustion product leachates. *Journal of Geotechnical and Geoenvironmental Engineering*, 144(3):04018008.

Chen, L.-C., Tien, C.-H., Ou, S.-L., Lee, K.-Y., Tian, J., Tseng, Z.-L., Chen, H.-T., Kuo, H.-C., and Sun, A.-C. (2019b). Perovskite cspbbr3 quantum dots prepared using discarded lead–acid battery recycled waste. *Energies*, 12(6):1117.

Chen, P. and Lu, N. (2018). Generalized equation for soil shrinkage curve. American Society of Civil Engineers.

Chen, Y.-m., Li, J.-c., Yang, C.-b., Zhu, B., and Zhan, L.-t. (2017). Centrifuge modeling of municipal solid waste landfill failures induced by rising water levels. *Canadian Geotechnical Journal*, 54(12):1739–1751.

Chertkov, V. (2000). Modeling the pore structure and shrinkage curve of soil clay matrix. *Geoderma*, 95(3-4):215–246.

Chertkov, V. (2003). Modelling the shrinkage curve of soil clay pastes. *Geoderma*, 112(1-2):71–95.

Cho, H., Oh, D., and Kim, K. (2005). A study on removal characteristics of heavy metals from aqueous solution by fly ash. *Journal of hazardous materials*, 127(1-3):187–195.

Cokca, E. and Yilmaz, Z. (2004). Use of rubber and bentonite added fly ash as a liner material. *Waste management*, 24(2):153–164.

Cornelis, W., Corluy, J., Medina, H., Diaz, J., Hartmann, R., Van Meirvenne, M., and Ruiz, M. E. (2006a). Measuring and modelling the soil shrinkage characteristic curve. *Geoderma*, 137(1-2):179–191.

Cornelis, W., Corluy, J., Medina, H., Hartmann, R., Van Meirvenne, M., and Ruiz, M. E. (2006b). A simplified parametric model to describe the magnitude and geometry of soil shrinkage. *European Journal of Soil Science*, 57(2):258–268.

Cowland, J. and Leung, B. (1991). A field trial of a bentonite landfill liner. *Waste management & research*, 9(4):277–291.

Crescimanno, G. and Provenzano, G. (1999). Soil shrinkage characteristic curve in clay soils: Measurement and prediction. *Soil Science Society of America Journal*, 63(1):25–32.

Cuevas, J., Ruiz, A. I., de Soto, I. S., Sevilla, T., Procopio, J. R., Da Silva, P., Gismera, M. J., Regadío, M., Jiménez, N. S., Rastrero, M. R., et al. (2012). The performance of natural clay as a barrier to the diffusion of municipal solid waste landfill leachates. *Journal of environmental management*, 95:S175–S181.

Cui, Y., Tang, A., Loiseau, C., and Delage, P. (2008a). Determining water permeability of compacted bentonite-sand mixture under confined and free-swell conditions. *Physics and Chemistry of the Earth*, 33:S462–S471.

Cui, Y.-J., Tang, A. M., Loiseau, C., and Delage, P. (2008b). Determining the unsaturated hydraulic conductivity of a compacted sand–bentonite mixture under constant-volume and free-swell conditions. *Physics and Chemistry of the Earth, Parts A/B/C*, 33:S462–S471.

Dafalla, M., Shaker, A. A., Elkady, T., Al-Shamrani, M., and Dhowian, A. (2015). Effects of confining pressure and effective stress on hydraulic conductivity of sand-clay mixtures. *Arabian Journal of Geosciences*, 8(11):9993–10001.

Daniel, D. E. (1984). Predicting hydraulic conductivity of clay liners. *Journal of Geotechnical Engineering*, 110(2):285–300.

Daniel, D. E. (1994). State-of-the-art: Laboratory hydraulic conductivity test for saturated soils. *ASTM Special Technical Publication*, 1142:30–30.

Daniel, D. E., Anderson, D. C., and Boynton, S. S. (1985). Fixed-wall versus flexible-wall permeameters. *Hydraulic barriers in soil and rock*, 874:107–126.

Daniel, D. E. and Benson, C. H. (1990). Water content-density criteria for compacted soil liners. *Journal of Geotechnical Engineering*, 116(12):1811–1830.

Daniel, D. E., Trautwein, S. J., Boynton, S. S., and Foreman, D. E. (1984). Permeability testing with flexible-wall permeameters. *Geotechnical Testing Journal*, 7(3):113–122.

Daniels, J. L., Inyang, H. I., and Chien, C. C. (2004). Verification of contaminant sorption by soil–bentonite barrier materials using scanning electron microscopy/energy dispersive x-ray spectrometry. *Journal of Environmental Engineering*, 130(8):910–917.

Das, A., Krishna, K., Kumar, R., Das, A., Sengupta, S., and Ghosh, J. G. (2016). Tracing lead contamination in foods in the city of kolkata, india. *Environmental Science and Pollution Research*, 23(22):22454–22466.

Das, A., Patel, S. S., Kumar, R., Krishna, K., Dutta, S., Saha, M. C., Sengupta, S., and Guha, D. (2018). Geochemical sources of metal contamination in a coal mining area in chhattisgarh, india using lead isotopic ratios. *Chemosphere*, 197:152–164.

Dash, S. K. and Hussain, M. (2012). Lime stabilization of soils: reappraisal. *Journal of materials in civil engineering*, 24(6):707–714.

de Leeuw, J., Shankman, D., Wu, G., de Boer, W. F., Burnham, J., He, Q., Yesou, H., and Xiao, J. (2010). Strategic assessment of the magnitude and impacts of sand mining in poyang lake, china. *Regional Environmental Change*, 10(2):95–102.

Deka, A. and Sekharan, S. (2017). Contaminant retention characteristics of fly ash–bentonite mixes. *Waste Management & Research*, 35(1):40–46.

Deka, A. and Sekharan, S. (2020). Water retention characteristics of fly ash–bentonite mix. *Geotechnical and Geological Engineering*, 38(3):3245–3252.

Deka, S., Dash, S., and Sreedeep, S. (2015). Strength of lime-treated fly ash using bentonite. *Geotechnical Engineering*, 46(3SI):73–81.

Dolinar, B. (2009). Predicting the hydraulic conductivity of saturated clays using plasticity-value correlations. *Applied Clay Science*, 45(1-2):90–94.

Dolinar, B., Miŝiĉ, M., and Trauner, L. (2007). Correlation between surface area and atterberg limits of fine-grained soils. *Clays and Clay Minerals*, 55(5):519–523.

Donat, R., Akdogan, A., Erdem, E., and Cetisli, H. (2005). Thermodynamics of pb2+ and ni2+ adsorption onto natural bentonite from aqueous solutions. *Journal of colloid and interface science*, 286(1):43–52.

Dong, Y. and Lu, N. (2017). Measurement of suction-stress characteristic curve under drying and wetting conditions. *Geotechnical Testing Journal*, 40(1):107–121.

dos Reis, G. S., Lima, E. C., Sampaio, C. H., Rodembusch, F. S., Petter, C. O., Cazacliu, B. G., Dotto, G. L., and Hidalgo, G. E. N. (2018). Novel kaolin/polysiloxane based organic-inorganic hybrid materials: Sol-gel synthesis, characterization and photocatalytic properties. *Journal of Solid State Chemistry*, 260:106–116.

Du, Y., Fan, R., Liu, S., Reddy, K., and Jin, F. (2015). Workability, compressibility and hydraulic conductivity of zeolite-amended clayey soil/calcium-bentonite backfills for slurry-trench cutoff walls. *Engineering Geology*, 195:258–268.

Du, Y. and Hayashi, S. (2006). A study on sorption properties of cd2+ on ariake clay for evaluating its potential use as a landfill barrier material. *Applied Clay Science*, 32(1-2):14–24.

Du, Y.-J., Bo, Y.-L., Jin, F., and Liu, C.-Y. (2016). Durability of reactive magnesia-activated slag-stabilized low plasticity clay subjected to drying–wetting cycle. *European Journal of Environmental and Civil Engineering*, 20(2):215–230.

Dutta, J. and Mishra, A. K. (2016). Influence of the presence of heavy metals on the behaviour of bentonites. *Environmental Earth Sciences*, 75(11):1–10.

EPA/ 530-SW-86-007-F (1987). Design, construction, and evaluation of clay liners for waste

management facilities, office of solid waste and emergency response. Technical report, USEPA, Washington DC, USA.

Eren, E. and Afsin, B. (2008). An investigation of cu (ii) adsorption by raw and acid-activated bentonite: A combined potentiometric, thermodynamic, xrd, ir, dta study. *Journal of Hazardous materials*, 151(2-3):682–691.

Eren, E., Afsin, B., and Onal, Y. (2009). Removal of lead ions by acid activated and manganese oxide-coated bentonite. *Journal of Hazardous Materials*, 161(2-3):677–685.

Esposito, G. (2000). Centrifuge simulation of light hydrocarbon spill in partially saturated dutch dune sand. *Bulletin of Engineering Geology and the Environment*, 58(2):89–93.

Fan, C., Li, K., Li, J., Ying, D., Wang, Y., and Jia, J. (2017). Comparative and competitive adsorption of pb (ii) and cu (ii) using tetraethylenepentamine modified chitosan/cofe2o4 particles. *Journal of Hazardous Materials*, 326:211–220.

Fang, G. and Zhang, M. (2020). Multiscale micromechanical analysis of alkali-activated fly ash-slag paste. *Cement and Concrete Research*, 135:106141.

Fattah, M. Y. and Al-Lami, A. H. (2016). Behavior and characteristics of compacted expansive unsaturated bentonite-sand mixture. *Journal of Rock Mechanics and Geotechnical Engineering*, 8(5):629–639.

Feng, S.-J., Chang, J.-Y., Shi, H., Zheng, Q.-T., Guo, X.-Y., and Zhang, X.-L. (2019). Failure of an unfilled landfill cell due to an adjacent steep slope and a high groundwater level: A case study. *Engineering Geology*, 262:105320.

Fernández-Jiménez, A., Palomo, A., and Criado, M. (2005). Microstructure development of alkali-activated fly ash cement: a descriptive model. *Cement and concrete research*, 35(6):1204–1209.

Fityus, S. and Buzzi, O. (2009). The place of expansive clays in the framework of unsaturated soil mechanics. *Applied Clay Science*, 43(2):150–155.

Fleming, I. and Rowe, R. (2004). Laboratory studies of clogging of landfill leachate collection and drainage systems. *Canadian Geotechnical Journal*, 41(1):134–153.

Fredlund, D. G. and Fredlund, M. D. (2020). Application of estimation procedures in unsaturated soil mechanics. *Geosciences*, 10(9):364.

Fredlund, M. D., Wilson, G. W., and Fredlund, D. G. (2002). Representation and estimation of the shrinkage curve. In *Proc., 3rd Int. Conf. on Unsaturated Soils, UNSAT 2002*, pages 145–149.

Freundlich, H. (2002). Adsorptionstechnik. by franz krzil. *The Journal of Physical Chemistry*, 40(6):857–858.

Fu, F. and Wang, Q. (2011). Removal of heavy metal ions from wastewaters: a review. *Journal of environmental management*, 92(3):407–418.

Futalan, C. M., Kan, C.-C., Dalida, M. L., Hsien, K.-J., Pascua, C., and Wan, M.-W. (2011). Comparative and competitive adsorption of copper, lead, and nickel using chitosan immobilized on bentonite. *Carbohydrate polymers*, 83(2):528–536.

Gapak, Y., Das, G., Yerramshetty, U., and Bharat, T. V. (2017). Laboratory determination of volumetric shrinkage behavior of bentonites: A critical appraisal. *Applied Clay Science*, 135:554–566.

Gapak, Y. and Tadikonda, V. B. (2018). Hysteretic water-retention behavior of bentonites. *Journal of Hazardous, Toxic, and Radioactive Waste*, 22(3):04018008.

Garbev, K., Beuchle, G., Bornefeld, M., Black, L., and Stemmermann, P. (2008). Cell dimensions and composition of nanocrystalline calcium silicate hydrate solid solutions. part 1: synchrotron-based x-ray diffraction. *Journal of the American Ceramic Society*, 91(9):3005–3014.

Garg, A., Reddy, N. G., Huang, H., Buragohain, P., and Kushvaha, V. (2020). Modelling contaminant transport in fly ash–bentonite composite landfill liner: mechanism of different types of ions. *Scientific Reports*, 10(1):1–8.

Garnier, P., Rieu, M., Boivin, P., Vauclin, M., and Baveye, P. (1997). Determining the hydraulic properties of a swelling soil from a transient evaporation experiment. *Soil Science Society of America Journal*, 61(6):1555–1563.

Geng, G., Myers, R. J., Li, J., Maboudian, R., Carraro, C., Shapiro, D. A., and Monteiro, P. J. (2017). Aluminum-induced dreierketten chain cross-links increase the mechanical properties of nanocrystalline calcium aluminosilicate hydrate. *Scientific reports*, 7(1):1–10.

Ghobadi, M., Abdilor, Y., and Babazadeh, R. (2014). Stabilization of clay soils using lime and effect of ph variations on shear strength parameters. *Bulletin of Engineering Geology and the Environment*, 73(2):611–619.

Ghosal, P. S. and Gupta, A. K. (2017). Determination of thermodynamic parameters from langmuir isotherm constant-revisited. *Journal of Molecular Liquids*, 225:137–146.

Ghosh, A. and Subbarao, C. (1998). Hydraulic conductivity and leachate characteristics of stabilized fly ash. *Journal of Environmental Engineering*, 124(9):812–820.

Gilbert, R. B., Fernandez, F., and Horsfield, D. W. (1996). Shear strength of reinforced geosynthetic clay liner. *Journal of geotechnical engineering*, 122(4):259–266.

Gilbert, U. A., Emmanuel, I. U., Adebanjo, A. A., and Olalere, G. A. (2011). Biosorptive removal of pb2+ and cd2+ onto novel biosorbent: defatted carica papaya seeds. *biomass and bioenergy*, 35(7):2517–2525.

Gimsing, A. L. and Borggaard, O. K. (2007). Phosphate and glyphosate adsorption by hematite and ferrihydrite and comparison with other variable-charge minerals. *Clays and Clay Minerals*, 55(1):108–114.

Giroud, J., Badu-Tweneboah, K., and Soderman, K. (1997). Comparison of leachate flow through compacted clay liners in landfill liner systems. *Geosynthetics International*, 4(3-4):391–431.

Glatstein, D. A. and Francisca, F. M. (2015). Influence of ph and ionic strength on cd, cu and pb removal from water by adsorption in na-bentonite. *Applied Clay Science*, 118:61–67.

Gleason, M. H., Daniel, D. E., and Eykholt, G. R. (1997). Calcium and sodium bentonite

for hydraulic containment applications. *Journal of geotechnical and geoenvironmental engineering*, 123(5):438–445.

Godelitsas, A., Astilleros, J. M., Hallam, K., Harissopoulos, S., and Putnis, A. (2003). Interaction of calcium carbonates with lead in aqueous solutions. *Environmental science & technology*, 37(15):3351–3360.

Gopi Kiran, M., Pakshirajan, K., and Das, G. (2016). Heavy metal removal using sulfate-reducing biomass obtained from a lab-scale upflow anaerobic-packed bed reactor. *Journal of Environmental Engineering*, 142(9):C4015010.

Goswami, L., Arul Manikandan, N., Pakshirajan, K., and Pugazhenthi, G. (2017). Simultaneous heavy metal removal and anthracene biodegradation by the oleaginous bacteria rhodococcus opacus. *3 Biotech*, 7(1):1–9.

Goswami, L., Kumar, R. V., Borah, S. N., Manikandan, N. A., Pakshirajan, K., and Pugazhenthi, G. (2018). Membrane bioreactor and integrated membrane bioreactor systems for micropollutant removal from wastewater: a review. *Journal of water process engineering*, 26:314–328.

Goswami, L., Pakshirajan, K., and Pugazhenthi, G. (2020). Biological treatment of biomass gasification wastewater using hydrocarbonoclastic bacterium rhodococcus opacus in an up-flow packed bed bioreactor with a novel waste-derived nano-biochar based biosupport material. *Journal of Cleaner Production*, 256:120253.

Gupta, G. and Torres, N. (1998). Use of fly ash in reducing toxicity of and heavy metals in wastewater effluent. *Journal of Hazardous Materials*, 57(1-3):243–248.

Gupta, S. S. and Bhattacharyya, K. G. (2012). Adsorption of heavy metals on kaolinite and montmorillonite: a review. *Physical Chemistry Chemical Physics*, 14(19):6698–6723.

Hamadneh, I., Abu-Zurayk, R., Abu-Irmaileh, B., Bozeya, A., and Al-Dujaili, A. (2015). Adsorption of pb (ii) on raw and organically modified jordanian bentonite. *Clay Minerals*, 50(4):485–496.

Hamidpour, M., Kalbasi, M., Afyuni, M., Shariatmadari, H., and Furrer, G. (2011). Sorption of lead on iranian bentonite and zeolite: kinetics and isotherms. *Environmental Earth Sciences*, 62(3):559–568.

Hefne, J., Mekhemer, W., Alandis, N., Aldayel, O., and Alajyan, T. (2008). Kinetic and thermodynamic study of the adsorption of pb (ii) from aqueous solution to the natural and treated bentonite. *International journal of physical sciences*, 3(11):281–288.

Heineck, K. S., Lemos, R. G., Flores, J. A. A., and Consoli, N. C. (2010). Influence of particle morphology on the hydraulic behavior of coal ash and sand. *Geotechnical and Geological Engineering*, 28(4):325–335.

Hettiaratchi, J., Achari, G., Joshi, R., and Okoli, R. (1999). Feasibility of using fly ash admixtures in landfill bottom liners or vertical barriers at contaminated sites. *Journal of Environmental Science & Health Part A*, 34(10):1897–1917.

Ho, Y.-S. and McKay, G. (1999). Pseudo-second order model for sorption processes. *Process biochemistry*, 34(5):451–465.

Holan, Z. and Volesky, B. (1994). Biosorption of lead and nickel by biomass of marine algae. *Biotechnology and bioengineering*, 43(11):1001–1009.

Hong, C. S., Shackelford, C. D., and Malusis, M. A. (2016). Adsorptive behavior of zeolite-amended backfills for enhanced metals containment. *Journal of Geotechnical and Geoenvironmental Engineering*, 142(7):04016021.

Hsu, T.-C., Yu, C.-C., and Yeh, C.-M. (2008). Adsorption of cu2+ from water using raw and modified coal fly ashes. *Fuel*, 87(7):1355–1359.

Huang, R., Wang, B., Yang, B., Zheng, D., and Zhang, Z. (2011). Equilibrium, kinetic and thermodynamic studies of adsorption of cd (ii) from aqueous solution onto hacc–bentonite. *Desalination*, 280(1-3):297–304.

Iacovita, C., Stiufiuc, R., Radu, T., Florea, A., Stiufiuc, G., Dutu, A., Mican, S., Tetean, R., and Lucaciu, C. M. (2015). Polyethylene glycol-mediated synthesis of cubic iron oxide nanoparticles with high heating power. *Nanoscale research letters*, 10(1):1–16.

İNEL, O., Albayrak, F., and AŞKIN, A. (1998). Cu and pb adsorption on some bentonitic clays. *Turkish Journal of Chemistry*, 22(3):243–252.

Jain, C. and Ali, I. (2000). Adsorption of cadmium on riverine sediments: Quantitative treatment of the large particles. *Hydrological processes*, 14(2):261–270.

Jang, Y.-C. and Townsend, T. G. (2003). Leaching of lead from computer printed wire boards and cathode ray tubes by municipal solid waste landfill leachates. *Environmental Science & Technology*, 37(20):4778–4784.

Jin, C., Xiac-Ping, Z., Wei-Li, S., Mao-Sheng, C., Yi, S., Gang-Qiang, Y., Xue-Ming, L., and Fu-Xue, Z. (2010). Shape-controlled synthesis and related growth mechanism of pb (oh) 2 nanorods by solution-phase reaction. *Chinese Physics Letters*, 27(5):057302.

Kakaei, S., Khameneh, E. S., Rezazadeh, F., and Hosseini, M. H. (2020). Heavy metal removing by modified bentonite and study of catalytic activity. *Journal of Molecular Structure*, 1199:126989.

Kale, R. C., Kapil, B., and Ravi, K. (2021). Response of compacted bentonite to hyperalkalinity and thermal history. *Scientific Reports*, 11(1):1–12.

Kanchanason, V. and Plank, J. (2018). Effectiveness of a calcium silicate hydrate–polycarboxylate ether (csh–pce) nanocomposite on early strength development of fly ash cement. *Construction and Building Materials*, 169:20–27.

Kapeluszna, E., Kotwica, Ł., Różycka, A., and Gołek, Ł. (2017). Incorporation of al in cash gels with various ca/si and al/si ratio: Microstructural and structural characteristics with dta/tg, xrd, ftir and tem analysis. *Construction and Building Materials*, 155:643–653.

Kapoor, A. and Viraraghavan, T. (1998). Use of immobilized bentonite in removal of heavy metals from wastewater. *Journal of Environmental Engineering*, 124(10):1020–1024.

Kara, M., Yuzer, H., Sabah, E., and Celik, M. (2003). Adsorption of cobalt from aqueous solutions onto sepiolite. *Water research*, 37(1):224–232.

Katti, D. R., Srinivasamurthy, L., and Katti, K. S. (2015). Molecular modeling of initiation of

interlayer swelling in na–montmorillonite expansive clay. *Canadian Geotechnical Journal*, 52(9):1385–1395.

Kaufhold, S., Dohrmann, R., Koch, D., and Houben, G. (2008). The ph of aqueous bentonite suspensions. *Clays and Clay Minerals*, 56(3):338–343.

Kaya, A. and Ören, A. H. (2005). Adsorption of zinc from aqueous solutions to bentonite. *Journal of hazardous materials*, 125(1-3):183–189.

Kenney, T., Veen, W. V., Swallow, M. A., and Sungaila, M. (1992). Hydraulic conductivity of compacted bentonite–sand mixtures. *Canadian Geotechnical Journal*, 29(3):364–374.

Kererata, C., Soralumpb, S., and Sasanakulc, I. (2013). Centrifuge simulation of lnapl transportation in sand deposits with containment under flow and no-flow conditions. *Science Asia*, 39(5):527–534.

Khan, S. A., Khan, M. A., et al. (1995a). Adsorption of chromium (iii), chromium (vi) and silver (i) on bentonite. *Waste Management*, 15(4):271–282.

Khan, S. A., Khan, M. A., et al. (1995b). Sorption of strontium on bentonite. *Waste Management*, 15(8):641–650.

Kim, D., Vereecken, H., Feyen, J., Boels, D., and Bronswijk, J. (1992). On the characterization of properties of an unripe marine clay soil: I. shrinkage processes of an unripe marine clay soil in relation to physical ripening. *Soil Science*, 153(6):471–481.

Kinuthia, G. K., Ngure, V., Beti, D., Lugalia, R., Wangila, A., and Kamau, L. (2020). Levels of heavy metals in wastewater and soil samples from open drainage channels in nairobi, kenya: community health implication. *Scientific Reports*, 10(1):1–13.

Klopp, H. W., Arriaga, F. J., Likos, W. J., and Bleam, W. F. (2019). Atterberg limits and shrink/swell capacity of soil as indicators for sodium sensitivity within a gradient of soil exchangeable sodium percentage and salinity. *Geoderma*, 353:449–458.

Kollannur, N. J. and Arnepalli, D. N. (2019). Methodology for determining point of zero salt effect of clays in terms of surface charge properties. *Journal of Materials in Civil Engineering*, 31(12):04019286.

Komine, H. and Ogata, N. (2003). New equations for swelling characteristics of bentonite-based buffer materials. *Canadian Geotechnical Journal*, 40(2):460–475.

Kong, Y., Wang, L., Ge, Y., Su, H., and Li, Z. (2019). Lignin xanthate resin–bentonite clay composite as a highly effective and low-cost adsorbent for the removal of doxycycline hydrochloride antibiotic and mercury ions in water. *Journal of hazardous materials*, 368:33–41.

Krisdani, H., Rahardjo, H., and Leong, E.-C. (2008). Effects of different drying rates on shrinkage characteristics of a residual soil and soil mixtures. *Engineering Geology*, 102(1-2):31–37.

Kul, A. R. and Koyuncu, H. (2010). Adsorption of pb (ii) ions from aqueous solution by native and activated bentonite: kinetic, equilibrium and thermodynamic study. *Journal of Hazardous materials*, 179(1-3):332–339.

Kumar, M., Goswami, L., Singh, A. K., and Sikandar, M. (2019). Valorization of coal fired-fly ash for potential heavy metal removal from the single and multi-contaminated system. *Heliyon*, 5(10):e02562.

Kushwaha, A., Hans, N., Kumar, S., and Rani, R. (2018). A critical review on speciation, mobilization and toxicity of lead in soil-microbe-plant system and bioremediation strategies. *Ecotoxicology and environmental safety*, 147:1035–1045.

Lakherwal, D. (2014). Adsorption of heavy metals: a review. *International journal of environmental research and development*, 4(1):41–48.

Lange, K., Rowe, R., and Jamieson, H. (2007). Metal retention in geosynthetic clay liners following permeation by different mining solutions. *Geosynthetics International*, 14(3):178–187.

Langmuir, I. (1918). The adsorption of gases on plane surfaces of glass, mica and platinum. *Journal of the American Chemical society*, 40(9):1361–1403.

Lauritzen, C. and Stewart, A. (1942). Soil-volume changes and accompanying moisture and pore-space relationships. *Soil Science Society of America Journal*, 6(C):113–116.

Lee, U., Han, J., and Wang, M. (2017). Evaluation of landfill gas emissions from municipal solid waste landfills for the life-cycle analysis of waste-to-energy pathways. *Journal of Cleaner Production*, 166:335–342.

LFE10. Using bentonite enriched soils in landfill engineering, environment agency, eu landfill directive. Technical report.

Li, J., Geng, G., Myers, R., Yu, Y.-S., Shapiro, D., Carraro, C., Maboudian, R., and Monteiro, P. J. (2019). The chemistry and structure of calcium (alumino) silicate hydrate: a study by xanes, ptychographic imaging, and wide-and small-angle scattering. *Cement and Concrete Research*, 115:367–378.

Li, L. Y. and Li, F. (2001). Heavy metal sorption and hydraulic conductivity studies using three types of bentonite admixes. *Journal of Environmental Engineering*, 127(5):420–429.

Li, L. Y. and Li, R. S. (2000). The role of clay minerals and the effect of h+ ions on removal of heavy metal (pb2+) from contaminated soils. *Canadian geotechnical journal*, 37(2):296–307.

Li, Q., Chen, J., Benson, C. H., and Peng, D. (2021). Hydraulic conductivity of bentonite-polymer composite geosynthetic clay liners permeated with bauxite liquor. *Geotextiles and Geomembranes*, 49(2):420–429.

Lima, E. C. et al. (2018). Removal of emerging contaminants from the environment by adsorption. *Ecotoxicology and environmental safety*, 150:1–17.

Lima, E. C., Hosseini-Bandegharaei, A., Moreno-Piraján, J. C., and Anastopoulos, I. (2019). A critical review of the estimation of the thermodynamic parameters on adsorption equilibria. wrong use of equilibrium constant in the van't hoof equation for calculation of thermodynamic parameters of adsorption. *Journal of molecular liquids*, 273:425–434.

Lin, C.-J. and Chang, J.-E. (2001). Effect of fly ash characteristics on the removal of cu (ii) from aqueous solution. *Chemosphere*, 44(5):1185–1192.

Liu, X., Hicher, P., Muresan, B., Saiyouri, N., and Hicher, P.-Y. (2016). Heavy metal retention properties of kaolin and bentonite in a wide range of concentration and different ph conditions. *Applied Clay Science*, 119:365–374.

Liu, Y. (2009). Is the free energy change of adsorption correctly calculated? *Journal of Chemical & Engineering Data*, 54(7):1981–1985.

Liu, Z.-r. and Zhou, S.-q. (2010). Adsorption of copper and nickel on na-bentonite. *Process safety and environmental protection*, 88(1):62–66.

Lo, I. M., Mak, R. K., and Lee, S. C. (1997). Modified clays for waste containment and pollutant attenuation. *Journal of Environmental Engineering*, 123(1):25–32.

Lo, I. M.-C. (1996). Characteristics and treatment of leachates from domestic landfills. *Environment International*, 22(4):433–442.

Lu, N., Dong, Y., et al. (2017). Correlation between soil-shrinkage curve and water-retention characteristics. *J. Geotech. Geoenviron. Eng*, 143(9):04017054.

Lu, N. and Kaya, M. (2013). A drying cake method for measuring suction-stress characteristic curve, soil–water-retention curve, and hydraulic conductivity function. *Geotechnical Testing Journal*, 36(1):1–19.

Lu, N. and Likos, W. (2004). *Unsaturated soil mechanicsr*. John Wiley & Sons New York.

Luckham, P. F. and Rossi, S. (1999). The colloidal and rheological properties of bentonite suspensions. *Advances in colloid and interface science*, 82(1-3):43–92.

Luo, Q., Liu, M., Wang, T., and Wu, P. (2020). Correction method for hydraulic conductivity measurements made using a fixed wall permeameter. *Mathematical Problems in Engineering*, 2020.

Marcial, D., Delage, P., and Cui, Y. J. (2002). On the high stress compression of bentonites. *Canadian Geotechnical Journal*, 39(4):812–820.

Marinho, F. A. M. (1994). *Shrinkage behaviour of some plastic soils*. PhD thesis, University of London London, UK.

Mazzieri, F., Di Emidio, G., Fratalocchi, E., Di Sante, M., and Pasqualini, E. (2013). Permeation of two gcls with an acidic metal-rich synthetic leachate. *Geotextiles and Geomembranes*, 40:1–11.

Mbonimpa, M., Aubertin, M., Maqsoud, A., and Bussière, B. (2006). Predictive model for the water retention curve of deformable clayey soils. *Journal of Geotechnical and Geoenvironmental Engineering*, 132(9):1121–1132.

McGarry, D. and Malafant, K. (1987). The analysis of volume change in unconfined units of soil. *Soil Science Society of America Journal*, 51(2):290–297.

Mechleb, G., Gilbert, R., Christman, M., Gupta, R., and Gross, B. (2014). Use of expanded shale amendment to enhance drainage properties of clays. In *Geo-Congress 2014: Geocharacterization and Modeling for Sustainability*, pages 3444–3454.

Meier, A. J. and Shackelford, C. D. (2017). Membrane behavior of compacted sand–bentonite mixture. *Canadian Geotechnical Journal*, 54(9):1284–1299.

Melichová, Z. and Hromada, L. (2013). Adsorption of pb 2+ and cu 2+ ions from aqueous solutions on natural bentonite. *Polish Journal of Environmental Studies*, 22(2).

Meng, X., Jiang, X., Li, Z., Wang, J., Cooper, K. M., and Xie, Z. (2018). Responses of macroinvertebrates and local environment to short-term commercial sand dredging practices in a flood-plain lake. *Science of the Total Environment*, 631:1350–1359.

Mesri, G. and Olson, R. E. (1971). Mechanisms controlling the permeability of clays. *Clays and Clay minerals*, 19(3):151–158.

Millero, F., Huang, F., Zhu, X., Liu, X., and Zhang, J.-Z. (2001). Adsorption and desorption of phosphate on calcite and aragonite in seawater. *Aquatic Geochemistry*, 7(1):33–56.

Mishra, A. K., Ohtsubo, M., Li, L. Y., Higashi, T., and Park, J. (2009). Effect of salt of various concentrations on liquid limit, and hydraulic conductivity of different soil-bentonite mixtures. *Environmental geology*, 57(5):1145–1153.

Mishra, P. N., Scheuermann, A., Bore, T., and Li, L. (2019). Salinity effects on soil shrinkage characteristic curves of fine-grained geomaterials. *Journal of Rock Mechanics and Geotechnical Engineering*, 11(1):181–191.

Mitchell, J. K., Soga, K., et al. (2005). *Fundamentals of soil behavior*, volume 3. John Wiley & Sons New York.

Mohammad, W. A., Fawwaz, I. K., and Akl, M. A. (2010). Adsorption of lead, zinc and cadmium ions on polyphosphate-modified kaolinite clay. *Journal of environmental chemistry and ecotoxicology*, 2(1):001–008.

Mohammadinia, A., Disfani, M. M., Conomy, D., Arulrajah, A., Horpibulsuk, S., and Darmawan, S. (2019). Utilization of alkali-activated fly ash for construction of deep mixed columns in loose sands. *Journal of Materials in Civil Engineering*, 31(10):04019233.

Mohan, S. and Gandhimathi, R. (2009). Removal of heavy metal ions from municipal solid waste leachate using coal fly ash as an adsorbent. *Journal of hazardous materials*, 169(1-3):351–359.

Mollamahmutoğlu, M. and Yilmaz, Y. (2001). Potential use of fly ash and bentonite mixture as liner or cover at waste disposal areas. *Environmental Geology*, 40(11):1316–1324.

Montes-h, G., Duplay, J., Martinez, L., and Mendoza, C. (2003). Swelling–shrinkage kinetics of mx80 bentonite. *Applied Clay Science*, 22(6):279–293.

Muhunthan, B. (1991). Liquid limit and surface area of clays. *Geotechnique*, 41(1):135–138.

Mukherjee, K. and Mishra, A. K. (2019). Evaluation of hydraulic and strength characteristics of sand-bentonite mixtures with added tire fiber for landfill application. *Journal of Environmental Engineering*, 145(6):04019026.

Mukherjee, K. and Mishra, A. K. (2020). Undrained performance of sustainable compacted sand-bentonite–glass fiber composite for landfill application. *Journal of Cleaner Production*, 244:118662.

Müller, W. W. and Wöhlecke, A. (2017). Zero leakage? landfill liner and capping systems

in germany. *Environmental Geotechnics*, 6(3):162–170.

Musso, T. B., Parolo, M., Pettinari, G., and Francisca, F. M. (2014). Cu (ii) and zn (ii) adsorption capacity of three different clay liner materials. *Journal of environmental management*, 146:50–58.

Musso, T. B., Parolo, M. E., and Pettinari, G. R. (2019). ph, ionic strength, and ion competition effect on cu (ii) and ni (ii) sorption by a na-bentonite used as liner material.

Muurinen, A. (2011). Measurements on cation exchange capacity of bentonite in the long-term test of buffer material (lot). Technical report, Posiva Oy.

Naiya, T. K., Bhattacharya, A. K., Mandal, S., and Das, S. K. (2009). The sorption of lead (ii) ions on rice husk ash. *Journal of hazardous materials*, 163(2-3):1254–1264.

Nakano, A., Li, L., Ohtsubo, M., Mishra, A., and Higashi, T. (2008). Lead retention mechanisms and hydraulic conductivity studies of various bentonites for geoenvironment applications. *Environmental technology*, 29(5):505–514.

Nalbantoglu, Z. and Tuncer, E. R. (2001). Compressibility and hydraulic conductivity of a chemically treated expansive clay. *Canadian geotechnical journal*, 38(1):154–160.

Narani, S., Abbaspour, M., Hosseini, S. M. M., Aflaki, E., and Nejad, F. M. (2020). Sustainable reuse of waste tire textile fibers (wttfs) as reinforcement materials for expansive soils: with a special focus on landfill liners/covers. *Journal of Cleaner Production*, 247:119151.

Naseem, R. and Tahir, S. (2001). Removal of pb (ii) from aqueous/acidic solutions by using bentonite as an adsorbent. *Water research*, 35(16):3982–3986.

Naveen, B., Mahapatra, D. M., Sitharam, T., Sivapullaiah, P., and Ramachandra, T. (2017). Physico-chemical and biological characterization of urban municipal landfill leachate. *Environmental Pollution*, 220:1–12.

Ng, C. W., Chen, R., Coo, J. L., Liu, J., Ni, J., Chen, Y. M., Zhan, L.-t., Guo, H. W., and Lu, B. W. (2019). A novel vegetated three-layer landfill cover system using recycled construction wastes without geomembrane. *Canadian Geotechnical Journal*, 56(12):1863–1875.

Ng, C. W. W. and Yung, S. (2008). Determination of the anisotropic shear stiffness of an unsaturated decomposed soil. *Géotechnique*, 58(1):23–35.

Nguyen, L. C., Chu, H. L., and Ho, L. S. (2019). Soil treatment by bentonite and fly ash for liners of waste landfill: A case study in vietnam. *GEOMATE Journal*, 17(63):315–322.

Nhan, C., Graydon, J., and Kirk, D. (1996). Utilizing coal fly ash as a landfill barrier material. *Waste Management*, 16(7):587–595.

Niriella, D. and Carnahan, R. (2006). Comparison study of zeta potential values of bentonite in salt solutions. *Journal of Dispersion Science and Technology*, 27(1):123–131.

Niu, M., Li, G., Cao, L., Wang, X., and Wang, W. (2020). Preparation of sulphate aluminate cement amended bentonite and its use in heavy metal adsorption. *Journal of Cleaner Production*, 256:120700.

Olgun, M. and Yıldız, M. (2010). Effect of organic fluids on the geotechnical behavior of a

highly plastic clayey soil. *Applied Clay Science*, 48(4):615–621.

Öman, C. and Hynning, P.-Å. (1993). Identification of organic compounds in municipal landfill leachates. *Environmental Pollution*, 80(3):265–271.

Ören, A. H., Kaya, A., and Kayalar, A. Ş. (2011). Hydraulic conductivity of zeolite–bentonite mixtures in comparison with sand–bentonite mixtures. *Canadian Geotechnical Journal*, 48(9):1343–1353.

Özcan, A. S., Gök, Ö., and Özcan, A. (2009). Adsorption of lead (ii) ions onto 8-hydroxy quinoline-immobilized bentonite. *Journal of Hazardous materials*, 161(1):499–509.

Pal, S. K. and Ghosh, A. (2013). Hydraulic conductivity of fly ash–montmorillonite clay mixtures. *Indian Geotechnical Journal*, 43(1):47–61.

Palma-Fleming, H., Quiroz, E., Gutierrez, E., Cristi, E., Jara, B., Keim, M. L., Pino, M., Huber, A., Jaramillo, E., Espinoza, O., et al. (2000). Chemical characterization of a municipal landfill and its influence on the surrounding estuarine system, south central chile. *Boletin De La Sociedad Chilena De Quimica*, 45(4):551–561.

Palmer, B. G., Edil, T. B., and Benson, C. H. (2000). Liners for waste containment constructed with class f and c fly ashes. *Journal of Hazardous Materials*, 76(2-3):193–216.

Palomino, A. M. and Santamarina, J. C. (2005). Fabric map for kaolinite: effects of ph and ionic concentration on behavior. *Clays and Clay minerals*, 53(3):211–223.

Pandey, L. M. S. and Shukla, S. K. (2019). An insight into waste management in australia with a focus on landfill technology and liner leak detection. *Journal of Cleaner Production*, 225:1147–1154.

Pandian, N., Rajasekhar, C., and Sridharan, A. (1996). Fly ash as a pre-filter material for the retention of lead ions. *Journal of testing and evaluation*, 24(3):181–186.

Pantazidou, M., Abu-Hassanein, Z. S., and Riemer, M. F. (2000). Centrifuge study of dnapl transport in granular media. *Journal of geotechnical and geoenvironmental engineering*, 126(2):105–115.

Papandreou, A., Stournaras, C., and Panias, D. (2007). Copper and cadmium adsorption on pellets made from fired coal fly ash. *Journal of Hazardous Materials*, 148(3):538–547.

Pardal, X., Pochard, I., and Nonat, A. (2009). Experimental study of si–al substitution in calcium-silicate-hydrate (csh) prepared under equilibrium conditions. *Cement and Concrete Research*, 39(8):637–643.

Pasha, A. Y., Aflaki, E., Hu, L., and Meegoda, J. N. (2013). Effect of soil fabric on transport of a lnapl through unsaturated fine-grained soils: a centrifugal model study. *Soil and Sediment Contamination: An International Journal*, 22(2):223–240.

Pathak, P. and Choppin (2006). Kinetic and thermodynamic studies of cesium (i) sorption on hydrous silica. *Journal of radioanalytical and nuclear chemistry*, 270(2):299–305.

Patra, C., Shahnaz, T., Subbiah, S., and Narayanasamy, S. (2020). Comparative assessment of raw and acid-activated preparations of novel pongamia pinnata shells for adsorption of hexavalent chromium from simulated wastewater. *Environmental Science and Pollution*

*Research*, 27(13):14836–14851.

Pehlivan, E., Cetin, S., and Yanık, B. (2006). Equilibrium studies for the sorption of zinc and copper from aqueous solutions using sugar beet pulp and fly ash. *Journal of hazardous materials*, 135(1-3):193–199.

Peng, X. and Horn, R. (2005). Modeling soil shrinkage curve across a wide range of soil types. *Soil Science Society of America Journal*, 69(3):584–592.

Peng, X. and Horn, R. (2013). Identifying six types of soil shrinkage curves from a large set of experimental data. *Soil Science Society of America Journal*, 77(2):372–381.

Permien, T. and Lagaly, G. (1995). The rheological and colloidal properties of bentonite dispersions in the presence of organic compounds v. bentonite and sodium montmorillonite and surfactants. *Clays and Clay Minerals*, 43(2):229–236.

Phani Kumar, B. and Sharma, R. S. (2004). Effect of fly ash on engineering properties of expansive soils. *Journal of Geotechnical and Geoenvironmental Engineering*, 130(7):764–767.

Piekos, R. and Paslawska, S. (1999). Fluoride uptake characteristics of fly ash. *Fluoride*, 32.

Poulose, A., Nair, S. R., and Singh, D. N. (2000). Centrifuge modeling of moisture migration in silty soils. *Journal of geotechnical and geoenvironmental engineering*, 126(8):748–752.

Prakash, A., Hazra, B., and Sekharan, S. (2020a). Probabilistic analysis of soil-water characteristic curve of bentonite: multivariate copula approach. *International Journal of Geomechanics*, 20(2):04019150.

Prakash, A., Hazra, B., and Sreedeep, S. (2020b). Uncertainties in water retention curve of bentonite. In *Advances in computer methods and geomechanics*, pages 13–24. Springer.

Prakash, K. and Sridharan, A. (2009). Beneficial properties of coal ashes and effective solid waste management. *Practice periodical of hazardous, toxic, and radioactive waste management*, 13(4):239–248.

Prashanth, J., Sivapullaiah, P., and Sridharan, A. (2001). Pozzolanic fly ash as a hydraulic barrier in land fills. *Engineering Geology*, 60(1-4):245–252.

Puls, R. W., Powell, R. M., Clark, D., and Eldred, C. J. (1991). Effects of ph, solid/solution ratio, ionic strength, and organic acids on pb and cd sorption on kaolinite. *Water, Air, and Soil Pollution*, 57(1):423–430.

Puppala, A. J., Intharasombat, N., and Vempati, R. K. (2005). Experimental studies on ettringite-induced heaving in soils. *Journal of Geotechnical and Geoenvironmental Engineering*, 131(3):325–337.

Ranganatham, B. (1961). Soil structure and consolidation characteristics of black cotton clay. *Geotechnique*, 11(4):333–338.

Rao, M., Parwate, A., and Bhole, A. (2002). Removal of cr6+ and ni2+ from aqueous solution using bagasse and fly ash. *Waste management*, 22(7):821–830.

Rao, S. M. and Acharya, I. P. (2014). Synthesis and characterization of fly ash geopolymer

sand. *Journal of materials in civil engineering*, 26(5):912–917.

Rao, S. M. and Ravi, K. (2013). Hydro-mechanical characterization of barmer 1 bentonite from rajasthan, india. *Nuclear Engineering and Design*, 265:330–340.

Rao, S. M. and Ravi, K. (2015). Influence of initial degree of saturation on swell pressures of compacted barmer bentonite specimens. *Annals of Nuclear Energy*, 80:303–311.

Ray, S., Mishra, A. K., and Kalamdhad, A. S. (2022). Equilibrium, kinetic and hydraulic study of different indian bentonites in presence of lead. *European Journal of Environmental and Civil Engineering*, 26(6):2184–2203.

Ren, X., Zhao, Y., Deng, Q., Kang, J., Li, D., and Wang, D. (2016). A relation of hydraulic conductivityvoid ratio for soils based on kozeny-carman equation. *Engineering Geology*, 213:89–97.

Rio, S. and Delebarre, A. (2003). Removal of mercury in aqueous solution by fluidized bed plant fly ash. *Fuel*, 82(2):153–159.

Rowe, R. K. (1995). *Leachate characteristics for MSW landfills*. University of Western Ontario, Department of Civil Engineering, Faculty of .

Rowe, R. K. (2012). Short-and long-term leakage through composite liners. the 7th arthur casagrande lecture. *Canadian Geotechnical Journal*, 49(2):141–169.

Saarenketo, T. and Scullion, T. (1996). Using electrical properties to classify the strength properties of base course aggregates. Technical report, Texas Transportation Institute, Texas A & M University System.

Saha, A. and Sekharan, S. (2021). Importance of volumetric shrinkage curve (vsc) for determination of soil–water retention curve (swrc) for low plastic natural soils. *Journal of Hydrology*, 596:126113.

Saja, S., Bouazizi, A., Achiou, B., Ouaddari, H., Karim, A., Ouammou, M., Aaddane, A., Bennazha, J., and Younssi, S. A. (2020). Fabrication of low-cost ceramic ultrafiltration membrane made from bentonite clay and its application for soluble dyes removal. *Journal of the European Ceramic Society*, 40(6):2453–2462.

Salem, A. and Sene, R. A. (2011). Removal of lead from solution by combination of natural zeolite–kaolin–bentonite as a new low-cost adsorbent. *Chemical engineering journal*, 174(2-3):619–628.

Samingan, A. S., Leong, E.-C., and Rahardjo, H. (2003). A flexible wall permeameter for measurements of water and air coefficients of permeability of residual soils. *Canadian geotechnical journal*, 40(3):559–574.

Sanchez, M., Atique, A., Kim, S., Romero, E., and Zielinski, M. (2013). Exploring desiccation cracks in soils using a 2d profile laser device. *Acta Geotechnica*, 8(6):583–596.

Sandeep, P., Sahu, S., Kothai, P., and Pandit, G. (2016). Leaching behavior of selected trace and toxic metals in coal fly ash samples collected from two thermal power plants, india. *Bulletin of environmental contamination and toxicology*, 97(3):425–431.

Sari, A., Tuzen, M., Citak, D., and Soylak, M. (2007). Equilibrium, kinetic and thermody-

namic studies of adsorption of pb (ii) from aqueous solution onto turkish kaolinite clay. *Journal of hazardous materials*, 149(2):283–291.

Sarode, D. B., Jadhav, R. N., Khatik, V. A., Ingle, S. T., Attarde, S. B., et al. (2010). Extraction and leaching of heavy metals from thermal power plant fly ash and its admixtures. *Polish Journal of Environmental Studies*, 19(6):1325–1330.

Sathe, S. S., Goswami, L., Mahanta, C., and Devi, L. M. (2020). Integrated factors controlling arsenic mobilization in an alluvial floodplain. *Environmental Technology & Innovation*, 17:100525.

Schanz, T., Tripathy, S., and Sridharan, A. (2018). Volume change behaviour of swelling and non-swelling clays upon inundation with water and a low dielectric constant fluid. *Applied Clay Science*, 158:219–225.

Shaikh, J., Bordoloi, S., Yamsani, S. K., Sekharan, S., Rakesh, R. R., and Sarmah, A. K. (2019). Long-term hydraulic performance of landfill cover system in extreme humid region: Field monitoring and numerical approach. *Science of the total environment*, 688:409–423.

Sharanya, A., Mudavath, H., and Thyagaraj, T. (2021). Review of methods for predicting soil volume change induced by shrinkage. *Innovative Infrastructure Solutions*, 6(2):1–16.

Sharma, A., Hazra, B., Spagnoli, G., and Sekharan, S. (2021). Probabilistic estimation of specific surface area and cation exchange capacity: A global multivariate distribution. *Canadian Geotechnical Journal*, 58(8):1077–1094.

Sharma, J. S. and Samarasekera, L. (2007). Effect of centrifuge radius on hydraulic conductivity measured in a falling-head test. *Canadian geotechnical journal*, 44(1):96–102.

Shen, Y., Liu, H., Zhang, S., Gao, Y., Li, B., Yan, Y., Hu, Y., Zhao, L., and Yang, B. (2017). Discrete face-to-face stacking of anthracene inducing high-efficiency excimer fluorescence in solids via a thermally activated phase transition. *Journal of Materials Chemistry C*, 5(38):10061–10067.

Shivpuri, K. K., Lokeshappa, B., Kulkarni, D. A., and Dikshit, A. K. (2011). Metal leaching potential in coal fly ash. *American Journal of Environmental Engineering*, 1(1):21–27.

Shizong, L., Yanrong, W., and Chen, L. (1995). Investigation on the formation of ettringite in the presence of bao. *Cement and concrete research*, 25(7):1417–1422.

Simatupang, M., Mangalla, L. K., Edwin, R. S., Putra, A. A., Azikin, M. T., Aswad, N. H., and Mustika, W. (2020). The mechanical properties of fly-ash-stabilized sands. *geosciences*, 10(4):132.

Singh, D. N. and Gupta, A. K. (2000). Modelling hydraulic conductivity in a small centrifuge. *Canadian Geotechnical Journal*, 37(5):1150–1155.

Singh, D. N. and Gupta, A. K. (2001). Falling head hydraulic conductivity tests in a geotechnical centrifuge. *Journal of testing and evaluation*, 29(3):258–263.

Singh, S., Nayak, K., and Pani, A. (2015). Assessment of coal ash-bentonite mixture as landfill liner. In *Proc. Indian Geotech. Conf*.

Sivapullaiah, P. and Lakshmikantha, H. (2004). Properties of fly ash as hydraulic barrier. *Soil & Sediment Contamination*, 13(5):391–406.

Sivapullaiah, P. and Lakshmikanthay, H. (2005). Lime-stabilised illite as a liner. *Proceedings of the Institution of Civil Engineers-Ground Improvement*, 9(1):39–45.

Sivapullaiah, P., Sridharan, A., and Stalin, V. (2000). Hydraulic conductivity of bentonite-sand mixtures. *Canadian geotechnical journal*, 37(2):406–413.

Sivapullaiah, P. V. and Baig, M. (2010). Leachability of trace elements from two stabilized low lime indian fly ashes. *Environmental Earth Sciences*, 61(8):1735–1744.

Sivapullaiah, P. V. and Baig, M. A. A. (2011). Gypsum treated fly ash as a liner for waste disposal facilities. *Waste Management*, 31(2):359–369.

Skempton, A. (1953). The colloidal activity of clays. *Selected papers on soil mechanics*, pages 106–118.

Slack, R. J., Gronow, J. R., Hall, D. H., and Voulvoulis, N. (2007). Household hazardous waste disposal to landfill: using landsim to model leachate migration. *Environmental Pollution*, 146(2):501–509.

Sobti, J. and Singh, S. K. (2017). Techno-economic analysis for barrier materials in landfills. *International Journal of Geotechnical Engineering*, 11(5):467–478.

Spagnoli, G. and Shimobe, S. (2019). A statistical reappraisal of the relationship between liquid limit and specific surface area, cation exchange capacity and activity of clays. *Journal of Rock Mechanics and Geotechnical Engineering*, 11(4):874–881.

Sridharan, A., Prashanth, J., and Sivapullaiah, P. (1997). Effect of fly ash on the unconfined compressive strength of black cotton soil. *Proceedings of the Institution of Civil Engineers-Ground Improvement*, 1(3):169–175.

Sridharan, A., Rao, S. N., and Rao, G. V. (1971). Shear strength characteristics of saturated montmorillonite and kaolinite clays. *Soils and Foundations*, 11(3):1–22.

Stewart, R. D., Abou Najm, M. R., Rupp, D. E., and Selker, J. S. (2012). An image-based method for determining bulk density and the soil shrinkage curve. *Soil Science Society of America Journal*, 76(4):1217–1221.

Sun, Q., Tian, S., Sun, Q., Li, B., Cai, C., Xia, Y., Wei, X., and Mu, Q. (2019). Preparation and microstructure of fly ash geopolymer paste backfill material. *Journal of Cleaner Production*, 225:376–390.

Svensson, P. D. and Hansen, S. (2013). Combined salt and temperature impact on montmorillonite hydration. *Clays and Clay Minerals*, 61(4):328–341.

Tahervand, S. and Jalali, M. (2017). Sorption and desorption of potentially toxic metals (cd, cu, ni and zn) by soil amended with bentonite, calcite and zeolite as a function of ph. *Journal of Geochemical Exploration*, 181:148–159.

Tahir, S. and Naseem, R. (2007). Removal of cr (iii) from tannery wastewater by adsorption onto bentonite clay. *Separation and purification Technology*, 53(3):312–321.

Tan, Y., Zhang, H., and Wang, Y. (2020). Evaporation and shrinkage processes of compacted

bentonite-sand mixtures. *Soils and Foundations*, 60(2):505–519.

Tariq, A.-u.-R. and Durnford, D. S. (1993a). Analytical volume change model for swelling clay soils. *Soil Science Society of America Journal*, 57(5):1183–1187.

Tariq, A.-u.-R. and Durnford, D. S. (1993b). Soil volumetric shrinkage measurements: a simple method. *Soil Science*, 155(5):325–330.

Tastan, E. O., Edil, T. B., Benson, C. H., and Aydilek, A. H. (2011). Stabilization of organic soils with fly ash. *Journal of geotechnical and Geoenvironmental Engineering*, 137(9):819–833.

Thusyanthan, N. and Madabhushi, S. (2003). Scaling of seepage flow velocity in centrifuge models. *Engineering*, 326.

Thyagaraj, T. and Soujanya, D. (2017). Polypropylene fiber reinforced bentonite for waste containment barriers. *Applied Clay Science*, 142:153–162.

Timms, W. and Hendry, M. (2008). Long-term reactive solute transport in an aquitard using a centrifuge model. *Groundwater*, 46(4):616–628.

Tohdee, K., Kaewsichan, L., et al. (2018). Enhancement of adsorption efficiency of heavy metal cu (ii) and zn (ii) onto cationic surfactant modified bentonite. *Journal of Environmental Chemical Engineering*, 6(2):2821–2828.

Tran, H. N., You, S.-J., Hosseini-Bandegharaei, A., and Chao, H.-P. (2017). Mistakes and inconsistencies regarding adsorption of contaminants from aqueous solutions: a critical review. *Water research*, 120:88–116.

Triantafyllou, S., Christodoulou, E., and Neou-Syngouna, P. (1999). Removal of nickel and cobalt from aqueous solutions by na-activated bentonite. *Clays and Clay Minerals*, 47(5):567–572.

Tripathi, K. and Viswanadham, B. (2012). Evaluation of the permeability behaviour of sand-bentonite mixtures through laboratory tests. *Indian Geotechnical Journal*, 42(4):267–277.

Tripathy, S., Bag, R., and Thomas, H. R. (2014a). Effect of stern-layer on the compressibility behaviour of bentonites. *Acta Geotechnica*, 9(6):1097–1109.

Tripathy, S., Sridharan, A., and Schanz, T. (2004). Swelling pressures of compacted bentonites from diffuse double layer theory. *Canadian Geotechnical Journal*, 41(3):437–450.

Tripathy, S., Tadza, M. Y. M., and Thomas, H. R. (2014b). Soil-water characteristic curves of clays. *Canadian geotechnical journal*, 51(8):869–883.

Tripathy, S., Thomas, H. R., and Bag, R. (2017). Geoenvironmental application of bentonites in underground disposal of nuclear waste: characterization and laboratory tests. *Journal of Hazardous, Toxic, and Radioactive Waste*, 21(1):D4015002.

Tseveendorj, E., Enkhdul, T., Lin, S., Dorj, D., Sh, O., and Soyol-Erdene, T. (2017). Biosorption of lead (ii) from an aqueous solution using biosorbents prepared from water plants. *Mongolian Journal of Chemistry*, 18(44):52–61.

Tu, H. and Vanapalli, S. K. (2016). Prediction of the variation of swelling pressure and one-dimensional heave of expansive soils with respect to suction using the soil-water

retention curve as a tool. *Canadian Geotechnical Journal*, 53(8):1213–1234.

Uddin, M. K. (2017). A review on the adsorption of heavy metals by clay minerals, with special focus on the past decade. *Chemical Engineering Journal*, 308:438–462.

Unuabonah, E., Adebowale, K., and Olu-Owolabi, B. (2007). Kinetic and thermodynamic studies of the adsorption of lead (ii) ions onto phosphate-modified kaolinite clay. *Journal of Hazardous Materials*, 144(1-2):386–395.

USEPA, 1989. Requirements for hazardous waste landfill design, construction, and closure. seminar publication. Technical Report 625/4e89/022, United States Environmental Protection Agency, Cincinnati, pp. 1e127.

Visa, M., Bogatu, C., and Duta, A. (2010). Simultaneous adsorption of dyes and heavy metals from multicomponent solutions using fly ash. *Applied Surface Science*, 256(17):5486–5491.

Wadanambi, L., Dubey, B., and Townsend, T. (2008). The leaching of lead from lead-based paint in landfill environments. *Journal of Hazardous Materials*, 157(1):194–200.

Walkley, B., San Nicolas, R., Sani, M.-A., Rees, G. J., Hanna, J. V., van Deventer, J. S., and Provis, J. L. (2016). Phase evolution of c-(n)-ash/nash gel blends investigated via alkali-activation of synthetic calcium aluminosilicate precursors. *Cement and Concrete Research*, 89:120–135.

Wang, S., Dong, Y., He, M., Chen, L., and Yu, X. (2009). Characterization of gmz bentonite and its application in the adsorption of pb (ii) from aqueous solutions. *Applied clay science*, 43(2):164–171.

Wang, Y.-P., Wang, Z., Zhao, Y., Yi, F.-C., and Zhu, B.-L. (2021). Swelling properties and permeability of gmz bentonite-sand mixtures during different solutions infiltration. *Sustainability*, 13(4):1622.

Weerasinghe, I., Gallage, C., and Dawes, L. (2021). Effect of overburden confining stress on hydraulic performance of geosynthetic clay liners (gcls). *Heliyon*, 7(1):e05770.

Weng, C.-H. and Huang, C. (2004). Adsorption characteristics of zn (ii) from dilute aqueous solution by fly ash. *Colloids and Surfaces A: Physicochemical and Engineering Aspects*, 247(1-3):137–143.

Wijaya, M., Leong, E. C., and Rahardjo, H. (2015). Effect of shrinkage on air-entry value of soils. *Soils and foundations*, 55(1):166–180.

Wilkinson, N., Metaxas, A., Quinney, C., Wickramaratne, S., Reineke, T. M., and Dutcher, C. S. (2018). ph dependence of bentonite aggregate size and morphology on polymer-clay flocculation. *Colloids and Surfaces A: Physicochemical and Engineering Aspects*, 537:281–286.

Xu, D., Shao, D., Chen, C., Ren, A., and Wang, X. (2006a). Effect of ph and fulvic acid on sorption and complexation of cobalt onto bare and fa bound mx-80 bentonite. *Radiochimica Acta*, 94(2):97–102.

Xu, D., Tan, X., Chen, C., and Wang, X. (2008). Adsorption of pb (ii) from aqueous solution to mx-80 bentonite: effect of ph, ionic strength, foreign ions and temperature. *Applied*

*Clay Science*, 41(1-2):37–46.

Xu, D., Wang, X., Chen, C., Zhou, X., and Tan, X. (2006b). Influence of soil humic acid and fulvic acid on sorption of thorium (iv) on mx-80 bentonite. *Radiochimica Acta*, 94(8):429–434.

Xu, X., Liu, X., Oh, M., and Park, J. (2020). Development of a novel base liner material for offshore final disposal sites and the assessment of its hydraulic conductivity. *Waste Management*, 102:190–197.

Yahya, N. A., Al-Gaashani, R., and Abd-Shukor, R. (2017). Synthesis and characterization of pbo–cdo nanocomposite and its effect on (bi, pb)-2223 superconductor. *Applied Physics A*, 123(3):1–7.

Yao, Z., Ji, X., Sarker, P., Tang, J., Ge, L., Xia, M., and Xi, Y. (2015). A comprehensive review on the applications of coal fly ash. *Earth-science reviews*, 141:105–121.

Yao, Z., Xia, M., Sarker, P., and Chen, T.-z. (2014). A review of the alumina recovery from coal fly ash, with a focus in china. *Fuel*, 120:74–85.

Yap, M., Mubarak, N., Sahu, J., and Abdullah, E. (2017). Microwave induced synthesis of magnetic biochar from agricultural biomass for removal of lead and cadmium from wastewater. *Journal of Industrial and Engineering Chemistry*, 45:287–295.

Yeheyis, M. B., Shang, J. Q., Yanful, E. K., et al. (2010). Feasibility of using coal fly ash for mine waste containment. *Journal of environmental engineering*, 136(7):682.

Yeo, S.-S., Shackelford, C. D., and Evans, J. C. (2005). Consolidation and hydraulic conductivity of nine model soil-bentonite backfills. *Journal of Geotechnical and Geoenvironmental Engineering*, 131(10):1189–1198.

Yilmaz, N. and Yapar, S. (2004). Adsorption properties of tetradecyl-and hexadecyl trimethylammonium bentonites. *Applied Clay Science*, 27(3-4):223–228.

Yin, J., Deng, C., Yu, Z., Wang, X., and Xu, G. (2018). Effective removal of lead ions from aqueous solution using nano illite/smectite clay: isotherm, kinetic, and thermodynamic modeling of adsorption. *Water*, 10(2):210.

Yong, R. N. (2000). *Geoenvironmental engineering: Contaminated soils, pollutant fate, and mitigation*. CRC press.

Yong, R. N., Nakano, M., and Pusch, R. (2012). *Environmental soil properties and behaviour*. CRC Press.

Yong, R. N. and Ouhadi, V. R. (2007). Experimental study on instability of bases on natural and lime/cement-stabilized clayey soils. *Applied clay science*, 35(3-4):238–249.

Younus, M. and Sreedeep, S. (2012a). Evaluation of bentonite-fly ash mix for its application in landfill liners. *Journal of Testing and Evaluation*, 40(3):357–362.

Younus, M. and Sreedeep, S. (2012b). Reevaluation and modification of plasticity-based criterion for assessing the suitability of material as compacted landfill liners. *Journal of materials in civil engineering*, 24(11):1396–1402.

Zahafa, F., Maroufa, R., Ouadjeniaa, F., and Schottb, J. (2018). Kinetic and thermodynamic

studies of the adsorption of pb (ii), cr (iii) and cu (ii) onto modified bentonite. *Desalin. Water Treat*, 131:282–290.

Zeng, Z., Cui, Y.-J., and Talandier, J. (2020). Evaluating the influence of soil plasticity on hydraulic conductivity based on a general capillary model. *Engineering Geology*, 278:105826.

Zhan, T., Guan, C., Xie, H., and Chen, Y. (2014). Vertical migration of leachate pollutants in clayey soils beneath an uncontrolled landfill at huainan, china: a field and theoretical investigation. *Science of the Total Environment*, 470:290–298.

Zhang, H., Tan, Y., Zhu, F., He, D., and Zhu, J. (2019a). Shrinkage property of bentonite-sand mixtures as influenced by sand content and water salinity. *Construction and Building Materials*, 224:78–88.

Zhang, M., Zhang, H., Cui, S., Jia, L., Zhou, L., and Chen, H. (2012). Engineering properties of gmz bentonite-sand as buffer/backfilling material for high-level waste disposal. *European journal of environmental and civil engineering*, 16(10):1216–1237.

Zhang, T., Cai, G., and Liu, S. (2018). Assessment of mechanical properties in recycled lignin-stabilized silty soil as base fill material. *Journal of Cleaner Production*, 172:1788–1799.

Zhang, Y., Zhu, C., Liu, F., Yuan, Y., Wu, H., and Li, A. (2019b). Effects of ionic strength on removal of toxic pollutants from aqueous media with multifarious adsorbents: A review. *Science of the Total Environment*, 646:265–279.

Zhirong, L., Uddin, M. A., and Zhanxue, S. (2011). Ft-ir and xrd analysis of natural na-bentonite and cu (ii)-loaded na-bentonite. *Spectrochimica Acta Part A: Molecular and Biomolecular Spectroscopy*, 79(5):1013–1016.

Zou, C., Jiang, W., Liang, J., Sun, X., and Guan, Y. (2019). Removal of pb (ii) from aqueous solutions by adsorption on magnetic bentonite. *Environmental Science and Pollution Research*, 26(2):1315–1322.

# List of Publications

**Published articles**

* **Gupt, C. B.,** Yamsani, S. K., Prakash, A., Medhi, C. R., and Sreedeep, S. (2018). Appropriate Liquid-to-Solid Ratio for Sorption Studies of Bentonite. Journal of Environmental Engineering, 145(2), 04018138. ASCE. (Impact Factor: 1.657; H-index: 95)

* **Gupt, C. B.,** Bordoloi, S., Sreedeep, S., and Sarmah, A. K. (2020). Adsorption characteristics of Barmer bentonite for hazardous waste containment application. Journal of hazardous materials, 396, 122594. Elsevier. (Impact Factor: 14.224; H-Index: 307)

* **Gupt, C. B.,** Bordoloi, S., Sreedeep, S., and Sarmah, A. K. (2020). A feasibility study of Indian fly ash-bentonite as an alternative adsorbent composite to sand-bentonite mixes in landfill liner. Environmental Pollution, 265, 114811. Elsevier. (Impact Factor: 9.988; H-Index: 249)

* **Gupt, C. B.,** Bordoloi, S., Sahoo, R. K., and Sreedeep, S. (2021). Mechanical performance and micro-structure of bentonite-fly ash and bentonite-sand mixes for landfill liner application. Journal of Cleaner Production, 292, 126033. Elsevier. (Impact Factor: 11.07; H-Index: 232)

* **Gupt, C. B.,** Prakash, A., Hazra, B., and Sreedeep S. (2021). Predictive Model for Soil Shrinkage Characteristic Curve of High Plastic Soils. Geotechnical Testing Journal. ASTM. (Impact Factor: 1.289; H-Index: 57)

* **Gupt, C. B.,** Sreedeep, S and Arnepalli, D. N. (2022). Impact of Buffering Agent on Lead Adsorption of Bentonite: An Appraisal. Journal of Environmental Engineering, 148(2), ASCE (Impact Factor: 1.657; H-index: 95)

* **Gupt, C. B.,** Sanandam Bordoloi, S. Metta Niranjan Bhatlu, M. N., and Sreedeep, S. (2022). Hydraulic conductivity variation in compacted bentonite-fly ash mixes under constant volume and free swelling conditions. Canadian Geotechnical Journal, 99(999), 1-18. NRC (Impact Factor: 3.725; H-index: 129)

* **Gupt, C. B.,** Sanandam Bordoloi, and Sreedeep, S. (2023). Contaminant retention affected by controlled and uncontrolled pH for fly ash-bentonite composites used as landfill liner material. Journal of Cleaner Production, 406, 136924. Elsevier. (Impact Factor: 11.07; H-Index: 232).

**Book Chapter**

* **Gupt, C. B.,** Younus, M. M., and Sreedeep, S. (2019). Utilization of Thermal Power Plant By-Product Fly Ash in Waste Management. In Advances in Waste Management (pp. 479-491). Springer, Singapore.

* **Gupt, C. B.,** Kushwaha, A., Prakash, A., Chandra, A., Goswami, L., and Sreedeep, S. (2021). Mitigation of groundwater pollution: Heavy metal retention characteristics of fly ash-based liner materials. In Fate and transport of subsurface pollutants (pp. 79-104). Springer, Singapore.

**Conference**

* **Gupt, C. B.,** and Sreedeep, S. (2014). Volumetric shrinkage characteristics curve of highly expansive soils. NES-STUDENT GEOCONGRESS at IIT Guwahati.

* **Gupt, C. B.,** and Sreedeep, S. (2014). Study on soil volumetric shrinkage curve for varying plasticity. IGC-2014 at Kakinada, India.

* **Gupt, C. B.,** and Sreedeep, S. (2014). Study on soil volumetric shrinkage curve for varying plasticity. IGC-2014 at Kakinada, India.

* **Gupt, C. B.,** and Sreedeep, S. (2015). Comparative assessment of volumetric shrinkage curves of cohesionless and cohesive soil. IGS Pune Chapter, India.

* **Gupt, C. B.,** and Sreedeep, S. (2017). Applications of Field Emission Scanning Electron Microscope in Civil Engineering. ICSIMR-2017 at IIT Guwahati.

**Articles submitted/preparation**

* **Gupt, C. B.,** and Sreedeep, S. Hydraulic conductivity of bentonite under constant volume and free swelling conditions at 1g and Ng (using small geotechnical centrifuge).

* **Gupt, C. B.,** Sahoo, R. K., and Sreedeep, S. Demonstrating the utility of accelerated physical modelling for determining hydraulic conductivity of hydraulic barriers.

* **Gupt, C. B.,** and Sreedeep, S. Impact of interaction time on the variation of hydraulic conductivity of bentonite  fly ash under constant volume and free swelling conditions.

* **Gupt, C. B.,** and Sreedeep, S., Patra, C., and Narayanasamy, S. Effect of interaction time on contaminant retention capacity of Indian bentonite-fly ash mixes for its potential application in waste containment.